



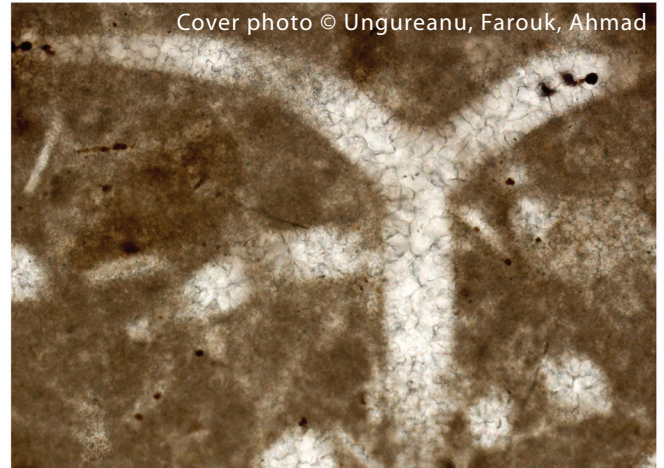
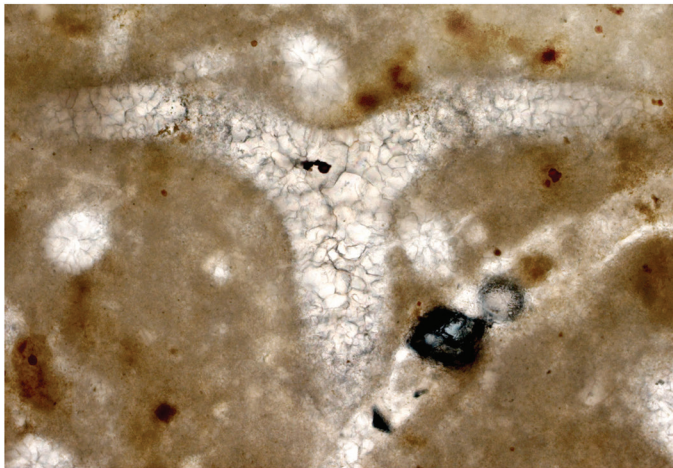
The Hashemite Kingdom of Jordan Scientific Research Support Fund The Hashemite University

JJEES

Jordan Journal of Earth
and Environmental Sciences



Volume (15) Number (3)



JJEES is an International Peer-Reviewed Research Journal

Jordan Journal of Earth and Environmental Sciences (JJEES)

JJEES is an International Peer-Reviewed Research Journal, Issued by Deanship of Scientific Research, The Hashemite University, in corporation with, the Jordanian Scientific Research Support Fund, the Ministry of Higher Education and Scientific Research.

EDITORIAL BOARD:

Editor –in-Chief:

- Prof. Dr. Eid A. Al Tarazi
The Hashemite University, Jordan

Editorial Board:

- Prof. Dr. Abdalla M. Abu Hamad
Jordan University
- Prof. Dr. Hani R. Al Amoush
Al al-Bayt University
- Prof. Dr. Ibrahim M. Oroud
Mutah University

Assistant Editor:

- Dr. Mohammed A. Salahat
The Hashemite University, Jordan
- Prof. Dr. Kamel K. Al Zboon
Balqa Applied University
- Prof. Dr. Khaldoun A. Al-Qudah
Yarmouk University
- Prof. Dr. Mahmoud M. Abu –Allaban
The Hashemite University

ASSOCIATE EDITORIAL BOARD: (ARRANGED ALPHABETICALLY)

- Professor Ali Al-Juboury
Al-Kitab University, Kirkuk, Iraq
- Dr. Bernhard Lucke
Friedrich-Alexander University, Germany
- Professor Dharendra Pandey
University of Rajasthan, India
- Professor Eduardo García-Meléndez
University of León, Spain
- Professor Franz Fürsich
Universität Erlangen-Nürnberg, Germany
- Professor Olaf Elicki
TU Bergakademie Freiberg, Germany

INTERNATIONAL ADVISORY BOARD: (ARRANGED ALPHABETICALLY)

- Prof. Dr. Ayman Suleiman
University of Jordan, Jordan.
- Prof. Dr. Chakroun-Khodjet El Khil
Campus Universitaire, Tunisienne.
- Prof. Dr. Christoph Külls
Technische Hochschule Lübeck, Germany.
- Prof. Dr. Eid Al-Tarazi
The Hashemite University, Jordan.
- Prof. Dr. Fayed Abdulla
Jordan University of Science and Technology, Jordan.
- Prof. Dr. Hasan Arman
United Arab Emirates University, U.A.E.
- Prof. Dr. Hassan Baioumy
Universiti Teknologi Petronas, Malaysia.
- Prof. Dr. Khaled Al-Bashaireh
Yarmouk University, Jordan.
- Dr. Madani Ben Youcef
University of Mascara, Algeria.
- Dr. Maria Taboada
Universidad De León, Spain.
- Prof. Dr. Mustafa Al- Obaidi
University of Baghdad, Iraq.
- Dr. Nedal Al Ouran
Balqa Applied University, Jordan.
- Prof. Dr. Rida Shibli
The Association of Agricultural Research Institutions in the Near East and North Africa, Jordan.
- Prof. Dr. Saber Al-Rousan
University of Jordan, Jordan.
- Prof. Dr. Sacit Özer
Dokuz Eylul University, Turkey.
- Dr. Sahar Dalahmeh
Swedish University of Agricultural Sciences, Sweden.
- Prof. Dr. Shaif Saleh
University of Aden, Yemen.
- Prof. Dr. Sherif Farouk
Egyptian Petroleum Institute, Egypt.
- Prof. Dr. Sobhi Nasir
Sultan Qaboos University, Oman.
- Prof. Dr. Sofian Kanan
American University of Sharjah, U.A.E.
- Prof. Dr. Stefano Gandolfi
University of Bologna, Italy.
- Prof. Dr. Zakaria Hamimi
Banha University, Egypt.

EDITORIAL BOARD SUPPORT TEAM:

- Language Editor
- Dr. Abdullah F. Al-Badarneh
- Publishing Layout
- Obada M. Al-Smadi

SUBMISSION ADDRESS:

Manuscripts should be submitted electronically to the following e-mail:

jjees@hu.edu.jo

For more information and previous issues:

www.jjees.hu.edu.jo



Hashemite Kingdom of Jordan



Scientific Research Support Fund



Hashemite University

Jordan Journal of Earth and Environmental Sciences

JJEES

An International Peer-Reviewed Scientific Journal

Financed by the Scientific Research Support Fund

Volume 15 Number (3)

<http://jjees.hu.edu.jo/>

ISSN 1995-6681

PAGES	PAPERS
146 - 155	Behavioral Responses to Hydrocarbon Stress in Marine Bacteria Isolated from Arzew Harbor in Northwestern Algeria <i>Samia Aliane, Amina Meliani, Samir Berkat, Hibat Errahmen Mazari, Youcef Bouhadda, Abdesselem Si Mohammed</i>
156 - 161	Assessment of Rainwater Harvesting Management in Jordan <i>Kamel K. Al-Zboon, Obada A. Mansi and Bashaar Y. Ammary</i>
162 - 173	Delineation of Potential Groundwater Area in Semi-arid and Arid Region: A Case Study of Wadi Mekerra North West Algeria Using Remote Sensing, GIS and Analytic Hierarchy Process <i>Zakaria Mahfoud, Noureddine Maref, Abdelkader Bemoussat</i>
174 - 182	Dolomitization Model of the Lower Jurassic Sarki Formation Depending on Petrography and Carbon/Oxygen Isotopes, Northeastern Iraq-Kurdistan region <i>Bzhar A. Delizy, Waleed S. Shingaly, Sardar M. Balaky</i>
183 - 191	b-value Estimation and Extreme Magnitude Assessment in the Source Region of Past Earthquakes in Central Himalaya and Vicinity <i>Ram Krishna Tiwari, Harihar Paudyal</i>
192 - 198	Stability Analysis of Shiraz Metro Line 1 Tunnel Using Flac2D Software <i>Naghme Nasiri, Fariba Kargaranbafghi, Hamid Mehrnahad, Javad Gholamnejad and Mojtaba Rahimi Shahid</i>
199 - 207	A Review on Water Quality Aspects of Urban Rainwater Harvesting in Jordan <i>Ayat Hazaymeh, Jens Lange</i>
208 - 215	Evaluating the Impact of Rubber Particles on the Swelling Potential and Pressure of Tizi Soil in an Area Located in North Western Algeria <i>Benamar Balegh, Hamid Sellaf, Adda Hadj Mostefa, Nourdinne, Mahmoudi</i>
216 - 224	The Development of Fine Precast Concrete Mix Using Local Materials <i>Mohmd Sarireh, Ayoup M. Ghrair, Sliiman M., M Zaidyeen, and Mohmd Al-Jaraba</i>

Behavioral Responses to Hydrocarbon Stress in Marine Bacteria Isolated from Arzew Harbor in Northwestern Algeria

Samia Aliane^{1*}, Amina Meliani², Samir Berkat¹,
Hibat Errahmen Mazari¹, Youcef Bouhadda³, Abdesselem Si Mohammed⁴

¹Mustapha Stambouli University, Faculty of Nature and Life Sciences, Laboratory of Geo-environment, and Space Development (LGEDE), 29000 Mascara, Algeria;

²Mustapha Stambouli University, Faculty of Nature and Life Sciences 29000 Mascara, Algeria;

³Mustapha Stambouli University, Faculty of Nature and Life Sciences, Laboratory of Physical Chemistry of Macromolecules and Biological interfaces, 29000 Mascara, Algeria;

⁴Ahmed ZABANA University, Faculty of Sciences and Technology, 29000 Relizane, Algeria

Received May 1st, 2023; Accepted March 9th, 2024

Abstract

Marine hydrocarbon pollution has emerged as a pressing concern, imperiling the ocean's abundant resources and disrupting the crucial services rendered by marine ecosystems. The presence of hydrocarbons in seawater poses a significant challenge to microorganisms, prompting adaptive modifications in bacterial behavior to thrive in these adverse conditions. A comprehensive investigation into marine bacteria's potential to utilize and break down hydrocarbons was conducted, focusing on strains isolated from Arzew harbor. These strains underwent rigorous phenotypic and biochemical characterization. Their ability to form biofilms in the presence of varying concentrations of sodium chloride, crude oil, and kerosene was meticulously assessed. Hydrophobicity and chemotactic responses of these strains were studied in media supplemented with crude oil and kerosene. Notably, the results unveiled that eight of these strains exhibited a profile akin to *Pseudomonas sp.* While one strain resembled *Aeromonas sp.*, all strains exhibited varying degrees of biofilm-forming capacity, ranging from low to high. A predominantly hydrophobic phenotype was observed among these strains. The majority of the bacteria displayed a noteworthy chemotactic attraction to crude oil. Strain S7 emerged as the most promising, displaying remarkable proficiency in handling the studied hydrocarbons, closely followed by strain S16. It's worth emphasizing that robust outcomes were associated with emulsification potential and chemotaxis towards both hydrocarbons, coupled with bacterial cell surface hydrophobicity. These findings illuminate the potential of these strains for enhancing water quality in hydrocarbon-contaminated environments.

© 2024 Jordan Journal of Earth and Environmental Sciences. All rights reserved

Keywords: Hydrocarbons, Biofilm, Emulsifying Activity, Hydrophobicity, Chemotaxis.

1. Introduction

Microbial communities, inhabiting marine environments, include different groups of bacteria, archaea, fungi, protists, and viruses (Fuhrman *et al.*, 2015). These microorganisms play a crucial role in the recycling of elements, taking the example of carbon, nitrogen, and sulfide cycling. These processes contribute to the insurance of nutrients in the marine environment and the regulation of global climate. It is important to note that the structure and function of microbial communities allow us to better understand their role in the marine environment (Jégousse *et al.*, 2022). These organisms can be phototrophs or chemotrophs as primary producers, as well as heterotrophs that represent the secondary producers. Recently, several studies have focused on molecular analysis to determine the organisms present in a given site and their spatiotemporal distribution. The data, generated by phylogenetic studies, is based on a limited number of genes citing 16S and 18S rRNA. Scientists have confirmed that these tools are insufficient to understand and assess environmental functions and community ecology. New tools are being developed to allow us to much understand about these functions. These tools are brief omics analysis which

includes metagenomic, metatranscriptomic, metaproteomic, and metabolomic analyses (Fuhrman *et al.*, 2015).

The analysis of total microbial communities is considered a rigorous criterion for seawater quality. It enhances sustainable development. As already noted, it is crucial to evaluate any change in the structure of microbial communities because of their contribution to biogeochemical cycles and the biodegradation of pollutants. Various parameters can influence community structures especially the gradient of inorganic substrates (N, P), season, adjacent habitat, depth, oxygen, protist predation, pressure, salinity, algal dominance, particulate organic carbon, human disturbance, and sand mining (Nimnoi and Pongsilp, 2020). It is known that oil pollution is an environmental concern in marine ecosystems. This is related to oil extraction and transportation activities, shipping, urban runoff, and industrial discharges. The hydrophobic nature of these compounds allows them to accumulate in sediments that act as a sink. Therefore, high concentrations can be accumulated in sediments with the potential to be quite harmful to the health of marine ecosystems. This nature makes bioremediation encouraging biotechnology to reduce the adverse effects associated with

* Corresponding author e-mail: samia.aliane@univ-mascara.dz

this type of pollution while avoiding negative implications such as the use of dispersants or oil burning (Lozada *et al.*, 2014; Perdigão *et al.*, 2021). The use of indigenous microorganisms can improve the efficiency of biodegradation due to their adaptation to the environment. Therefore, several studies have recommended the importance of using indigenous microbial communities for the bioremediation of petroleum hydrocarbons in marine ecosystems (Perdigão *et al.*, 2021). It highlights that Polycyclic Aromatic Hydrocarbons (PAHs), resulting from pyrolytic processes and mainly anthropogenic activities, are considered priority pollutants due to their carcinogenic and mutagenic properties (Imarhiagbe and Obayagbona, 2029). Microbial degradation plays a key role in remedying environmental contamination caused by petroleum spills. Numerous strains of bacteria and fungi have showcased their remarkable capability to selectively break down distinct fractions of petroleum compounds, signifying their important role in restoring affected ecosystems (Olaemi *et al.*, 2021).

Remarkably, hydrocarbon degrading bacteria can exhibit chemotactic behavior as a signaling system in order to make these compounds accessible (AlKaabi *et al.*, 2020). Moreover, the chemotaxis allows bacteria to migrate to favorable environments or to move away from unfavorable environments (Wang *et al.*, 2022). This process in *Escherichia coli*, *Pseudomonas aeruginosa*, *Pseudomonas putida*, and *Rhodococcus erythropolis*, has demonstrated their ability to detect and adapt to chemical changes in their environment (Liang *et al.*, 2021). *P. aeruginosa* with a polar flagellum has demonstrated a directed mobility that allows it to accumulate at the hydrocarbon-water interface. The monitoring of the unicellular mobility near the hydrocarbon-water interface revealed four types of movements. The first type is a visitor that visits the interface and then leaves. Other bacteria have proved their ability to stay at the interface for at least 60s by passive diffusion, otherwise, they are known as “diffusive”. Some bacteria swim in circle perpendicular trajectories “pirouettes” or flat “loops” by locating themselves at the hydrocarbon-water interface (Conrad, 2020).

Bioremediation represents an environmentally-friendly waste management approach, harnessing the power of living organisms to efficiently eliminate or render harmless pollutants, present within a tainted location (Mercy *et al.*, 2019). The efficiency of biodegradation relies on the interactions between the bacterial cells and the hydrocarbon, as does the hydrophobicity of the cell surface (AlKaabi *et al.*, 2020). The hydrophobicity of bacterial cells is considered to be an important factor in controlling bacterial growth and adhesion to surfaces (Meliani and Bensoltane, 2014). It should be noted that microbial adhesion to hydrocarbons is one of the methods to determine the affinity of bacteria for dispersed hydrocarbons (Conrad, 2020). Many microorganisms can produce biosurfactants. These products increase the interaction between hydrocarbons and microbial cells, bioavailability which subsequently improves the bioremediation of hydrocarbons in polluted sites (Shahaliyan *et al.*, 2015). The production of biosurfactants is associated with the emulsification potential of strains. It was also described that an effective emulsification of hydrocarbons and the

stabilization of emulsion in marine environment, represent a crucial requirement for hydrocarbon remediation (Gong *et al.*, 2015). Our study signifies a novel research endeavor, focused on observing and understanding the responses of native bacteria in the Arzew region when exposed to hydrocarbon stress. Two main characteristics of the indigenous marine bacteria are assessed: the cells’ surface hydrophobicity and their emulsification potential. The profiling of communal traits such as biofilm formation and chemotaxis of native marine bacteria improves potent data related to the future application of these strains for environmental purposes.

2. Material and methods

2.1. Sampling and bacterial isolation

Arzew harbor is located on the eastern side of Cape Carbon in Arzew Bay, approximately 350 kilometers west of Algeria and 500 kilometers to the east of the Strait of Gibraltar (35°51'38.196 N 0°18'26.1864 W) (Fig.1). Its main activity is the exportation of hydrocarbons (Bensari *et al.*, 2020). Water sampling was performed during early winters in December 2020 and December 2021 from the border and depth of 20 cm. One millimeter of each sample was transferred into a flask, containing 100 ml of Bushnell and Haas Broth at pH = 7. Flasks were kept in incubator at 30 °C under shaking for 48 to 72h. A 100µl of each bacterial suspension was transferred to BH agar plates. Colonies were purified and stored at 4°C in fresh BH medium supplemented with 20% of sterile glycerol (Borah *et al.*, 2019).

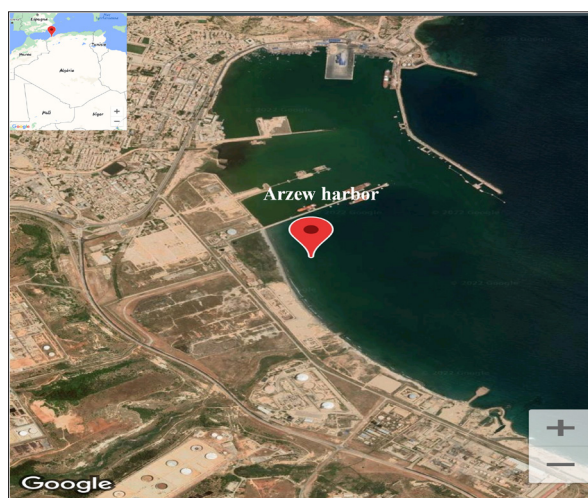


Figure 1. Map of Arzew harbor of Oran (Map Data© 2022, Google Maps.)

2.2. Morphological and biochemical characterization

All isolates were identified by studying their morphology and biochemical profile. The morphological study of the colony concerns its shape, color, diameter, and contour. These characteristics were observed on *Pseudomonas* F agar plates after incubation at $35 \pm 2^\circ\text{C}$ for 24h. Bacterial identification is based on Gram staining, catalase, and oxidase test by using commercial disks (Sigma Aldrich), and biochemical and carbohydrates fermentation profiles were studied by using API 20NE (Biomerieux: API (Analytical Profile Index) is a standardized system for the identification of non-fastidious, non-enteric Gram-negative rods, containing 20 miniature of biochemical tests (combines 8 conventional tests, 12 assimilation tests, and a database) multitests. All strains were

conserved in LB with glycerol 30 per cent at -80°C (Celik *et al.*, 2008).

2.3. Biofilm formation

Biofilm formation evaluation was performed using the microplate method. Bushnell and Haas Broth were used to fill transparent 96-well polystyrene microplates. Each well was inoculated with a pre-culture prepared with the studied strains, and the control wells were filled with sterile BH broth. The microplates were then incubated at 37°C for 24h. After incubation, the microplates were emptied of their contents and then rinsed three times with phosphate buffer (PBS). The microplates were inverted to dry slightly and then stained with 0.5% (W/V) crystal violet solution. After 15 min. of staining, the dye excess was removed, and the wells were rinsed three times with sterile bi-distilled water. The microplates were dried for 15 min. at room temperature. The crystal violet, retained by adhered cells to the polystyrene surface, is recovered by 95% ethanol, and it was determined by reading the absorbance at the wavelength (λ) = 595 nm by Eliza reader (YSENMED) (Stephanovic *et al.*, 2007; Wijesinghe *et al.*, 2019).

The evaluation of biofilm formation is performed by comparing values of the optical density of the bacterial film against the optical density of negative controls (sterile media). Biofilm formation ability is expressed using the threshold value (DO_c). The threshold value (DO_c) is defined as the mean of the negative controls plus three times the standard deviation of the negative controls (Diaz *et al.*, 2016).

2.3.1. The Effects of salinity on biofilm formation

In order to test the effect of salinity on the bacterial adhesion, different concentrations of NaCl were tested (0, 0.3M, 0.5M, 0.8, 1M, 2M, and 3M). 96-well polystyrene microplate was incubated at 37°C for 24h. After incubation, the optical density was determined by an Eliza reader at λ = 595 nm.

2.3.2. The Effects of hydrocarbons on biofilm formation

Various concentrations of the crude oil and kerosene have been tested in order to evaluate their effect on the biofilm formation. In this goal, seven concentrations were used (0, 0.5%, 1%, 1.5%, 2%, 3%, and 4%). It should be noted that the same conditions were kept. After incubation, the optical density was read at λ = 595 nm by Eliza reader.

2.4. Bacterial chemotaxis toward Hydrocarbons

Chemotactic responses of marine strains towards hydrocarbons were detected by the capillary method as previously described (Gordillo *et al.*, 2007; Shu *et al.*, 2018). First, Eppendorfs were used as a chamber to introduce a volume equal to 200 μ l of the bacterial suspension ($OD=2.5$) into the chemotactic buffer. A needle of 2 cm in length was used as a capillary and attached to a syringe containing 200 μ l of the tested substances. After 90 minutes of incubation at room temperature, the syringe was removed from the bacterial suspension, and its content was diluted and spread on Pseudomonas F agar, the incubation was performed at 37°C for 24h. After incubation, the developed colonies were counted and expressed as CFU.ml⁻¹(CFU: Colony-Forming Unit).

2.5. Bacterial adhesion to hydrocarbons (BATH)

The bacterial adhesion to hydrocarbons assay serves to evaluate the hydrophobicity of bacterial cell suspension (Rosenberg *et al.*, 1980). Briefly, the bacteria were grown in Lauria Bertani broth at 30 °C. They reach their exponential phase overnight ($OD_{600} = 0.6$). A volume of 2 ml of bacterial suspension was suspended in an eppendorf tube and centrifuged at 1500×g. The supernatant was removed and the bacteria were resuspended in 2 ml of fresh motility buffer. This operation was repeated three times before transferring the bacterial suspension to round bottom test tubes. Then, 15 μ l of the tested hydrocarbon was added and a thin layer of oil formed which covers the bacterial suspension. After 2 minutes of agitation, the mixtures were left 15 minutes to settle for phase separation. A volume of 1 ml of aqueous phase was transferred to cuvette for optical density reading at 600 nm (Chao *et al.*, 2014; May *et al.*, 2019).

$$RH = (OD_{\text{initial}} - OD_{\text{residual}}) / OD_{\text{initial}} \times 100\%$$

RH: Relative hydrophobicity

OD initial: Optical density of the preculture before adding the hydrocarbons

OD residual: Optical density of the preculture after adding the hydrocarbons

2.6. Hydrocarbon emulsifying activity

To determine the emulsifying activity of bacterial strains, a tube containing an overnight culture inoculated previously in LB (Lauria Bertani) broth. An equivalent volume of crude oil and kerosene were introduced under vortexing for 3 min. at a maximum speed. A tube containing sterile broth with an equivalent volume of the hydrophobic phase was used as a negative control. Incubation was performed at 37°C for 24 h. After incubation, the emulsification index was calculated according to the following formula (Cooper *et al.*, 1987).

$$E24 = (He / Ht) \times 100$$

He: height of emulsion

Ht: total height of the mixture

2.7. Statistical analysis

All experiments were performed in triplicates. The results were analyzed by one-way ANOVA ($P < 0.05$). All data were presented as the average and standard deviation (SD) The results were followed up with Bonferroni test ($P < 0.05$) groupings. The descriptive statistics, Principal Component Analysis (PCA), Hierarchical Cluster analysis (HCA), and correlation were executed. All statistical treatments were undertaken using STAISTICA software (version 10).

The biofilm formation capacity was expressed using cut-off values (ODc). ODc value can be defined as the mean of negative controls (OD_{nc}) plus three standard deviations (SDs) (Diaz *et al.*, 2016). Strains were classified into the following categories: $ODc < OD \leq 2 \times ODc$: weak biofilm producer, $2 \times ODc < OD \leq 4 \times ODc$: moderate biofilm producer, and $OD > 4 \times ODc$: strong biofilm producer.

3. Results

3.1. Isolates characterization

A total of 9 strains were isolated and subjected to conventional phenotypical and physiological tests. As the phenotypical study, all strains are characterized on the basis of Gram staining and cultural aspect of colonies on agar medium. However, the physiological study consists in the catalase and oxidase test. The biochemical profile was determined by a classical gallery, API 20NE.

According to the obtained results on *Pseudomonas* F agar, 8 strains have proved a similar aspect with yellow-green

pigments (S5, S6, S7, S8, S9, S11, S16 and S25), and one strain with beige colonies (S30). All strains are Gram negative rods, aerobics, oxidase and catalase positive. They grow well at 42°C, and none has the capacity to grow at 4°C (Fig. 2).

The resulting biochemical profiles were interpreted using the API-web software (bioMérieux). The similarity index of eight isolates was found to be 99.98% for *Pseudomonas* taxa and only S30 strain with 99.92% as a similarity index for *Aeromonas* taxa. The phenotypical and biochemical traits are summarized in Table 1.

Table 1. Phenotypical and biochemical characteristics of marine strains.

	S5	S6	S7	S8	S9	S11	S16	S25	S30
Gram	-	-	-	-	-	-	-	-	-
Oxydase	+	+	+	+	+	+	+	+	+
Catalase	+	+	+	+	+	+	+	+	+
Motility	+	+	+	+	+	+	+	+	+
Pigment	+	+	+	+	+	+	+	+	-
Growth at 4°C	-	-	-	-	-	-	-	-	-
Growth at 42°C	+	+	+	+	+	+	+	+	+
Mannitol	+	+	+	+	+	-	+	-	-
Citratase	+	+	+	+	+	+	+	+	+
ONPG	+	+	+	+	+	+	+	+	+
ADH	+	+	+	+	+	+	+	+	+
LDC	+	+	+	+	+	+	+	+	+
ODC	+	+	+	+	+	+	+	+	+
H ₂ S	-	-	-	-	-	-	-	-	-
Urease	-	-	-	-	-	-	-	-	-
Indole	-	-	-	+	-	-	-	-	-
Gelatinase	+	+	+	+	+	+	+	+	+
VP	-	-	-	-	-	-	-	-	-
NO ₃	+	+	+	+	+	+	+	+	+
TRP	-	-	-	-	-	-	-	-	+
GLU	-	-	-	+	-	-	-	-	+
ESC	-	-	-	+	-	-	-	-	+
PNPG	-	-	-	+	-	-	-	-	+
GLUa	+	+	+	+	+	+	+	+	+
ARa	-	-	-	-	-	-	-	-	+
MNEa	-	-	-	-	-	-	-	-	+
MANa	+	+	+	+	+	+	+	+	+
NAGa	+	+	+	+	+	+	+	+	+
MALa	-	-	-	-	-	-	-	-	+
GNTa	+	+	+	+	+	+	+	+	+
CAPa	+	+	+	+	+	+	+	+	+
ADLa	+	+	+	+	+	+	+	+	-
MLTa	+	+	+	+	+	+	+	+	+
CITa	+	+	+	+	+	+	+	+	-
PACa	-	-	-	-	-	-	-	-	-

+ : Positive

- : Negative

3.2. Biofilm formation

The evaluation of biofilm formation on microplate presents a method of quantification based on the demonstration of cell adhesion to a polystyrene surface. All strains were tested for their ability to form biofilms on polystyrene microplate as mentioned above. This ability was tested by varying the concentration of sodium chloride, crude oil, and kerosene. After incubation, the wells were stained with crystal violet to visualize the bacterial adhesion. The categorization of strains (weak, moderate, or high biofilm-forming) was based on the comparison between the optical densities, read at 595 nm with the critical optical density (OD_c) (Fig.3).

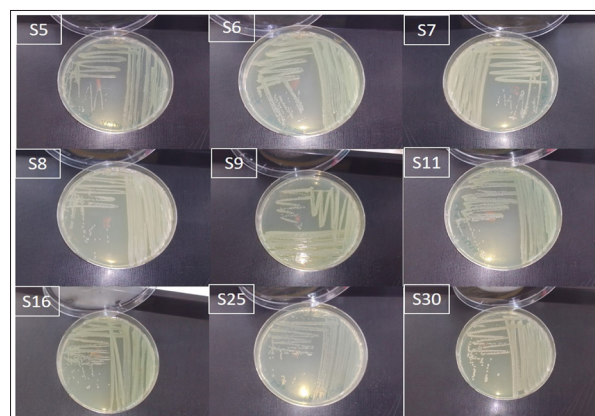


Figure 2. Cultural aspect of marine isolates on Lauria Bertani agar.

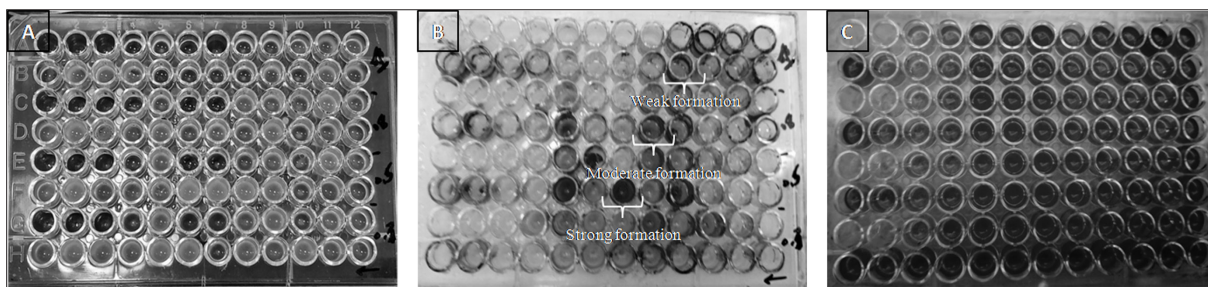


Figure 3. Results of biofilm formation demonstrating the ability of marine strains, to adhere to polystyrene microplate. **A:** Before coloration with Crystal violet; **B:** After crystal violet Removal and drying; **C:** Crystal violet recovery by ethanol

3.2.1. Effect of salinity on bacterial communities

In the absence of sodium chloride stress, most strains display a moderate level of adherence to the polystyrene surface. However, only one strain (S16) exhibited strong biofilm-forming ability, as evidenced by its significantly higher optical density value ($P < 0.05$), indicating substantial adherence. Conversely, this same strain demonstrated robust biofilm formation at varying concentrations, ranging from 0.5M to 2M of sodium chloride. In other words, these concentrations amplified bacterial adhesion to the polystyrene surface. Bacterial adhesion predominantly ranged from weak to moderate across concentrations fluctuating from 0.3M to 1M. Interestingly, 88.89% of the strains exhibited moderate adhesion at a concentration of 3M. However, this particular concentration had an adverse effect on bacterial adhesion, except for the S16 strain, which maintained strong biofilm formation under the same conditions. Most of the tested concentrations moderately enhance the biofilm-forming capacity of marine isolates, possibly due to their halophilic traits. However, this observation doesn't hold true for the 2M concentration, as it significantly strengthens bacterial adhesion. Consequently, most strains can now be classified as strong biofilm formers. The most robust biofilm formation was evident in S6 (0.906) at the 2M concentration and S16 (0.963) at the 3M concentration ($P < 0.05$) (see Fig. 4).

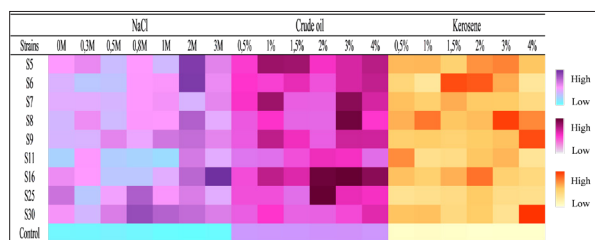


Figure 4. Bacterial ability to form biofilm at different concentrations of sodium chloride; crude oil and kerosene ($p < 0.05$).

3.3.2. Effect of hydrocarbons on bacterial communities

The impact of hydrocarbons on the biofilm-forming capability of bacterial isolates was studied by varying the concentrations of crude oil and kerosene. A range of concentrations, spanning from 0.5% to 4%, was selected for investigation. In the case of crude oil, marine strains have generally demonstrated a moderate capacity to create biofilms when the concentrations range from 0.5% to 2%. However, when the concentrations increase to 3% and 4%, there is a noteworthy enhancement in biofilm formation in 55.55% of our strains ($P < 0.05$). This concentration enhanced biofilm formation can be attributed to the marine strains' ability to degrade and utilize hydrocarbons as a carbon source.

However, the introduction of both 0.5% and 1.5% concentrations of kerosene exerts a detrimental impact on biofilm formation. This adverse effect is primarily attributed to the fact that a significant portion of strains within the population exhibits weak adhesion properties. Conversely, when exposed to concentrations of 1%, 2%, 3%, and 4% of kerosene, these strains display a noticeable shift towards moderate biofilm formation, as depicted in Figure 2. These findings suggest that the marine strain may not be adept at utilizing kerosene as a carbon source, possibly due to its toxic nature.

3.3. Bacterial chemotaxis toward hydrocarbons

All strains underwent assessment for their chemotactic responses across various sodium chloride concentrations. Remarkably, all of our strains exhibited positive chemotaxis responses to both crude oil and kerosene. Particularly intriguing was the chemotactic behavior displayed by the S7 strain, with a concentration of 980.104 CFU.ml⁻¹ showing a notable response to crude oil and 396.104 CFU.ml⁻¹ towards kerosene. The majority of strains demonstrated a moderate level of chemotaxis. When comparing bacterial chemotaxis to the tested hydrocarbons, it became evident that the most robust cell concentrations were observed in response to crude oil. Notably, crude oil significantly enhanced the chemotactic behavior of the S7 strain ($P < 0.05$), while no statistically significant differences were observed for the majority of strains (refer to Fig. 5).

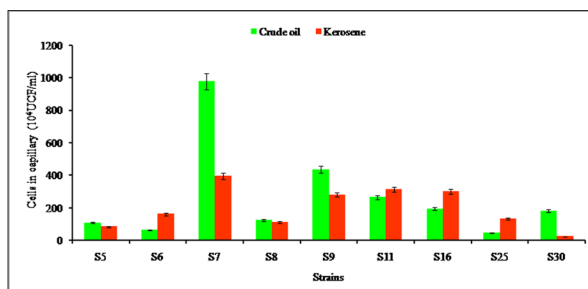


Figure 5. Cells accumulation in capillary, in presence of crude oil and kerosene in after 24h of incubation at 37°C. Data represent means \pm SD of three experiments ($p < 0.05$).

3.4. Bacterial cell surface hydrophobicity

To investigate the surface cell hydrophobicity concerning crude oil and kerosene, a comparison was made between the initial optical density and the residual optical density. The outcomes of these cell hydrophobicity assessments are illustrated in Figure 6. A standout observation emerges with the S11 strain, showcasing a remarkable 61.33% hydrophobicity towards crude oil, and the S16 strain displaying a significant

59.33% hydrophobicity towards kerosene. Evidently, the presence of crude oil substantially amplifies surface cell hydrophobicity across the majority of marine isolates.

Regarding kerosene, the majority of marine isolates exhibited a moderate level of hydrophobicity, with the notable exception of the S16 strain, which displayed a particularly intriguing degree of hydrophobicity (as illustrated in Figure 4). When comparing the hydrophobicity of these strains across the tested hydrocarbons, it becomes apparent that they demonstrated relatively similar hydrophobic characteristics. However, it is worth highlighting that this trait appears to be particularly pronounced in response to crude oil.

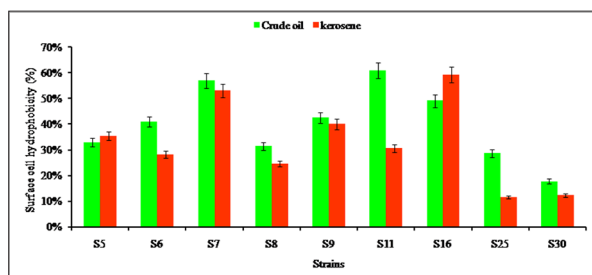


Figure 6. Bacterial cell hydrophobicity of marine strains toward crude oil and kerosene, after 24h of incubation at 37°C. Data represent means \pm SD of three experiments ($p < 0.05$).

3.5. Emulsifying activity

The emulsification index served as a quantifiable measure for evaluating the capacity of the studied strains to emulsify hydrocarbons. Interestingly, nine strains exhibited emulsifying potential, with nine strains demonstrating emulsifying activities against crude oil within a range of 29.27% to 59.79%. A lower emulsifying potential was observed in 22.22% of the strains. In the case of kerosene, all strains exhibited emulsification indices varying between 17.38% and 58.19%, as depicted in Figure 7.

An interesting emulsifying capability was observed in 44.44% of the tested strains. Among these, the most noteworthy performance was exhibited by the S25 strain, showcasing an impressive 59.25% emulsification index when interacting with crude oil. In contrast, both the S7 and S16 strains displayed comparable emulsification indices of 58.19% when exposed to kerosene. The emulsification indices of the S5 and S8 strains were also quite similar. It is striking that there was a notably higher emulsifying potential for crude oil, compared to kerosene within this study.

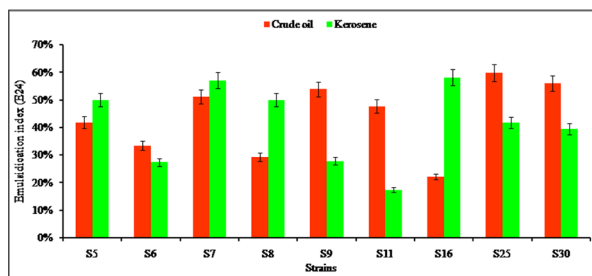


Figure 7. Emulsification index of marine strains, toward crude oil and kerosene after 24h of incubation at 37°C. Data represent means \pm SD of three experiments ($p < 0.05$).

3.6. Principal component analysis (PCA)

Correlation circle plots serve as a valuable tool within Principal Component Analysis (PCA) to unveil relationships among variables (as illustrated in Fig. 8). Our examination of these variables unveiled two principal components, where PC1 accounted for a substantial 47.73% of the total variance while PC2 contributed significantly at 28.45%. The inherent correlation between two variables is visually apparent through the angular orientation of their vectors. When the angle is acute, it signifies a positive correlation. An obtuse angle indicates a negative correlation, and a right angle implies a null correlation. Notably, the correlation circle closely envelops the chemotaxis towards kerosene (EK), rendering it exceptionally well-represented on the map.

The narrow angle between Chemotaxis towards kerosene (CK) and Hydrophobicity towards crude oil (HC) signifies a robust correlation, as indicated by a correlation coefficient of 0.932478. This same strong correlation is evident between Chemotaxis towards crude oil (CC) and both Chemotaxis towards kerosene (CK) ($r = 0.745503$) and Hydrophobicity towards crude oil (HC) ($r = 0.636069$). Additionally, the angle formed between the vectors representing Hydrophobicity towards kerosene (HK) and the Emulsification index towards kerosene (EK) reveals a positive correlation ($r = 0.493149$). Conversely, the Emulsification index towards crude oil appears largely independent of the other parameters.

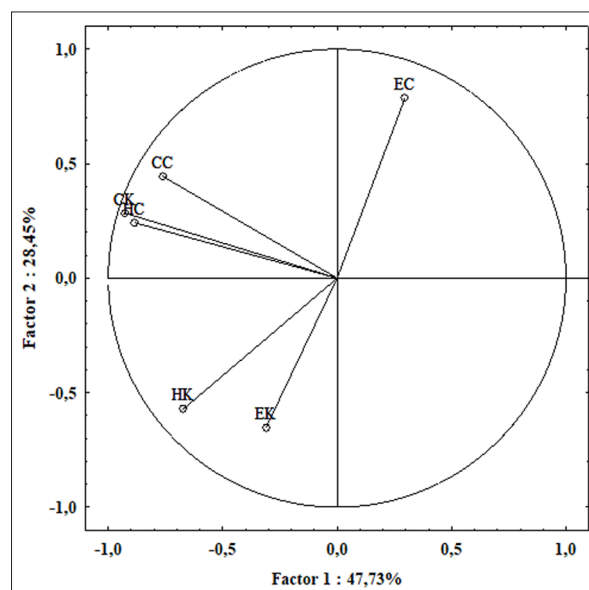


Figure 8. Correlation circle plot for PCA between the studied variable. EC: Emulsification index towards crude oil; EK: Emulsification index towards Kerosene; HC: Hydrophobicity towards crude oil; HK: Hydrophobicity towards Kerosene; CC: Chemotaxis towards crude oil; CK: Chemotaxis towards Kerosene.

3.6. Principal component analysis (PCA)

Correlation circle plots serve as a valuable tool within Principal Component Analysis (PCA) to unveil relationships among variables (as illustrated in Fig. 8). Our examination of these variables unveiled two principal components, where PC1 accounted for a substantial 47.73% of the total variance while PC2 contributed significantly at 28.45%. The inherent correlation between two variables is visually apparent through the angular orientation of their vectors. When the angle is

acute, it signifies a positive correlation. An obtuse angle indicates a negative correlation, and a right angle implies a null correlation. Notably, the correlation circle closely envelops the chemotaxis towards kerosene (EK), rendering it exceptionally well-represented on the map.

The narrow angle between Chemotaxis towards kerosene (CK) and Hydrophobicity towards crude oil (HC) signifies a robust correlation, as indicated by a correlation coefficient of 0.932478. This same strong correlation is evident between Chemotaxis towards crude oil (CC) and both Chemotaxis towards kerosene (CK) ($r = 0.745503$) and Hydrophobicity towards crude oil (HC) ($r = 0.636069$). Additionally, the angle formed between the vectors representing Hydrophobicity towards kerosene (HK) and the Emulsification index towards kerosene (EK) reveals a positive correlation ($r = 0.493149$). Conversely, the Emulsification index towards crude oil appears largely independent of the other parameters.

3.7. Hierarchical cluster analysis (HCA)

The analysis of bacterial behaviors concerning crude oil and kerosene reveals a classification of marine strains into three distinct clusters: Cluster 1 (comprising strains S5, S8, S6, S25, S30), Cluster 2 (with strains S9, S11, S16), and Cluster 3 (represented by strain S7). Within each cluster, there is a remarkable similarity in various traits. This hierarchical clustered heatmap illustrates that these behaviors can be categorized as low, medium, or high, as shown in Figure 9.

Notably, S7 emerges as the most significant strain, demonstrating compelling results in its interactions with the studied hydrocarbons, closely followed by the S16 strains. These strong results are equally associated with emulsification activity (44.44%) and chemotaxis toward both hydrocarbons (44.44%), with bacterial cell surface hydrophobicity contributing at 22.22%.

The analysis of the variables shows a clear division of our parameters into two distinct clusters. The first cluster comprises chemotaxis towards hydrocarbons, specifically crude oil and kerosene, while the second cluster encompasses hydrophobicity and emulsification related to hydrocarbons. Notably, our study reveals a high correlation in chemotactic behaviors between crude oil and kerosene. Consequently, our strains exhibit correlated responses to both hydrocarbons, primarily due to variations in chemotactic outcomes from other variables. Furthermore, their emulsification and hydrophobicity towards hydrocarbons demonstrate relatively close similarities. These findings are strongly supported by the correlation circle plot (Fig. 6).

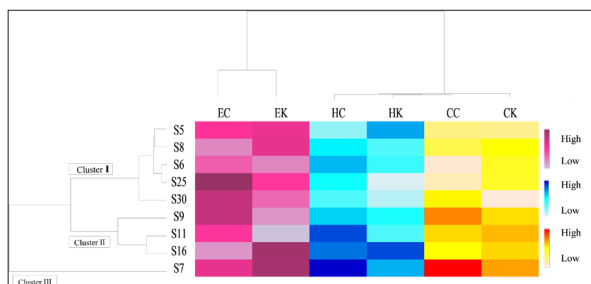


Figure 9. Correlation between the bacterial behaviors toward the tested hydrocarbons.

4. Discussion

This study aims to illuminate the intricate behaviors, exhibited by bacteria in response to varying levels of salinity and the presence of hydrocarbons within contaminated environments. Our primary objective is to unravel the specific bacterial traits that contribute to their superior adhesion and emulsifying capabilities in the context of hydrocarbons. Our results unequivocally establish that elevated salinity levels promote the formation of biofilms among marine strains. This phenomenon is in accord with prior research, as it can be attributed to the protective effects of biofilm structures against salt-induced stressors, as highlighted by Qurashi et al. (2012). Furthermore, *A. hydrophila* is shown to have an ability to form biofilms at lower concentrations of sodium chloride, as elucidated by Jahid et al. (2015). These findings reinforce the concept that biofilm formation bolsters bacterial resilience in the face of environmental challenges, particularly salinity. In highly saline environments, the formation of biofilms by halophilic bacteria emerges as a crucial strategy to counteract the detrimental effects of salinity. This was evident in a study on *Halomonas stenophila* HK30, an isolate from a saline wetland in Brikcha, Morocco, which exhibited a remarkable capacity to form biofilms even in the presence of a high salt concentration (5% w/v). Our exploration of the impact of salt stress on biofilm formation in *Vibrio* sp. B2, isolated from seawater, unveiled that these bacteria not only retained robust cell activity but also exhibited increased production of extracellular polymeric substances (EPS). This surge in EPS production is a key factor in the establishment of biofilms, as reported by Yin et al. (2019). Surprisingly, our research has unveiled fascinating findings, the presence of crude oil significantly amplifies the formation of biofilms within our examined bacterial strains. Notably, strains of *Pseudomonas aeruginosa* exhibit an extraordinary propensity for biofilm development when crude oil serves as their exclusive carbon source, as detailed in the works of Dasgupta et al. (2013) and Dutta and Singh (2016). In the context of crude oil reservoirs, the microbial biofilm communities feature a diverse array of genera, including *Achromobacter*, *Arcobacter*, *Pseudomonas*, and *Bacillus*, which have showcased their remarkable capacity to metabolize and degrade hydrocarbons, with a particular focus on aromatic hydrocarbons. In this intricate metabolic pathway, these microorganisms leverage various metabolites, such as enzymes and biosurfactants, to facilitate the degradation of hydrocarbons, as expounded upon by Elumalai et al. (2021). An aggregation of dense biomass at the oil-water interface was observed (Dasgupta et al., 2013). This phenomenon revealed a diverse range of biofilm-forming microorganisms in produced water within oilfields, which have been linked to the onset of biocorrosion in X80 steel (de Oliveira et al., 2021). As reported, the most frequently found bacteria contaminating kerosene include *Bacillus simplex*, *P. synxantha*, and *Sphingomonas zea*. These microorganisms have displayed a notable capacity for biofilm formation, acting as primary colonizers in the initial stage of biofilm development (Chiciudean et al., 2019). A recent study delved into the structures and composition of microbial biofilms cultivated in kerosene-based fuels, utilizing Scanning Electron Microscopy (SEM). The SEM imaging unveiled a complex,

multilayered structure of these biofilms. Detailed analysis of the images identified various bacterial and fungi-like structures, highlighting the cells capability to produce exopolymeric substances. Additionally, it became evident that three-dimensional microbial aggregates were prominently present in both the biofilm and water samples (Krohn et al., 2021). It has been reported that kerosene exhibits a low level of toxicity, falling within the range of 2.41% to 3.09%, when present at a contamination level of 10% over a 24-hour period. This effect pertains to its impact on the logarithmic survival rates of hydrocarbonoclastic bacteria such as *Bacillus sp.*, *Pseudomonas sp.*, *Serratia sp.*, and *Micrococcus sp.* The remarkable survival capabilities of these microorganisms can be attributed to their proficiency in hydrocarbon degradation, particularly kerosene, and their adeptness in utilizing it as a carbon and energy source for metabolic processes. Conversely, a different pattern emerges in the case of other microorganisms exclusively identified in pristine soil samples, including *Streptococcus sp.*, *Salmonella sp.*, *Staphylococcus aureus*, and *Escherichia coli*. These microorganisms exhibit a notably higher susceptibility to kerosene toxicity, with survival rates within the range of 26.82% to 36.8% during the same exposure and incubation period. Their resilience against the toxic effects of kerosene is underpinned by a suite of resistance mechanisms, encompassing genetic adaptation, enzyme-mediated resistance, efflux pumps, biofilm metabolic activity, and outer membrane structural attributes (Nseabasi and Antai, 2012). Chemotaxis plays a crucial role in the behavior of bacteria, enabling them to navigate toward areas rich in chemicals that serve as valuable nutrients and energy sources. This process also empowers them to exploit resources that would, otherwise, be inaccessible, such as petroleum hydrocarbons. Bacteria are guided in their movement by specific chemical cues known as chemoattractants, while substances that repel them are referred to as chemorepellents (Murphy et al., 2020; Zhao and Ford, 2022). Interestingly, our research uncovered a positive chemotactic response to both hydrocarbons in the entirety of tested strains, suggesting their capability to utilize them as substrates or carbon sources. Intriguingly, bacterial migration towards crude oil surpassed that towards kerosene. Consistent findings demonstrated that *Pseudomonas* strains exhibited a strong attraction to refined petroleum oil. Our study further elucidated the role of bacterial adhesion and biofilm formation in confirming the directed mobility of bacteria towards refined oil (Dutta and Singh, 2016). Indeed, chemotactic microorganisms possess an interesting ability to detect changes in chemical gradients within their environments, leading to specific behavioral responses under the influence of this environmental stress. Based on the results obtained from the BATH analysis, it is evident that the various strains displayed a range of hydrophobic characteristics, fluctuating between being highly hydrophobic to distinctly hydrophilic. To provide a clearer understanding, strains were categorized based on a hydrophobicity index. Those with an index exceeding 80% were considered highly hydrophobic, while those with an index lower than 30% were regarded as strongly hydrophilic, as described by Wang et al. 2019. As per these criteria, our findings revealed that approximately 77.78% of the strains

displayed a marked preference for hydrophobic interactions with crude oil. However, 22.22% of the strains exhibited a pronounced hydrophilic tendency when exposed to crude oil. Shifting the focus to kerosene, around 66.67% of the strains showcased different hydrophobic characteristics while 33.33% of strains manifested a hydrophilic phenotype in the presence of kerosene. Comparing the hydrophobicity of these strains across the two tested hydrocarbons, it was evident that our recovered strains exhibited a particularly intriguing preference for hydrophobic interactions with crude oil. These findings align partially with those described by Priji and colleagues, who observed significant hydrophobicity indices in *Pseudomonas sp.* strains toward crude oil in comparison to kerosene (Pijit et al., 2017). Notably, our results highlighted the exceptional hydrophilicity of the S30 strain, which is consistent with the findings of another study that characterized an environmental strain of *A. hydrophila* as having hydrophilic properties when exposed to hexadecane as a carbon source. In this case, the hydrophobicity indices reported were notably low (Kaczorek et al., 2010). Understanding the hydrophobicity of microbial surfaces is essential, as it plays a crucial role in adhesion to both abiotic and biotic surfaces, as well as in penetrating host tissues. Importantly, the hydrophobic properties of bacteria are integral to various beneficial processes, such as hydrocarbon degradation. Some environmental contaminants, such as toluene, are recognized for their high hydrophobicity and cell membrane-disrupting toxicity. Hydrophobic bacteria possess the ability to accumulate on such compounds and facilitate their degradation (Krasowska and Sigler, 2014). Remarkably, our assessment of the emulsification index unveils a compelling trait shared by a significant proportion of *Pseudomonas sp.* strains, as they exhibit noteworthy emulsifying capabilities when faced with crude oil and kerosene. Notably, the pinnacle of emulsification prowess was observed in *Pseudomonas* strains, with exceptional indices recorded in their interactions with diesel, kerosene, and motor oil, as elucidated by Viramontes-Ramos et al. 2010. Furthermore, our results reveal that *A. hydrophila* boasts substantial emulsification potential, particularly when confronted with crude oil. The emulsification activity of *A. hydrophila*, reaching an impressive 57.63%, surpassed that of *Acinetobacillus sp.* and *Vibrio parahaemolyticus* in the context of kerosene, as documented by Adetitun et al. in 2016. The analysis of statistical data has demonstrated a fascinating relationship, intricately tied to emulsification activity and chemotaxis towards both hydrocarbons. This is closely followed by the bacterial cell surface's hydrophobic characteristics. Notably, a robust correlation was observed between chemotaxis and hydrophobicity traits. However, The emulsification potential remained largely unaltered by other variables. The combined attributes of chemotaxis, cell surface hydrophobicity, and emulsification potential within these marine strains play a pivotal role in their resilience, capacity to adapt to hydrocarbon-induced stress, and ability to utilize these compounds as sources of energy and carbon. These findings hint at the potential of these strains to ameliorate water quality in sites contaminated by hydrocarbon contamination.

5. Conclusion

The behaviorome profiling of indigenous marine bacteria has yielded intriguing results in relation to the studied hydrocarbons. A pivotal discovery lies in their remarkable ability to form biofilms, enabling them to effectively combat hydrocarbon-induced stress. These bacterial strains have also exhibited substantial halotolerance, a crucial trait for survival in their marine habitat. Additionally, chemotaxis, a social behavior among these bacteria, has been emphasized. Notably, these marine strains exhibit an intriguing hydrophobicity and possess significant emulsifying potential, indicative of their significant capability in addressing hydrocarbon-related challenges. This emulsifying activity is intricately linked to the production of biomolecules, which serve as highly effective bioemulsifiers for hydrocarbons.

This study presents several noteworthy limitations, with one of the most significant concerns revolving around potential interactions between hydrophobicity and various surface properties. These interactions encompass factors like surface tension, the application of techniques such as PCR for molecular strain identification and HPLC for bioemulsifier detection, along with considerations related to their environmental relevance. From a broader perspective, the study explores the potential of these strains to produce valuable biomolecules for various biotechnological applications. The purification and molecular characterization of these metabolites will be facilitated through the use of analytical tools, including gel filtration chromatography and HPLC. Furthermore, the identification of robust producer strains will be accomplished by delving into their S16 rRNA profiles. In sum, these findings offer substantial support for the viability of employing these strains to promote the principles of sustainable development, particularly in scenarios marked by water contamination with hydrocarbons.

6. Conflicts of interest

The authors declare no conflict of interest

Acknowledgement

This study was supported by the Algerian Ministry of Higher Education and Scientific Research (MESRS), General Directorate for Scientific Research and Technological Development (DGRSTD).

References

- Adetitun, D.O., Awoyemi, O.D., Adebisi, O.O., Kolawole, O.M., and Olayemi AB. (2016). Biodegradative activities of some Gram-negative bacilli isolated from kerosene treated soil grown with cowpea (*Vigna unguiculata*). *Agrosearch*, 16(1): 41-57.
- AlKaabi, N., Al-Ghouti, M., Jaoua, S., and Zouari, N. (2020). Potential for native hydrocarbons-degrading bacteria to remediate highly weathered oil-polluted soils in Qatar through sel-purification and bioaugmentation in biopiles. *Biotechnology Reports*, 28(2020): 1-10.
- Bensari, B., Bahbah, L., Lounaoui, A., Fahci, S., Bouda, A., and Bachari, N. (2020). First record of non-indigenous species in port of Arzew (Algerian Southwestern Mediterranean). *Mediterranean Marine Science*, 21(2): 393-399.
- Borah, D., Agarwal, K., Khataniar, A., Konwar, D., Gogoi, S.B., and Kallel, M. (2019). A newly strains of *Serratia sp.* from an oil spillage site of Assam shows excellent bioremediation potential. *3 Biotech*, 9(7):1-12.
- Celik, G.Y., Aslim, B., and Benyatli, Y. (2008). Characterization and production of the exopolysaccharides (EPS) from *Pseudomonas aeruginosa* G1 and *Pseudomonas putida* G12 strains. *Carbohydrate Polymers*, 73(1):178-182.
- Chao, Y., Guo, F., Frang, H.H.P., and Zhang, T. (2014). Hydrophobicity of diverse bacterial populations in activated sludge and biofilm revealed by microbial adhesion to hydrocarbons assay and high-throughput sequencing. *Colloids and Surfaces B: Biointerfaces*, 114(1): 379-385.
- Chiciudean, I., Mereuta, I., Ionescu, R., Vassu, T., Tanase, A., and Stoican, I. (2019). Jet A-1 bacterial contamination: a case study of cultivable bacteria diversity, alkane degradation and biofilm formation. *Polish Journal of Environmental Studies*, 28(6): 4139-4146.
- Conrad, C.J. (2020). Biophysical methods to quantify bacterial behaviors at oil-water interfaces. *Journal of Industrial Microbiology and Biotechnology*, 47(9-10): 725-738.
- Cooper, D.G., and Goldenberg B.G. (1987). Surface-active agents from two *Bacillus*. *Applied and Environmental Microbiology*, 53(2): 224-229.
- Dasgupta, D., Ghosh, R., Sengupta, T. (2013). Biofilm-mediated enhanced crude oil degradation by newly isolated *Pseudomonas* species. *ISRN Biotechnology*, 250749(2013): 1-13
- de Oliveira, E.S.D., Pereira, R.F., Lima, M.A.G.A., and Filho, S.L.U.F. (2021). Study on Biofilm Forming Microorganisms Associated with the Biocorrosion of X80 Pipeline Steel in Produced Water from Oilfield. *Journal of Materials Research*, 24(6): 1-10.
- Diaz, M., Ladero, V., del Rio, B., Redruella, B., Fernandez, M., Martin, M.C., and Alvarez, MA. (2016). Biofilm-forming capacity in biogenic amine-producing bacteria isolated from dairy products. *Frontiers in Microbiology*, 7(591): 1-10.
- Dutta, S., and Singh, P. (2016). Chemotaxis of biofilm producing *Pseudomonas spp.* towards refined petroleum oil. *Journal of Scientific Research*, 8(2): 199-207.
- Elumalai, P., Parthipan, P., AlSalhi, M.S., Huang, M., Devanesan, S., Karthikeyan, O.P., Kim, W., and Rajasekar A. (2021). Characterization of crude oil degrading bacterial communities and their impact on biofilm formation. *Environmental Pollution*, 286 (2021): 1-10.
- Fuhrman, J.A., Cram, J.A., and Needham, D.M. (2015). Marine microbial community dynamics and their ecological interpretation. *Nature Reviews*, 13(3):133-146.
- Gong, H., Li, Y., Bao, M., Lv, D., and Wang, Z. (2015). Petroleum hydrocarbon degrading bacteria associated with chitosan as effective particle-stabilizers for oil emulsification. *RSC Advances*, 5(47): 37640-37647.
- Gordillo, F., Chavez, F.P., and Jerez, C.A. (2007). Motility and chemotaxis of *Pseudomonas sp.* B4 towards polychlorobiphenyls and chlorobenzoates. *FEMS Microbiology Ecology*, 60(2): 322-328.
- Jahid, I.K., Mizan, M.D.F.R., Ha A.J., and Ha S. (2015). Effect of salinity and incubation time of planktonic cells on biofilm formation, motility, exoprotease production, and quorum sensing of *Aeromonas hydrophila*. *Food Microbiology*, 49(2015): 142-151.
- Jégousse, C., Vannier, P., Groben, R., Guomundsson, K., and Marteinsson, T.V. (2022). Marine microbial communities of north and south Shelves of Iceland. *Frontiers in Marine Science*, 9(2022): 1-13.
- Kaczorek, E., Imarhiagbe, E., and Obayagbona N. (2019). Polycyclic Aromatic Hydrocarbon, Physio-Chemical Properties, and Culturable Microbial Flora of Human Urine-Impacted Topsoils at Commercial Tricycle Parks Along Benin-Sapele Expressway, Benin City, Nigeria. *Jordan Journal of Earth and Environmental Sciences*. 10 (3): 167-172

- Krasowska, A., and Sigler, K. (2014). How microorganisms use hydrophobicity and what does this mean for human needs?. *Frontiers in Cellular and Infection Microbiology*, 4(112): 1-7.
- Krohn, I., Bergmann, L., Qi, M., Indenbirken, D., Han, Y., Perez-Garcia, P., Katzowitzsch, E., Hägele, B., Lübcke, T., Siry, C., Riemann, R., Alawi, M., and Streit, W.R. (2021). Deep (Meta) genomics and (Meta) transcriptome Analyses of Fungal and Bacteria Consortia from Aircraft Tanks and Kerosene Identify Key Genes in Fuel and Tank Corrosion. *Frontiers in Microbiology*, 12: 1-14.
- Liang, K., Gao, R., Wang, C., Wang, W., and Yan, W. (2021). Chemotaxis towards crude oil by an oil-degrading *Pseudomonas aeruginosa* 6-1B strain. *Polish Journal of Microbiology*, 70(1): 69-78.
- Lozada, M., Maros, M.S., Commendatore, M.G., Gil, M.N., and Dionisi, H.M. (2014). Structure of the bacterial community of marine environments polluted by hydrocarbons as a basis for the definition of an ecological index of exposure to hydrocarbons. *Microbes & Environment*, 29(3): 269-276.
- May, H.C., Yu, J., Shrihari, S., Seshu, J., Klose, K.E., Cap, A.P., Chambers, J.P., Guentzel, M.N., and Arulanandam, B.P. (2019). Thioredoxin modulates cell surface hydrophobicity in *Acintiothacter baumannii*. *Frontiers in Microbiology*, 10(2019): 1-9.
- Meliani, A., and Bensoltane, A. (2014). Enhancement of Hydrocarbons Degradation by Use of *Pseudomonas* Biosurfactants and Biofilms. *Journal of Petroleum and Environmental Biotechnology*, 5 (1): 1-7.
- Mercy, A., Eseosa, I., and Frederick, E. (2019). Total Petroleum Hydrocarbon and Heavy Metal Reduction: A Case Study of Enhanced Degradation Potential of Animal Waste by Fungal Isolates. *Jordan Journal of Earth and Environmental Sciences*. 10 (1): 21-27.
- Murphy, A.W.M., Davis, G.B., Rayner, J.L., Walsh, T., Bastow, T.P., Butler, A.P., Puzon, G.J., and Morgan, M.J. (2022). The role of predicted chemotactic and hydrocarbon degrading taxa in natural source zone depletion at a legacy petroleum hydrocarbon site. *Journal of Hazardous Material*, 430(2020):1-12.
- Nimnoi, P., and Pongsilp, N. (2020). Marine bacterial communities in the upper gulf of Thailand assessed by illumine next-generation sequencing platform. *BMC Microbiology*, 20 (19): 1-11.
- Nseabasi, N.O., and Antai, S.P. (2012). Toxic effect of kerosene contamination on the survival of bacterial and fungal species in soil from Niger Delta, Southern Nigeria. *International Research Journal of Microbiology*, 3(12): 382-387.
- Olalemi, A., Arotupin, D., Ojuolape, O., Ogunmolu, F. (2021). Assessment of Microorganisms Isolated from Steeping Maize (*Zea mays* L.) and Sorghum (*Sorghum bicolor* L.) on the Hydrolysis of some Hydrocarbon Products. *Jordan Journal of Earth Environmental Sciences*. 12 (1): 44-49
- Perdigão, R., Almeida, M.R., Magalhaers, C., Ramos, S., Caralas, A.L., Ferreira, B.S., Carvalho, M.F., and Mucha, AP. (2021). Bioremediation of Petroleum Hydrocarbons in Seawater: Prospects of Using Lyophilized Native Hydrocarbon-degrading bacteria. *Microorganisms*, 9 (11): 1-19.
- Pijit, P., Sreedharan, S., Unni, K.N., Anderson, R.C., and Benjamin, S. (2017). *Pseudomonas* sp. BUP6, a novel isolate from malabari goat produces an efficient rhamnolipid type biosurfactant. *Journal of Basic Microbiology*, 57(1): 21-33.
- Qurashi, A.W., and Sabri, A.N. (2012). Bacterial exopolysaccharides and biofilm formation stimulate chickpea growth and soil aggregation under salt stress. *Brazilian Journal of Microbiology*. 43 (3): 1183-1191.
- Rosenberg, M., Gutnick, D., and Rosenberg, E. (1980). Adherence of bacteria to hydrocarbons: A simple method for measuring surface hydrophobicity. *FEMS Microbiology Letters*. 9(1): 29-33.
- Shahaliyan, F., Safafieh, A., and Abyar, H. (2015). Evaluation of Emulsification Index in marine bacteria *Pseudomonas* sp. and *Bacillus* sp. *Arabian Journal for Science and Engineering*, 40(7): 1-7.
- Shu, L., Zhang, B., Queller, D., and Strassmann, E.J. (2018). *Burkholderia* bacteria use chemotaxis to find social amoeba *Dictyostelium discoideum* hosts. *ISME*. 12(8): 1977-1993.
- Stephanovic, S., Vukovic, D., Hola, V., Bonaventura, G.D., Djukic, S., Cirkovic, I., and Ruzicka, F. (2007). Quantification of biofilm in microtiter plates: overview of testing conditions and practical recommendations for assessment of biofilm production by staphylococci. *Acta Pathologica et Microbiologica Scandinavica*, 115(8): 891-899.
- Urbanowics, M., and Olszanowski, A. (2010). The influence of surfactants on cell surface properties of *Aeromonas hydrophila* during diesel oil biodegradation. *Colloids and Surfaces B: Biointerfaces*, 81(1): 363-398.
- Viramontes-Ramos, S., Portillo-Ruiz, M.C., and Nevarez-Moorillon, G.V. (2010). Selection of biosurfactant/bioemulsifier producing bacteria from hydrocarbon-contaminated soil. *Brazilian Journal of Microbiology*, 41(3): 668-675.
- Wang, D., Lin, J., Lin, J., Wang, W., and Li, S. (2019). Biodegradation of petroleum hydrocarbons by *Bacillus subtilis* BL-27, a strain with weak hydrophobicity. *Molecules*, 24(17):1-15.
- Wang, Y., Huang, Z., Zhou, N., Liu, C., Jiang, C., Li, D., and Liu S. (2022). The response regulator FlmD regulates biofilm formation in *Camamonas testosteroni* through the transcriptional activator SoxR. *Microorganisms*, 10(2): 1-16.
- Wijesinghe, G., Dilhari, A., Gayani, B., Kottegoda, N., Samaranyake, L., and Weerasekera, M. (2019). Influence of laboratory culture media on in vitro growth, adhesion, and biofilm formation of *Pseudomonas aeruginosa* and *Staphylococcus aureus*. *Medical Principles Practice*, 28 (1): 28-35.
- Yin, W., Wang, Y., Liu, L., and He, J. (2019). Biofilms: the "protective clothing" in extreme environments. *International Journal of Molecular Sciences*, 20(14): 1-18.
- Zhao, X., and Ford, R.M. (2022). Marine Bacteria Chemotaxis to Crude Oil Components with Opposing Effects. *BioRxiv*. 10(2022): 1-26.

Assessment of Rainwater Harvesting Management in Jordan

Kamel K. Al-Zboon^{1*}, Obada A. Mansi¹ and Bashaar Y. Ammary¹

Environmental Engineering Department, Al-Balqa' Applied University, P.O. Box 50, 21510 Al-Huson, Jordan

Received Dec. 28, 2023; Accepted March 22nd, 2024

Abstract

Rainwater harvesting (RWH) has the potential to provide a sustainable solution to the problem of water scarcity. Therefore, this study aims to assess the management of (RWH) by distributing a questionnaire to householders in the northern region of Jordan. The questionnaire covered all the parameters that have an impact on water use, management, and quality of RWH. The results of the statistical analysis showed that 25.5% of the cisterns were constructed in the last 15-30 years. About (60.2%) of cisterns were made of concrete, and 46.6% of them have capacities between 30-50 m³. The largest percentage of these cisterns (43.7%) are used for all purposes, including drinking, while 23.3%, 18.45%, and 10.7% are used for irrigation, washing, and cooking, respectively. HRW is mainly collected from rooftops (72.8%) while 25.2% is collected from home yards. Regarding the surrounding environment, 62.1% of the houses have no sanitary system and depend on cesspools for sewage disposal, and 8.7% have an animal barn near the cistern. Roof cleaning before the rainy season was implemented by 84.5% of the households, while 12.6% reported complaints due to water quality. 4.9% of them visited the hospital. About 24.3% visually inspected water quality, and 3.9%, 4.9%, and 2.9% of them reported abnormal pain, change of water taste, and presence of impurities in water, respectively. It is recommended to establish public awareness programs to enhance RWH management. The program should outline the best practices to collect and store rainwater and to take appropriate corrective measures to get high water quality for drinking purposes.

© 2024 Jordan Journal of Earth and Environmental Sciences. All rights reserved

Keywords: Rainwater Harvesting, Water management, Jordan, Water Quality, Health Risk.

1. Introduction

In Jordan, the annual available renewable water resources are less than 100 m³/c, which is significantly below the threshold limit of 500 cubic meters. It is classified as "absolute water scarcity (Kharabshah and Alzboon, 2021). Until 2100, water stress levels are projected to increase at an average annual rate of 1.1%–1.4 %, exposing more than 90% of Jordan's low-income households to a critical water vulnerability (UNICEF, 2022).

In spite of Jordan, receiving low precipitation, rainwater is the key parameter in Jordan water budget. About 77% of the area receives less than 100 mm of rainfall, 90% of the area receives < 200 mm, and only 1.05% receives more than 500mm (Tabieh and Al-Horani, 2010.). The total average precipitation in Jordan is approximately 8.5 billion/year. However, 93 percent of this amount is lost due to evaporation (Barjenbruch and Alzboon, 2010). It was reported that the available water from all resources in Jordan is 1,034 million cubic meters per year (MCM/y), of which 886 MCM/y are renewable water resources while the remaining is nonrenewable. In contrast, the total demand of all sectors in Jordan is about 1,442 MCM/y, which indicates a deficit value of 408 MCM/y, representing 28.3% of the total demand and 46.05% of the total RWR for the year 2018 (Al Qatarneh and Al-Zboon, 2022, Alzboon et al., 2021). High water pressure makes Jordan among the most water-stressed countries and poses a significant environmental, social, and economic load on the country's development plans. The Jordanian government has long been under permanent pressure to find

a long-term solution to the country's water problems. There are many options to bridge the gap between resources and demand, including water desalination, water reuse, better management, and water harvesting (Al Tabbal Jalal, et al., 2019).

Rainwater harvesting is a comprehensive process, which includes collecting, storage, and conservation of precipitation from the surface to be used later for drinking, irrigation, and domestic uses. The rainwater harvesting system depends on three components. The catchments area, in which tiled cement roofs are the most common in Jordan. The second component is the conveyance system, which includes the pipes or gutters that transport water to the storage facility, and the storage facility (wells or storage tanks (Abdulla and Al-Shareef, 2009). Rainwater harvesting (RWH) is a widely used technique for collecting and storing rainwater that falls on a catchment area and is connected directly to a cistern or well for future use (Kloss, 2008).

RWH is an ancient practice of collecting and storing rainwater from roofs and other surfaces. Perhaps one of the most effective methods currently applied in the world to conserve water resources is the application of various water harvesting techniques. This is because it has a clear positive impact in conserving large quantities of water through collecting, storing, and using it promptly for various purposes, instead of wasting it.

When the harvested rainwater is used domestically, its quality comes first. Many factors affect the quality of RWH.

* Corresponding author e-mail: kalzboon@yahoo.com

These factors include the environment, such as how close it is to heavy industry or main roads, as well as whether or not there are birds or rodents (Förster, 1998; Taylor et al. 2000). Temperatures, past dry periods, and rainfall patterns are examples of meteorological conditions that also affect the quality of rainwater harvesting (Simmons et al. 2001; Van Metre and Mahler, 2003).

Rainwater harvesting has long been used in Jordan to provide water for domestic and agricultural use. Several historical examples of effective water harvesting systems still exist in the country, i.e., the Nabatean city of Petra's cut-stone reservoirs, underground cisterns, and traditional village houses, etc. (Abdulla and Al-Shareef, 2009). About 81 % of rainwater harvesting wells are located in Irbid governorate, where rainwater harvesting is widely practiced. Approximately 34% of collected rainwater is used for drinking and cooking, while the remaining is used for watering gardens, cleaning indoor and outdoor spaces, and flushing toilets (DOS, 2004).

According to Almur (2016), adopting RWH systems has several advantages, including increasing water supply and providing safe, clean, and dependable drinking water, in addition to decreasing soil erosion and flooding. Furthermore, this technology is less expensive and environmentally a good choice for governments, especially when given the rising cost of water.

The main disadvantage of this system is that the supply is limited by the amount of rainfall and the size of the catchment area and wells. Therefore, it is not a dependable water source in dry weather and prolonged drought. Another disadvantage is the associated health risks. When a well is not properly sealed, it can become a mosquito breeding ground, and rainwater can become contaminated by air pollution, animal or bird droppings, insects, dirt, and organic matter, which may pose health risks. (Worm and Hattum, 2006).

Radaideh et al. (2009) conducted a study that aimed to assess the suitability of rainwater for domestic use, and the results showed that the water quality of these cisterns varies depending on their catchment area, location, and the availability of public sewer systems. The study found that the average concentrations of Fecal Coliform (FC), Total Coliform (TC), and *Escherichia coli* (*E. Coli*) in samples obtained from rooftop catchments were 2.4, 6.3, and 2.1 MPN/100ml, respectively. In contrast, the average concentrations in the samples collected from storage tanks with land catchments were 11.1, 24.6, and 5.2 MPN/100 ml, respectively. They concluded that RWH is unfit for drinking purposes, but it could be used for garden irrigation in residential areas.

Shubo et al. (2022) evaluated the quality of rainwater harvesting for a year, observing several microbiological parameters such as (*E. coli*), total coliforms, human JC polyomavirus (JCPyV), and human adenovirus (HAdV), Group A rotavirus (RVA), and norovirus GII and GI. They reported the presence of total coliform in 44 samples (91.7%), *E. coli* was detected in 28 samples (58.2%), and HAdV and JCPyV were present in 10 samples (20.8%) and 6 samples (12 %), respectively. HAdV viral values ranged from 102 to 103 (GC/L), while JCPyV viral values ranged from 101

to 104. The samples contained no RVA, Norovirus GI, or GII. According to FIB, 15 of 16 samples (94%) contained compatible viruses.

Harvested rainwater was studied for microbial contamination by Chubaka et al. (2018). The analysis of 53 rainwater tanks from the Adelaide region was performed, using the Colilert TM IDEXX Quanti-Tray*/2000. The results showed that there is a relationship between the presence of television antennas in the rainwater harvesting area and the abundance of *E. coli*. On the other hand, neither seasonality nor the materials used in the roofs or tanks had any effect on the prevalence of *E. coli*. There was *E. coli* present in 28 out of the 53 tanks, and the levels in 10 samples were above the recommended recreational limit of 150 MPN/100 ml. Regarding the benefits of treatment, the results showed that a 0.45 µm filter cartridge was able to effectively remove all detectable levels of *E. coli*, down to 0 MPN/100 ml.

Al-Houri and Al-Omari (2022) evaluated the current status of RWH practices and public opinion in Ajloun governorate/Jordan. A structured questionnaire was prepared and distributed to randomly selected residents. It was reported that the amount of water that could be harvested in the dry year (2017) was about 0.40 (MCM), compared to a wet year with a volume of 0.97 MCM (2018). The results showed that rooftop rainwater harvesting in Ajloun governorate can provide 7.6% in the dry year and 16.8% in the wet year of the total water used for domestic purposes. Also, it was found that 14.2% of the households are currently practicing rooftop rainwater harvesting. Due to the high one-time investment required for the construction of RWH systems, almost all people (96.7%) agreed that the government should help in covering the cost of the system.

The present study aims to identify RWH management in the northern region of Jordan by distributing a questionnaire and interviews with 103 householders in the rural areas. The prepared questionnaire covers the type of catchment area, storage characteristics, water uses, the surrounding environment, water treatment, and complaints about water quality. The outcomes of this research will help in better improving the management of RWH and are expected to enhance public awareness about the importance of RWH which subsequently will provide a significant safe renewable source of water.

2. Methodology

2.1 Study area

Irbid Governorate is located in the northern part of Jordan, as shown in Figure 1. The Governorate covers a total area of approximately 1572 km² and lies on the geographical coordinates between 32° 45' 48" and 35° 33' 21" N and 32° 14' 11" and 36° 4' 36" E. It is bordered on the north by the Syrian Arab Republic, on the west by Palestine, on the east by the Mafraq governorate, and on the south by the governorates of Al-Balqa, Ajloun, and Jerash governorates. The governorate is divided into nine subregions: AL-Kasbah, AL-Ramtha, AL-Koora, Bani Kinanah, Bani Obaid, Northern Shuna, the Northern Mazar, the AL-Wastiyah, and the AL-Taibah (DOS, 2017).

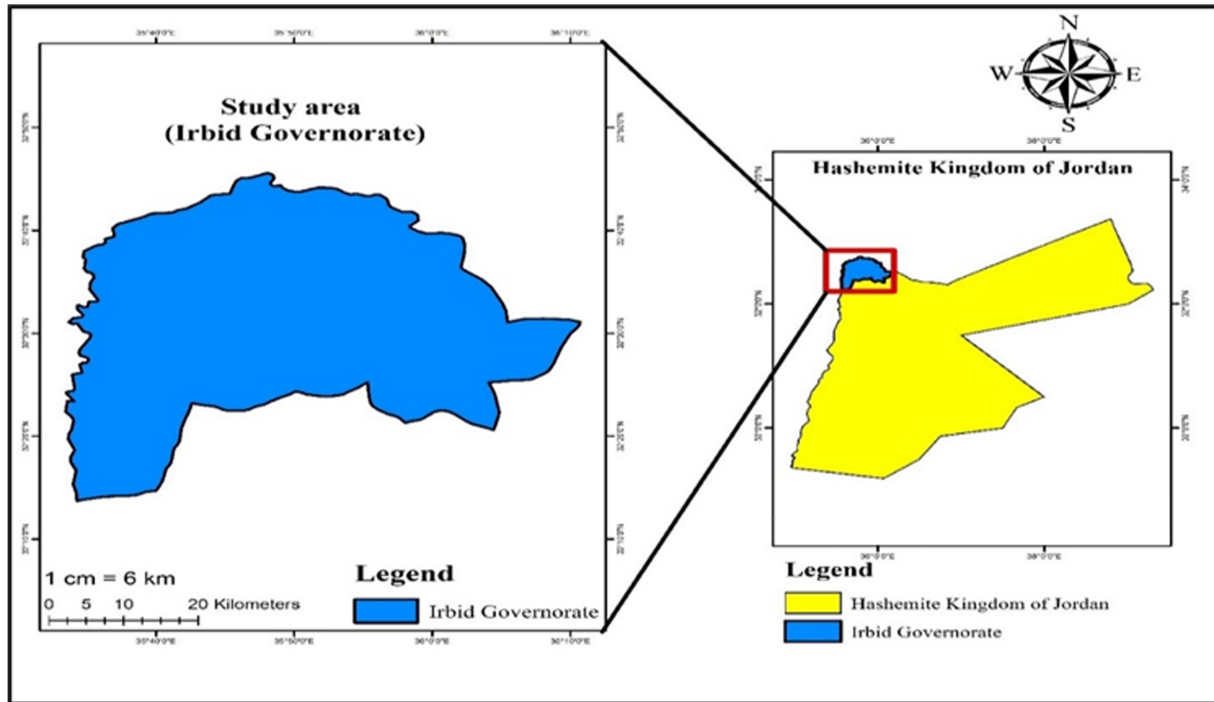


Figure 1. The Study area location.

2.2 Climate

Irbid climate, like the rest of the Levant, is a Mediterranean climate, with hot, dry summers and cold, rainy winters. In summer, temperatures reach around 35 °C, while in winter, temperatures drop to around 5 °C and may drop to zero °C, and snow rarely falls. Green grass grows, and flowers spread in the spring, especially in valleys and plains (JMD, 2022). In Irbid Governorate, the average annual precipitation ranges from 488 mm over the mountains in the west and southwest to 157 mm in the flat terrain in the east. The potential evaporation in the region ranges from 2,000 to 2,400 mm per year (Al Azzam and Al Kuisi, 2021). Figure 2 shows the cumulative rainfall of four stations in Irbid Governorate for the years 2015-2021 (JMD, 2022).

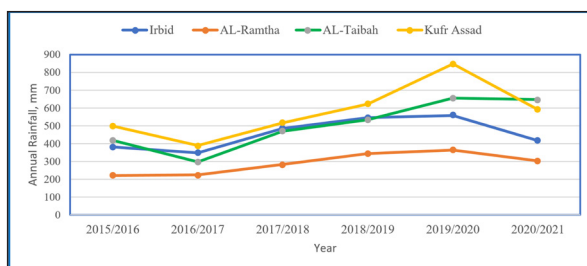


Figure 2. Cumulative rainfall period in Irbid Governorate, 2015-2021.

2.3. Materials and Method

A questionnaire was designed to assess the applied management of water harvesting in the study area. In the first round, approximately 20 questionnaires were distributed to the owners of the cisterns as a trial. This was performed to detect any weaknesses or gaps in the questionnaire. Also, the trial round would be beneficial to determine the problems that can be encountered during data collection. After that, 103 questionnaires were distributed to the targeted group of cistern owners. Yes/No questions and multiple-choice questions have

been used. Personal interviews with water specialists were conducted to ensure that the questionnaire covers the required data adequately.

The questionnaire consists of three parts:

- The first part is related to demographic information, including age, education, and number of family members.
- The second part consists of questions regarding the characteristics of rainwater collection sites and a description of the surrounding environment.
- The final part comprises questions about water quality and practices related to monitoring, cleaning, complaints, and health risks.

2.4 Statistical Analysis

After the field survey, the data obtained from the answers to the questionnaires had been tabulated and analyzed using the Statistical Package for Social Sciences (SPSS) program to determine the internal interactions between the different variables that affect the rainwater harvesting management.

3. Result and Discussions

The purpose of this study was to investigate the management practices of rainwater collection from rooftops and home yards in Irbid Governorate. It also examined the characteristics of the collected rainwater, the description of the surrounding environment, and the level of residents' awareness of the factors that impact the quality of the collected rainwater.

3.1 Characteristics of the cisterns

To investigate the characteristics of the rainwater harvesting sites and to describe the surrounding environment, a descriptive statistical analysis was conducted, and the results are shown in Table 1. It was found that most of the cisterns (43.7%) have been built during the last 15 years.

This indicates the increase in population awareness of the importance of water harvesting. This may also be seen as result of the governmental programs and public awareness which encouraged residents to build water cisterns. Climate change, combined with water scarcity may be the driving force for more attention to water harvesting.

It was found that about 83.5% of the cisterns have capacities of less than 50 m³. The larger capacity means a higher cost of construction, which may explain the smaller size of cisterns in the study area, especially for low-income households. According to the long-term metrological data, the average precipitation in the study area ranged between 221-621 mm/y, and only 60% can be harvested (0.132-0.372 m³/m² of the rooftop area), so most of the cisterns are not filled during dry seasons.

As for well construction, there are mainly two methods of cisterns construction. The first is constructed using a capsulated box of reinforced concrete either underground or above ground surface. The second type is a pear-shaped cistern that is usually excavated in rocky soils. While concrete type can be built in most types of soil, rock-cut type is excavated in rocky soil. The concrete type is more costly, but it is more popular due to its reliability, durability, and it is easier to clean. This explains why 60.2% of the householders prefer concrete cisterns. Even though the rock-cut type has lower cost than the concrete type, some households are reluctant to use them due to potential leakages, which explain their limited use.

Regarding the catchment area, more than 72% of the households are relying on rooftops as a source of rainwater, while 25.2% depend on home yards. Previously, there were wide non-constructed areas which were used for rainwater harvesting. Nowadays, most of the urbanized areas are covered with houses and buildings. This population density explains the higher percentage of using rooftops as a source of rainfall water. Also, the collection of rainwater from rooftops is easier and no additional investment is required.

Table 1. Characteristics of the cisterns.

Category		Percent, %
The age of the cistern, year	(1-15)	43.7
	(15-30)	25.2
	> 30	31.1
Well capacity, m ³	< 30	36.9
	(30-50)	46.6
	> 50	16.5
Well type	Concrete	60.2
	(pear-shaped well)	37.9
	Tanks	1.9
Catchment area	rooftop	72.8
	home yard	25.2
	other	1.9

3.2 Sources of water inside the well

The results of the questionnaire analysis showed that 58% of the study population use collection wells to harvest rainwater separately. Meanwhile, 14.6% reported that they

depended only on municipal water to fill the cistern. The rest (25.2%) resorted to filling the cistern with both municipal and rainwater. When the rainy season ends, the owners might use cistern for storage of municipal water and tankers which might be used in case of insufficient supply of municipal water. About (68.9%) of the study population pump water from the cisterns to the rooftop tanks and, then, use it, while the rest pump it directly to the indicated purpose.

3.3 Harvested rainwater uses

The results of the field survey revealed that 43.7% of the cisterns' owners use the water for all purposes including drinking. while 23.3%, 18.45%, and 10.7% of households use water for irrigation, washing, and cooking, respectively as shown in Table 2. Most people, especially in rural areas, strongly believe that rainwater is clean and suitable for all purposes. In contrast, some people, mainly in the cities, consider that rainwater can only be used for irrigation, cooking, and washing but not suitable for drinking.

Table 2. Uses of RWH.

Sources of cistern water	Frequency	Percent, %
Rainwater	60	58.3
municipal water	15	14.6
Rainwater + municipal water	26	25.2
Other	2	1.9
Total	103	100.0

3.4 Description of the surrounding environment

To determine the relationship between water quality and the surrounding environment, a descriptive analysis was carried out for the considered samples. The results of the questionnaire in Table 3 showed there were trees near 55.3% of the cisterns, and most of these trees were olives (45.6%), citruses (26.3%), and other types (28.1%). The roots of the trees may penetrate the cistern walls and cause water leakage from the cistern or contamination of water by organic and other contaminants. Also, the presence of trees may become an attractive habitat for birds which may increase the contamination of water by animal waste. Additionally, harvested water may become contaminated by the leaves of trees, applied fertilizers, and pesticides.

A conducted research revealed that just 8.7% of households owned pet animals, including chickens and rabbits, within their backyards. On the other hand, 13.6% of households reported that their neighbors owned such pets. The practice of keeping pets in backyards may result in the contamination of water due to animal waste.

The field survey found that there are floating materials in 51.5% of the cisterns, and there is a significant correlation between the presence of trees and the floating materials in water (P <0.05).

Table 3. Characteristics of the surrounding environment.

Parameter			Count	Percent, %	
Are there trees near the well.	Yes	If there are trees nearby, mention their type	Olive trees	26	45.6%
			citrus trees	15	26.3%
			Other	16	28.1%
	No		I do not have	46	100.0%
Do you raise pets or animals near the well?	Yes		9	8.7%	
	No		94	91.3%	
Do the neighbors raise animals near the well?	Yes		14	13.6%	
	No		89	86.4%	
The presence of waste	Yes		20	19.4%	
	No		83	80.6%	
Do you notice floating impurities	Yes		53	51.5%	
	No		50	48.5%	

3.5 Complaints about water quality

According to the results, a small percentage of respondents (12.6%) reported that someone in their family had complained about the water, with only (4.9%), reporting a visit to the hospital due to these complaints. The most commonly reported complaints were a change in the taste of the water (4.9%), abdominal pain (3.9%), and the presence of impurities (2.9%).

3.6 Awareness of water quality

Public awareness of water quality depends on many socioeconomic parameters including education, awareness programs, income, uses of RWH, and the surrounding environment. About 84.5% of respondents reported cleaning the roof of their house before the rainy season, suggesting that this is a common practice among the study population. During the dry season, the roof may be contaminated due to

air pollution, dust, birds, and other sources. For this reason, it is necessary to clean the roof before the rainy season starts to ensure getting clean RWH. Most households (66.0%) clean the cistern and get rid of the remaining water for irrigation, of which 47.6% clean the cistern annually while 54.4% clean it biannually. A small percentage (24.3%) of the owners conducted a visual inspection of water quality inside the cistern while 75.7% didn't check. The results also showed that only 26.2% of the owners added chlorine to the cistern to control the biological growth. Based on the field survey, the identified sources of contaminants are the presence of trees and waste near the cistern, raising of animals and the cleanliness of the rooftop and the cistern. These results indicated that most people are aware of cleaning the rooftop and the cisterns while most of them are not aware of the continuous monitoring of water quality, sources of contamination, and the necessity of disinfection.

Table 4. Some indicators of public awareness.

Parameter	Answer	Percent, %
The presence of waste near the cistern	Yes	19.4%
	No	80.6%
Clean the well and get rid of the remaining water	Yes	66.0%
	No	34.0%
Is the roof of the house cleaned before the rainy season?	Yes	84.5%
	No	15.5%
Do you notice floating impurities?	Yes	51.5%
	No	48.5%
Have you ever done checks for the water quality of the well?	Yes	24.3%
	No	75.7%
Do you raise pets or animals near the well?	Yes	8.7%
	No	91.3%
Add chlorine and other materials	Yes	26.2%
	No	73.8%

4. Conclusion

Rainwater harvesting represents an attractive option to bridge the gap between supply and demand in Jordan and one of the key elements in climate change control. This study attempted to shed light on rainwater harvesting from rooftops and yards and collecting it in cisterns. A questionnaire was

distributed for the owners of the cistern to assess harvested water management in the study area.

The statistical package for the social sciences (SPSS) program was used for statistical analyses. Based on the obtained results and the field survey, the following points can

be concluded:

1. Water harvesting represents a significant source of water in the study area.
2. Most of householders are interested in water harvesting, but some do not apply that due to financial constraints.
3. The presence of trees in the household yard and raising animals have significant impact on water quality.
4. Most of the owners clean the rooftop before the first rainwater splashes.
5. It is necessary to conduct a national public awareness program for management of water harvesting including emphasizing the importance of RWH, the quality of RWH, and the best practices that should be taken by households.

Acknowledgment

I am grateful to the Deanship of Scientific Research at Al-Balqa Applied University for the support provided during this research program.

Conflicts of interest

The authors declare no conflict of interest

References

- Abdulla, F. A., and Al-Shareef, A. W. (2009). Roof rainwater harvesting systems for household water supply in Jordan. *Desalination*, 243(1–3): 195–207.
- Al-Houri, Z., and Al-Omari, A. (2022). Assessment of rooftop rainwater harvesting in Ajloun, Jordan. *Journal of Water Reuse and Desalination*, 12(1): 22–32.
- Al Azzam, N., and Al Kuisi, M. (2021). Determination of Flash Floods Hazards and Risks for Irbid Governorates Using Hydrological and Hydraulic Modelling. *Jordan Journal of Earth and Environmental Sciences*, 12(1): 81–91.
- Almur, S. A. (2016). Assessing Water Quality of Cisterns in Sha'rawiya Area "Tulkarm Governorate" for Drinking Purposes, MSC Theses, An Najah National University.
- Al Qatarneh Ghada, Kamel K. AlZboon, 2022, Water Poverty Index: a Tool for Water Resources Management in Jordan, *Water Air Soil Pollution* (2022) 233:461 <https://doi.org/10.1007/s11270-022-05892-3>.
- Al Tabbal Jalal, Kamel K. Al-Zboon, 2019, The Potential of the Application of Olive Cake and Stone Cutting Waste for Soil Amendment, *Jordan Journal of Earth and Environmental Sciences*, 10(1): 7 – 17.
- Alzboon Kamel K. , La'aly A Al-Samraie, Khalideh Al Rawashdah, (2021), Climate Change Indicators in Jordan: A New Approach Using Area Method, *Jordan Journal of Civil Engineering* 15(1): 142-155.
- Barjenbruch, M., and Alzboon, K. K. (2010). North-The north-south wastewater management: A comparative study for Germany and Jordan. *Green Energy and Technology*, 31: 545–554, Springer.
- Chubaka, C. E., Whiley, H., Edwards, J. W., and Ross, K. E. (2018). Microbiological values of rainwater harvested in Adelaide. *Pathogens*, 7(1): 21.
- DOS. (2004). Department of Statistics Annual Report, Amman, Jordan,.
- DOS. (2017). Estimated Population of the Kingdom by Governorate, Locality, Gender, and Household.
- Förster, J. (1998). The influence of location and season on the concentrations of macroions and organic trace pollutants in

roof runoff. *Water Science and Technology*, 38(10): 83–90.

JMD, Jordan Meteorological Department (2022). The Hashemite Kingdom of Jordan Jordan Meteorological Department. Department of Meteorology. Retrieved January 1, 2022, from <http://jmd.gov.jo/en> (5 July, 2023).

kharabshah Noor, kamel Alzboon, (2021), WW treatment and reuse in Jordan, 10 years of development, *Desalination and water reuse*, 2021(238): 15–27.

Kloss Christopher. (2008). *Managing Wet Weather with Green Infrastructure Municipal Handbook Rainwater Harvesting Policies*, EPA.

Radaidah Jamal, Kamel, A.-Z., Adnan, A.-H., and Rida, A.-A. (2012). Quality Assessment of Harvested Roof Top Rainwater for Domestic Uses, *Jordan Journal of Earth and Environmental Sciences* 6(2):149–155.

Shubo, T., Maranhão, A. G., Ferreira, F. C., de Silva e Mouta Júnior, S., de Pedrosa Macena, L. da G., do Rosário Vaz Morgado, C., ... Miagostovich, M. P. (2022). Microbiological characterization of stormwater in a high-income neighborhood in Rio de Janeiro, Brazil. *Environmental Monitoring and Assessment* 2022 194:2, 194(2): 1–16.

Simmons, G., Hope, V., Lewis, G., Whitmore, J., and Gao, W. (2001). Contamination of potable roof-collected rainwater in Auckland, New Zealand. *Water Research*, 35(6), 1518–1524.

Taylor, R., Sloan, D., Cooper, T., Morton, B., and Hunter, I. (2000). A waterborne outbreak of Salmonella Saintpaul. *Communicable Diseases Intelligence*, 24(11): 336–339.

Tabieh Mohammad A.S. and Ala'a Al-Horani, (2010), An Economic Analysis of Water Status in Jordan. *Journal of Applied Sciences*, 10: 1695-1704.

UNICEF, J. and E. I. (2022). Tapped out: The costs of water stress in Jordan, available: <https://www.unicef.org/jordan/costs-water-crisis-jordan>.

Van Metre, P. C., and Mahler, B. J. (2003). The contribution of particles washed from rooftops to contaminant loading to urban streams. *Chemosphere*, 52(10): 1727–1741.

Worm, J., and Hattum, T. van. (2006). Rainwater harvesting for domestic use. ICCO and AIDEnvironment, available: https://sswm.info/sites/default/files/reference_attachments/HATUM%20and%20WORM%202006%20Rainwater%20Harvesting%20for%20Domestic%20USE.pdf (20 Dec. 2023).

Delineation of Potential Groundwater Area in Semi-arid and Arid Region: A Case Study of Wadi Mekerra North West Algeria Using Remote Sensing, GIS and Analytic Hierarchy Process

Zakaria Mahfoud^{1*}, Nouredine Maref¹, Abdelkader Bemoussat¹

¹Department of hydraulics, Faculty of Technology, Djillali Liabès University of Sidi Bel Abbès, Algeria

Received August 12th, 2023; Accepted Oct 18th, 2023

Abstract

Groundwater is a vital natural resource and has an important role in the economy. It is the main source of water for irrigation and food industry. In general, groundwater is a reliable water source for agriculture and can be used flexibly during dry periods. Moreover, the use of geographic information systems (GIS) has shown great effectiveness in the study of groundwater since they present a very essential and rapid result. It allows the establishment of thematic maps that are useful for future developments and to control the quality of groundwater.

For this reason, the present study aims to delimit the potential of Wadi Mekerra groundwater basin, located in the North-Western part of Algeria, characterized by an arid and semi-arid climate. This aquifer, which extends over more than 2800 km², is unconfined, drained through Wadi Mekerra, and exploited by a fairly impressive number of wells and deep wells, almost the majority of which are used to irrigate agricultural land. In the current study, an analytical hierarchical process technique (AHP) was integrated with a geographic information system.

A total of eight thematic layers were established and assessed for groundwater potential zone delineation, including geomorphology, geology, land use/cover, lineament density, drainage density, rainfall, soil and slope. All thematic maps' weights for each class are determined by the AHP approach based on each class's attributes and water potential capacity. Data from springs, wells, and deep wells and their chemical analyses were carefully used for validation. The map of the groundwater potential zone was, then, divided into five categories: very good, good, moderate, low, and very low.

The study shows a very low and low groundwater potential zone that covers around 50.55% of the study area. The percentages of areas with very good and good groundwater potential are 4.15 and 11 percent, respectively. The moderate groundwater potential zone covers 59 % of the basin.

© 2024 Jordan Journal of Earth and Environmental Sciences. All rights reserved

Keywords: Groundwater potential zones (GWPZ), Analytic hierarchy process (AHP), Wadi Mekerra North West Algeria, Remote-sensing (RS), Geographic information system (GIS), Water Resources.

1. Introduction

Water is an essential element for life and is present in the atmosphere in the form of clouds, vapour, or rain. It is also reserved in the underground layers, which contain enormous quantities. Seasonal climatic extremes and irregular rainfall variations are characteristics of arid and semi-arid zones. Compared to drought, which can occur in both arid and humid climates, it is a structural climatic event.

Groundwater is the most essential component of the hydrological cycle (Chiedozié and Tosan, 2022). It can be vulnerable to many sources of contamination and land cover change resulting from human activities (Rehman et al., 2019). An aquifer's function is to store groundwater and control how much water is held and released. The ability of the aquifer to recover and convey water is determined by hydrodynamic parameters (Mallick et al., 2015). They are crucial in understanding the aquifer and the amounts of water that

are produced by a well. These traditional methods, used to identify, delineate, and map the groundwater potential zones, are expensive. Furthermore, groundwater aquifers may be evaluated and managed rapidly and effectively by combining the use of remote sensing, GIS, and satellite data (Adiat et al., 2012; Verma and Singh, 2013; Alqahtani and Qaddah, 2019).

Some researchers have reported on a variety of techniques for groundwater monitoring and management, such as identifying potential zones (Thakur et al., 2018; Pande et al., 2020; Bhattacharya et al., 2021). As an illustration, several studies have used probabilistic models such as the frequency ratio (Razandi et al., 2015), multi-criteria decision analysis (Rahmati et al., 2015), and logistic regression (Pourtaghi and Pourghasemi, 2014).

The groundwater potential zones were identified in the present study using Analytical Hierarchy Process (AHP) and GIS approaches (Machiwal et al., 2011). The Analytical

* Corresponding author e-mail: mahfoud.univsba@gmail.com

Hierarchy Process (AHP) is an approach for organizing and evaluating complicated decisions. Thomas L. Saaty developed the AHP in 1980 (Saaty, 1980). By quantifying its criteria and alternative choices and integrating these components into the overall purpose, the AHP offers a coherent framework for a critical decision, particularly in domains related to groundwater (Saaty, 2001).

Groundwater is influenced by many factors, such as water quality, the available amount of water, management costs, environmental aspects, etc. The Analytic Hierarchy Process (AHP) is a decision-making methodology commonly used in the field of groundwater management. This approach offers the possibility of structuring and comparing various criteria and options, thus contributing to the formulation of informed decisions. Several studies have demonstrated the effectiveness of this method in this specific context. A research has used the AHP to assess the vulnerability of groundwater to pollution, taking into account various hydrogeological parameters (Gangadharan and Vinoth, 2016). In another study, this method is used in the selection of drilling sites based on criteria such as recharge, water quality, and accessibility (Gdoura et al., 2016; Li et al., 2023). Additionally, for the mapping of groundwater quality, the AHP can be applied by considering various chemical and physical parameters, as illustrated by a study on the struggling Asan River in India (Mishra et al., 2022). Furthermore, this method is employed as a bottom-up strategy to track changes in soil characteristics (Tobore et al., 2023).

This study makes it possible to adjust priorities and approaches according to new information and new challenges since groundwater conditions can change over time due to factors, such as climate change or human activity. The proposed methodology also makes it possible to integrate scientific data and research results into the groundwater management process, thus ensuring that decisions are based on solid data.

This study is significant as it proves the possibility to managing water resources optimally and dynamically and collecting reliable preliminary information on the state of the hydrogeological environment. In addition, the data the study provides can be so efficient in any potential decision-making to solve the difficult problem of groundwater quality.

The main objective of the study is to delimit, identify, and map the area of groundwater potential of the Wadi Mekerra

basin located in the North-West of Algeria. This study area is subject to an arid and semi-arid climate characterized by very irregular rainfall. For this reason, this study is an example of the application of the principles of sustainable development to the water resources sector, and decisions are made methodically and can be explained and justified.

2. Study Area

The Oued-Mekerra sub-basin study area is located in the western part of the Macta basin, in northwestern Algeria. Geographically, the study site is located between latitude 34°19'20" to 35°21'34" N and longitude 0°56'39" to 0°25'22" W with an aerial extent of 2120 Km² and the main Wadi length is about 106 km. The main stream of the Mekerra sub-basin is of the fifth order and has a dendritic drainage pattern. Figure 1 shows that the study area is generally expected to have a higher elevation in the north and northwest areas and a lower elevation in the south with a minimum and maximum elevation of 295 m and 1484 m from the mean level of the sea (datum), respectively, and the standard deviation is of 280.94m. The climate of the study area is arid to semi-arid, characterized by cold, wet winters and hot, dry summers with the average annual rainfall in the region being between 310 and 450 mm over five months (December to April) (Otmame et al., 2019). The average temperatures of the maxima and minima are respectively 39°C and -2°C with an annual average of 19.52°C. The relative humidity is high all year round (more than 50%) and becomes maximum during the winter months when it oscillates between 68% and 80% when the temperatures are minimum. In addition, the geology of the study area is characterized by the formation of limestone and alluvial deposits, which occupy more than 79% of the surface of this sub-basin and play a role in increasing the permeability of the rocks (Hallouche, 2017).

3. Materials and Methods

3.1 Data used and preparation of thematic layers:

Topographic elevation (DEM), slope, and drainage density maps are developed from ASTER DEM images that have been downloaded from (www.search.earthdata.nasa.gov/search). These topographical maps were georeferenced using the WGS 84 datum, UTM zone 30 N projections in ArcGIS 10.4.1. The geomorphological and geological maps were downloaded respectively, from the Global Landform classification (Meybeck et al., 2001; Iwahashi and Pike, 2007) and the Surface geology of Africa, in order to prepare the thematic layers (Table1).

Table 1. Data sources used for thematic layers preparation.

Thematic layers	Data type	Scale/resolution	Data sources
Administrative boundary shapefile	Polygon	1:15 000 000	DIVA-GIS (https://www.diva-gis.org/)
Slope	Raster (ASTER)	30m	NASA website (www.search.earthdata.nasa.gov/search)
Drainage density			
Lineament density			
Geology	Polygon	1:750 000	Surficial geology of Africa(https://catalog.data.gov/)
Geomorphology	Raster (ASTER)	30m	Global Landform classification (https://esdac.jrc.ec.europa.eu)
Soil	Polygon	1: 5 000 000	FAO-UNESCO Soil Map of the World(https://data.apps.fao.org/)
Rainfall	CSV	Hight resolution	Global weather data (https://globalweather.tamu.edu/) 1979-2014
Land use/land cover	Polygon	10m	global land use/land cover (LULC) (Esri Inc.) (https://www.arcgis.com/)

Soil data for the study area were downloaded from Digital Soil Map of the World in ESRI shape file format. In addition, shaded relief maps of eight different azimuth angles are respectively 0°, 45°, 50°, 60°, 90°, 100°, 200°, and 315°. They were developed from ASTER DEM and processed in ArcGIS to extract the Mekerra Wadi sub-basin lineaments (Das and Pardeshi, 2018). Therefore, the line density tool was used to prepare a lineament density map of the study area. The land use/land cover map of the study area was extracted after downloading the layer which displays an overall land use/land cover (LULC) map. This map is derived from the ESA Sentinel-2 imagery at 10 m resolution. It is a composite of LULC predictions for 10 classes throughout the year to

generate a representative snapshot of 2020. Daily rainfall data for the study area were uploaded to (globalweather.tamu.edu) over the 36 years from 1979 to 2014 (Ahl, Woods, et al. 2008). These data were used to generate the rainfall map using the inverse distance weighting (IDW) method of interpolation.

Geospatial techniques have been applied in this paper to delineate potential groundwater areas of the Mekerra Wadi sub-basin. Eight thematic maps, such as geomorphology, rainfall, lineament density, lithology, slop, soil, LULC, and drainage density were prepared (Rajaveni et al., 2017). The flowchart in Figure 2 shows the processes for delineating groundwater potential zones in our study area.

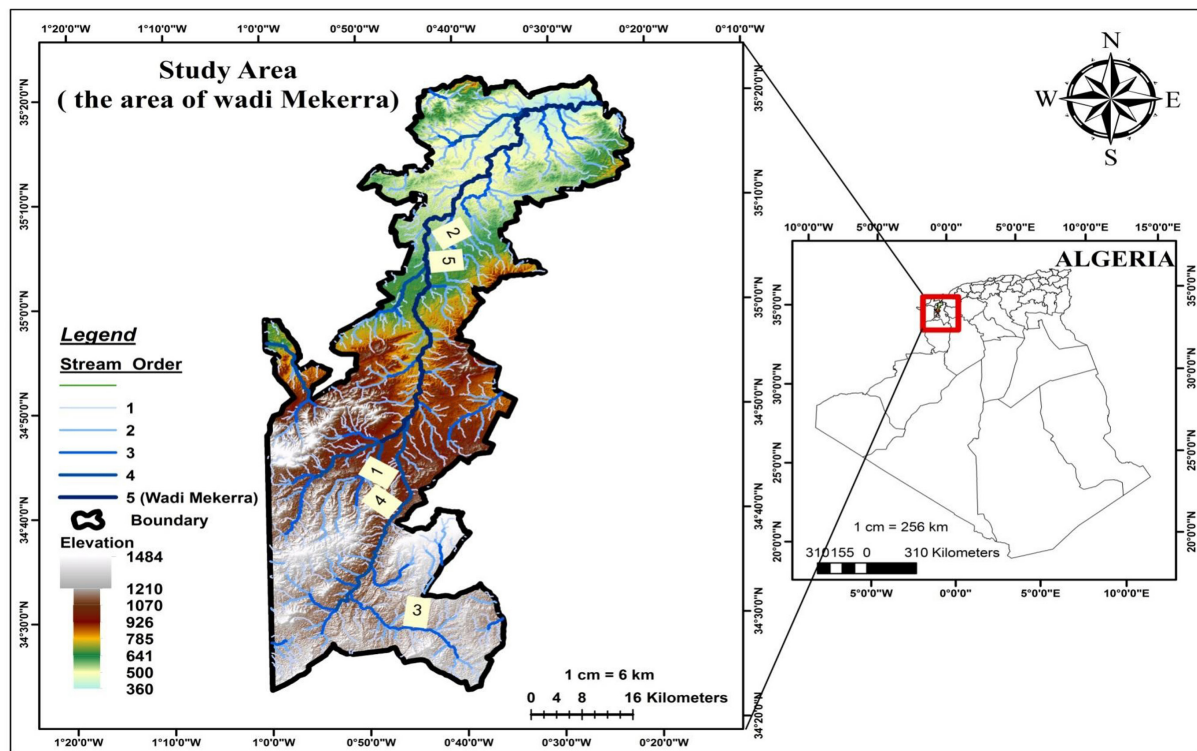


Figure 1. Location of Wadi Mekerra and Study area.

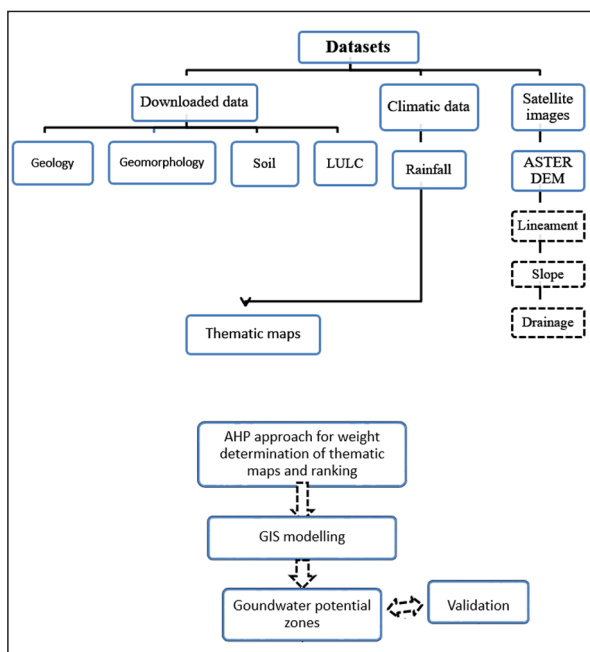


Figure 2. Flowchart of the methodology applied in the study area.

3.2 Geomorphology

Geomorphology addresses the landform and landform evolution of an area and is one of the main factors generally utilized for the depiction of groundwater potential zones. It offers data about the distribution of diverse landform features. Processes, like understanding issues of deforestation, soil properties, and seasonal precipitation, can better assess frequencies of flooding events and their potential danger of freezing and thawing (Rajaveni et al., 2017; Thapa et al., 2017). (Figure 3).

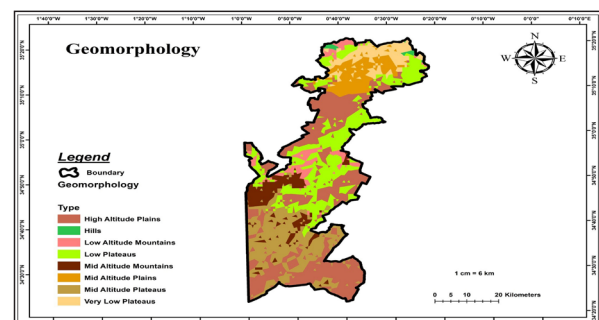


Figure 3. Geomorphology map of the study area.

3.3 Rainfall

Rain is the primary source of water in the hydrological cycle and the most important element, influencing groundwater in a region (Shekhar and Pandey, 2015). The intensity and duration of precipitation are crucial for infiltration and the amount of runoff (Abuzied et al., 2016). For the present study, precipitation data from 1979 to 2014 are used, with yearly precipitation, varying between 486 and 695 mm. The precipitation map was constructed using the IDW interpolation approach (Figure 4).

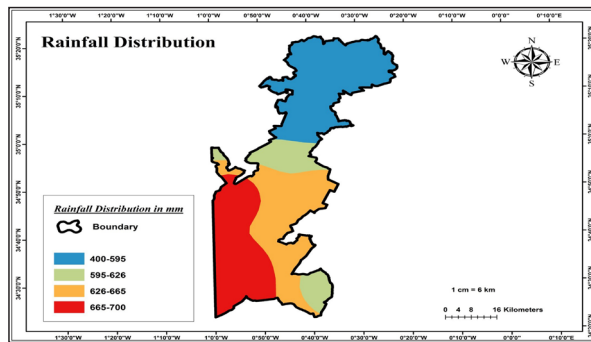


Figure 4. Rainfall distribution map of the study area.

3.4 Lineament density

Lineaments are linear geological or geomorphological elements such as faults, fractures, watercourse, roads, etc. (Pradhan and Youssef, 2010). Linear geologic features are expected to be primarily the fractured zone with good porosity and permeability (Devi et al., 2001). The Lineament density was determined according to the following formula (Edet et al., 1998):

$$Ld = \sum_{i=0}^{i=n} Li / A \text{ (K}m^{-1}\text{)} \tag{1}$$

Where $\sum Li$ is the total length of all lineaments (km), and A is the area of the grid (km²).

3.5 Lithology

Lithology describes the geochemical, mineralogical, and physical properties of rocks. It plays a fundamental role in the processes that control, on the surface, the flow of materials to soils, ecosystems, rivers, and oceans. It impacts both the porosity and the permeability of aquifer rocks and plays an important role in the apparition and movement of groundwater (Acharya et al., 2012).

3.6 Slope

Overall, a steep slope promotes runoff at the expense of infiltration (Gupta et al., 2018), while flat areas have high infiltration and can accumulate more groundwater (Rahman et al., 2012). The slope is important for many applications, particularly in geomorphology, natural resource management, and spatial planning. The slope map can be useful for identifying areas with low, moderate, or high slopes.

3.7 Soil

Soil governs the natural cycle of water, air, and organic and mineral substances. It filters and purifies water and stores and transforms substances. It represents an essential link in the permanent flows of energy and matter in the Earth's ecosystem, thus influencing the control of runoff and infiltration rates and then groundwater recharge (Fagbohun, 2018).

3.8 Land use/Land cover

The thematic map of land use in an area to be studied is a factor to be taken into account when prospecting groundwater. It is also a good indicator to quantify recharge, runoff, soil erosion (Al-Sababhah and Al maqablah, 2022) and infiltration (Ibrahim-Bathis and Ahmed, 2016; Bera et al., 2020). LULC map represents the spatial distribution of the different categories of land in the study area.

3.9 Drainage density

Drainage density is indicative of the infiltration and permeability of a drainage basin and plays a tremendous role in groundwater availability and contamination (Bera et al., 2019). It is also important in geomorphology, hydrology, and water resource management. To calculate the drainage density, The following formula is used:

$$\text{Drainage density} = (\text{Total length of drainage}) / (\text{Total area of the study area}) \tag{2}$$

3.10 Analytic hierarchy process weightage analysis

This study determines thematic map weights, using the Analytical Hierarchy Process (AHP). The AHP was developed by Tomas L. Saaty in (1980), and, as a multicriteria, decision-making analysis arranges the factors in a hierarchic structure. The structure is composed of an overall goal of criteria, sub-criteria, and alternatives (Satty, 1990). The advantage of AHP in multi-criteria decision-making is that it takes into account the intuitive knowledge of the decision-maker in the analytical decision (Saaty, 2000). The AHP is structured in two parts: the problem structure and the weighting of the different parts of the problem structure. The decision maker must first analyse the decision into hierarchical sub-problems that are easier to understand (Saaty,1987) . Second, decision-makers need to assess the different elements systematically, comparing them to each other in pairs. This comparison is made using Saaty's basic comparison scale, ranging from 1 to 9, (see Table 2 in the appendix, Saaty, 1987). This scale of importance defines the value 1 as factors having "equal importance", and 9 defines the "extreme importance" of a factor compared to another factor. The analytical hierarchy process in GIS has been widely studied (Malczewski, 2006). The topics examined are agriculture (Beigbabayi and Azadi,2011), environment (Ying et al., 2007), particularly in the field of groundwater, exploration, and management (Gangadharan and Vinoth,2016; Arulbalaji et al., 2019; Al-Djazouli et al., 2021). Accordingly, the criteria are analysed using the AHP matrix (Table 2, Table 3). We give the parameter geomorphology the highest weight, whereas precipitation, and lineament density were given moderate weight, and land use/land cover, lithology, soil, slope, and drainage density, were given low weight (Table 4). In addition, Table 2 shows the rank and weights assigned to the thematic layers.

Table 2. Saaty's 1–9 scale of relative importance.

Intensity of importance	Definition
1	Equal importance
2	Weak
3	Moderate importance
4	Moderate plus
5	Strong importance
6	Strong plus
7	Very strong or demonstrated importance
8	Very , very strong
9	Extreme importance

LuLc : Land use/Land cover.

Table 3. Pair-wise comparison matrix (eight layers) developed for AHP based groundwater potential zoning.

Factors	Geomorphology	Rainfall	Lineament Density	Lithology	Slope	Soil	LuLc	Drainage Density	Weight
Geomorphology	8	7	6	5	4	3	2	1	0.37
Rainfall	8/2	7/2	6/2	5/2	4/2	3/2	2/2	1/2	0.18
Lineament Density	8/3	7/3	6/3	5/3	4/3	3/3	2/3	1/3	0.12
Lithology	8/4	7/4	6/4	5/4	4/4	3/4	2/4	1/4	0.09
Slope	8/5	7/5	6/5	5/5	4/5	3/5	2/5	1/5	0.07
Soil	8/6	7/6	6/6	5/6	4/6	3/6	2/6	1/6	0.06
LuLc	8/7	7/7	6/7	5/7	4/7	3/7	2/7	1/7	0.05
Drainage Density	8/8	7/8	6/8	5/8	4/8	3/8	2/8	1/8	0.046

Table 4. Categorization of factors influencing of Groundwater Potential Zoning.

Parameter	Classes	weight	Influence (%)	Rank	Area (sq km)
Geomorphology	High Altitude Plains	0.37	37	4	1277.903826
	Hills			3	16.049945
	Low Altitude Mountains			4	148.644935
	Low Plateaus			5	654.784206
	Mid Altitude Mountains			5	246.023682
	Mid Altitude Plains			3	204.127049
	Mid Altitude Plateaus			6	652.713914
Rainfall	Very Low Plateaus	0.18	18	5	187.193251
	1(486-595)			1	954.542709
	2(595-626)			1	348.481986
	3(626-665)			2	785.447755
Lineament Density	4(465-694)	0.12	12	3	732.698764
	Very High(1.12-1.40)			5	129.650732
	High (0.84-1.12)			4	369.002481
	Medium(0.56-0.84)			3	608.18116
	Low(0.28-0.56)			2	847.286627
Lithology	Very Low(0.08-0.28)	0.09	9	1	887.438973
	Jurassic			4	660.193015
	Cretaceous			4	269.970883
	Lower Cretaceous			4	623.878811
	Quaternary			2	10.334615
	Pleistocene			2	247.792056
Slope(degree)	Tertiary	0.07	7	3	1023.882024
	0-3.6			5	1317.924085
	3.6-7.4			4	918.882549
	7.4-12.7			3	412.453821
	12.7-20.1			2	102.929178
Soil	20.1-48.4	0.06	6	1	69.514624
	Chromic cambisols			4	1808.159408
	Calcic Cambisols			3	967.607736
LuLc	Xerosols	0.05	5	2	57.409059
	Annual Broadleaf Vegetation			5	665.237595
	Broadleaf Crops			5	0.586084
	Barren Land			1	93.091426
	Built			1	79.337862
	Closed Shrublands			4	1819.016725
	Shrubs			5	162.057048
Drainage Density	Water	0.046	4.6	5	2.562314
	Very High (4.05-5.05)			1	157.200871
	High(3.04-4.04)			2	298.854688
	Medium(2.03-3.03)			3	475.094541
	Low(1.02-2.02)			4	565.915158
Drainage Density	Very Low (0.05-1.01)	0.046	4.6	5	617.676699

The groundwater potential map was created by summing the weight values of eight thematic maps: geomorphology, lithology, slopes, soils, land use/land cover, precipitation, lineament density, and drainage density map. The overall weights of various polygons inside the included layer had been derived from the subsequent equation to acquire groundwater potential index (Rao and Briz-Kishore, 1991; Kumar et al., 2016):

$$\text{GWPI} = ((GM_w)(GM_{wi}) + (RF_w)(RF_{wi}) + (LD_w)(LD_{wi}) + (LG_w)(LG_{wi}) + (SP_w)(SP_{wi}) + (SL_w)(SL_{wi}) + (LC_w)(LC_{wi}) + (DD_w)(DD_{wi})) \quad (3)$$

GWPI= groundwater potential index, GM = geomorphology, RF=Rainfall, LD=LineamentDensity, LG=Lithology, SP=Slope, SL=Soil, LC= land use/land cover, DD=Drainage Density, and the subscripts "w" and "wi" talk to the normalized weight of a topic and the normalized weight of individual features of a topic, respectively.

Specific diagrams have been developed to represent the results of hydrochemical analyses and to derive particular information from them using the DIAGRAM software, developed by Roland SIMLER from the University of Avignon. The use of these diagrams (Chadha, Piper's, Riverside) proves to be valuable because it makes it simple and direct to interpret rich analyses that are difficult to interpret. The Piper diagram uses the major elements to represent the different groundwater facies. The Riverside diagram is mainly used to assess the risk of soil salinization. For this, he uses the electrical conductivity (EC) or the total dissolved charge, both relating to the salinity of the water and the sodium absorption index (SAR) which is a measure of the risk of sodization of the soil due to irrigation. Finally, geochemical classification and hydrochemical processes of surface and groundwater samples are illustrated in a Chadha diagram.

4. Results and Discussion

The study area presents diverse geomorphological features, including High and Mid-Altitude Plains, Low and Mid-Altitude Mountains, Low and Very Low Plateaus, Mid-Altitude Plateaus, and Hills (Figure 3). The High Altitude Plains are expansive, with varying elevations from 830m in the middle to 1120m in the south and 523m in the north. They feature Calcimagnesian clayey loam soils with textures, ranging from coarse to fine, and have relatively moderate groundwater permeability.

In contrast, the Mid-Altitude Plains in the north are relatively uniform, with altitudes ranging from 447m to 554m, slightly undulating and are often affected by rainwater runoff and soil erosion. The Hills occupy an altitude between 253m and 500m and have limited groundwater potential. The Low and Mid-Altitude mountains are predominantly forested and unsuitable for agriculture due to steep slopes, interrupted wadis, and severe erosion. The Low and Mid-Altitude Plateaus are relatively flat (Meybeck et al., 2001), mainly covered by forests and plantations, with calcimagnesian, Limono-clay soils. Additionally, Very low Plateaus at elevations of 400m to 550m are characterized by coarse, stony materials in major wadi beds and glacia formations connected to mountains and

hills, occasionally intersected by faint gullies.

Rainfall has been categorized into five groups every year: (486-595mm), (595-626mm), (626-665mm), and (665-694 mm) (Figure 4). High weights are ascribed to heavy precipitation and vice versa. In the study region, we discovered that very low and low lineament densities, along with medium lineament density, occupy a major part, whereas high and very high lineament densities are represented by minor parts (Figure 5). The lineaments density was divided into five categories: Very Low (0.08-0.28 km/km²), Low (0.28-0.56 km/km²), Medium (0.56-0.84 km/km²), High (0.84-1.12 km/km²), and Very High (1.12-1.40 km/km²) (Figure 5).

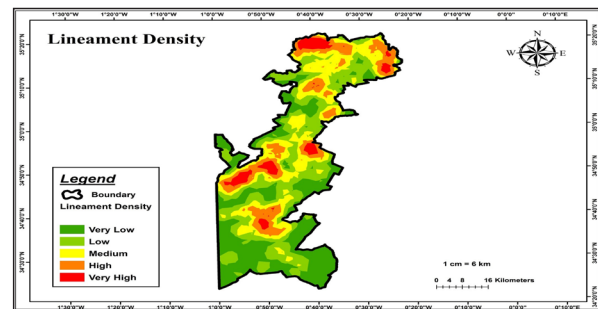


Figure 5. Lineament density map of the study area.

The geological map of the study area reveals a diverse range of lithologies spanning different geological periods, including Jurassic, Cretaceous, Lower Cretaceous, Quaternary, Pleistocene, and Tertiary formations (Figure 6). The predominant Tertiary strata, particularly in the northern part of the basin, comprise marine Pliocene deposits consisting of robust conglomerate banks, layers of coarse sandstone intercalated with greyish silt, and occasionally lacustrine limestone. The Pleistocene layer essentially encompasses the entire Quaternary period. In additionally, we encounter the Tensiftian, Soltanian, and Moulouyen climatic cycles (Choubert and Faure-Muret, 1956), representing the late Pleistocene and manifesting in various forms: gravelly and stony crusted formations along the Mekerra Wadi, silts embedded with calcareous granules further from the Wadi, and the presence of calcareous crusts. The coloration of the silt ranges from pale red to brownish-red, depending on whether the area has been cultivated or not.

The degree of slope of the study area varies between 0° and 50°. The study area was divided into five slope classes (Figure 7), namely, gentle (0–3.6°), low (3.6–7.4°), relatively high (7.4–12.7°), high (12.7–20.1°) and steep (20.1–48.4°). Most of the area of the basin falls into a gently sloping category with a coverage of 1317.92 km². The class with the high slope value receives the lowest rank due to relatively highest runoff and low infiltration. Figure 8 shows the soil map, which is dominated by Chromic Cambisols (1808.16 km²), Calcic Cambisols (967.60 km²), and Xerosols (57.40 km²). The calcimorphic soils are carbonated in the majority of the horizons, which is due to the calcareous rocks and the semi-arid climate. The soil is classified into two types: The poorly developed soils of alluvial contribution and calcimagnesian soils (Mahfoud et al., 2020). Land use and cover in the study area are classified into seven categories: Annual Broadleaf Vegetation, Broadleaf Crops, Barren Land, Built-

up Areas, Closed Shrublands, Shrubs, and Water (as shown in Figure 9). The high weights are assigned to waterlogged areas, agricultural land, and forests due to their favorable groundwater percolation capabilities, whereas low weights are allocated to built-up areas and arid lands, as they have limited potential for groundwater recharge. Figure 10 shows the drainage density of Wadi Mekerra is classified into five classes, such as very low (<1.01km/km²), Low (1.02-2.02km/km²), Medium (2.03-3.03km/km²), High (3.04-4.04km/km²) and Very High (4.05-5.05 km/km²), occupying an area of 617.67 km², 565.91 km², 475.09 km², 298.85 km², and 157.20 km², respectively. We assign high weight values to areas with high drainage density.

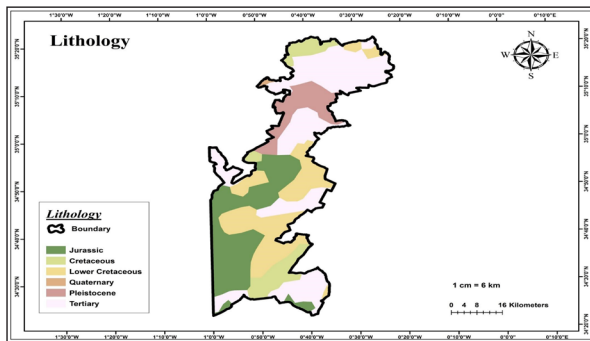


Figure 6. Lithology map of the study area

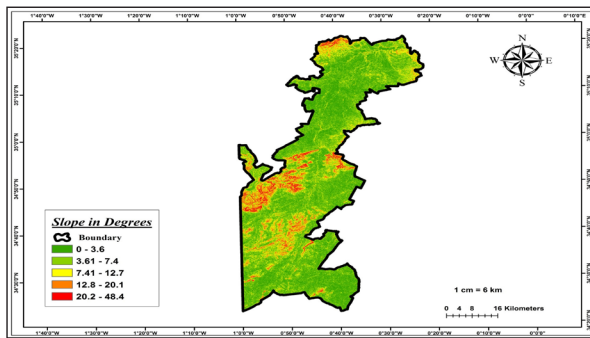


Figure 7. Slope map of the study area.

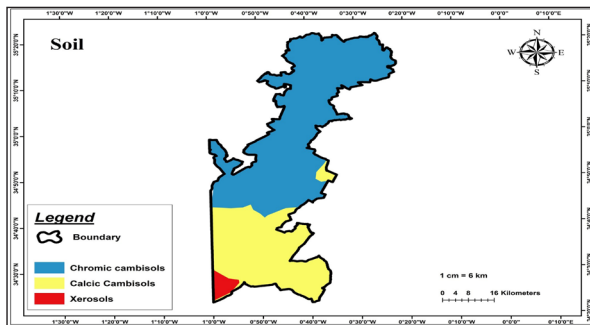


Figure 8. Soil map of the study area.

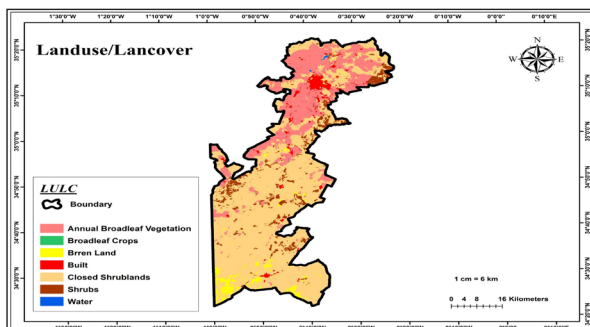


Figure 9. Land use/land cover map of the study area.

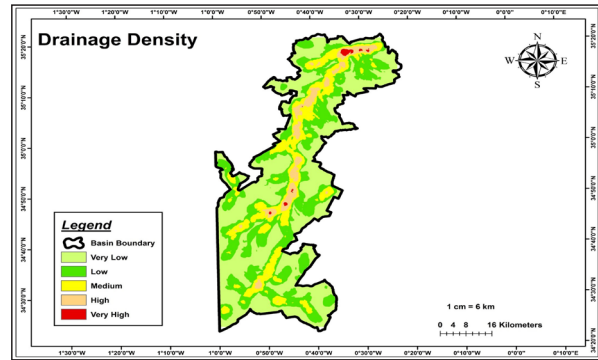


Figure 10. Drainage density map of the study area.

Figure 11 shows the groundwater potential map, which has been divided into five classes with groundwater potentials of very good, good, moderate, low, and very low, and the aerial distribution of these categories is 69.51km², 102.92 km², 412.45 km², 918.88 km², and 1317.92 km². Except for a small area in the northwest, the north and center of the study area are considered very low to low water potential, while areas, considered potentially moderate, good to very good, occupy large areas in the south-western region of the Mekerra Wadi, which explains— by a good permeability— a good density of lineaments, and a density of drainage.

Piper’s diagram (Figure12a) shows that the majority of the waters of the Plio-Quaternary aquifer in the northern area is sulphated chloride and magnesium calcium. The diagram of Chadha (1999) (Figure13a) (Figure13b), shows that the majority of the samples represents water of the Cl-Ca-Mg type in the northern and southern study area. These water types have a permanent hardness and do not deposit residual sodium carbonate when they are used for irrigation (Chadha 1999). Figure14a shows, according to the Riverside diagram, that the groundwater in the northern area of the study area belongs to 3 classes: C4S1, C4S2, and C3S1 and the conditions of usage are in Table.6. The Piper diagram of the southern of study area shows that the groundwater is chloride-sulfated (Figure12b). The 17 examined wells of southern area all include water that is C3S1-class, which includes water suitable for crop irrigation according to SAR value (Figure14b).

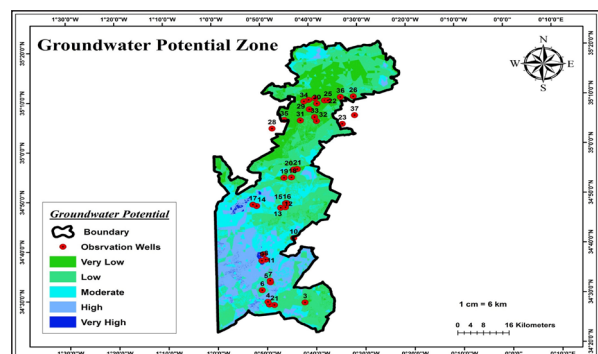


Figure 11. Groundwater potential zones of the study area.

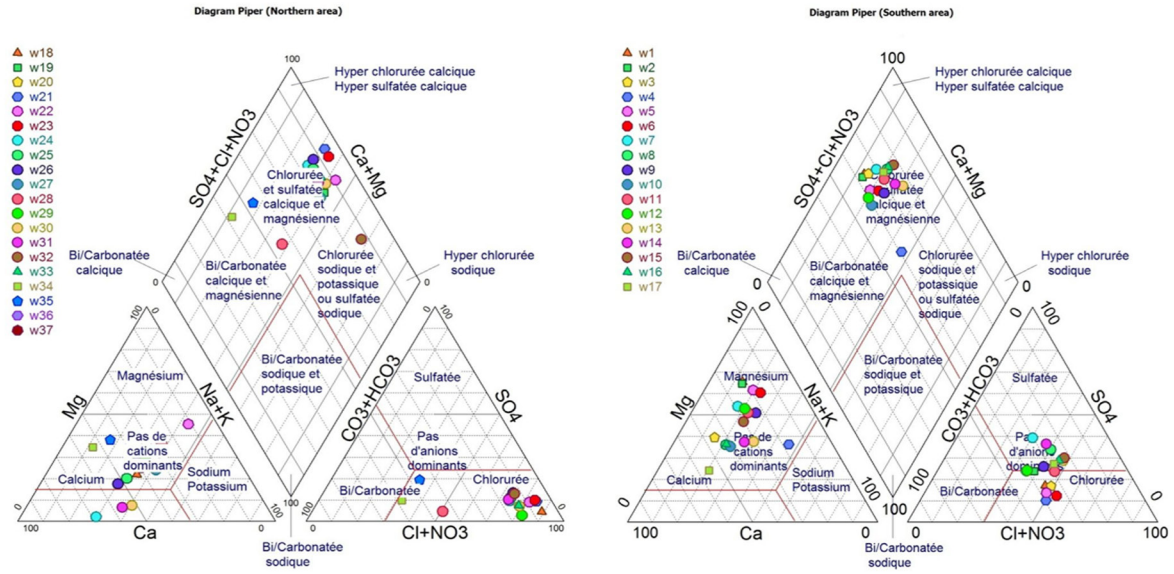


Figure 12. (a) diagram Piper in the northern of the study area ; (b) diagram Piper in the southern of the study area.

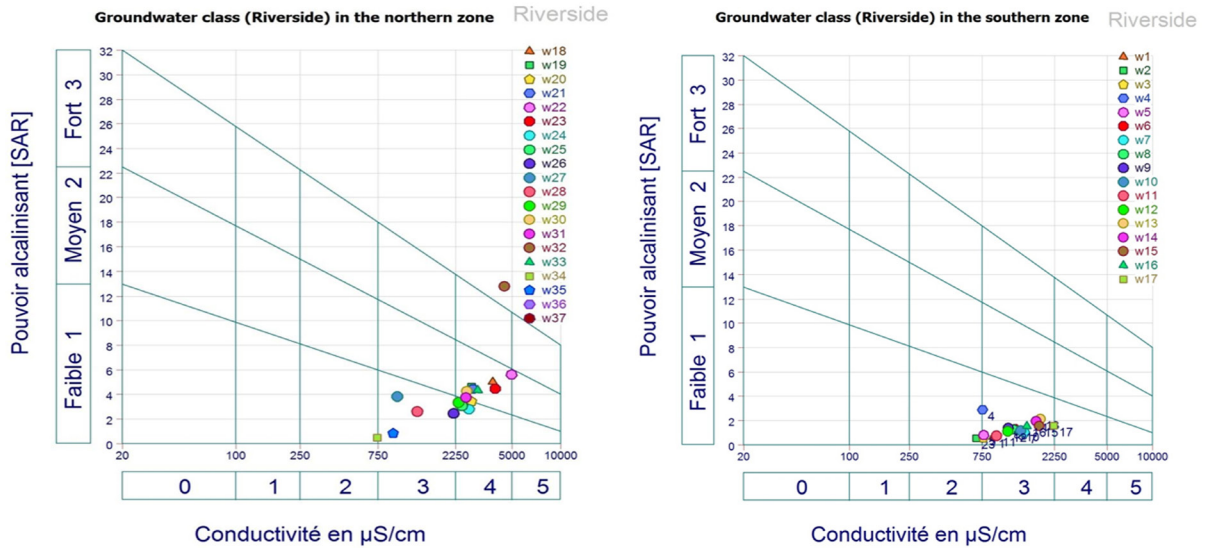


Figure 13. (a) diagram Chadha groundwater in the northern of the study area ; (b) diagram Chadha groundwater in the southern of the study area.

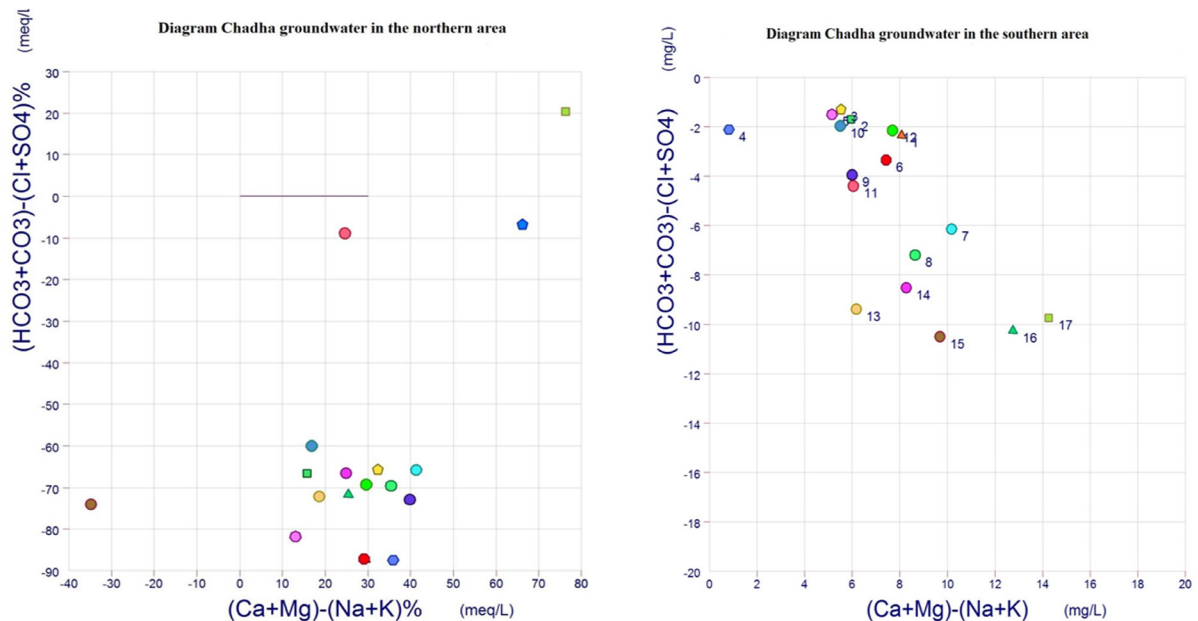


Figure 14. (a) diagram Riverside groundwater in the northern of the study area ; (b) diagram Riverside groundwater in the southern of the study area.

Table 5. Location and physico-chemical characteristics of the observation well-2018

n°	Name	Department	X1	Y1	TDS	pH	Ca ²⁺	Mg ²⁺	Na ⁺	K ⁺	Cl ⁻	SO ₄ ²⁻	NO ₃ ⁻	HCO ₃ ⁻	EC	Depth (m)	GWL (m)	Yield
1	Puits Sidi Naïmi	Radjm Demouch	701456.673	3817337.63	2732	7.61	47	87.48	32.2	2.35	150.66	82.13	24.8	220.86	886	100	2.3	(63-100)
2	Dar EL Beida	Ras El Ma	699894.686	3817497.93	2213	7.27	36	63.67	24.15	1.56	103.87	98.94	27.9	200.11	685	150	2.72	(15-80)
3	Forage Faraat Zit	Ras El Ma	710988.395	3818298.39	2238	7.44	72	38.03	25.07	3.91	95.01	62.92	71.3	164.13	763	150	2.6	(15-80)
4	Forage Z'hina	Ras El Ma	699425.961	3818502.77	3211	7.12	38	47.26	112.93	2.35	198.87	57.64	22.94	286.14	756	80	2.1	(15-80)
5	Sidi Hamli 3	Ras El Ma	700209.496	3825770.07	3030	7.31	32	63.18	35.42	3.91	130.1	60.52	47.12	209.87	770	180	2.92	(15-80)
6	Sidi Hamli 2	Ras El Ma	697652.342	3822848.53	3563	6.91	46	100.9	70.15	5.08	220.14	75.41	42.16	270.27	1237	160	3.83	(15-80)
7	Forage Titten Yahia	Ras El Ma	700152.082	3826399.260	2122	7.19	90	101.1	57.73	4.69	166.97	309.79	17.98	305.05	1432	155	3.3	(15-80)
8	F OS1	Oued Sbaa	698723.079	3834223.73	1985	7.25	129	65.97	71.07	5.08	210.93	252.16	19.22	244.04	1200	125	5.5	(15-100)
9	F OS2	Oued Sbaa	697543.712	3833832.16	1678	7.66	58	76.91	70.84	5.47	168.03	148.41	13.02	236.72	1120	200	6.8	(30-100)
10	Hqaiba	CW39A-Hqaiba	707451.229	3842250.74	1725	7.53	86	44.47	53.59	4.3	137.9	131.12	11.16	283.7	1348	150	7.2	(20-80)
11	F OS	Oued Sbaa	697988.213	3836237.225	1352	7.29	58	68.65	36.8	35.19	180.8	138.33	37.82	219.03	933	50	9.28	(15-80)
12	Serradj Zouaoui	Mouley Slissen	703391.735	3853538.7	1687	7.13	70	83.84	59.8	3.13	159.53	168.11	45.26	357.52	1102	150	6.3	(15-80)
13	Serradj Zouaoui2 RN95	Mouley Slissen	704883.823	3853725.28	1898	7.12	104	76.55	119.6	4.69	300.62	254.56	26.04	267.22	1813	160	10.53	(27-100)
14	Tamatouna 1	Mouley Slissen	695888.890	3854206.44	1532	7.3	131	85.66	119.14	5.08	228.3	365.03	83.7	336.78	1715	138	9.86	(27-100)
15	Serradj Zouaoui3 RN95	Mouley Slissen	704896.972	3855229.05	1678	7.01	109	102.1	93.38	2.74	319.05	288.18	37.2	274.55	1794	132	6.34	(27-100)
16	Mouley Slissen 1	Mouley Slissen	705293.516	3855302.1	1783	7.2	188	98.05	106.03	3.91	333.94	304.99	45.88	336.17	1480	200	7.3	(27-100)
17	Tamatouna 2	Mouley Slissen	694758.691	3854692.06	1810	7.09	269	70.96	112.93	3.91	354.15	320.84	68.82	422.19	2240	80	8.2	(43-100)
18	Ighti 2	Bordj Jaafar	706744.215	3864855.3	2352	6.88	120	63.06	74.75	1.17	159.88	146.01	29.14	347.15	1228	150	11.8	60>
19	Sidi Ali Benyoub	Sidi Ali Benyoub	704447.395	3864722.23	1113	7	104	56.5	38.87	1.56	123.01	71.56	19.22	334.94	867	150	9.88	60>
20	Source Ain Mekareg	Bordj Jaafar	707388.778	3867738.49	1418	6.91	98	38.27	24.15	1.17	99.97	46.59	24.18	350.2	739		5.2	130
21	Source Skhouna	CW48-Sidi Ali Benyoub	708567.898	3867967.14	1389	7.03	109	55.65	45.54	2.35	158.11	124.88	6.82	376.43	924	60	5.76	101
22	P-Belawliadi	Amarnas	717106.743	3893515.59	2356	7.32	580	180	541	11	2061	145	67	252	4796	60	3.7	(3-10)
23	Cité El HORIA	Sidi Bel Abbas	722622.081	3884815.940	4423	7.12	240	111	345	13	965	168	32	376	2812	80	6.2	(3-10)
24	Sidi Khaled	Sidi Khaled	712287.038	3890229.29	2123	7.05	295	115	275	16	815	190	195	340	2801	82	4.56	(3-10)
25	Cité El HORIA1 CW4	Sidi Bel Abbas	718105.491	3893573.57	3125	6.9	530	225	481	10	1905	300	196	246	4866	65	3.2	(3-10)
26	Douar Gouassem	Tilmouni	726037.702	3895036.25	4120	7.18	109	270	481	13	1909	290	45	367	4960	55	5.9	(3-10)
27	RN 95 Route de Boukhanefis	Sidi Bel Abbas	714052.543	3894340.44	3185	7.02	420	160	425	9	1578	265	85	210	3940	73	7.3	(2-18)
28	RN7 Route Lamtar	Lamtar	700679.739	3883041.79	1695	7.13	455	9	220	7	870	160	90	350	2701	100	4.5	(5-15)
29	Sidi Laheen	Sidi Laheen	712084.092	3893725.05	1152	6.92	305	78	232	8	839	178	26	299	2456	75	6.15	(2-18)
30	P-Belawliadi	Amarnas	714667.883	3892371.82	1782	7.09	270	55	171	12	721	191	96	233	2186	80	4.9	(2-18)
31	RN 95 Route de Boukhanefis1	Boukhanefis	709522.803	3886060.29	1854	7	175	75	240	6	550	264	71	320	2126	92	3.7	(3-17)
32	RN13 Sidi Khaled	Sidi Khaled	714545.29	3885850.67	1685	6.93	85	71	135	9	270	35	19	426	1312	88	4.1	(3-17)
33	RN13 Sidi Khaled1	Sidi Khaled	713959.005	3887319.87	1532	7.01	221	105	240	10	916	43	54	295	2355	90	7.75	(3-17)
34	Sidi Laheen1	Sidi Laheen	710615.018	3893138.66	1798	6.94	350	30	310	7	957	120	54	292	2650	75	9.2	(3-17)
35	Habara	Sidi Khaled	704500.44	3886269.83	1865	7.11	355	25	270	5	880	171	50	347	2628	70	6.3	(3-17)
36	R7 Route Tilmouni	Tilmouni	722042.559	3894804.34	3462	6.97	119	165	920	13	1520	360	45	457	4498	60	7.6	(3-17)
37	P-Belarbi	Belarbi	726443.379	3888044.19	3328	7	320	141	370	12	1109	142	25	344	3078	109	5.5	(3-17)

Table 6. Classification of waters according to SAR (Richards (USSL), 1954).

Degree	Quality	Classe	Condition of use
1	Excellent	C1S1	Waters that can be used safely for irrigation for most crops, on most soils.
2	Good	C2S1 C1S2	Generally, water that can be used without control, especially for irrigation of plants moderately tolerant to salts on the ground.
3	Acceptable	C3S1 C2S3 C3S2	Generally, water suitable for irrigation of salt-tolerant crops on well-drained soil. However, the evolution of salinity must be controlled.
4	Poor	C4S1 C4S2 C3S3	Highly mineralized water that may be suitable for the irrigation of certain species that are well tolerant to salts on the ground and well drained.
5	Very poor	C3S4 C4S3 C4S4	Water not generally suitable for irrigation but can be used under certain conditions: very permeable soil, well leached, plants tolerant to salts.

5. Validation

By comparing the areas of groundwater potential, delineated in this study, to data from deep wells and springs, the validity of the groundwater potential map was achieved. It is done by overlaying only the point data of the two springs, 36 deep wells with the map generated, using the weighted index overlay analysis. Moreover, within the framework of the good integrated management of water resources, the validity was also achieved by the hydrochemical classification of groundwater in the study area. For this purpose, several methods have been defined by various authors to classify and know the different chemical facies of the waters of the Plio-Quaternary aquifer. The wells (well n°:16-37) and 02 springs (source n°: 18-19) located in the northern of study area, are located in areas with very low and low groundwater potential and have a water production capacity comprised between 2 and 18 liters per minute (LPM). However, the other wells in the study area are located in areas with moderate, high and very high groundwater potential and have a water production capacity of about 20-80 LPM, 80-100 LPM, respectively. Six wells, including four wells (No. 10, 23, 28, and 37) (see figure) located outside our study area and two other wells (No. 1, 14) are not perfectly suited for various reasons (Table.5).

6. Conclusion

The Mekerra Wadi area is located in the department of Sidi Bel Abbes in the Northwestern region of Algeria and is situated in a region with a very diverse geomorphology (plateaus, mountains, plains, hills, etc). Moreover, the wadis of the semi-arid and arid regions of North Africa are the best known intermittent and ephemeral watercourses. Thus, these watercourses are important sources of groundwater supply (Fovet et al., 2021). In addition, the Wadi Mekerra is known by its ephemeral main stream.

The present study aims to delineate potential groundwater areas, using a combination of AHP, remote sensing and GIS techniques. The groundwater potential zones were defined in this study using a total of eight thematic layers, including geomorphology, Rainfall, Lineament Density, Lithology, Slope, Soil, LuLc, and Drainage Density.

The results, obtained according to the final map, the study area could be grouped into five classes, such as very high, high, moderate, low, and very low. Areas, with very high and high water potential, are mainly found in the lower parts of the study area. A large portion of the very low groundwater

potential areas are located in the northern part of the area, and the low potential areas are scattered over the entire surface. The northern portion of the basin has the majority of the very low groundwater potential areas, and the low potential areas are dispersed over the entire region. The results show that 59% is covered by an area with moderate water potential. Areas with very low and low groundwater potential occupy 50.55% of the total area. In addition, areas with very high and very low water potential occupy 4.15 and 11%, respectively. Using flow data and results of chemical analyses of wells, deep wells, and springs in the study area, the delineated map of potential groundwater zones was validated.

The Mekerra Wadi area is located in the department of Sidi Bel Abbes in the Northwestern region of Algeria and is situated in a region with a very diverse geomorphology (plateaus, mountains, plains, hills, etc). Moreover, the wadis of the semi-arid and arid regions of North Africa are the best known intermittent and ephemeral watercourses. Thus, these watercourses are important sources of groundwater supply (Fovet et al., 2021). In addition, the Wadi Mekerra is known by its ephemeral main stream.

The present study aims to delineate potential groundwater areas, using a combination of AHP, remote sensing and GIS techniques. The groundwater potential zones were defined in this study using a total of eight thematic layers, including geomorphology, Rainfall, Lineament Density, Lithology, Slope, Soil, LuLc, and Drainage Density.

The results, obtained according to the final map, the study area could be grouped into five classes, such as very high, high, moderate, low, and very low. Areas, with very high and high water potential, are mainly found in the lower parts of the study area. A large portion of the very low groundwater potential areas are located in the northern part of the area, and the low potential areas are scattered over the entire surface. The northern portion of the basin has the majority of the very low groundwater potential areas, and the low potential areas are dispersed over the entire region. The results show that 59% is covered by an area with moderate water potential. Areas with very low and low groundwater potential occupy 50.55% of the total area. In addition, areas with very high and very low water potential occupy 4.15 and 11%, respectively. Using flow data and results of chemical analyses of wells, deep wells, and springs in the study area, the delineated map of potential groundwater zones was validated.

For this purpose, the map of the zones groundwater potential of this study provides decision makers with an overview of integrated groundwater management for urban and agricultural uses to avoid environmental, economic and social risks. Since most of the study area is covered with agricultural land and agriculture remains one of the main sources of groundwater pollution due to the use of pesticides and livestock effluents, this study will improve irrigation facilities and preserve the quality of water in the area. It can be used as a communication and stakeholder engagement tool. By involving different actors in the process of prioritizing criteria and decision-making, it is possible to reach a consensus and a better acceptance of the decisions taken.

Conflict of Interests

The authors declare no conflict of interest

References

- Acharya, T., S.K. Nag, and S. Basumallik, Hydraulic significance of fracture correlated lineaments in precambrian rocks in Purulia district, West Bengal. *Journal of the Geological Society of India*, 2012. 80 (5): p. 723-730.
- Adiat, K., M. Nawawi and K. Abdullah (2012). "Assessing the accuracy of GIS-based elementary multi criteria decision analysis as a spatial prediction tool—a case of predicting potential zones of sustainable groundwater resources." *Journal of Hydrology* 440: 75-89.
- Ahl, R. S., S. W. Woods and H. R. Zuuring (2008). "Hydrologic calibration and validation of swat in a snow-dominated rocky mountain watershed, montana, USA 1." *JAWRA Journal of the American Water Resources Association* 44(6): 1411-1430.
- Al-Djazouli, M. O., K. Elmorabiti, A. Rahimi, O. Amellah and O. A. M. Fadil (2021). "Delineating of groundwater potential zones based on remote sensing, GIS and analytical hierarchical process: a case of Waddai, eastern Chad." *GeoJournal* 86(4): 1881-1894.
- Alqahtani, F. and A. A. Qaddah (2019). "GIS digital mapping of flood hazard in Jeddah–Makkah region from morphometric analysis." *Arabian Journal of Geosciences* 12(6): 1-20.
- Al-Sababhah, N., and Al maqablah, M. 2022. "Integrated Evaluation of Soil Erosion-prone Areas based on the GIS Technique and the Analytic Hierarchy Process on Hillside Slopes, Northwest of Jordan ". *Jordan Journal of Earth and Environmental Sciences*, 14 (2).
- Arulbalaji, P., D. Padmalal and K. Sreelash (2019). "GIS and AHP techniques based delineation of groundwater potential zones: a case study from southern Western Ghats, India." *Scientific reports* 9(1): 1-17.
- Beigbabayi, B and M. M. Azadi (2011). "Using ahp modeling and gis to evaluate the suitability of site with climatic potential for cultivation of autumn canola in ardabil province." *Scholars Research Library*. 3 (5):2307-2317
- Bera, A., B.P. Mukhopadhyay, and S. Barua, Delineation of groundwater potential zones in Karha river basin, Maharashtra, India, using AHP and geospatial techniques. *Arabian Journal of Geosciences*, 2020. 13(15): p. 1-21.
- Bera, A., B.P. Mukhopadhyay, and D. Das, Landslide hazard zonation mapping using multi-criteria analysis with the help of GIS techniques: a case study from Eastern Himalayas, Namchi, South Sikkim. *Natural Hazards*, 2019. 96(2): p. 935-959.
- Bhattacharya, S., S. Das, S. Das, M. Kalashetty and S. R. Warghat (2021). "An integrated approach for mapping groundwater potential applying geospatial and MIF techniques in the semiarid region." *Environment, Development and Sustainability* 23(1): 495-510.
- Chadha, D. (1999). "A proposed new diagram for geochemical classification of natural waters and interpretation of chemical data." *Hydrogeology journal* 7(5): 431-439.
- Chiedozi, O., and Tosan, A. O. (2022). Groundwater Quality Around Active and Non-Active Dumpsites in Benin City, Nigeria. *Jordan Journal of Earth and Environmental Sciences*, 13(4).
- Choubert, G. and A. Faure-Muret (1956). *Lexique stratigraphique du Maroc: par Georges Choubert, avec la collaboration de Anne Faure-Muret. Introduction géologique, les grands traits de la géologie du Maroc, par Georges Choubert et Jean Marçais, Éditions du Service géologique du Maroc.*
- Das, S. and S. D. Pardeshi (2018). "Integration of different influencing factors in GIS to delineate groundwater potential areas using IF and FR techniques: a study of Pravara basin, Maharashtra, India." *Applied Water Science* 8(7): 1-16.
- Devi, S.P., S. Srinivasulu, and K.K. Raju, Delineation of groundwater potential zones and electrical resistivity studies for groundwater exploration. *Environmental Geology*, 2001. 40(10): p. 1252-1264.
- Edet, A., et al., Application of remote-sensing data to groundwater exploration: a case study of the Cross River State, southeastern Nigeria. *Hydrogeology journal*, 1998. 6(3): p. 394-404.
- Fagbohun, B. J. (2018). Integrating GIS and multi-influencing factor technique for delineation of potential groundwater recharge zones in parts of Ilesha schist belt, southwestern Nigeria. *Environmental earth sciences*, 77(3), 69.
- Fovet, O., A. Belemtougri, L. Boithias, I. Braud, J. b. Charlier, M. Cottet, K. Daudin, G. Dramais, A. Ducharne and N. Folton (2021). "Intermittent rivers and ephemeral streams: Perspectives for critical zone science and research on socio-ecosystems." *Wiley Interdisciplinary Reviews: Water* 8(4): e1523.
- Gangadharan, R. and S. Vinoth (2016). "Assessment of groundwater vulnerability mapping using AHP method in coastal watershed of shrimp farming area." *Arabian Journal of Geosciences* 2(9): 1-14.
- Gdoura, K., M. Anane, and S. Jellali, Geospatial and AHP-multicriteria analyses to locate and rank suitability sites for groundwater recharge with reclaimed water. *Resources, Conservation and Recycling*, 2015. 104: p. 19-30.
- Gupta, D., S. Yadav, D. Tyagi and L. Tomar (2018). "Multi-criteria decision analysis for identifying of groundwater potential sites in Haridwar." *The Engineering Journal of Application and Scopes* 3(2): 9-15.
- Hallouche, B. (2017). *bassin versant de la haute de mekerra (nw algerien): hydrologie, geochimie, pollution* PhD in science, university of Tlemcen (Abu Baker Belkaid).
- Ibrahim-Bathis, K. and S. Ahmed, Geospatial technology for delineating groundwater potential zones in Doddahalla watershed of Chitradurga district, India. *The Egyptian Journal of Remote Sensing and Space Science*, 2016. 19(2): p. 223-234.
- Iwahashi, J. and R. J. Pike (2007). "Automated classifications of topography from DEMs by an unsupervised nested-means algorithm and a three-part geometric signature." *Geomorphology* 86(3-4): 409-440.
- Kumar, P., S. Herath, R. Avtar and K. Takeuchi (2016). "Mapping of groundwater potential zones in Killinochi area, Sri Lanka, using GIS and remote sensing techniques." *Sustainable Water Resources Management* 2(4): 419-430.
- Li, M., et al., Groundwater Quality Evaluation and Analysis Technology Based on AHP-EWM-GRA and Its Application. *Water, Air, and Soil Pollution*, 2023. 234(1): p. 19.
- Machiwal, D., M. K. Jha and B. C. Mal (2011). "Assessment of groundwater potential in a semi-arid region of India using

- remote sensing, GIS and MCDM techniques." *Water resources management* 25(5): 1359-1386.
- Mahfoud, Z., A. Khaldi, and K. Korichi, Wastewater reuse and mapping of irrigable soils: Case of Sidi Bel Abbes City, Algeria. *Journal of Water and Land Development*, 2020.
- Malczewski, J. (2006). "GIS-based multicriteria decision analysis: a survey of the literature." *International journal of geographical information science* 20(7): 703-726.
- Mallick, J., C. K. Singh, H. Al-Wadi, M. Ahmed, A. Rahman, S. Shashtri and S. Mukherjee (2015). "Geospatial and geostatistical approach for groundwater potential zone delineation." *Hydrological Processes* 29(3): 395-418.
- Meybeck, M., P. Green and C. Vörösmarty (2001). "A new typology for mountains and other relief classes." *Mountain research and development* 21(1): 34-45.
- Mishra, A.P., et al., Assessment of water quality index using Analytic Hierarchy Process (AHP) and GIS: a case study of a struggling Asan River. *International Journal of Environmental Analytical Chemistry*, 2022: p. 1-13.
- Otmame, A., K. Baba Hamed and A. Bouanani (2019). "Apport de la variabilité spatiale des caractéristiques physiques du bassin versant dans la modélisation hydrologique et les sous-produits du bilan hydrologique: cas du bassin versant de l'aval Mekerra, Algérie." *Revue des sciences de l'eau/Journal of Water Science* 32(2): 117-144.
- Pande, C. B., K. N. Moharir, S. K. Singh and A. M. Varade (2020). "An integrated approach to delineate the groundwater potential zones in Devdari watershed area of Akola district, Maharashtra, Central India." *Environment, Development and Sustainability* 22(5): 4867-4887.
- Pourtaghi, Z. S. and H. R. Pourghasemi (2014). "GIS-based groundwater spring potential assessment and mapping in the Birjand Township, southern Khorasan Province, Iran." *Hydrogeology Journal* 22(3): 643-662.
- Pradhan, B. and A.M. Youssef, Manifestation of remote sensing data and GIS on landslide hazard analysis using spatial-based statistical models. *Arabian Journal of Geosciences*, 2010. 3(3): p. 319-326.
- Rahman, M. A., B. Rusteberg, R. Gogu, J. L. Ferreira and M. Sauter (2012). "A new spatial multi-criteria decision support tool for site selection for implementation of managed aquifer recharge." *Journal of environmental management* 99: 61-75.
- Rahmati, O., A. Nazari Samani, M. Mahdavi, H. R. Pourghasemi and H. Zeinivand (2015). "Groundwater potential mapping at Kurdistan region of Iran using analytic hierarchy process and GIS." *Arabian Journal of Geosciences* 8(9): 7059-7071.
- Rajaveni, S., K. Brindha and L. Elango (2017). "Geological and geomorphological controls on groundwater occurrence in a hard rock region." *Applied Water Science* 7(3): 1377-1389.
- Rao, B. V. and B. Briz-Kishore (1991). "A methodology for locating potential aquifers in a typical semi-arid region in India using resistivity and hydrogeologic parameters." *Geoexploration* 27(1-2): 55-64.
- Razandi, Y., H. R. Pourghasemi, N. S. Neisani and O. Rahmati (2015). "Application of analytical hierarchy process, frequency ratio, and certainty factor models for groundwater potential mapping using GIS." *Earth Science Informatics* 8(4): 867-883.
- Rehman, H. U., Z. Ahmad, A. Ashraf and S. S. Ali (2019). "Predicting groundwater potential zones in Upper Thal Doab, Indus Basin through integrated use of RS and GIS techniques and groundwater flow modeling." *Arabian Journal of Geosciences* 12(19): 1-13.
- Saaty, R. W. (1987). "The analytic hierarchy process—what it is and how it is used." *Mathematical modelling* 9(3-5): 161-176.
- Saaty, T. L. (1980). "The analytic hierarchy process McGraw-Hill." New York 324.
- Saaty, T. L. (2000). *Fundamentals of decision making and priority theory with the analytic hierarchy process*, RWS publications.
- Saaty, T. L. (2001). *Decision making for leaders: the analytic hierarchy process for decisions in a complex world*, RWS publications.
- Satty, T. (1990). "How to make a decisin: The Analytical Hierarchy Process."
- Shekhar, S. and A.C. Pandey, Delineation of groundwater potential zone in hard rock terrain of India using remote sensing, geographical information system (GIS) and analytic hierarchy process (AHP) techniques. *Geocarto International*, 2015. 30(4): p. 402-421.
- Thakur, D., S. Bartarya and H. Nainwal (2018). "Mapping groundwater prospect zones in an intermontane basin of the Outer Himalaya in India using GIS and remote sensing techniques." *Environmental Earth Sciences* 77(10): 1-15.
- Thapa, R., S. Gupta and D. Reddy (2017). "Application of geospatial modelling technique in delineation of fluoride contamination zones within Dwarka Basin, Birbhum, India." *Geoscience Frontiers* 8(5): 1105-1114.
- Tobore, A., et al., Geospatial Soil Suitability Assessment for Maize (*Zea mays*) Production in Derived Savanna of Agricultural Research and Training, OYO STATE, Nigeria. *Jordan Journal of Earth and Environmental Sciences*, 2023. 14(1).
- Verma, A. and T. Singh (2013). "Prediction of water quality from simple field parameters." *Environmental earth sciences* 69(3): 821-829.
- Ying, X., G.-M. Zeng, G.-Q. Chen, L. Tang, K.-L. Wang and D.-Y. Huang (2007). "Combining AHP with GIS in synthetic evaluation of eco-environment quality—A case study of Hunan Province, China." *Ecological modelling* 209(2-4): 97-109.

Dolomitization Model of the Lower Jurassic Sarki Formation Depending on Petrography and Carbon/Oxygen Isotopes, Northeastern Iraq-Kurdistan region

Bzhar A. Delizy¹, Waleed S. Shingaly², Sardar M. Balaky¹

¹ Department of Petroleum Geosciences, Faculty of Science, Soran University-Erbil, Kurdistan region, Iraq

² Department of Earth Science and Petroleum, College of Science, Salahaddin University-Erbil, Kurdistan region, Iraq

Received April 17th, 2023; Accepted Oct. 16th, 2023

Abstract

The shallow marine carbonate strata of the Lower Jurassic Sarki Formation are exposed at the northeastern limb of the Handreen and Spibalties anticlines in Rawanduz area, Kurdistan region, northeastern Iraq. The Sarki Formation is made up of light grey dolomitic limestone, dark grey dolomite, brecciated dolomite, grey brecciated dolomitic limestone, and thin-bedded dark grey marlstone. Based on the crystal size and geometry, five dolomite textures are identified, Dolomite-1: fine crystalline, planar-s (subhedral); Dolomite-2: fine to medium crystalline planar-e (euhedral); Dolomite-3: medium to coarse, planar-e (euhedral) to planar-s (subhedral) dolomites; Dolomite-4: coarse crystalline, planar-s (subhedral) to nonplanar-a (anhedral) dolomites; Dolomite-5: planar (subhedral) pore-filling dolomite cement. The Sarki dolomites have depleted values of $\delta^{18}\text{O}$ from Dolomite-1 to Dolomite-5. The notable decrease in $\delta^{18}\text{O}$ is due to an increase in the temperature of the dolomitization fluid relative to the increase of burial depth. Fine to medium crystalline dolomite is associated with the early stages of dolomitization, whereas coarse crystalline dolomite is associated with the late diagenetic stage. The petrographic study, that is, stable carbon and oxygen isotope analysis, suggests a sabkha and mixing zone models of the Sarki dolomites.

© 2024 Jordan Journal of Earth and Environmental Sciences. All rights reserved

Keywords: Dolomitization, Stable Isotope, Lithostratigraphy, Sarki Formation, Iraqi Kurdistan

1. Introduction

The shallow marine Sarki Formation is a carbonate succession outcropping in the north and northeastern Iraq. It was deposited in an intertidal-supratidal setting (Delizy and Shingaly, 2021). It was first defined by Dunnington (1952) in (Bellen et al., 1959) from Chia Gara mountain, south of Amadyia, northern Iraq, which constitutes a part of the Arabian Plate (AP 6) tectonostratigraphic megasequence that ranges from middle Permian to middle Jurassic (Sharland et al., 2001). The lateral equivalent of the Sarki Formation in central Iraq is the Butma Formation. The thickness of the formation varies from one place to another. At the type locality, the thickness is estimated to be 300m: the upper part is 180m, and the lower part is 120m (Buday, 1980). The thickness of the studied sections is 176m in the Warte section, and 115m in the Zarwan section. Lithologically, the Sarki Formation is composed of dolomites and brecciated dolomites in the upper part with some ghosts of bivalves and ostracods. The lower part of the formation consists of brecciated dolomitic limestones, interbedded with marly thin beds in the middle part. The lower contact of the Sarki Formation is gradational with the Baluti Formation, and the upper contact is conformable with Sehkanian Formation (Jassim and Goff, 2006). The lower boundary of the Sarki Formation in the Zarwan section is not exposed.

The Sarki Formation outcrops of Northern Iraq were investigated by Bellen et al., (1959), Buday (1980), Surdashy

(1999), Jassim and Goff (2006), AL- Badry (2012), AL-Jboury and Mccann (2013), Delizy and Shingaly (2022), and Omar (2022). The main aim of the current study is to describe the dolomite textures, the dolomitization model, and the origin of the dolomites based on the isotopic analysis and petrographic study.

2. Geologic Setting

The Sarki Formation is well exposed in the core and limbs of several anticlines in the imbricated and Northern thrust zone of Iraq. During the Middle Permian to Triassic and Jurassic periods, breaking off north and northeast microplates of the Arabian portion of Gondwana land occurred due to the active extinction and rifting (Alsharhan and Nairn, 2003). The opening of the Neo-Tethys ocean involved two stages. The first one started during the Permian and Triassic periods when the Iranian Plate (microplate) began to move towards the Eurasian Plate away from the Arabian Plate. The next stage occurred as the Neo-Tethys reached its greatest width of 4000 km during the Late Triassic to Middle Jurassic periods (Sadooni and Alsharhan, 2004).

The platform part of the Iraqi territory is separated into two main units: a stable and an unstable shelf (Buday, 1980). The stable shelf is characterized by a relatively thin sedimentary cover and a lack of significant folding (Al-Ghreri et al., 2018). The unstable shelf has a thick and folded sedimentary cover, and the intensity of the folding increases toward the northeast (Al-Juboury et al., 2023). During the

* Corresponding author e-mail: bzhar.kheder@soran.edu.iq

present work, two outcrops were measured in the imbrication zone in northern Iraq. The Warte section is located 3 km to the south of Warte town, close to the Karukh Mountain, and approximately 39 km to the east and southeast of Rawnduz district within the Erbil Governorate (Lat. $36^{\circ} 28' 24''$ N and Long. $44^{\circ} 45' 14''$ E), whereas the Zarwan section was chosen in Zarwan village, which is located 500m to the north of the Zarwan village, about 15 km in northeastern Rawanduz district in Erbil Governorate (Lat. $36^{\circ} 38' 44''$ N and Long. $44^{\circ} 39' 53''$ E) (Fig. 1).

Structurally, the Sarki Formation in Warte section is located in the core of Handreen anticline in the imbrication zone (Fig. 2). The Handreen anticline is asymmetrical: the fold axis is trending NW-SE and plunging in the NW, and its length is around 30 km. The NE limb dips steeply, and the SW limb dips gently at 40° approximately. The Zarwan section is exposed at the northeastern limb of asymmetrical Spibalies anticline, with fold axis trending NW-SE (Balaki, 2004). The anticline is doubly plunging around 26 km length, the NE limb steep dips angle, and the SW limb dips 50° approximately (Delizy and Shingaly, 2022).

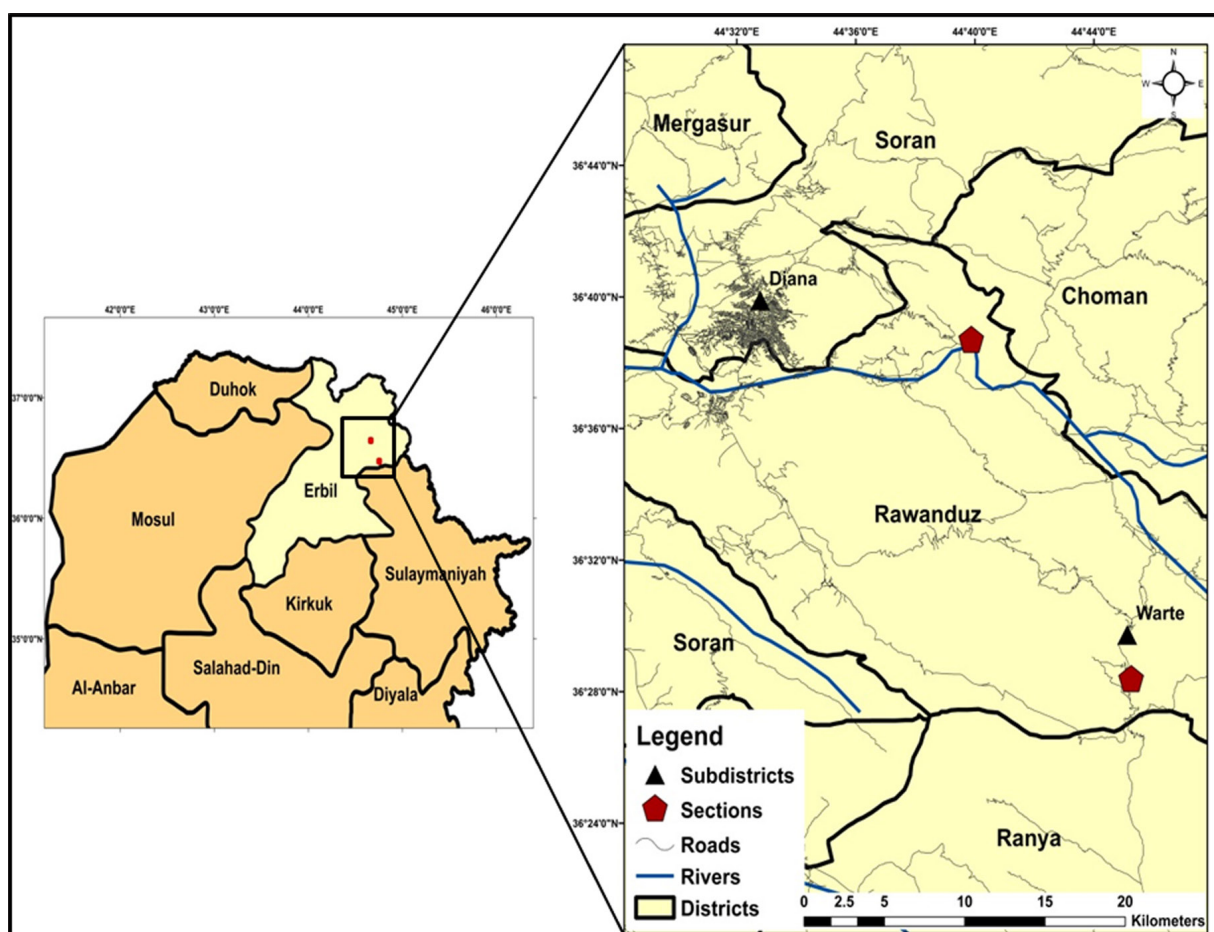


Figure 1. Location map of the studied sections.

3. Materials and Methods

The selected outcrops around the imbrication zone were described and measured in detail in terms of lithology, sedimentary structures, and mineralogy. A total of ninety samples were collected from the two studied sections. 80 samples belonged to the Sarki Formation, and other several samples crossed the contacts of the underlying Baluti Formation and the overlying Sehkanian Formation. Samples were taken perpendicularly to the beds' strikes. The interval between samples is generally determined by changes in the lithology and color. All of the beds have been measured and lithologically described. A total of 80 thin sections were prepared in the workshop of Scientific Research Center, Soran University. For each sample, at least one thin section was prepared. The thin sections were

marked, using Alizarin Red Solution (ARS) to differentiate calcite from dolomite minerals according to the procedure suggested by Friedman (1959). To identify the relationships between dolomite fabrics and type of dolomite, scanning electron microscopy was used in the scanning lab of Scientific Research Center of Soran University. For the classification of dolomite textures, the work of Sibley and Gregg (1987) is used to describe different dolomite fabrics based on the microscopic and scanning electron microscope. Twenty samples of the carbonates of Sarki Formation from the two studied sections are chosen for stable carbon and oxygen isotope in order to determine the origin of dolomite. The C and O isotope analyses, employing the conventional digestion method, were performed at the Cornell Isotope Laboratory (COLL), Cornell University, New York, USA.

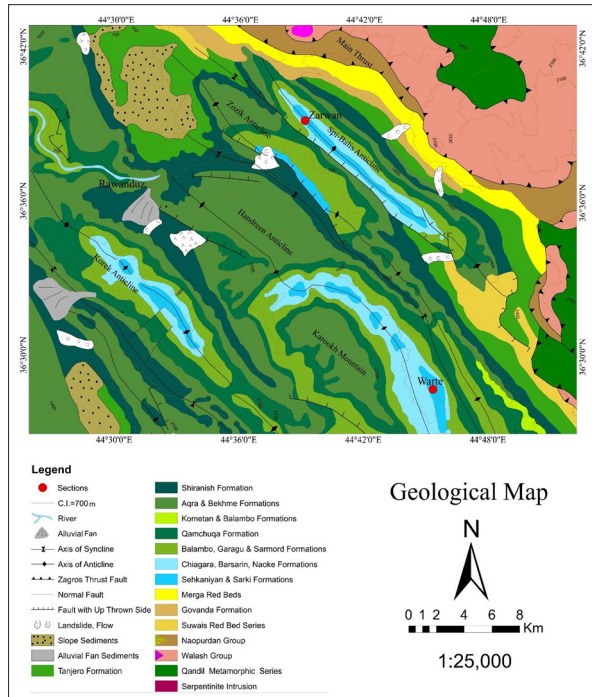


Figure 2. Geological map of the studied area (modified from Abdula et al., 2021).

4. Results and Discussion

4.1. Lithostratigraphy

The total thickness of Sarki Formation in the Warte section is 176 meters thick, and it is 115 meters thick in the Zarwan section. The formation consists of dolomitic limestone, dark grey dolomite, thick-bedded brecciated dolomitic limestone and brecciated dolomite with thin-bedded marlstones. Based on the field observations and petrographic analysis, the Sarki Formation can be subdivided into three lithostratigraphic units: Lower unit (A), Middle unit (B), and Upper unit (C) (Figs. 3 and 4).

A- Lower unit (Thick-bedded brecciated dolomitic limestone)

This unit is overlying the Baluti Formation and is underlying the medium to thick bedded dolomitic limestone and marl (unit B) in Warte section. while in Zarwan section, the lower part of this unit is covered by slope deposits. In Warte section, this unit consists of brecciated dolomitic limestone and dolomitic limestone, but in Zarwan section, it is mostly composed of brecciated dolomitic limestone (Fig. 5a). The thickness of this unit is approximately 40m in Warte section and 30m in Zarwan section. It consists of 40-100cm massive, grey to light grey brecciated dolomitic limestone (Fig. 5b). This unit represents the lower part of the Sarki Formation.

B- Middle unit (Medium-to-thick bedded dolomitic limestone and thin marl)

This unit overlies the thick bedded brecciated dolomitic limestone and is overlain by the medium to thick bedded

dolomite. The unit is the thickest among the other units of the studied formation. It is about 80m thick in Warte section and 50m in Zarwan section. It is composed of medium to thick bedded, yellowish grey dolomitic limestone which is interbedded with thin grey marly beds, most precisely to the lower part of the unit (Fig. 6a). The marl in this unit is commonly compacted between hard beds of dolomitic limestone particularly in the Zarwan section (Fig. 6b). The dolomitic limestone beds have a thickness of (5-60cm), and the beds of marl range from 2-15cm in thickness.

C- Upper unit (Thick bedded dolomite and medium-to-thick bedded brecciated dolomite)

The upper unit (Unit C) forms the upper part of the Sarki Formation in the two studied sections. The unit has a thickness of 55m in Warte section and 35m in Zarwan section. It can be separated into lower and upper parts. The lower part of this unit in Warte section is about 25m, and it consist of thick 20-80cm grey brecciated dolomite (Fig. 6c). The lower part in this unit is overlain by thick bedded of dolomite and underlain by medium to thick beds of dolomitic limestone. The upper part of this unit is 30m and consists of thick beds 40-100cm of grey to dark grey dolomite and is overlain by massive and thick beds of dolomitic limestones of Sekhanyian Formation from the two studied sections (Fig. 6d).

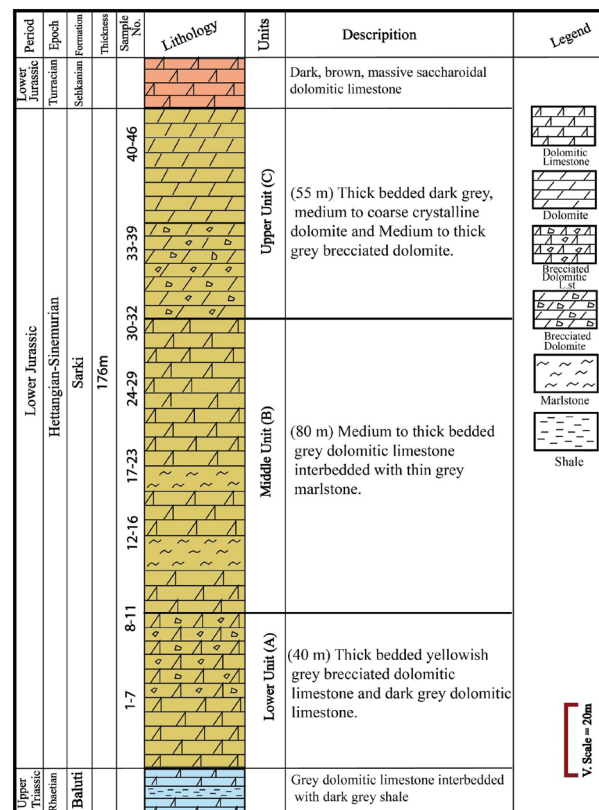


Figure 3. Stratigraphic column of the Sarki Formation, Warte section. Northern Iraq.

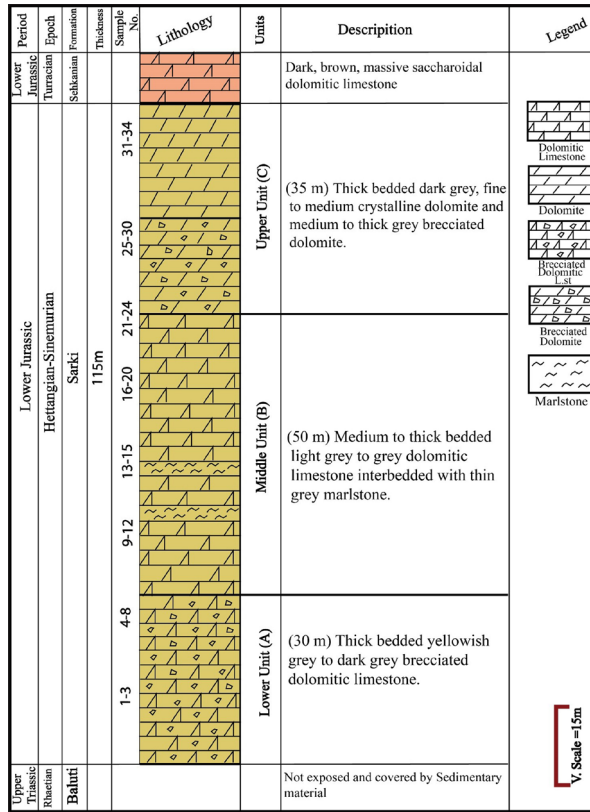


Figure 4. Stratigraphic column of the Sarki Formation, Zarwan section, Northern Iraq.



Figure 5. Field photographs showing: (a) The lower contact separating the Sarki Formation and the underlying Baluti Formation in Warte section marking the brecciated dolomitic limestone of the Lower unit (A). (b) The lower unit of the Sarki Formation in the Zarwan section showing the brecciated dolomitic limestone.

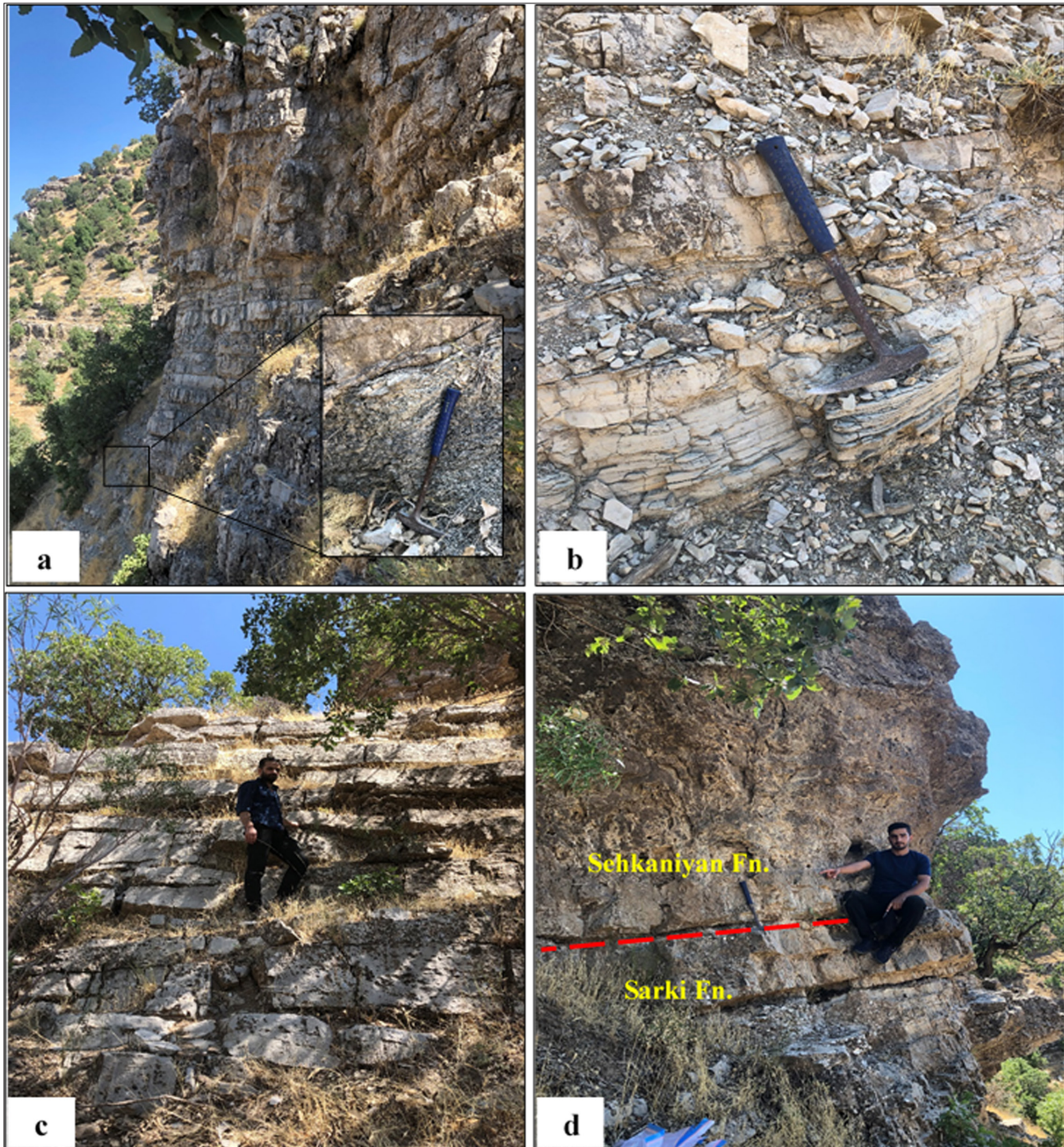


Figure 6. Field photographs showing: (a) Light grey dolomitic limestone interbedded with grey marl from the middle unit, (B) of Sarki Formation, (b) Thin marly beds between hard dolomitic limestones at the middle unit (B), (c) Thick bedded of grey to dark grey brecciated dolomite from upper unit (C) of the Sarki Formation, (d) The upper contact of the Sarki Formation underneath the Sehkaniyan Formation in Warte section, and showing the thick dolomite beds of Sarki Formation which is overlain by the massive saccharoidal dolomitic limestone of Sehkaniyan Formation.

4.2. Dolomite types

By using the petrographic microscope, SEM, stable isotope analysis, crystal size distribution, boundary shapes (planar and non-planar), and according to the classification scheme of Sibley and Gregg (1987), five dolomite textures have been recognized and classified in the Sarki Formation from the two studied sections. The time of dolomitization is determined based on crystal size (fabric) and $\delta^{18}\text{O}$ isotopic composition of different types of dolomite. The carbon and oxygen isotopes for different types of dolomite are plotted in Fig. 7, Table 1.

1- Fine crystalline, planar-s (subhedral) dolomite (Dolomite type 1)

Fine crystalline dolomicrite to dolomicrosparite ranges in size from 10 to 35 μm (with an average of 20 μm) and is typically characterized by planar-s (subhedral) mosaic with regular intercrystalline boundaries in micritic groundmass (Fig.8 a, b). Dolomite type 1 is developed under near-surface low temperatures during an early diagenetic stage, indicating a supratidal to upper intertidal environments (Machel, 2004). Dolomite type 1 is characterized by a dense and fine texture of dolomitized mudstone, lacking allochems and porosity. The crystal size is usually used to determine boundaries between early and late diagenetic dolomite phases (Gregg and Sibley, 1984; Wright, 2001). This type of dolomite is the most commonly studied succession and is widely distributed

in the lower and middle parts of the Warte section. Dolomite 1 is a microcrystalline dolomite (dolomicrite), having $\delta^{18}\text{O}$ and $\delta^{13}\text{C}$, and ranges from (-1.88‰ to -2.33‰) and (-0.89‰ to 2.75‰) respectively. The high micrite content indicates an early stage of dolomitization. The $\delta^{18}\text{O}$ values in this type of dolomite are less negative and not heavier than those of other dolomite types which indicate a low temperature and shallow burial depths during the earliest stages (Schidlowski, 2000).

2- Fine to medium crystalline planar-e (euhedral) to planar-s (subhedral) dolomite (Dolomite type 2)

This type of texture is characterized by a mixed distribution of fine and medium dolomite crystal sizes with a dense crystalline mosaic. The fine crystals component is subhedral to euhedral planar-s crystal shape, and the medium dolomite crystals component is commonly euhedral and ranges in size from 20-80 μm (average: 60 μm) (Figs. 8c, d). Commonly, this type shows a cloudy texture and represents the end of early to intermediate diagenetic replacement dolomites. Dolomite type 2 is observed in the lower and middle parts of the Sarki Formation in the Warte section, and the middle part of the Zarwan section. The $\delta^{18}\text{O}$ of this type of dolomite ranges from (-2.40‰ to -2.61‰), and the $\delta^{13}\text{C}$ ranges from (-1.12‰ to 2.80‰). The $\delta^{18}\text{O}$ of dolomite 2 is more depleted than dolomite 1, indicating that dolomite 2 has generated at early to intermediate stages with increasing temperatures. Dolomite 2 represents fine to medium crystalline dolomite texture. The increase in crystal size from fine to medium indicates the early and shallow burial diagenesis.

3- Medium to coarse, planar-e (euhedral) to planar-s (subhedral) dolomite (Dolomite 3)

This type of dolomite is common in the middle part of the Zarwan section and consists mainly of medium to coarse, planar-e (euhedral) to planar-s (subhedral) crystals. It ranges from 80- 300 μm (Fig. 8, e). The voids and spaces between crystals are mostly infilled by bitumen, and fractures are infilled by cement. This texture type is dominantly formed in an intermediate diagenetic stage during a high rate of burial temperatures. It resulted in the recrystallization of finer dolomites during burial or near the surface meteoric zone and in the mixed marine-meteoric zone too. The results of stable carbon and oxygen isotope analysis show that the $\delta^{18}\text{O}$ for dolomite 3 ranges from -2.55‰ to -7.39‰, whereas $\delta^{13}\text{C}$ ranges from -2.03‰ to 1.48‰. This type is related to the presence of chemical solution (stylolites). The $\delta^{18}\text{O}$ in dolomite type 3 is lighter than it is in types 1 and 2 dolomites, but it is heavier than dolomite types 4 and 5. The oxygen isotope of the dolomite 3 is more negative and indicates an increasing degree of temperature and depth of burial.

4- Coarse crystalline, planar-s (subhedral) to nonplanar-a (anhedral) dolomite (Dolomite type 4)

This type of dolomite is composed of dense, clear boundaries and close-packed coarse crystals, ranging in size

from (200-500 μm). Two different crystal shapes of dolomite 4 are observed: planar-s (subhedral) type and nonplanar-a (anhedral) type (Fig. 8f). In the Sarki Formation; this type of dolomite is observed in the middle part of the Zarwan section and indicated development in deep burial during the late diagenetic stage. The $\delta^{18}\text{O}$ value of dolomite 4 is -3.82‰, and the $\delta^{13}\text{C}$ value is -1.23‰. Dolomite type 4 has more depleted $\delta^{18}\text{O}$ values, compared to other types of dolomite. The coarse crystals' size and the more negative oxygen isotope of $\delta^{18}\text{O}$ are indicators of temperature increase and deep burial.

5- Planar (subhedral) void-filling dolomite cement (Dolomite type 5)

This type of dolomite consists of coarse crystals, pores filling, milky clusters, vugs, and fractures (Fig. 8g, h). Dolomite type 5 occurs in ghost filling of bioclasts and small veins, indicating a late stage of dolomitization. The crystals ranged in size from 100-600 μm , and their shapes refer to planar-s (subhedral) mosaic dolomite. It occurs in the upper part of the Sarki Formation in the Warte section, particularly, in the molds of bivalves and ostracods. The values of $\delta^{18}\text{O}$ and $\delta^{13}\text{C}$ for dolomite 5 are similar and nearly equal to dolomite 4 values which range between -3.86‰ and -0.17‰ respectively. The crystals' sizes and values of $\delta^{18}\text{O}$ for pore filling dolomite 5 are similar to those of dolomite 4 and may have occurred during the late deeper burial diagenesis stage compared to other types of dolomite.

Table 1. Carbon and oxygen isotopic ratios of dolomites sample of the Sarki Formation in the Warte and Zarwan sections.

Dolomite texture	Sample no.	$\delta^{18}\text{O}$ VPDB	$\delta^{13}\text{C}$ VPDB
Dolomite 1	W.S. 12	-2.04	2.75
	W.S. 30	-1.99	1.01
	W.S. 40	-2.08	-0.89
	Z.S. 14	-1.90	0.87
	Z.S. 24	-2.33	1.18
	Z.S. 30	-1.88	2.02
Dolomite 2	Z.S. 8	-2.45	-1.12
	Z.S.15	-2.51	-0.25
	W.S. 10	-2.40	1.03
	W.S. 11	-2.61	2.80
Dolomite 3	W.S. 22	-7.39	-3.32
	W.S. 28	-3.17	1.30
	W.S. 31	-3.31	-0.76
	W.S. 32	-3.62	-1.07
	W.S. 34	-4.07	0.91
	Z.S. 16	-2.64	0.52
	Z.S. 17	-2.93	-2.03
	Z.S. 28	-2.55	1.48
Dolomite 4	W.S. 23	-3.82	-1.23
Dolomite 5	W.S. 46	-3.86	-0.17

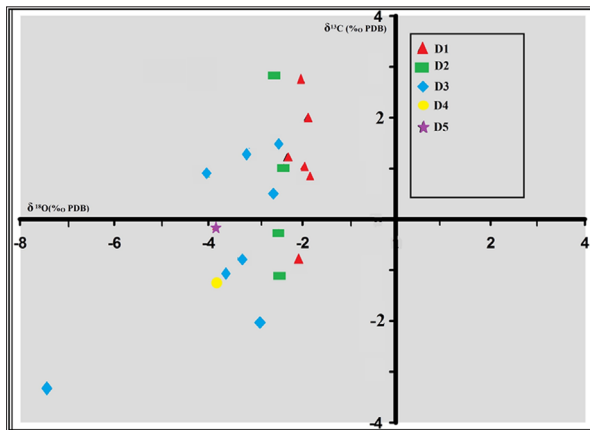


Figure 7. Plot of $\delta^{18}\text{O}$ and $\delta^{13}\text{C}$ values of the different types of dolomite in Sarki Formation.

4.3. Dolomitization stage

Delizy and Shingaly (2022) indicated that the the Sarki Formation was deposited in peritidal shelf lagoon and shoal environments. The presence of micrite and rims of skeletal and non-skeletal grains indicates an early diagenetic stage. The sediments in the studied sections are mostly affected

by different types of marine and meteoric cementation before reaching the burial environments. Depending on the petrographic, stable carbon and oxygen isotope analysis of different types of dolomite, the time of diagenesis can be determined (Fig. 9). Fine crystalline dolomite (dolomite type 1) is formed under the near surface (shallow burial) and low-temperature degree in the supratidal environment, whereas the depleted values of $\delta^{18}\text{O}$ and sizes of crystals in type 2 dolomite suggest that this type is formed in shallow burial depths. Dolomite type 3 is characterized by planar crystal boundaries and more depleted $\delta^{18}\text{O}$ than dolomite types 1 and 2. This result indicates a formation in the early to late stages of burial. Dolomite types 4 and 5 have more depleted $\delta^{18}\text{O}$ and coarser crystal sizes, indicating the advanced stage of diagenesis and the formation under high rate of temperature and deep burial.

Both early and late stages of dolomitization are noticed in the Sarki Formation in which the early diagenetic dolomitization is characterized by fine crystalline dolomites while coarse crystalline types indicate a late diagenetic dolomitization.

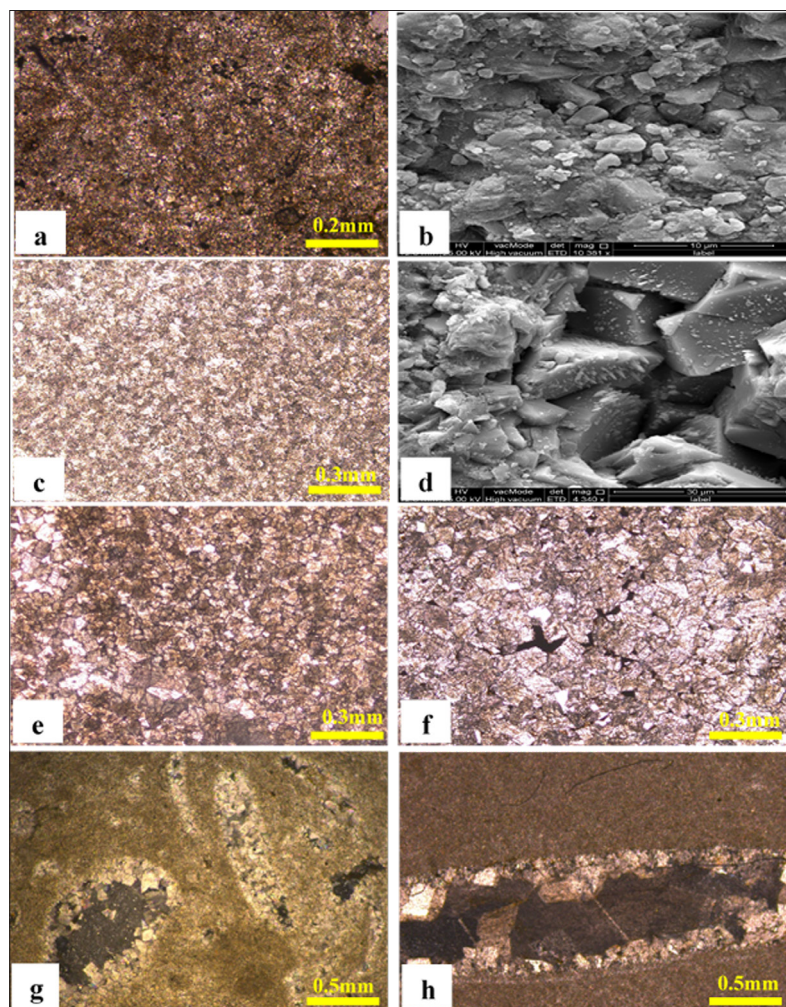


Figure 8. Photomicrographs of Sarki Formation dolomites: (a) Fine crystalline planar-s (subhedral) dolomite 1, ZS. 24, P.P. (b) SEM image of fine crystalline planar-s (subhedral) dolomite 1, WS. 40 (c) Fine to medium crystalline planar-e (euhedral) to planar-s (subhedral) dolomite 2, WS. 10, P.P. (d) SEM image of fine to medium crystalline planar-e (euhedral) to planar-s (subhedral) dolomite 2, WS. 11 (e) Medium to coarse, planar-e (euhedral) to planar-s (subhedral) dolomite 3, WS. 22, P.P. (f) Coarse crystalline, planar-s (subhedral) to nonplanar-a (anhedral) dolomite 4, WS. 23, P.P. (g) Planar (euhedral) to planar (subhedral)-filling dolomite cement, dolomite 5, WS. 46, P.P. (h) Planar (euhedral) to planar (subhedral) void-filling dolomite cement, ZS. 23, P.P.

WS: Warte –Sarki, ZS: Zarwan-Sarki, P.P: Plane Polarized light. X.N: Crossed Nichol

4.3.1. Early diagenetic dolomitization

The dolomitization in the Sarki Formation is of an early diagenetic type and is characterized by fine crystals. The crystal size ranges from 10 to 100um and has a planar-e to planar-s morphology. It includes the textures of dolomite type 1, dolomite type 2, and medium size of dolomite type 3. It is supposed that these dolomite types were developed under shallow burial and probably during the mixing of a meteoric phreatic wedge with marine water (Machel, 2004). This type of dolomitization is more common in all parts of the Sarki Formation in the Warte section, but it is more common in the lower part of the Zarwan section.

4.3.2. Late diagenetic dolomitization

The late diagenetic dolomitization is characterized by a coarse crystalline dolomite mosaic of planar-e to planar-s fabrics of coarse crystal size dolomite 3 and dolomite 4. Most coarse crystalline dolomite in this stage developed in the fractures and moldic ghosts (dolomite type 5). The pore filling with euhedral, equant, and coarse dolomite crystals that increase in size inwards are more common. The coarse crystalline dolomite fabric, microfracture healing, and moldic pore-filling indicate late diagenetic events in a deep-burial environment (Amthor and Friedman, 1991; Machel, 2004). Late diagenetic dolomites are observed in the Sarki Formation, especially in the middle part of the Zarwan section and the upper part of Warte section.

Dolomite Textures	Stage of Diagenesis	
	Early Stage	Late Stage
Dolomite 1	██████████	
Dolomite 2	██████████	
Dolomite 3		██████████
Dolomite 4		██████████
Dolomite 5		██████████

Figure 9. Paragenetic sequence of different dolomite textures in the Sarki Formation.

4.4. Dolomitization Model

Dolomitization is a heterogeneous process, developed under various conditions and can be divided into two groups including primary and secondary dolomites (Pichler and Humphrey, 2001). Primary dolomites are precipitated directly while secondary dolomites are produced by the replacement process and are also called replacement dolomites (Machel, 2004).

Based on the detailed petrographic study of stable carbon and oxygen isotope analysis, the dolomites of the Sarki Formation are formed in two diagenetic environments: the Sabkha and the mixing zone (Fig. 10).

4.4.1. Sabkha model

The Sarki Formation is a shallow water carbonate succession, deposited in peritidal environments which include intertidal-supratidal subenvironments (Delizy and Shingaly, 2022). The $\delta^{18}O$ values of dolomicrite (dolomites 1), close to positive and fine crystal size of crystals (euhedral to subhedral rhombs), indicate a hypersaline environment. Based on petrographic data such as the fine crystalline texture, syndepositional dolomites and very early diagenetic dolomites are indicators of the Sabkha model

for dolomite 1. In terms of mechanism and hydrogeological circumstances, the Sabkha dolomitization is very similar to reflux dolomitization (Machel, 2004). This type of dolomite is characterized by a fine crystalline texture that is formed in shallow burial, low temperature, and saline environment. Moreover, the existence of fine-crystal dolomites in Sabkha fine-grained micritic sediments indicates appropriate locations for nucleation of coarser dolomite crystals (Sibley and Gregg, 1987). In shallow burial subsurface, dolomitizing fluids have been recharged through seawater flowing by tidal currents and a high rate of evaporation in supratidal and intertidal areas (Yoo and Lee, 1998).

4.4.2. Mixing zone model

In mixing zone model, the dolomitizing fluids are generated by mixing seawater and subsurface meteoric water. When CO_2 -saturated subsurface meteoric water is combined with seawater, the new solution is undersaturated in $CaCO_3$ and supersaturated in dolomites (Machel, 2004). Based on the stable isotopic analysis of different types of dolomite, it shows that the depleted $\delta^{18}O$ values and relatively light $\delta^{13}C$ values indicate dolomitization by mixing fresh and marine waters. Isotopic analysis of dolomite in the Sarki Formation shows more negative $\delta^{18}O$ and depleted values in $\delta^{13}C$ v (Table 1), hence the mixing between fresh and marine water is indicative of the mixing zone model for dolomitization of the Sarki Formation.

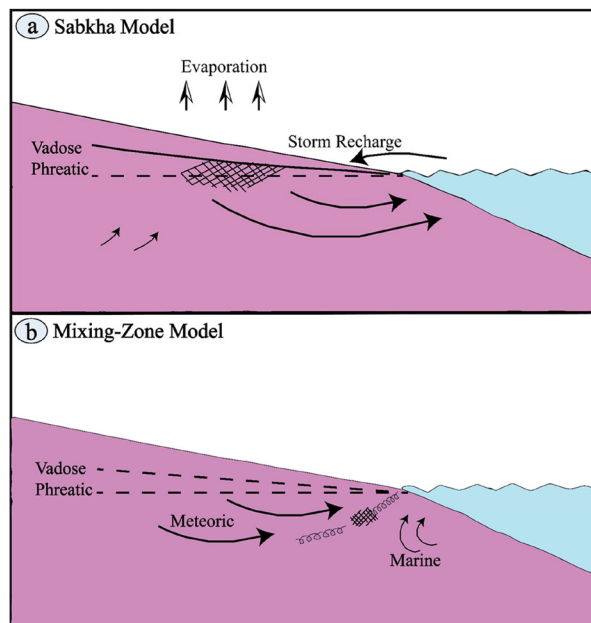


Figure 10. Dolomitization models of the Sarki Formation (after Warren, 2000).

5. Conclusions

It concluded that the Sarki Formation is composed of light grey dolomitic limestone, dark grey dolomite, brecciated dolomite, grey brecciated dolomitic limestone, and thin-bedded dark grey marlstone. The total thickness of the formation is 176 m in the Warte section and 115 m in the Zarwan section. Three different lithostratigraphic units were recognized through the petrographic study and field observation: thick-bedded brecciated dolomitic limestone, medium to thick-bedded dolomitic limestone and thin marl, and thick-bedded dolomite and medium to thick-bedded

brecciated dolomite.

In the Sarki Formation, there are five different dolomite rock textures: Dolomite 1 fine crystalline, planar-s (subhedral) dolomite, Dolomite 2 fine to medium crystalline planar-e (euhedral) dolomites, Dolomite 3 medium to coarse, planar-e (euhedral) to planar-s (subhedral) dolomites, Dolomite 4 coarse crystalline, planar-s (subhedral) to nonplanar-a (anhedral) dolomites, and Dolomite 5 planar (subhedral) pore-filling dolomite cement. Based on the stable oxygen isotope values of dolomite samples, the Sarki dolomites show depleted values of $\delta^{18}\text{O}$ from dolomite 1 to dolomite 5. This reduced value in $\delta^{18}\text{O}$ indicated a temperature increase of the dolomitization fluid that is related to increasing depth of burial from early diagenetic to late diagenetic stage. The Sarki Formation was associated to the Sabkha and mixing zone models, according to a detailed petrographic study and analysis of stable carbon and oxygen isotopes. Fine to medium crystalline dolomite (dolomite 1, dolomite 2 and medium crystalline dolomite 3) indicated an association with an early stage dolomitization while coarse crystalline dolomite (coarse crystalline dolomite 3, dolomite 4 and dolomite 5) indicated a late diagenetic stage.

6. Conflicts of interest

The authors declare no conflict of interest

References

- Abdula, R., Fatah, S., Salih, G., Mustafa, M., Ali, M. (2021). Source rock evaluation of the Chia Gara Formation in the Bekhme-1 well, Harir District, Kurdistan Region, Iraq. *Jordan Journal of Earth and Environmental Sciences (JJEES)*, 106.
- Al-Ghreri, M. F., AS, A. G., Abed, A. A. (2018). Microfacies analysis and paleoenvironment interpretation of Upper Oligocene Azkand Formation in western Iraq. *Jordan Journal of Earth and Environmental Sciences*, 9(3), 146-152.
- Al-Badry, A.M.S. (2012). Stratigraphy and geochemistry of Jurassic formations in selected sections-north Iraq, (Doctoral dissertation, College of Science, University of Baghdad).
- Al-Juboury, A., and Maccann, T. (2013). Petrological and geochemical interpretation of Triassic–Jurassic boundary sections from northern Iraq, *Geological journal*. 2013;1-16. DOI: 10.1002/gj.2537.
- Al-Juboury, A. I., Al-Auqadi, R. S., Al-Lhaebi, S. H., Rowe, H. D., Hussein, S. H. (2023). Anoxic Marine Conditions Recorded from the Middle Paleozoic Black Shales (Kaista and Ora formations), Northern Iraq: A multi-Proxy Approach. *Jordan Journal of Earth and Environmental Sciences (JJEES)*, 14(1), 50-63.
- Alsharhan, A.S., and Nairn, A.E.M. (1997). *Sedimentary basins and petroleum geology of the Middle East*. Elsevier.
- Amthor, J.E., and Friedman, G.M. (1991). Dolomite-rock textures and secondary porosity development in Ellenburger Group carbonates (Lower Ordovician), west Texas and southeastern New Mexico. *Sedimentology*, 38(2), pp.343-362.
- Balaki, H.G. (2004). Geometry and structural history of Zozik-Rola and Spi Balies-Mama Ruta structures of the Zagros fold thrust belt in NE Iraqi Kurdistan. Unpub. Thesis, University of Salahadin, Iraq. 103p.
- Bellen, R.C. Van, Dunnington, H.V., Wetzel, R., Morton, D. (1959). *Lexique Stratigraphique Internationa*, Vol. III, Asie, Fascicule 10a Iraq, Paris, 333p.
- Buday, T. (1980). *The Regional Geology of Iraq*, Vol. 1, Stratigraphy and Paleogeography, Dar Al-Kutub Publishing House, University of Mosul, Mosul, Iraq, 445p.
- Delizy, B.A., and Shingaly, W.S. (2022). Microfacies Analysis and Depositional Environment of Sarki Formation (Early Jurassic), Rawanduz Area, Kurdistan Region, Northern Iraq. *Tikrit Journal of Pure Science*, 27(1), pp.24-35.
- Dunnington H. V. (1958). Generation, migration, accumulation and dissipation of oil northern Iraq. In: Weeks GL (ed) *Habitat of oil, a symposium*. American. Association of Petroleum Geologists, Tulsa.
- Friedman, G.M. (1959). Identification of carbonate minerals by staining methods. *Journal of Sedimentary Research*, 29(1), pp.87-97.
- Gregg, J.M., and Sibley, D.F. (1984). Epigenetic dolomitization and the origin of xenotopic dolomite texture. *Journal of Sedimentary Research*, 54(3), pp.908-931.
- Jassim, S.Z., and Goff, J.C. (2006). *Geology of Iraq*: Dolin. Prague and Moravian Museum, Brno, Czech Republic, 5.
- Machel, H.G. (2004). Concepts and models of dolomitization: a critical reappraisal. *Geological Society, London, Special Publications*, 235(1), pp.7-63.
- Omar, N., McCann, T., Al-Juboury, A. I., Ustinova, M. A., Sharezwri, A. O. (2022). Early Jurassic–Early Cretaceous Calcareous Nannofossil Biostratigraphy and Geochemistry, Northeastern Iraqi Kurdistan: Implications for Paleoclimate and Paleocological Conditions. *Geosciences*, 12(2), 94.
- Pichler, T., and Humphrey, J.D. (2001). Formation of dolomite in recent island-arc sediments due to gas-seawater-sediment interaction. *Journal of Sedimentary Research*, 71(3), pp.394-399.
- Sadooni, F.N., and Alsharhan, A.S. (2004). Stratigraphy, lithofacies distribution, and petroleum potential of the Triassic strata of the northern Arabian plate. *AAPG bulletin*, 88(4), pp.515-538.
- Schidrowski, M. (2000). Carbon isotopes and microbial sediments. In *Microbial sediments* (pp. 84-95). Springer, Berlin, Heidelberg.
- Sibley, D.F., and Gregg, J.M. (1987). Classification of dolomite rock textures. *Journal of sedimentary Research*, 57(6), pp.967-975.
- Sharland, P.R., Archer, R., Casey, D.M., Davies, R.B., Hall, S.H., Heward, A.P., Horbury, A.D., Simmons, M.D. (2001). Arabian plate sequence stratigraphy. *GeoArabia* “, spec Publ 2, gulf PetroLink.
- Surdashy, A.M. (1999). Sequence stratigraphic analysis of the Early-Jurassic central and northern Iraq, (Doctoral dissertation, Science College, University of Baghdad).
- Warren, J. (2000). Dolomite: occurrence, evolution and economically important associations. *Earth-Science Reviews*, 52(1-3), pp.1-81.
- Yoo, C.M., and Lee, Y.I. (1998). Origin and modification of early dolomites in cyclic shallow platform carbonates, Yeongheung Formation (Middle Ordovician), Korea. *Sedimentary Geology*, 118(1-4), pp.141-157.

b-value Estimation and Extreme Magnitude Assessment in the Source Region of Past Earthquakes in Central Himalaya and Vicinity

Ram Krishna Tiwari*, Harihar Paudyal

Birendra Multiple Campus, Tribhuvan University, Bharatpur, Chitwan, Nepal

Received Dec. 21st, 2023; Accepted Jan. 9th, 2024

Abstract

The Gutenberg-Richter (GR) and Gumbel methodologies were applied to analyze seismic activity parameters (specifically, b-values) in the central Himalaya region, covering latitudes between 26° and 31° E and longitudes between 80° and 88° N during the time frame from 1964 to 2021. Additionally, Gumbel's techniques were utilized to gauge the frequency of occurrence for moderate-to-large magnitude earthquakes. Within a circular area with a diameter of 250 kilometers, we determined the b-values for the primary source regions of the ten past major earthquakes. The estimated b-value based on GR relation varies from 0.82 ± 0.06 to 1.02 ± 0.10 , whereas the b-value based on Gumbel's method ranges from 0.86 ± 0.30 to 1.88 ± 0.32 . The results indicate that Gumbel's distribution approach is effective for regions where large earthquake data is available, and the b-values, estimated from the GR method, are found to be more appropriate for the tectonics of the source regions. The Lo-Mustang earthquake region and Bajhang earthquake regions are identified as probable regions for the occurrence of a large earthquake in less than 100 years, which also supports the existence of a western Nepal seismic gap between Uttarakhand, India, and central Nepal. The findings describe the seismic risk in the epicenters of previous earthquakes in terms of b-value, recurrence intervals, and earthquake probability for each magnitude.

© 2024 Jordan Journal of Earth and Environmental Sciences. All rights reserved

Keywords: GR relation, Gumbel distribution, b-value, Central seismic gap

1. Introduction

The central Himalayan and adjoining region, delineated by latitude 26°–31°N and longitude 80°–88°E, has been considered as the study region. This region includes Nepal's entire territory and some parts of India and China. The region can be traditionally classified into distinct tectonic divisions when moving from south to north (Yin, 2006) (Figure 1). These divisions include the Sub-Himalaya, Lesser Himalaya, Higher Himalaya, and Tethyan Himalaya. They are demarcated by the presence of four significant east-west trending faults, namely the Main Frontal Thrust (MFT), the Main Boundary Thrust (MBT), the Main Central Thrust (MCT), and the South Tibetan Detachment System (STDS) (Thakur et al., 2019). Tanakpur Lineament (TL), Karnali Lineament (KL), and Samea Lineament (SL) are the transverse lineaments in western Nepal (Tiwari and Paudyal, 2023a). In contrast, Judi Lineament (JL), Thaple Lineament (TL), Kathmandu Lineament (KTML), Motihari-GauriShanker Lineament (MGL), Motihari-Everest Lineament (MEL), Arun Lineament (AL), and Kanchenjunga Lineament (KANL) are lineaments from central Nepal to eastern Nepal (Tiwari et al., 2022).

The central portion of the Himalayan Mountain range has witnessed a series of catastrophic earthquakes, as outlined in Table 1. One such event was the devastating 2015 Gorkha earthquake, which registered a magnitude of 7.8 on the Richter scale. This earthquake had profound impacts, resulting in approximately 9,000 fatalities and the destruction

of over fifty thousand structures, leading to substantial economic losses in the affected region (Bilham, 2019; Wyss and Chamlagain, 2019). While the Gorkha Earthquake was significant, it was smaller in magnitude, compared to the great earthquakes that have been anticipated in central Nepal (Bilham et al., 2017; Hussain et al., 2020; Morell et al., 2017). Puzzlingly, this event raised the probability of more catastrophic earthquakes, occurring in the future along the Himalayan orogenic belt.

The main objective of the present study is to estimate the b-value, using the Gutenberg-Richter (GR) and Gumbel methods, establishing a connection between b-values and tectonics, and determining earthquake recurrence probabilities in the central Himalayas and its surroundings.

B-value by Gutenberg-Richter

The b-value of GR relation (Gutenberg and Richter, 1944) is the slope of the equation

$$\log N(M) = a - bM \quad (1)$$

Where the seismicity metric $N(M)$ indicates the cumulative count of earthquakes that have a magnitude equal to or greater than the completeness threshold M , additionally, a metric "a" is used to quantify seismicity (Ahmed et al., 2021; Tiwari and Paudyal, 2022, 2021). Another important factor is known as the b-value, which quantifies the frequency of small and large earthquakes, occurring within a specific region (Ahmed et al., 2021; Amelung and King, 1997).

* Corresponding author e-mail: ram.tiwari@bimc.tu.edu.np

The b-value is influenced by various factors. For instance, an increase (or decrease) in stress applied to a geological volume will result in a corresponding decrease (or increase) in the b-value (Jordan et al., 2019; Schorlemmer et al., 2005; Wang et al., 2021; Wiemer and Wyss, 2002). The b-value is closely connected to various aspects of crustal deformation, including faulting, cracking, folding, and fracturing, as well as processes like liquid migration and magmatic intrusions (Chen et al., 2006; Numan and Ghaeb, 2019; Scholz, 1968; Tiwari and Paudyal, 2023a). It also exhibits associations with tectonic features and focal mechanisms, with distinct fault regimes corresponding to different b-values. Typically, in strike-slip faulting, the b-value is around 1.0, whereas in normal faulting, it tends to be greater than 1.0, and in thrust faulting regimes, it is usually less than 1.0 (Abed et al., 2023; Amelung and King, 1997; Gulia and Wiemer, 2010; Tiwari and Paudyal, 2022). Furthermore, the b-value is greater than one for earthquake swarms (Aswini et al., 2021; Tiwari and Paudyal, 2023b).

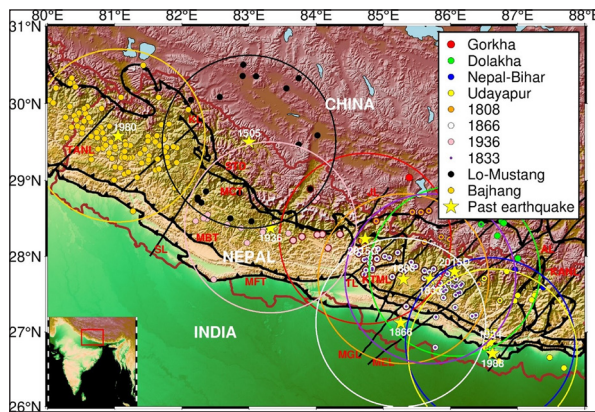


Figure 1. Tectonic map and source region of past earthquakes (yellow stars) inscribed by different colors circle. The center of the circle is at the epicenter location of earthquakes. MCT, MBT, and MFT are major thrust faults in the Himalayas, namely, Main Central Thrust, Main Boundary Thrust, and Main Frontal Thrust. TL, KL, and SL are Tanakpur Lineament, Karnali Lineament, and Samea Lineament, respectively. Other lineaments from central Nepal to eastern Nepal are Judi Lineament (JL), Thaple Lineament (TL), Kathmandu Lineament (KTML), Motihari-GauriShanker Lineament (MGL), Motihari-Everest Lineament (MEL), Arun Lineament (AL), and Kanchenjunga Lineament (KANL) (Öztürk et al., 2008; Shanker et al., 2007; Yadav et al., 2015).

B-value by the Gumbel method

Gumbel distribution is a probability distribution that models the maximum or minimum value of a set of random variables. In the context of earthquakes, it can be utilized to gauge the likelihood of the most significant seismic event that could occur within a specific region over a defined time. This probability estimation is directly derived from the premise that earthquakes originate from a straightforward Poisson process and adhere to the Gutenberg-Richter relation (Epstein and Lomnitz, 1966; Kijko and Ahjos, 1985). The earthquake distribution, based on the Gumbel distribution, is given as

$$G(M) = \exp(-\alpha e^{-\beta M}), M \geq 0 \quad (2)$$

The linear form of the equation is

$$\ln(-\ln G(M)) = \ln(\alpha) - \beta M \quad (3)$$

Where $G(M)$ represents the probability of earthquakes with magnitudes not exceeding M within a one-year

timeframe, α represents the average annual count of earthquakes with a magnitude greater than 0, while β stands for the reciprocal of the average magnitude of earthquakes occurring in the specific region under consideration. Finally, M denotes the magnitude or intensity of an earthquake event. The coefficients of GR law and Gumbel distribution could be related as the following:

$$\alpha = \frac{\ln \alpha}{\ln 10} \quad (4)$$

and

$$b = \frac{\beta}{\ln 10} \quad (5)$$

Finally, the cumulative count of earthquakes (N) can be expressed as

$$N = \alpha e^{-\beta M} = -\ln[G(M)] \quad (6)$$

(Epstein and Lomnitz, 1966; Ray et al., 2019)

Mean or average return period

The mean return period stands as a crucial hazard parameter for any given geographic area (Ahmed et al., 2016; Al-Tarazi and Qadan, 1997; Husein et al., 1995). It quantifies the average time interval, denoted as T in years between occurrences of earthquakes with a magnitude surpassing M and given by

$$T = \frac{1}{N} = e^{\beta M / \alpha} \quad (7)$$

2. Material and Methods

The analysis in this study covers a period of 57 years (1964-2021), which ensures the reliability of quantitative analysis. The earthquake data was obtained from the International Seismological Center (ISC) catalog, containing 3153 earthquakes (Di Giacomo et al., 2018, 2015). To ensure accuracy, the catalog was declustered using the Reasenber method (Reasenber, 1985) in ZMAP software (Wiemer, 2001) with specific parameters: a confidence limit of 0.95, minimum magnitude cutoff of 1.5, interaction radius factor of 10, epicenter error of 1.5, and depth error of 2. This process resulted in the identification of 76 earthquake clusters, and after declustering, 2571 earthquakes were retained for analysis. To assess the completeness of the data, the maximum likelihood method was used, revealing a completeness magnitude of 4.5 mb. Therefore, the final dataset includes 478 earthquakes, all with a magnitude equal to or greater than the completeness value of 4.5 (Figure 2).

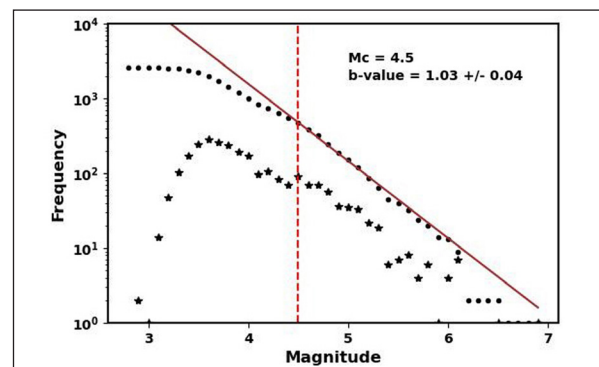


Figure 2. Magnitude of completeness (M_c) and b-value of frequency magnitude distribution where stars stand for non-cumulative frequency magnitude distribution. The b-value 1.03 ± 0.04 shows that the study area is seismically active (Ghosh, 2020; Hamdache et al., 2018).

3. Results and Discussions

To compare the effectiveness of the approach to reflect the tectonic characteristics of the study area, b-values for the specified region were calculated from two methods namely, the Gutenberg and Richter frequency magnitude relationship approach (Gutenberg and Richter, 1944). Gumbel's annual extreme values method (Öztürk et al., 2008; Yadav et al., 2015) and details are presented in Table 1.

Table 1. The estimates of the GR parameter and Gumbel parameter in the source regions of the central Himalayan and adjoining region.

SN	Source region	Epicenter		No. of events	GR parameter			Gumbel parameter			
		Longitude	Latitude		a-value	b-value	R ²	β -value	R ²	b-value	R ²
1	Lo-Mustang earthquake (1505)	82.00°E	30.00°N	20	3.87	0.95 ±0.16	0.89	2.71 ± 0.00	0. 72	1.18 ±0.00	0.72
2	1808 earthquake	86.63°E	26.71°N	66	4.03	0.87 ±0.09	0.68	2.26 ± 0.22	0. 58	0.98 ±0.10	0.58
3	1833 earthquake	85.70°E	27.70°N	72	4.09	0.88 ±0.08	0.68	2.36 ± 0.19	0. 58	1.02 ±0.08	0.58
4	1866 earthquake	85.26°E	27.12°N	55	4.61	1.02 ± 0.10	0.81	2.96 ± 0.28	0. 62	1.28 ±0.12	0.62
5	Nepal-Bihar earthquake (1934)	86.59°E	26.86°N	44	3.75	0.85 ±0.10	0.78	2.17 ± 0.30	0. 61	0.94 ±0.13	0.61
6	1936 earthquake	83.32°E	28.38°N	26	4.24	1.02 ±0.11	0.99	4.33 ± 0.74	0. 82	1.88 ±0.32	0.82
7	Bajhang earthquake (1980)	81.05°E	29.58°N	103	3.96	0.82 ±0.06	0.89	2.79 ± 0.68	0. 72	1.21 ±0.30	0.72
8	Udayapur earthquake (1988)	84.73°E	28.23°N	34	3.75	0.87 ±0.13	0.74	1.99 ± 0.69	0. 57	0.86 ± 0.30	0.57
9	Gorkha earthquake (2015)	84.73°E	28.23°N	47	3.88	0.88±0.1	0.66	2.17 ± 0.67	0. 56	0.94 ±0.29	0.56
10	Dolakha earthquake (2015)	86.06°E	27.80°N	70	4.23	0.91 ±0.08	0.87	2.94 ± 0.64	0. 68	1.28 ±0.28	0.68

The b-values in 10 regions are exhibited in Figure 3, in which b-value is represented by the slope of the red solid line. The legend box in each image depicts b-values with the corresponding standard deviation, magnitude of completeness (M_c), and coefficient of determination (R^2). Evidently, Figure 3 shows the different b-values in each, suggesting different evolutions of stress states in different places. The 1866 and the 1936 earthquake regions were registered as areas with b-values 1.02 ± 0.10 , and 1.02 ± 0.11 , respectively, close to the global mean value of 1.0, whereas other regions were characterized as having a b-value less than 1.0, as shown in Figure 3. This increase suggests that the 1866 and 1936 earthquake regions were seismically active while other regions having comparative low b-values were more prone to seismic activity.

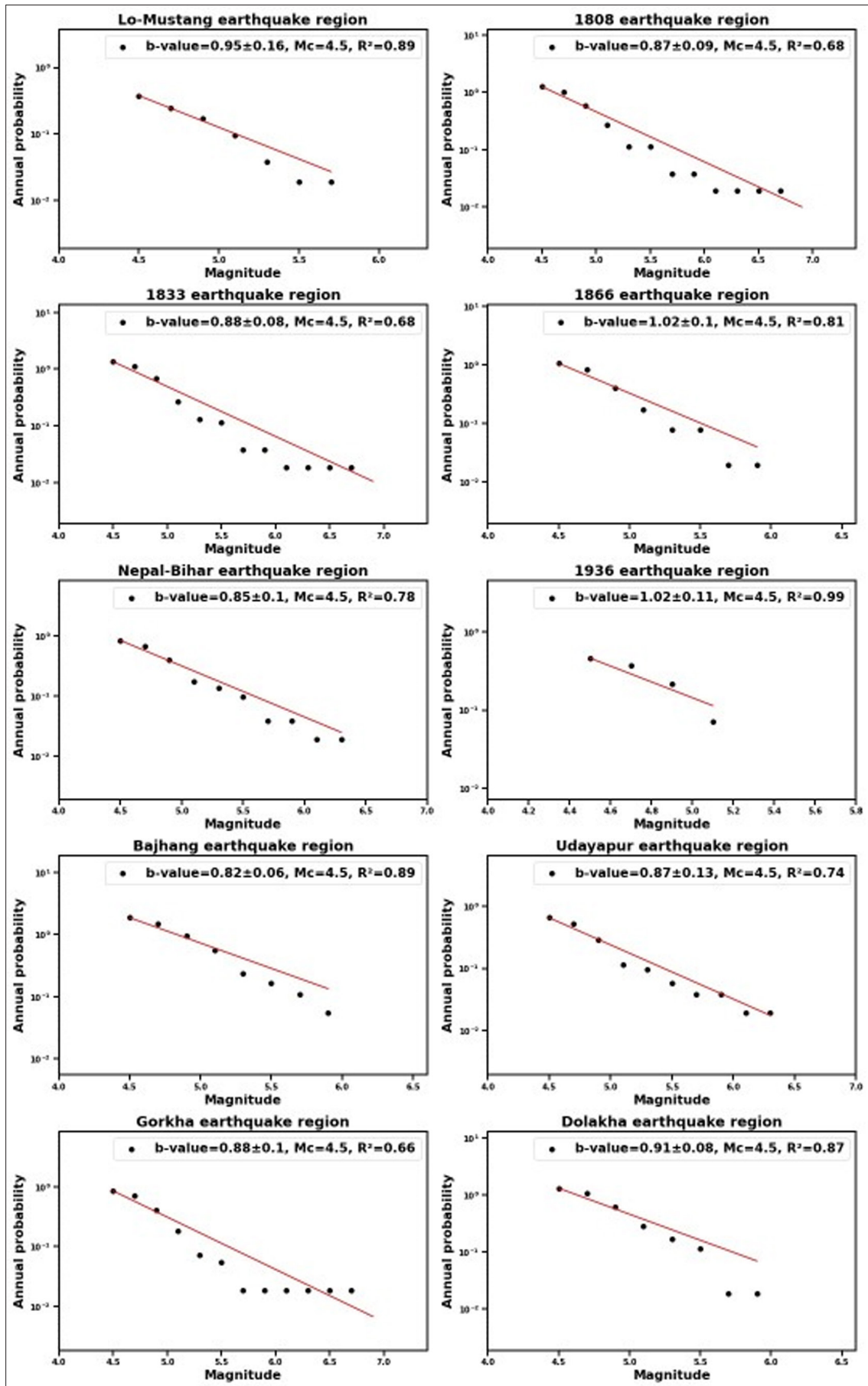


Figure 3. Frequency-Magnitude plot of the (a) Lo-Mustang earthquake region (b) 1808 earthquake region (c) 1833 earthquake region (d) 1866 earthquake region (e) Nepal-Bihar earthquake region (f) 1936 earthquake region (g) Bajhang earthquake region (h) Udayapur earthquake region (i) Gorkha earthquake region (j) Dolakha earthquake region

The highest β value (4.33 ± 0.74) or b value (1.88 ± 0.32) is observed in the 1936 earthquake region, while the lowest β value (1.99 ± 0.69) or b value (0.86 ± 0.30) is observed for Udayapur earthquake region (Figure 4). The subsequent high β values (2.96 ± 0.28) or b value (1.28 ± 0.12) are observed in the 1866 earthquake and Dolakha earthquake regions (2.94 ± 0.64 or 1.28 ± 0.28). The earthquake regions of Nepal-Bihar and Gorkha show similar values of $\beta = 2.17 \pm 0.30$ or b value = 0.94 ± 0.13 and $\beta = 2.17 \pm 0.67$ or b value = 0.94 ± 0.29 , respectively, revealing a parallel style of tectonic stress accumulation, coupled with a low frequency of earthquake

events. The source region of Lo-Mustang earthquake and Bajhang earthquake region show β value of 2.71 ± 0.00 or b value = 1.18 ± 0.00 and β value of 2.79 ± 0.68 or b value = 1.21 ± 0.30 , respectively. The source region of the 1808 earthquake and the 1833 earthquake show β value of 2.26 ± 0.22 or b value = 0.98 ± 0.10 and β value of 2.36 ± 0.19 or b value of 1.02 ± 0.08 , respectively. The variation in the estimated values, observed in our study, can likely be attributed to several factors, including disparities in earthquake data utilized for analysis, variations in the sizes of seismic zones, and differences in the applied analytical techniques.

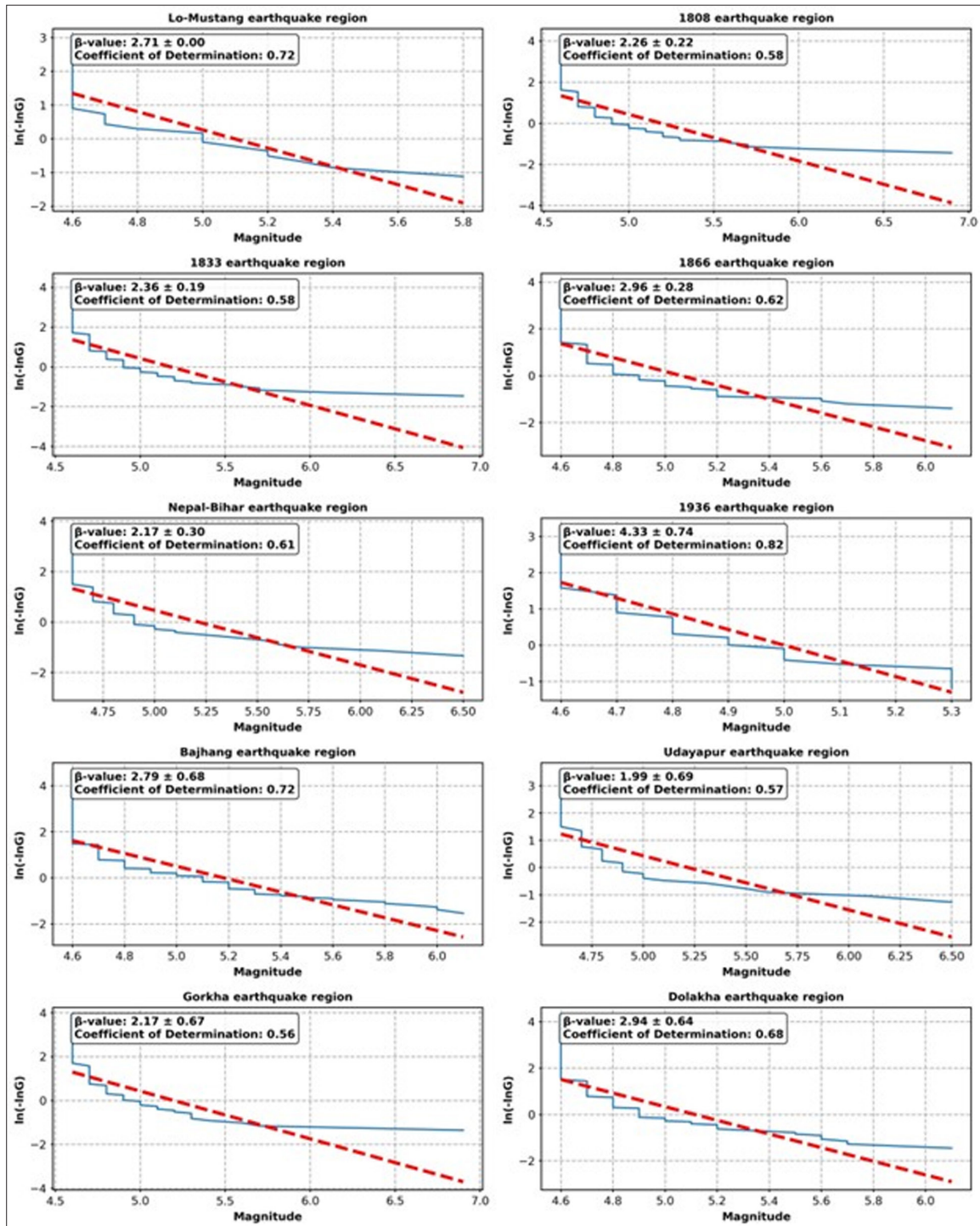


Figure 4. The Gumbel distribution characterization of the extreme values of the (a) Lo-Mustang earthquake region (b) 1808 earthquake region (c) 1833 earthquake region (d) 1866 earthquake region (e) Nepal-Bihar earthquake region (f) 1936 earthquake region (g) Bajhang earthquake region (h) Udayapur earthquake region (i) Gorkha earthquake region (j) Dolakha earthquake region.

The mean return period curves for 10 different regions are plotted in Figure 5. The 1808, 1833, 1866 the Nepal-Bihar, the Udayapur, the t and the Gorkha earthquake regions, exhibit a reduced likelihood of earthquake occurrences and extended return periods when compared to other zones, indicating a lower susceptibility to future moderate seismic events. The remaining regions are seismically active in terms of return periods. The mean return period for a magnitude 5.8 earthquake is estimated to be 85–90 years

in the Lo-Mustang region. A return period of around 12 years for magnitude 5.2 is expected for the 1936 earthquake region. A return period of around 90 years is expected for the Bajhang earthquake region, while a return period of more than 250 years is expected for magnitude 6 earthquakes in the Dolakha earthquake region. Observing the study region, it is evident that there are pockets of very high seismicity and other small areas of comparatively less activity.

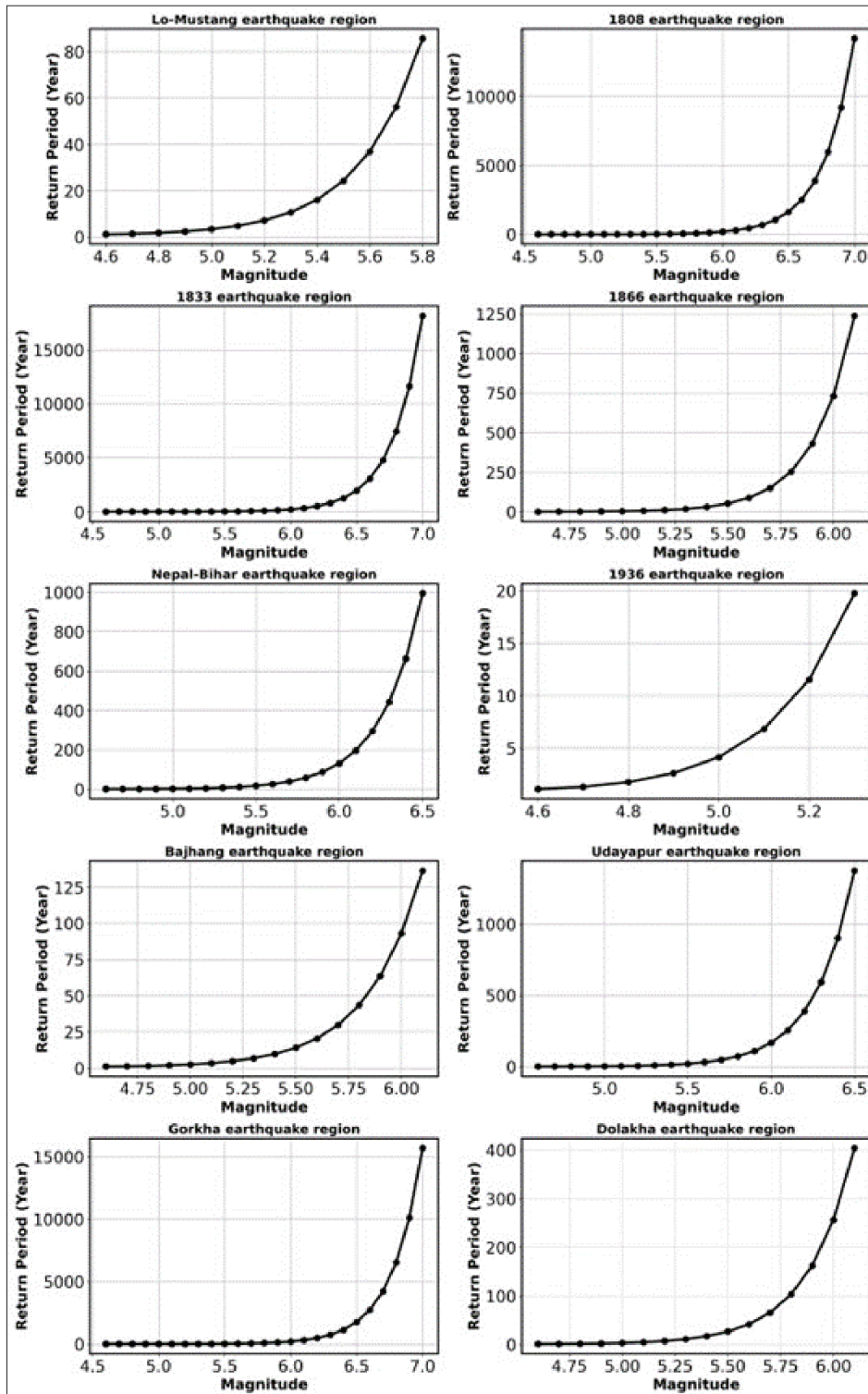


Figure 5. The average time intervals anticipated for specific magnitudes for (a) Lo-Mustang earthquake region (b) 1808 earthquake region (c) 1833 earthquake region (d) 1866 earthquake region (e) Nepal-Bihar earthquake region (f) 1936 earthquake region (g) Bajhang earthquake region (h) Udayapur earthquake region (i) Gorkha earthquake region (j) Dolakha earthquake region.

The exceedance curve $[1-G(m)]$ represents the annual probability of an earthquake magnitude (Figure 6) surpassing a given value across various seismic source regions. Figure 6 shows that the cumulative probability distribution for

exceedance, $1-G(m)$ of magnitudes ≤ 4.9 is greater than 50% and a distribution curve for non-exceedance is less than 50% for the regions considered.

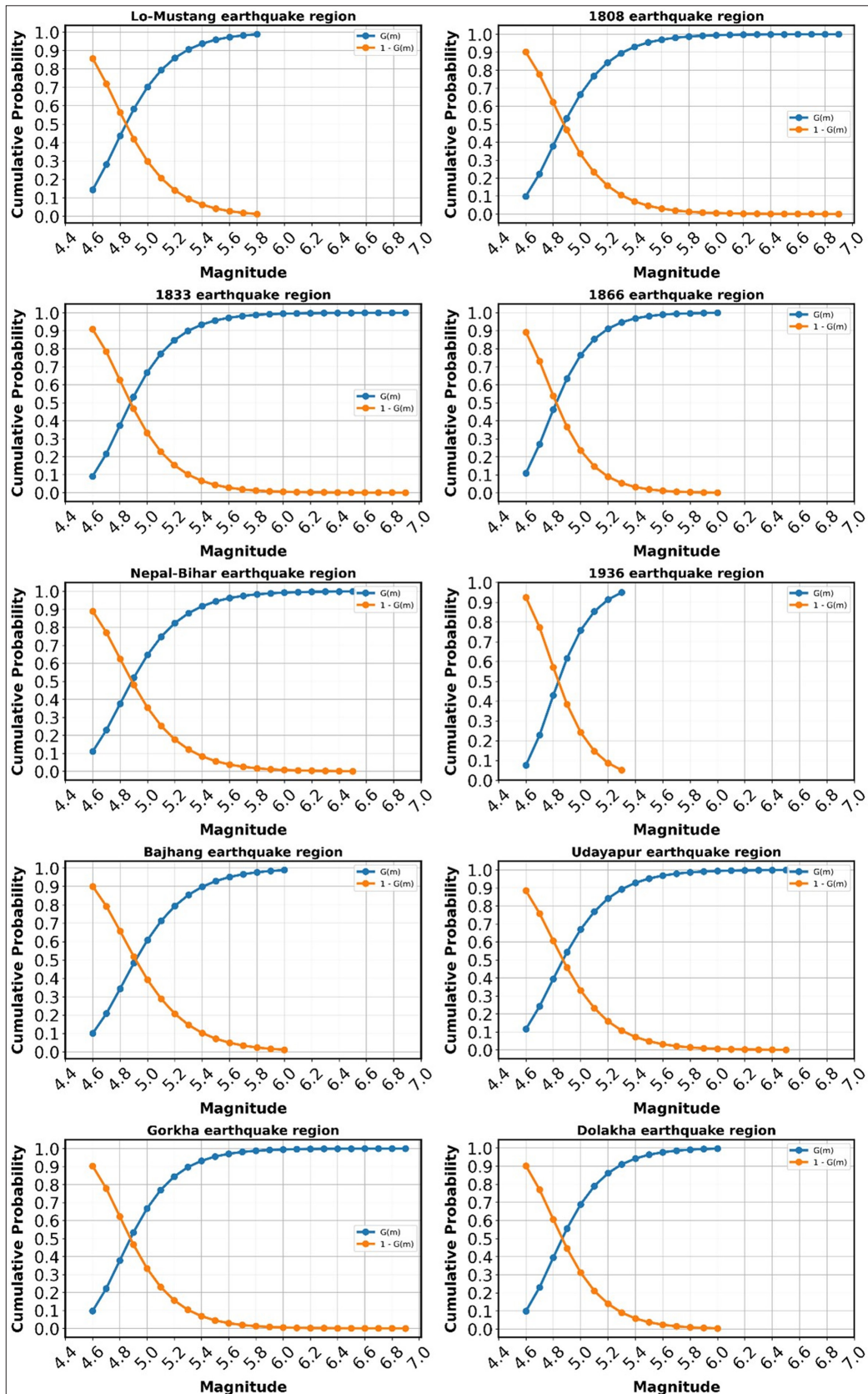


Figure 6. Probability of non-exceedance $[G(m)]$ and exceedance $[1-G(m)]$ for (a) Lo-Mustang earthquake region (b) 1808 earthquake region (c) 1833 earthquake region (d) 1866 earthquake region (e) Nepal-Bihar earthquake region (f) 1936 earthquake region (g) Bajhang earthquake region (h) Udayapur earthquake region (i) Gorkha earthquake region (j) Dolakha earthquake region.

In comparison to past research, the b-values were estimated in the ranges 0.88 to 1.08, 0.77 to 1.08, and 0.71 to 0.96 in the western, central, and eastern Nepal, respectively after 2015 Gorkha earthquake (Gunti et al., 2022). The study reveals that anticipated annual magnitude of the largest earthquakes in the Himalayan thrust zone are close to 5.5 (Yadav et al., 2011). Furthermore, it is estimated that the most probable annual earthquakes in the region 25°- 34°N and 73°- 85° E is 5.0 in magnitude with a probability of occurrence exceeding 50% annually (Shanker et al., 2007).

In conclusion, the b-values for the past 10 major earthquake source regions (central Himalaya and vicinity) are estimated through both GR relation and Gumbel's extreme value method. Furthermore, the return period of earthquake and assessment of extreme magnitude of the earthquake of same regions are estimated through Gumbel extreme value method. The estimated b-value through GR method varies from 0.82 ± 0.06 to 1.02 ± 0.10 whereas b-value through Gumbel's method ranges from 0.86 ± 0.30 to 1.88 ± 0.32 . The high b-value (1.88 ± 0.32), estimated for the 1936 earthquake region (Gumbel's method), does not seem suitable, which may be because of inadequate earthquake events and lack of historical data. In general, it can be concluded that the b-values, estimated using the Gutenberg-Richter (GR) approach, provide a more accurate reflection of the tectonic characteristics in the studied area, whereas Gumbel's distribution approach found effective for the regions where large events are available. Based on the findings, it can be inferred that both the Lo-Mustang and the Bajhang earthquake regions are potential locations for experiencing a significant earthquake in less than 100 years. These regions in a western Nepal seismic gap between Uttarakhand and central Nepal and has not been visited by a large earthquake since 1505.

Conflict of Interests

The authors declare no conflict of interest

References

- Abed, A.M., Al-Halboosi, J.M., Al-Jibouri, A.S., Al-Hetty, S. O. (2023). 2D Seismic Stratigraphic Analysis of Harthaand Kifl Formations in Balad Area- Center of Iraq. *Jordan Journal of Earth and Environmental Sciences*, 14(1):64–69.
- Ahmed, J., Javed, F., Zafar, W.A., Iqbal, T., Shah, M.A. (2021). Spatial variation of b-value, creep rate, and seismic moment release along Chaman fault system. *Arabian Journal of Geosciences*, 14:1623.
- Ahmed, N., Ghazi, S., Khalid, P. (2016). On the variation of b-value for Karachi region, Pakistan through Gumbel's extreme distribution method. *Acta Geodaetica et Geophysica*, 51:227–235.
- Al-Tarazi, E., and Qadan, H. (1997). Seismic hazard potential expected for the dams in Jordan. *Natural and Engineering Sciences*, 24(2).
- Amelung, F., and King, G. (1997). Earthquake scaling laws for creeping and non-creeping faults. *Geophysical Research Letters*, 24: 507–510.
- Aswini, K.K., Kamesh Raju, K.A., Dewangan, P., Yatheesh, V., Singha, P., Ramakrushana Reddy, T. (2021). Seismotectonic evaluation of off Nicobar earthquake swarms, Andaman Sea. *Journal of Asian Earth Science*, 221:104948.
- Bilham, R. (2019). Himalayan earthquakes: A review of historical seismicity and early 21st century slip potential. *Geological Society Special Publication*. 483:423–482.
- Bilham, R., Mencin, D., Bendick, R., Bürgmann, R. (2017). Implications for elastic energy storage in the Himalaya from the Gorkha 2015 earthquake and other incomplete ruptures of the Main Himalayan Thrust. *Quaternary International*, 462:3–21.
- Chen, C.C., Wang, W.C., Chang, Y.F., Wu, Y.M., Lee, Y.H. (2006). A correlation between the b-value and the fractal dimension from the aftershock sequence of the 1999 Chi-Chi, Taiwan, earthquake. *Geophysical Journal International*, 167:1215–1219.
- Di Giacomo, D., Bondár, I., Storchak, D.A., Engdahl, E.R., Bormann, P., Harris, J. (2015). ISC-GEM: Global Instrumental Earthquake Catalogue (1900-2009), III. Re-computed MS and mb, proxy MW, final magnitude composition and completeness assessment. *Physics of the Earth and Planetary Interiors*. 239:33–47.
- Di Giacomo, D., Robert Engdahl, E., Storchak, D. A. (2018). The ISC-GEM Earthquake Catalogue (1904-2014): Status after the Extension Project. *Earth System Science Data*, 10(4):1877–1899.
- Epstein, B., Lomnitz, C. (1966). A Model for the Occurrence of Large Earthquakes. *Nature*, 211:954–956.
- Ghosh, U. (2020). Seismic Characteristics and Seismic Hazard Assessment: Source Region of the 2015 Nepal Earthquake Mw 7.8 in Central Himalaya. *Pure and Applied Geophysics*, 177:181–194.
- Gulia, L., and Wiemer, S. (2010). The influence of tectonic regimes on the earthquake size distribution: A case study for Italy. *Geophysical Research Letters*, 37:1–6.
- Gunti, S., Roy, P., Narendran, J., Pudi, R., Muralikrishnan, S., Vinod Kumar, K., Subrahmanyam, M., Israel, Y., Satish Kumar, B. (2022). Assessment of geodetic strain and stress variations in Nepal due to 25 April 2015 Gorkha earthquake: Insights from the GNSS data analysis and b-value. *Geodesy and Geodynamics*, 13:288–300.
- Gutenberg, B., and Richter, C.F. (1944). Frequency of earthquakes in California. *Bulletin of the Seismological Society of America*. 34, 185–188.
- Hamdache, M., Peláez, J.A., Gospodinov, D., Henares, J. (2018). Statistical Features of the 2010 Beni-Ilmane, Algeria, Aftershock Sequence. *Pure and Applied Geophysics*, 175:773–792.
- Husein, A.I., Al-Homoud, A.S., Al-Tarazi, E., Nusier, O.K. (1995). Probabilistic seismogenic ground motion hazard assessment of Karak City in Jordan. *Environmental & Engineering Geoscience*. 1(2):207–218.
- Hussain, H., Shuangxi, Z., Usman, M., Abid, M. (2020). Spatial variation of b-values and their relationship with the fault blocks in the western part of the tibetan plateau and its surrounding areas. *Entropy*, 22(9).
- Jordan, N.W., Abutaha, S., Atallah, M., Abed, A. (2019). Structural Evolution of Wadi Hudaydun in Wadi Shueib Area, NW Jordan. *Jordan Journal of Earth and Environmental Sciences*, 10(3):152–160.
- Kijko, A., and Ahjos, T. (1985). Seismic hazard in Finland: evaluation of Mmax. *Geophysica*, 21(1):39-50
- Morell, K.D., Sandiford, M., Kohn, B., Codilean, A., Fülöp, R.H., Ahmad, T. (2017). Current strain accumulation in the hinterland of the northwest Himalaya constrained by landscape analyses, basin-wide denudation rates, and low temperature thermochronology. *Tectonophysics*, 721:70–89.
- Numan, N., and Ghaeb, F. (2019). Geological and Hydrogeological Implications of Gravity Data in the Agra

- Plain Iraqi Kurdistan Region. *Jordan Journal of Earth and Environmental Sciences*, 10(3):145–151.
- Öztürk, S., Bayrak, Y., Çınar, H., Koravos, G.C., Tsapanos, T.M. (2008). A quantitative appraisal of earthquake hazard parameters computed from Gumbel I method for different regions in and around Turkey. *Natural Hazards*, 47:471–495.
- Ray, S., Alam, M.J.B., Haque, M., Das, S.K., Tanmoy, B.B., Hasan, M.N. (2019). A study on b-value and investigation of seismic hazard in Sylhet seismic region, Bangladesh using Gumbel's extreme value distribution method. *SN Applied Science*, 1(5).
- Reasenberg, P. (1985). Second-order moment of central California seismicity, 1969-1982. *Journal of Geophysical Research Solid Earth*, 90:5479–5495.
- Scholz, C.H. (1968). The frequency-magnitude relation of microfracturing in rock and its relation to earthquakes. *Bulletin of the Seismological Society of America*, 58:399–415.
- Schorlemmer, D., Wiemer, S., Wyss, M. (2005). Variations in earthquake-size distribution across different stress regimes. *Nature*, 437:539–542.
- Shanker, D., Yadav, R.B.S., Singh, H.N. (2007). On the seismic risk in the Hindukush-Pamir-Himalaya and their vicinity. *Current Science*, 92:1625–1630.
- Thakur, V.C., Jayangondaperumal, R., Joevivek, V. (2019). Seismotectonics of central and nw himalaya: Plate boundary–wedge thrust earthquakes in thin-and thick-skinned tectonic framework. *Geological Society Special Publication*, 481:41–63.
- Tiwari, R.K., Paudyal, H. (2023a). Spatial mapping of b-value and fractal dimension prior to November 8 , 2022 Doti Earthquake, Nepal. *PLoS One*, 18:1–13.
- Tiwari, R.K., Paudyal, H. (2023b). Fractal Characteristics of the Seismic Swarm Succeeding the 2015 Gorkha Earthquake , Nepal. *Indian Geotechnical Journal*, 53:789–804.
- Tiwari, R.K., Paudyal, H. (2022). Frequency magnitude distribution and spatial correlation dimension of earthquakes in north-east Himalaya and adjacent regions. *Geologos*, 28:115–128.
- Tiwari, R.K., Paudyal, H. (2021). Statistics of the earthquakes in the central Himalaya and its vicinity in last 56 years , with an emphasis in the 25 April 2015 Gorkha , Nepal earthquake. *Contributions to Geophysics and Geodesy*, 51:321–343.
- Tiwari, R.K., Paudyal, H., Shanker, D. (2022). On the spatio-temporal variation in b-value after 25 April 2015 Gorkha, Nepal earthquake. *Geodesy and Geodynamics*, 13:525–533.
- Wang, R., Chang, Y., Miao, M., Zeng, Z., Chen, H., Shi, H., Li, D., Liu, L., Su, Y., Han, P. (2021). Assessing earthquake forecast performance based on b value in yunnan province, China. *Entropy*, 23(6).
- Wiemer, S. (2001). A software package to analyze seismicity: ZMAP. *Seismological Research Letters*, 72:373–382.
- Wiemer, S., and Wyss, M. (2002). Mapping spatial variability of the frequency-magnitude distribution of earthquakes. *Advances in Geophysics*, 45(C).
- Wyss, M., and Chamlagain, D. (2019). Estimated casualties in possible future earthquakes south and west of the M7.8 Gorkha earthquake of 2015. *Acta Geophysica*, 67(2):423–429.
- Yadav, R.B.S., Koravos, G.C., Tsapanos, T.M., Vougiouka, G.E. (2015). A Probabilistic Estimate of the Most Perceptible Earthquake Magnitudes in the NW Himalaya and Adjoining Regions. *Pure and Applied Geophysics*, 172:197–212.
- Yadav, R.B.S., Tripathi, J.N., Shanker, D., Rastogi, B.K., Das, M.C., Kumar, V. (2011). Probabilities for the occurrences of medium to large earthquakes in northeast India and adjoining region. *Natural Hazards*, 56:145–167.
- Yin, A. (2006). Cenozoic tectonic evolution of the Himalayan orogen as constrained by along-strike variation of structural geometry, exhumation history, and foreland sedimentation. *Earth-Science Reviews*, 76:1–131.

Stability Analysis of Shiraz Metro Line 1 Tunnel Using Flac2D Software

Naghme Nasiri¹, Fariba Kargaranbafghi^{1*}, Hamid Mehrnahad², Javad Gholamnejad³
and Mojtaba Rahimi Shahid⁴

¹ Department of Geology, Faculty of Sciences, Yazd University, 89195741-, Iran.

² Department of Civil Engineering, Faculty of Engineering, Yazd University, Iran.

³ Department of Mining and Metallurgical Engineering, Faculty of Engineering, Yazd University, Iran.

⁴ Department of Geology, Faculty of Sciences, Ferdowsi University of Mashhad, Iran

Received July 14th, 2022; Accepted Dec. 25th, 2023

Abstract

The growing reliance on subterranean infrastructure, spurred by the expansion of urban landscapes, the escalating population densities, the pressing need for efficient transit systems, the many environmental imperatives, and spatial constraints on surface development accentuate the pivotal role of metro tunnels akin to those found in Shiraz. These tunnels, crafted, using Earth Pressure Balance (EPB) and Tunnel Boring Machines, and fortified with segmental linings, undergo meticulous scrutiny for displacement and stability, employing static and quasi-static methodologies. Employing the sophisticated FLAC 2D software, the investigation delves into the nuanced impact of altering segmental lining thickness on displacement dynamics. Analysis results unveil a notable augmentation in displacement under quasi-static conditions, notably accentuated when the lining thickness is reduced.

© 2024 Jordan Journal of Earth and Environmental Sciences. All rights reserved

Keywords: Metro, Lining, Displacement, Numerical Analysis, Flac 2D.

1. Introduction

Underground facilities are an integral part of modern society and have various manifestations such as subways, railroads, highways, etc. The design of each of the above spaces requires access to appropriate data and the application of special measures. In each case, the designer must first seek to improve the quality of the materials in which the tunnel has to be drilled considering the ground conditions. In many areas, the tunnels are not self-support, and it is necessary to use tunnel lining, whose selection requires a lot of studies (Alkhaza'leh et al., 2023).

The investigation of soil behavior against tunnel construction is one of the topics in the field of geotechnics, discussed in many papers and studies in recent years (Meng et al., 2020; Han et al., 2022; Al-Hawari, 2008; Azeez et al., 2019). Therefore, the current study examined the displacement around the tunnel in a case study (Shiraz metro line 1). Stability analysis of metro tunnels, along with taking the necessary measures to stabilize them, is an essential study project. Several studies have been conducted in this regard, some of which are mentioned. Stability analysis was performed in a tunnel in Shanghai using FLAC3D software (Zhang et al., 2009). Another study investigated the stability of drilled tunnels in soft clay soils (Lee et al., 2006). Other studies have examined the stability of the underwater tunnels using numerical methods and the Mohr-Coulomb criterion (Hofle et al., 2008). The stability of tunnels with support systems has been studied using numerical methods in Japan (Funatsu et al., 2008). Another study modelled the stability of shallow tunnels by the finite element method (Fellin et al.,

2010). Also, some research in China has focused on changing soil properties in FPB mechanized drilling to increase stability (Yang et al., 2013).

The surrounding soils near tunnel crown and invert or across tunnel horizontal diameter are very critical to the tunnel convergence (Huang et al., 2017).

The numerical results reveal that compared to the moving-train load, the effect of earthquake action on the dynamic response of the subway tunnel is more prominent (Li et al., 2021).

The study area is located in the southeast of Shiraz, between Allah Square and Valiasr (Modarres Boulevard). This area includes a part of Shiraz urban railway with a length of about 7.5 km, including two tunnels with a diameter of nearly 7 meters in the vicinity, with a distance of 15 meters between their centers. As the tunnels are symmetrical and parallel, the present study has considered only one of them for modelling. A TBM device of EPB type has been proposed for tunnel drilling and lining implementation as the geological conditions of the region, clay along with silt and water content are taken into consideration. The tunnel has been modeled using geotechnical information of the soil and the characteristics of the segments used in the tunnel in the BHA11 borehole area with approximately 15 meters of overburden as the highest overburden in the study area. FLAC 2D software was used to measure the displacements in the studied tunnel. FLAC 2D is a finite difference numerical modelling software used in continuum contexts with static and quasi-static analyses. A 2D numerical study has been

* Corresponding author e-mail: fkargaran@yazd.ac.ir

used to investigate the factors that affect the behavior of segmental tunnel linings (Do et. al., 2013).

The aim of this study is to assess the stability of the Shiraz metro line tunnel. To achieve this goal, the engineering and geomechanically properties of materials will be identified, and static as well as pseudo-static analyses will be conducted using the Flac2D software. For enhanced result clarity, various two-dimensional models with distinct color schemes will be presented.

2. Materials and Methods

2.1. General Geology of Shiraz

The city of Shiraz has developed on the young alluvium of the fourth period, whose origin is the function of sediment transport by dry river and sedimentation in Maharloo Lake. The alluvium of the fourth period of Shiraz Plain ranges from coarse-grained debris sediments and alluvial fans in the margins of heights to lake fine-grained sediments along Maharloo Lake. Sediments are mostly coarse-grained in the north and northwest of the plain, including sand, gravel, and cobble, resulting from the erosion of the surrounding calcareous heights and sedimentation by the dry river. The deposits are often medium-grained in the central part of the plain and include sand and gravel with a mixture of clay and silt. Sediments are often fine-grained in the western and southwestern parts of the plain, adjacent to Sultanabad Mountain, due to the presence of the Fars Group formations and the ChenarRahdar River, which transports and deposits sediments from the Fars Group formations in the west of Shiraz basin. Sediments gradually become fine-grained in the eastern and southeastern parts of the plain and around Maharloo Lake, consisting of clay, silt, gypsum, and swamp and lake sludge.

In addition to surface changes, the type and granularity of deep sediments are also variable, with deep sediments of the northern and northwestern areas having coarser grains. However, surface sediments in the central and eastern parts of the plain are mostly fine-grained. Fine-grained and coarse-grained sediments are deposited alternately with increasing depth. Figure 1 shows the geological profile of the study route.

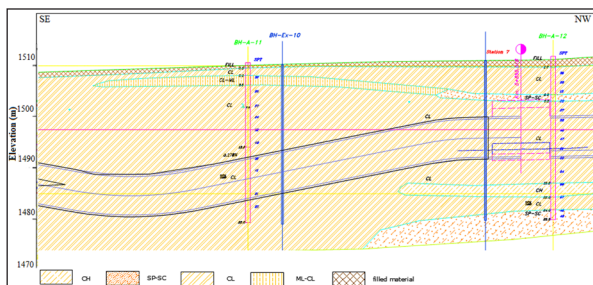


Figure 1. Geological profile of the study area.

2.2 Geometric and Geo-Mechanical Characteristics of Shiraz metro

Phase 1 plan of the Shiraz metro with a length of approximately 24 km includes three deep, semi-deep, and surface parts, depending on the geological conditions of the project. The deep tunnels, with a length of approximately 15 km, are drilled in the alluvial environment below the water

table. Excavation of this tunnel is carried by two shield TBMs using the Earth Pressure Balance (EPB) method in the form of twin tunnels with a drilling diameter of 6.88 meters and a final effective diameter of 6 meters. The permanent support of these tunnels is by prefabricated concrete parts called segments with an arrangement of 1 + 2 + 2 + 1. A6 is the largest segment, called the Counter Key, and A1 is the smallest segment, called the Key in the shape of a trapezoid. Other segments, including A2, A3, A4, and A5, have the shape of a parallelogram and are placed next to the Counter Key and Key segments (Figure 2). A6 segments have the largest approximate width of 1.42 m, while segments of the Key have the smallest approximate width of 1.38 m. Table 1 presents the mechanical characteristics of the segments. The study area was in the BHA11 borehole. The depth of the overburden is about 15 meters in this area, and the groundwater level is approximately 7 meters below the ground. In general, the soil section in the BHA11 borehole can be divided into three layers located up to a depth of 25 meters from the ground surface. From a depth of 25 m, the type of soil is similar to the second layer in the BHA11 borehole, with mainly clay and silty clay layers, which is generally considered in four-layer modeling. Table 2 shows the geo-mechanical parameters of the layers. Figure 3 shows the plastic zones after the drilling stage. According to the figure, the tensile zones dominate the shear zones in the figure, and most of the collapse is of the tensile type.

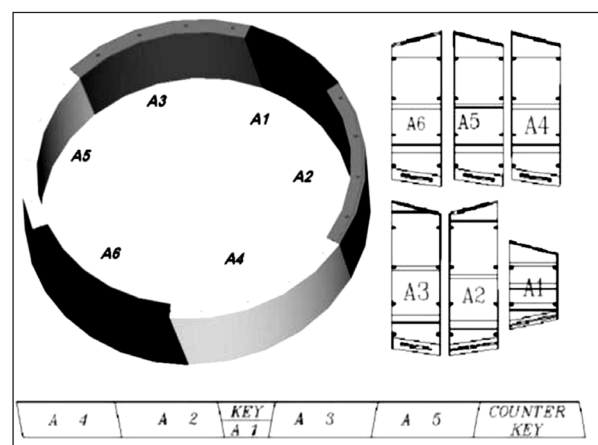


Figure 2. Arrangement of segments used in Shiraz metro line 1 tunnel.

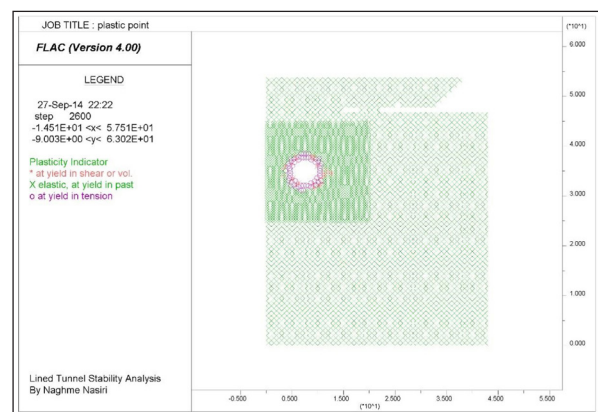


Figure 3. Plastic zones after the drilling stage without support lining.

Table 1. Mechanical parameters of the lining used in the tunnel.

Material	Concrete
f'c	510 Kg/cm ²
Elastic Modulus	3.17*10 ⁵ KN/m ²
Poisson Ratio	0.2
Thickness	0.3 m
I	0.00225 m ⁴
A	0.42m ²
EI	7.13*10 ⁴ KN.m
EA	9.5*10 ⁶ KN
Weight per Unit Length	8 KN/m/m

Table 2. Geomechanical parameters of layers.

Type of materials	Depth (m)	Cohesion (Kpa)	Internal friction (degrees)	Density (Kg/m ³)	Bulk modulus (Mpa)	shear modulus (Mpa)
1 st layer	0-3	33	35	2000	37.33	22.4
2 nd layer	3-20	52	29	2080	33.33	20
3 rd layer	3-25	28	37	2000	31.33	18.8
4 th layer	25-54	52	29	2080	3.33	20

3. Results

3.1 Investigation of Displacements Around the Tunnel During Static Analysis Tunnel Modeling Without Support Lining

As EPB type, TBM machine has been used in Shiraz metro tunnel drilling, and the body of the tunnel is raveling ground, the support system is applied without time interruption and simultaneously with the drilling process. Figure 4 illustrates the historical progression of unbalanced forces after the drilling stage, focusing on conditions where no segmental lining has been implemented. This visual representation tracks the evolution of forces exerted within the tunneling environment over time, providing a detailed timeline of the unbalanced forces as the tunnel progresses. It offers insights into the structural stability and integrity of the tunnel in the absence of segmental lining. The maximum permissible displacement in tunnel construction is crucial in ensuring structural stability and safety.

The assessment of the tunnel's structural integrity becomes paramount where tunnel drilling occurs before the implementation of a support system,. In cases where the model doesn't attain equilibrium or where the tunnel collapses, the consequences are evident, as depicted in Figure 5, showcasing vertical stress contours post-drilling. High displacement, as evident in this figure, indicates significant instability and structural displacement within the tunnel itself. This instability highlights the critical need for a robust support system to maintain stability and prevent potential collapses or structural failures within the tunneling process. At this stage, the vertical and horizontal displacements are plotted for points with different angles in the tunnel. Also, Figures 6 and 7 show displacements in two horizontal and vertical directions. As shown, the displacement is considerable in this case and even reaches one meter in the vertical direction. Therefore, the application of the support lining is essential in this tunnel.

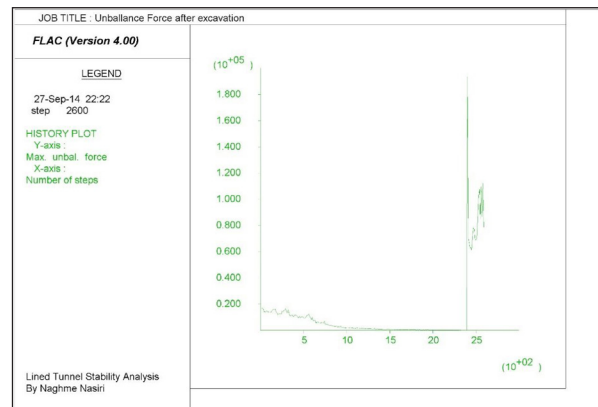


Figure 4. History of unbalanced forces after the drilling stage without segmental lining.

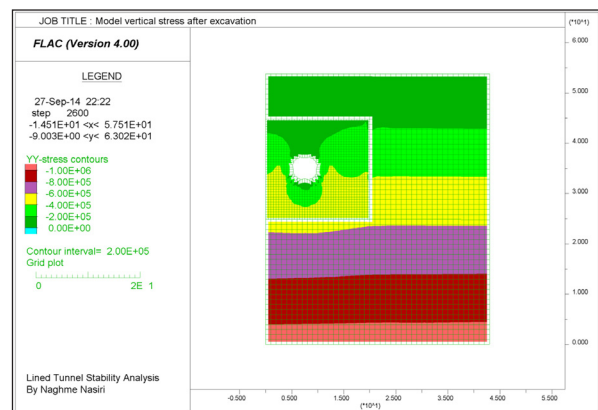


Figure 5. Vertical stress contours after the drilling stage without segmental lining

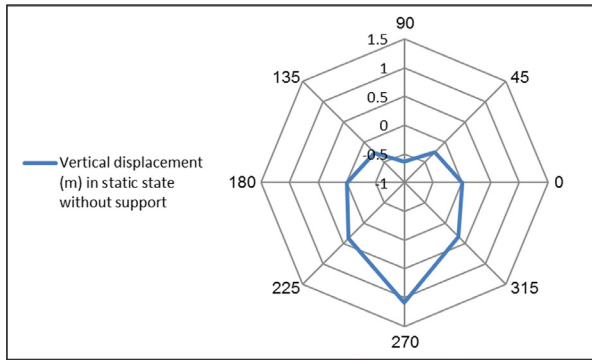


Figure 6. Vertical displacement in static state without support.

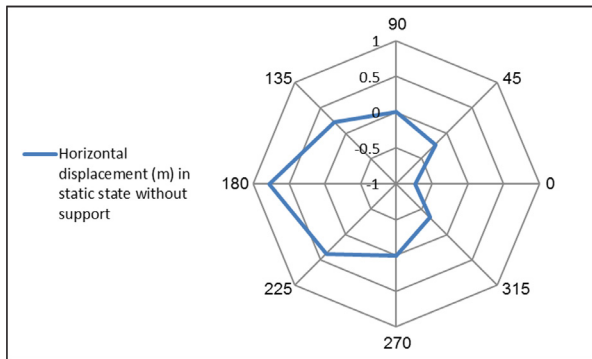


Figure 7. Horizontal displacement in static state without support.

3.2 Modeling with Support Lining

In the next step, drilling was done, having the support system in a static state. As mentioned before, the drilling and lining installation steps were done simultaneously. Figure 8 shows the history of unbalanced forces after drilling. Accordingly, there is a lack of balance of forces after drilling, and finally, equilibrium is established in the model.

Figure 9 shows the vertical displacement contours after drilling with a segmental lining. In this case, the vertical displacement in the tunnel ceiling is between 5-10 mm as subsidence, and the vertical displacement in the form of tunnel floor heave is between 1.5-2 cm. The amount of surface subsidence, in this case, is about 5 mm. Figures 10 and 11 show the values of the displacements in the vertical and horizontal directions on the diagram. It is evident that the displacement is much less than it is in the previous case, and it can be, therefore, said that the tunnel is stable. Figure 12 compares the displacements in the vertical direction in the above two states. According to the diagram, the displacement in the static state with the support lining is much less than the state without the support lining system, and the use of the lining in this tunnel is necessary.

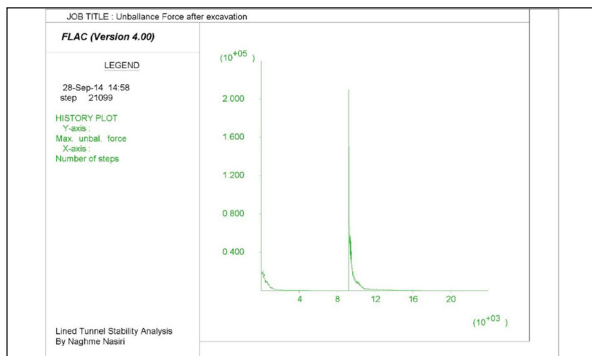


Figure 8. History of unbalanced forces after the drilling stage with a support lining.

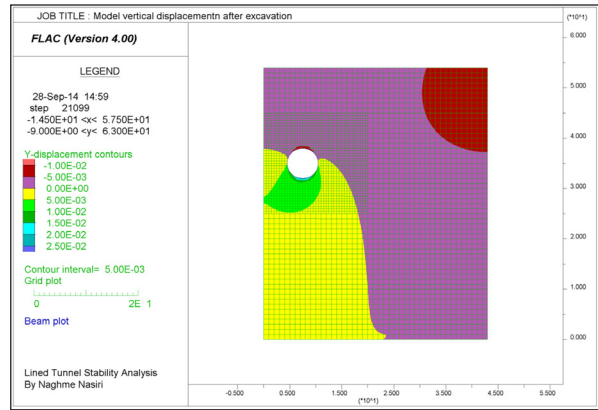


Figure 9. Vertical stress contours after the drilling stage with a support lining.

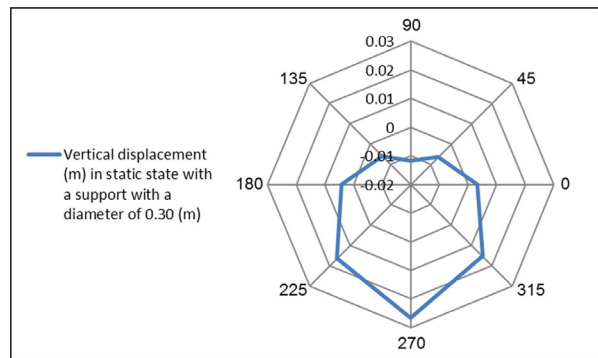


Figure 10. Vertical displacement in static state with a support lining.

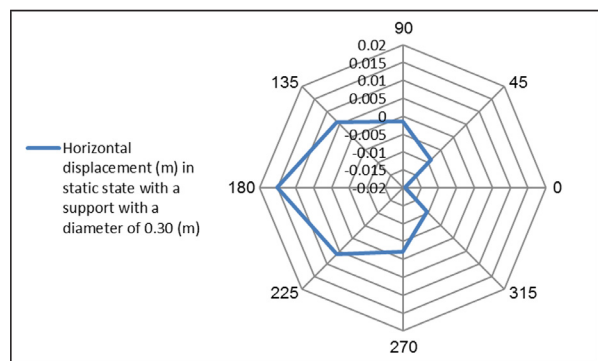


Figure 11. Horizontal displacement in static state with a support lining.

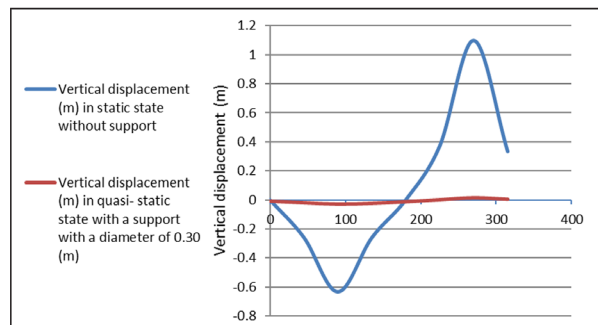


Figure 12. Comparison of displacements in the vertical direction in static state with and without lining.

For modeling in quasi-static analysis, the procedure is similar to the previous steps. The only difference is that the earthquake horizontal acceleration in the area is considered 0.3 g according to the 2800 code of practice, an Iranian code of practice for seismic resistant design of buildings (Road, Housing and Urban Development Research Center, 2014). As shown in Figure 13, the model has also reached

equilibrium after the drilling stage in this case. Figure 14 shows the vertical displacement after the drilling stage in the quasi-static state, indicating an increase in the displacement compared to the static state. The surface subsidence also reaches 2 cm.

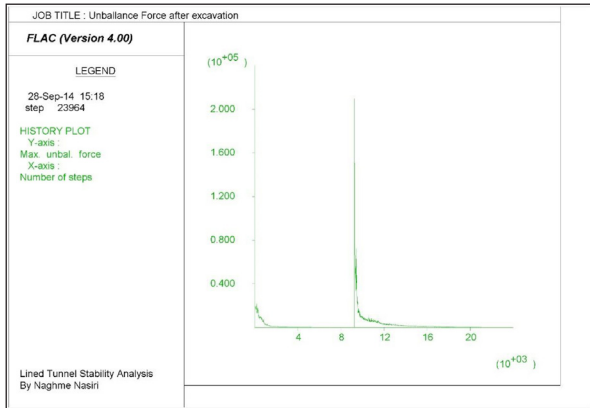


Figure 13. History of unbalanced forces in quasi-static state with support lining.

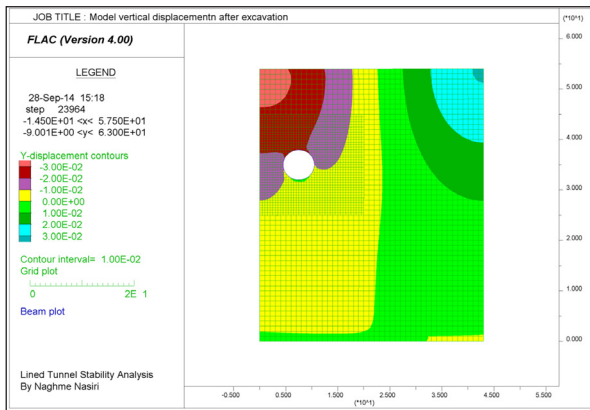


Figure 14. Vertical displacement contours after the drilling stage in quasi-static state with support lining.

According to Figures 15 and 16, the displacement in both vertical and horizontal directions has increased in the quasi-static, compared to the static state, and the tunnel is still stable.

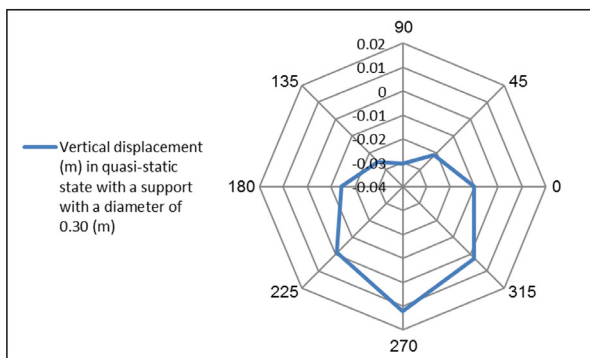


Figure 15. Vertical displacement in a quasi-static state with support lining.

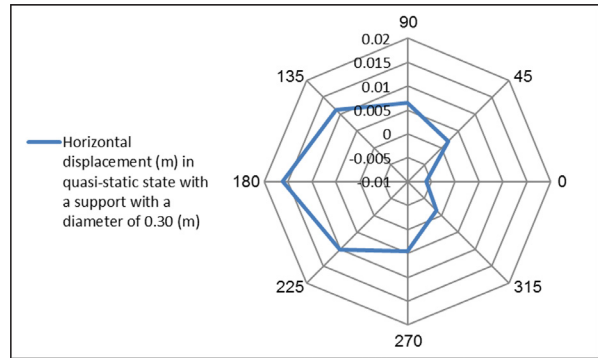


Figure 16. Horizontal displacement in a quasi-static state with support lining.

3.3 Investigation of Displacements by Changing the Lining Thickness During Quasi-Static Analysis

The displacement values were obtained for linings with a thickness of 0.25, 0.20, 0.15, and 0.10 meters in the vertical and horizontal directions. It should be noted that as the thickness of the lining changes, the properties of the lining also change. According to the diagrams in Figures 17 and 18, the displacement increases with decreasing the lining thickness. Accordingly, the lining with a thickness of 0.3 m has less displacement than the others. Thus, it is the most suitable case for use as a support lining in the relevant tunnel among the studied thicknesses.

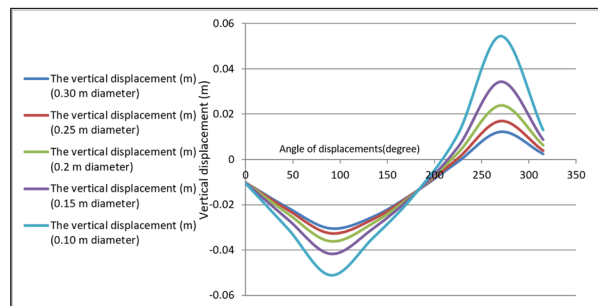


Figure 17. Comparison of vertical displacement in quasi-static state with different thicknesses of support lining.

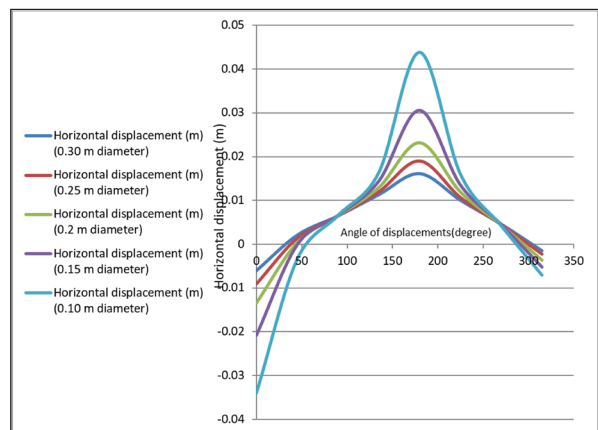


Figure 18. Comparison of horizontal displacement in quasi-static state with different thicknesses of support lining.

4. Discussion:

The study's findings underscore the pivotal role of support lining in ensuring the stability and integrity of tunnels during and after drilling processes. The absence of support lining led to notable instabilities, marked by high displacements and the inability to reach equilibrium, resulting in the collapse of the tunnel model. This result aligns with established research emphasizing the importance of support systems in underground constructions (Zhang et al., 2017).

Simultaneous application of support lining during drilling proved instrumental in establishing equilibrium and mitigating displacements. This strategy resonates with previous studies emphasizing the real-time implementation of support systems during excavation to counteract unbalanced forces and maintain stability (Qin et al., 2022). The analysis showcased that the support lining effectively reduced both vertical and horizontal displacements, promoting stability and structural integrity.

Moreover, the investigation into different lining thicknesses yielded valuable insights. The varying displacements, corresponding to different thicknesses, highlighted those thinner linings and resulted in higher displacements. They emphasize the critical role of proper lining thickness selection. This finding corroborates with the body of research, focusing on the relationship between lining properties and tunnel stability (Xu et al., 2021; Chen et al., 2019).

The study's implications extend to practical applications in tunnel construction and engineering practices. Engineers and construction teams can utilize these findings to make informed decisions regarding the implementation of support lining strategies. Optimal thickness selection, such as the identified 0.3-meter thickness, emerges as a crucial consideration to minimize displacements and ensure stability during tunnel construction. However, further research could explore additional variables, impacting support lining effectiveness, such as material properties, installation methods, and geological conditions. Additionally, conducting field studies to validate these findings in real-world tunnel construction scenarios would strengthen the practical applicability of the results.

This study emphasizes the indispensability of support lining systems in maintaining tunnel stability during and after drilling processes. The insights into simultaneous application and optimal thickness selection serve as a foundation for enhancing tunnel engineering practices, contributing to safer and more resilient underground infrastructure.

5. Conclusions

The metro route, primarily clay with low plasticity and occasional silt and sand, necessitates sealed prefabricated concrete parts due to soil permeability. Analysis affirms tunnel instability without support lining, evident in unbalanced force diagrams and displacement contours. However, appropriately designed linings, detailed in Table 1, stabilize the tunnel, limiting maximum vertical

displacement to 20 mm. Both static and quasi-static analyses confirm tunnel stability with designed support linings, with the only discrepancy being increased displacement due to seismic factors in the latter case. Reducing lining thickness exacerbates displacement, as depicted in relevant diagrams.

Conflicts of interest

The authors declare no conflict of interest

References

- Al-Hawari, Z. (2008). Characterization of A Hard Opaline Clayey Bed Overlying Phosphates from Esh-Shidiya Area, SE of Jordan. *The Jordan Journal of Earth and Environmental Sciences (JJEES)*, 1(2): 89-94.
- Alkhaza'leh, H., Abu-Awwad, A., & Alqinna, M. (2023). Effect of Irrigation with Treated Wastewater on Potatoes' Yields, Soil Chemical, Physical and Microbial properties. *Jordan Journal of Earth & Environmental Sciences*, 14(2): 135-145.
- Azeez, J., Blessing, O., Debo, A., & Olabisi, O. (2019). Estimating Lime Equivalence of Animal Manure Ashes and Soil Reaction Kinetics in Southwestern Nigerian Soils: An Incubation Study. *Jordan Journal of Earth & Environmental Sciences*, 10(3): 178-186.
- Chen, F., Wang, L., & Zhang, W. (2019). Reliability assessment on stability of tunnelling perpendicularly beneath an existing tunnel considering spatial variabilities of rock mass properties. *Tunnelling and Underground Space Technology*, 88: 276-289.
- Do, N.-A., Dias, D., Oreste, P., Djeran-Maigre, I. (2013). 2D numerical investigation of segmental tunnel lining behavior. *Tunneling and underground space technology* 37: 115- 127.
- Fellin, W., King, J., Kirsch, A., Oberguggenberger, M. (2010). Uncertainty modeling and sensitivity of tunnel face stability. *Structural safety* 32: 402- 410.
- Funatsu, T., Hoshino, T., Sawae, H., Shimizu, N. (2008). Numerical analysis to better understand the mechanism of the effects of ground supports and reinforcements on the stability of tunnels using the distinct element method. *Tunneling and underground space technology* 23: 561- 573.
- Han, L., Liu, H., Zhang, W., Ding, X., Chen, Z., Feng, L., & Wang, Z. (2022). Seismic behaviors of utility tunnel-soil system: With and without joint connections. *Underground Space*, 7(5): 798-811.
- Hofle, R., Fillibeck, J., Norbert, V. (2008). Time dependent deformations during tunneling and stability of tunnel faces in fine-grained soils under groundwater. *Acta geotechnica* 3: 309-316.
- Huang., H.W., Xiao., L., Zhang., D.M., Zhang., J. (2017). Influence of spatial variability of soil Young's modulus on tunnel convergence in soft soils. *Engineering geology* 228: 357- 370.
- Lee, C.J., Wu, B.R., Chen, H.T., Chiang, K.H. (2006). Tunnel stability and arching effects during tunneling in soft clayey soil. *Tunneling and underground space technology* 21: 119-132.
- Li, J., Lou, Y., Yang, X., Jin, X. (2021). Nonlinear seismic analysis of a train-tunnel-soil system and running safety assessment of metro vehicles. *Soil dynamics and earthquake engineering* 147: 106772.
- Meng, F. Y., Chen, R. P., Wu, H. N., Xie, S. W., & Liu, Y. (2020). Observed behaviors of a long and deep excavation and collinear underlying tunnels in Shenzhen granite residual soil. *Tunneling and Underground Space Technology*, 103, 103504.
- Qin, Y., Lai, J., Gao, G., Yang, T., Zan, W., Feng, Z., & Liu, T. (2022). Failure analysis and countermeasures of a tunnel constructed in loose granular stratum by shallow tunnelling method. *Engineering Failure Analysis*, 141, 106667.
- Road, Housing & Urban Development Research Center. (2014). Iranian code of practice for seismic resistant design of building (PN 253), Iranian building codes and standards. 2800 Standard, 4th edition, p.212.

Xu, Z., Luo, Y., Chen, J., Su, Z., Zhu, T., & Yuan, J. (2021). Mechanical properties and reasonable proportioning of similar materials in physical model test of tunnel lining cracking. *Construction and Building Materials*, 300, 123960.

Yang, Y., Wang, G., Li, H., Huang, X. (2013). The new clay mud and its improvement effects of tunnels. *Applied clay science* 79: 49- 56.

Zhang, Q., Zhang, X., Wang, Z., Xiang, W., & Xue, J. (2017). Failure mechanism and numerical simulation of zonal disintegration around a deep tunnel under high stress. *International Journal of Rock Mechanics and Mining Sciences*, 93: 344-355.

Zhang, Z.X., Kastner, R., Emeriault, F., Li, F. (2009). Stability analysis of large slurry shield- driven tunnel in soft clay. *Tunneling and underground space technology* 24: 472-481.

A Review on Water Quality Aspects of Urban Rainwater Harvesting in Jordan

Ayat Hazaymeh^{1*}, Jens Lange²

¹ Ayat Hazaymeh, PhD Candidate, Hydrology, Faculty of Environment and Natural Resources, University of Freiburg, Freiburg, Germany.

² Prof. Dr. Jens Lange, Hydrology, Faculty of Environment and Natural Resources, University of Freiburg, Freiburg, Germany.

Received Aug. 11th, 2023; Accepted Jan. 14th, 2024

Abstract

Rainwater harvesting has regained importance in light of increasing water scarcity, particularly in arid and semi-arid regions such as Jordan, as it can be utilized for a variety of uses, including drinking and irrigation. However, the quality of harvested rainwater is of vital importance in determining its intended use, as it may be vulnerable to contamination from different sources during its journey from the atmosphere to storage facilities. Several studies have investigated the water quality issues of the rainwater harvesting system in Jordan, including the quality of direct rain, runoff water, and stored water in cisterns. The factors affecting water quality were also investigated. This paper reviews the rainwater quality harvesting systems in Jordan. The findings revealed that microbial contaminants were frequently reported, exceeding the allowable limits set by the Jordanian standard for drinking purposes. In contrast, direct rain was found to be of better quality. Despite the importance of organic and emerging contaminants in recent water research, minimal attention has been paid to these contaminants. Future research should also focus on options for improving water quality, such as prior treatment measures.

© 2024 Jordan Journal of Earth and Environmental Sciences. All rights reserved

Keywords: Water harvesting, Direct rain, Runoff, Cistern, Water quality, Contamination, Irrigation, Drinking, Water quality standards.

1. Introduction

Jordan is one of the countries with the most severe water scarcity worldwide, with renewable freshwater resource availability of only 61 m³ per capita by 2021 (Ministry of Water and Irrigation, 2023). This scarcity level is primarily attributed to the arid to semi-arid climatic conditions that prevail in the country, with 80% of Jordan receiving an average annual rainfall of less than 100 mm (Hadadin et al., 2010).

Rapid population growth in recent years, due to both natural growth and immigration, has further exacerbated the water scarcity situation (Al-Shibli et al., 2017; Food and Agriculture Organization of the United Nations (FAO), 2016). This increase in water scarcity has resulted in increasing pressure on the limited availability of water resources and a corresponding continuous decrease in per capita access to safe and reliable supplies of potable water.

To address this issue, Jordan has implemented various strategies and plans, including promoting the use of non-conventional water resources, such as the expansion of the reuse of treated wastewater in agriculture, desalinated seawater, and investing more in rainwater harvesting in rural and urban areas, particularly from rooftops (Ministry of Water and Irrigation, 2016). Rainwater harvesting is a traditional, common, and socially acceptable solution for Jordanian communities, and has been widely practiced throughout history for irrigation and water supply.

Rainwater harvesting is the process of collecting and storing rainwater in tanks and other storage facilities. Thereby, roof runoff water refers to the flow of water that

is generated when rain falls on the rooftop of a building and then moves downward through the gutters into a tank or cistern, whereas ground or surface runoff is generated when rain falls on urban ground such as roads, parking lots, courtyards, pavements, and other impervious surfaces. The collected rainwater can be used for different domestic and non-domestic purposes, such as drinking, washing, cleaning, toilet flushing, and irrigation. However, the quality of the collected rainwater is crucial because it is a limiting factor in determining its intended use. Contrary to the common belief that rainwater is pure and uncontaminated, research has revealed that rainwater can contain a wide variety of contaminants, such as physical, chemical, microbiological, organic compounds, trace, and heavy metals, as well as emerging contaminants (i.e., pharmaceutical, and personal care product residues, pesticide residues, microplastics, per- and poly-fluoroalkyl substances (PFAS), and others) (Deng, 2021). This is because there are many potential sources of contamination to which rainwater can be exposed during its journey from the atmosphere to the roofs and storage facilities.

Throughout the years, many studies in Jordan have explored the water quality of urban rainwater harvesting systems in terms of the main sources of contamination, chemical composition, and potential use of water. However, there remains a lack of comprehensive overviews. Therefore, there is a need to provide a holistic picture of published articles on the water quality of urban rainwater harvesting systems, with a focus on evaluating and reviewing the findings and identifying gaps in the research in this field, which can be beneficial for researchers, scientists for future

* Corresponding author e-mail: ayat.hazaymeh@hydrology.uni-freiburg.de

research, and policymakers.

This paper presents a systematic literature review that addresses the water quality, collected through urban rainwater harvesting systems, more specifically, the main sources of contamination and the chemical composition and potential uses of water. The present review includes 21 studies that were published in international databases, followed by a narrative and quantitative data synthesis and suggestions for further studies.

2. Materials and Methods

2.1 Search strategy

The search for articles was conducted using the following bibliographic databases: ScienceDirect, Springer, EBSCOhost, ProQuest, WorldCat, and Worldwide Science. The searches were also performed using Google Scholar, which included relevant articles that were not recorded in bibliographic databases. The search used specific keywords and terms related to urban rainwater harvesting (Figure 1).

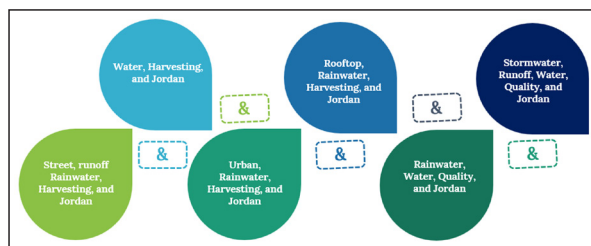


Figure 1. Specific keywords used in the search of bibliographic databases.

2.2 Inclusions and exclusion criteria of research articles

Explicit inclusion and exclusion criteria were set to screen the search and select articles. These criteria outlined the specific characteristics that the articles needed to be included in the review, such as publication date, language, and relevance to the research topic (Figure 2).

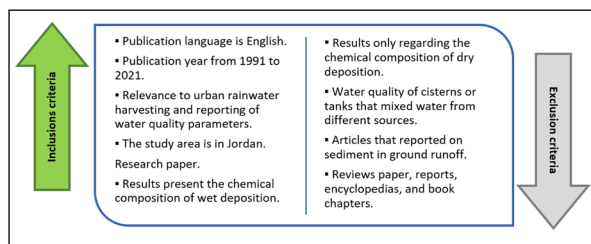


Figure 2. Inclusions and exclusion criteria

2.3 Extraction, synthesis, and presentation of data

Twenty-one articles were selected based on the inclusion criteria described above. Unique Identification Codes (IDs) from WQ-1 to WQ-21 were assigned to these articles, which were then grouped into four main water quality (WQ) categories according to the investigated water quality: rainwater, roof runoff, ground runoff, and stored water in cisterns. Out of each article, information about the authors, year of publication, study area, average annual rainfall amount, source of tested water, sampling period, number of samples, investigated factors, and conditions, was extracted and summarized in tables in the supplementary material.

In a quantitative synthesis, the reported average concentrations of water quality variables were extracted and

tabulated in an Excel spreadsheet for each WQ category. Thereafter, the reported water quality variables were converted to the same units as stated in Jordanian standards for drinking and irrigation water. Basic descriptive statistics (including minimum, maximum, average, and count values) were calculated and tabulated for each investigated water quality variable. Subsequently, the extracted values of the water quality parameters for each WQ category were compared with the limits specified in the Jordanian standards for drinking and irrigation. For this purpose, the percentage of compliance with drinking and irrigation standards for physical, chemical, microbial, trace, and heavy metals was calculated, and water quality parameters that exceeded the standard limits were identified. Additionally, the ionic balance was calculated for all the reported anions and cations in each study to ensure analytical quality (the results are available in the supplementary materials). In a qualitative synthesis, the potential factors that affect the quality of rainwater, roof runoff, ground runoff, and water stored in the cistern were discussed. Figure 3 summarizes the extraction, synthesis, and presentation processes of the data.

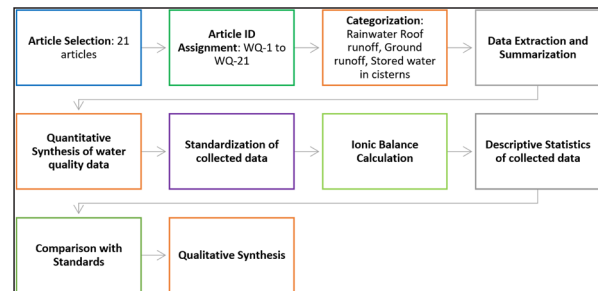


Figure 3. The flowchart for the process of extraction, synthesis, and presentation of data

3. Results and Discussion

The following sections present a meta-analysis of the results, collected from the selected studies regarding the study areas, the investigated water quality parameters, and the investigated water sources. This section also includes a discussion of the factors that affect different water quality parameters and a comparison with Jordanian standards to assess the suitability of rainwater harvesting for drinking and irrigation purposes. However, the comparison between different water quality categories was not conducted due to the heterogeneity of test methods and units, as well as the limited number of results for each WQ parameter, which precludes statistical analysis.

3.1. Characteristics of reviewed articles

The investigated locations in the reviewed articles revealed the following frequency: Amman was the most frequent, followed by Irbid, Jerash, and Maan. After that, Ajloun and Karak had equal frequencies, and then, Zarqa and Mafraq had the same frequency as well (Figure 4). Most studies focused on the quality of rainwater rather than on runoff and rainwater stored in the cisterns. Studies, investigating the quality of harvested rainwater in cisterns, mainly focused on the northern and middle parts of Jordan, particularly Irbid, Ajloun, Jerash, Zarqa, and Amman. This focus can be attributed to the spatial variation of rainfall amounts in Jordan, where the western, northern, and

middle regions receive higher amounts of rainfall, whereas the eastern and southern regions receive less (Tarawneh and Şen, 2012). Thus, rainwater harvesting systems at the household level are more common in northern and central Jordan. According to the 2015 Jordan National Census, the Irbid Governorate had the highest percentage of houses that depended on water harvesting as their main source of drinking water (21%), followed by the Ajloun Governorate (Figure 4).

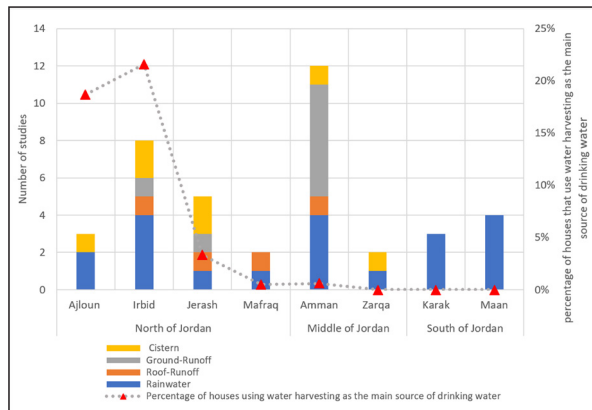


Figure 4. Distribution of study areas in the reviewed articles within Jordanian governorates, water type, and percentage of houses that use water harvesting as the main source of drinking water (Department of Statistics (DOS), 2015).

Chemical water quality parameters, such as pH, Chloride (Cl), Total Dissolved Solids (TDS), Electrical conductivity (EC), Sulfate (SO₄), Calcium (Ca), Magnesium (Mg), Sodium (Na), and Potassium (K), received most attention in the reviewed articles, as indicated in Figure 5. For the heavy metals, the focus was on lead (Pb) and iron (Fe). In terms of microbial indicators, faecal coliforms were the most often tested, as they are considered a better indicator of animal or human waste than total coliforms. Overall, microbial indicators were mainly examined in rainwater stored in cisterns rather than in rainfall or runoff water. Organic compounds (polycyclic aromatic hydrocarbons (PAHs), dissolved organic compounds (DOC), and others) were only investigated in two articles on ground runoff water and direct rain.

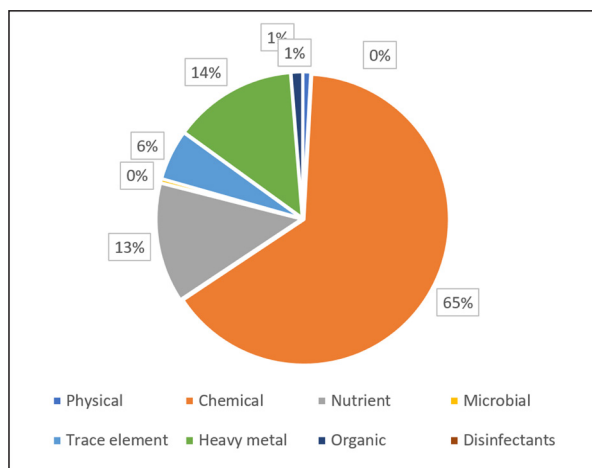


Figure 5. Categorization of water quality parameters reported in reviewed articles.

Figure 6 shows a mind map of the distribution of the selected articles according to the investigated water source, where most of the selected articles focused on assessing the quality of rainwater (direct rain). Only a few studies, such as those conducted by Al-Amoush et al., (2018); Almanaseer (2019) compared rainwater quality with roof runoff. Jiries et al. (2003) compared the quality of rainwater with ground runoff water, whereas Awawdeh et al. (2012) compared the quality of roof runoff with ground runoff water.

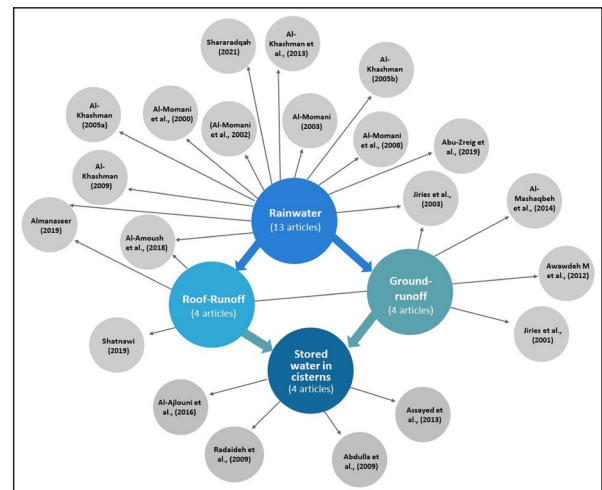


Figure 6. Mind map of the distribution of selected articles according to the investigated water sources.

3.2. Investigated factors affecting the quality of rainwater harvesting categories.

3.2.1 Rainwater (direct rain)

The quality of direct rain was a major concern in the selected articles, and several factors were found to have an impact. The reviewed studies mainly focused on the impact of rainfall event characteristics, anthropogenic sources, and natural sources. For rainfall event characteristics, temporal variations in rainwater quality during the rainfall season were observed, with elevated concentrations in all investigated water quality parameters at the beginning of the rainfall season. These elevated concentrations were attributed to the accumulation of large amounts of dust and contaminants in the atmosphere during the dry summer period, which were scavenged by rainfall (Abu-Zreig et al., 2019; Al-Khashman 2005b, 2009; Al-Khashman et al., 2013; Jiries et al., 2003). The number of rainy days and rain events was also found to be a decisive factor affecting rainwater chemistry, whereas the non-continuity of rain events, followed by dry days, resulted in the release of pollutants into the atmosphere before the next event (Al-Momani et al., 2002).

Studies on the natural sources, conducted by Al-Khashman (2005b, 2005a, 2009); Al-Khashman et al., (2013); Al-Momani (2003); Al-Momani et al. (2000, 2002), found that atmospheric neutralization processes were the main factors contributing to neutral or alkaline pH in rainwater samples. These processes were attributed to local alkaline dust that contained large amounts of Calcium carbonate (CaCO₃), calcite, and dolomite. In addition, the studies, conducted by Al-Momani (2003) and Al-Momani et al. (2000, 2002, 2008) highlighted the impact of Saharan soil dust, which was indicated by the high concentrations of calcium (Ca) in

rainwater samples. The Dead Sea also affected the chemical composition of rainwater, particularly in areas closest to the Dead Sea (Al-Khashman (2005b, 2009); Al-Khashman et al., 2013; Shararadqah 2021). Sulfate (SO_4) was attributed to both natural and anthropogenic sources (Al-Momani et al., 2000, 2002, 2008).

Regarding the influence of anthropogenic sources, agricultural activities were identified as influencing factors to rainwater chemistry, particularly in the area close to the Jordan Valley (Ghour), with fertilizers as a potential source of high concentrations of Ammonium (NH_4) and Nitrate (NO_3) (Al-Khashman (2005a, 2009); Al-Khashman et al., 2013; Al-Momani et al., 2000; Shararadqah 2021). Al-Khashman (2009) found that agricultural activities affected rainwater quality throughout the year. Local industries, such as cement and phosphate mining activities, refineries, thermal power stations, wastewater treatment plants, solid waste landfills and other light industries, were also identified as potential sources that influence the chemical composition of rainwater, particularly in terms of trace and heavy metal content (Al-Khashman (2005b, 2009); Al-Khashman et al., 2013; Al-Momani et al., 2002). Road traffic emissions and fuel consumption also led to high concentrations of Nitrate (NO_3) in rainwater samples (Al-Khashman 2009; Al-Momani et al., 2000; Shararadqah 2021). Al-Momani (2003) reported that heavy metal concentrations in rainwater, particularly Lead (Pb) and Zinc (Zn), could be related to road traffic sources, whereas Al-Amoush et al., (2018) attributed heavy metal concentrations in rainwater samples to industrial emissions. Heating activities during the cold period were also identified as anthropogenic sources of heavy and trace metals in rainwater (Al-Khashman 2005b; Al-Khashman et al., 2013).

Also in a worldwide context, rainwater chemistry varies between different geographical locations. According to Keresztesi et al., (2020), anthropogenic activities, including coal-fired power plants, oil refineries, significant industries, agricultural activities, terrestrial sources, and marine sources, had an impact on the chemical composition of precipitation in contemporary United States. Due to the buildup of significant amounts of dust in the atmosphere that rain scavenges, Chakraborty and Gupta (2018) conducted a study in India and discovered that rainwater had the highest concentration of contaminants at the start of the rainfall season. In addition, industrial activities, vehicular emissions, and other anthropogenic activities were found to affect Indian rainwater quality. On Upolu Island, Imo et al., (2021) revealed that marine sources had a larger influence on rainwater composition than anthropogenic and terrestrial sources. In China, Zeng and Han (2021) identified terrestrial sources (dust) and anthropogenic emissions (long-distance transport) as the main factors influencing rainwater quality in Guiyang City, China. According to research by Rivera-Rivera et al., (2020), the characteristics of air masses, local transportation, regional advection, and the solubility of trace metals all have a significant impact on the quality of rainwater in Mexico City.

3.2.2 Roof-runoff water

In Jordan, less attention was paid to factors that influence the quality of roof runoff (the impact of roof materials and first flush only) compared to direct rain. The impact of roof materials on water quality was studied by Al-Amoush et al., (2018). They found that runoff from metal insulation had the lowest water quality, followed by mixed concrete, mixed asphalt, concrete, water, seal coat, roll asphalt, and thermal insulation. Almanaseer (2019) reported the effects of the first flush by contrasting the quality of roof runoff water between the first and second storms. The results revealed that the water quality improved in the second storm owing to the wash-off of accumulated substances and dust from the roof. Shatnawi (2019) examined the relationship between the length of the dry period before rainfall and the runoff water quality and found that this was not significant. She then successfully tested a manually designed filtration system to reduce turbidity and suspended solid levels.

International studies provide a broader view of roof runoff quality. According to Förster (1996), decisive factors include roof material (chemical characteristics, roughness, surface coating, age, weather ability, etc.), the physical boundary condition of the roof (size, inclination, and exposure), precipitation event intensity, wind, pollutant concentration in the rain, and other meteorological factors (season, weather characteristics, and antecedent dry time). In addition, the chemical properties of the pollutants (vapor pressure, solubility in water, Henry's constant, etc.), concentrations of pollutants in the atmospheric boundary layer (emission, transport, half-life, phase distribution, etc.), and location of the roof (proximity to pollution sources) were found to affect water quality. Furthermore, the age of the roof and the operation and maintenance strategy of the catchments were found to have a significant influence, as reported by Meera and Ahammed (2018); Emmanuel et al., (2021).

3.2.3 Ground runoff water

Factors, affecting Jordanian ground runoff water quality, were discussed in two studies. Al-Mashaqbeh et al. (2014) found that a higher traffic density in an urban area led to higher concentrations in organic pollutants and heavy metals compared to rural areas. There, the use of chemical and natural fertilizers in agriculture could be attributed to higher levels of total suspended solids, nutrients, and microbial indicators. Jiries et al. (2001) reported that anthropogenic activities and vehicle emissions were contributing factors in lowering the quality of street runoff water in the city center area of Amman as compared to residential areas. Thereby, high concentrations of all constituents, including polycyclic aromatic hydrocarbons (PAHs), were most prominent in the first rainy month of sampling, mainly due to low rainfall and a protracted dry period (Jiries et al., 2001, and 2003).

In worldwide studies, land use was found to significantly influence runoff water quality, such as the case in the capital state of Kuwait (Al-Jaralla and Al-Fares, 2009). More specifically, the ratio of agricultural area to total land use area was identified as the main contributing factor in the Geum River Basin, Korea (Kim et al., 2007). Nearby, Lee et

al. (2016) identified the main sources of runoff pollution in the Geumhak watershed to be agrochemicals and road traffic, apart from groundwater, native soils, domestic sewage, and other urban sources.

3.2.4 Stored water in cisterns

In Jordan, Radaideh et al. (2009) found a significant impact of geographical location and rainfall intensity on water quality in cisterns. Abdulla et al. (2009) reported that rainfall intensity and the number of dry days preceding a rainfall event significantly affected the quality of harvested rainwater. Al-Ajlouni, et al. (2016) observed higher contamination of samples when they were collected shortly after rain.

Radaideh et al. (2009) found that cistern water harvested from rooftops generally tended to have better quality than water collected from other catchment areas, because the latter were exposed to many additional contamination sources, including fertilizers, pesticides, chicken and livestock manure, dissolved minerals, sediments, sewage, decaying plants, algae, bacteria, and detergents. Yet, Assayed et al. (2013) identified fecal deposits from birds on roofs as a possible source of microbial contamination. According to both Assayed et al. (2013) and Radaideh et al. (2009), microbial contamination was more likely when the rainwater tanks were situated near cesspits. Finally, using a rope and bucket to retrieve water from the cistern could cause microbial contamination (Assayed et al., 2013).

It is generally important to ensure that stored water stays safe for consumption, particularly for drinking and other domestic purposes. Therefore, a set of recommendations and measures were suggested by Abdulla et al., (2009), which included chlorinating the stored water at least once per rainy season, cleaning the catchment area before the start of the rainy season and raising awareness on the importance of regular cistern maintenance to prevent contamination.

Worldwide literature has identified additional factors affecting the quality of cistern waters. Despins et al. (2009) revealed that the water stored in plastic tanks tended to have a slightly acidic pH, whereas the water in concrete tanks was more alkaline. Similarly, Simmons et al. (2001) found that water stored in ferrocement tanks tends to have higher pH values. Furthermore, Despins et al. (2009) found that some tank materials might affect water quality by leaching chemicals (e.g., metal from metal tanks and organic compounds from plastic tanks). Thereby, warmer temperatures may accelerate the rate of metal leaching from galvanized iron tanks (Martin et al., 2010). Both Abbasi and Abbasi (2011) and Sung et al. (2010) found that the cistern water quality tended to decline as the storage period increased.

Abbasi and Abbasi (2011) suggested extracting water from the top of the tank to avoid disturbing sediments at

the bottom, where water tended to be the dirtiest. They additionally recommended tank designs with overflows that flush the dirtiest water at the bottom. Lee et al. (2010) and Meeraand Ahammed (2006) also suggested diverting the first flush of rainfall away from the rainwater harvesting system. Several researchers indicated that regular maintenance and cleaning of catchment surfaces, gutters, and storage tanks can improve cistern water quality (Domènechand Sauri 2011; Lee et al., 2010; Meeraand Ahammed 2006).

4. Suitability of rainwater harvesting categories for drinking and irrigation purposes according to Jordanian standards

4.1 Rainwater (direct rain)

In general, 86% of the reported water quality parameters were within the allowable limits for drinking water in Jordan (Table 1). Exceptions included pH values, reported by Al-Momani et al., (2000), turbidity values reported by Abu-Zreig et al., (2019), and the Ammonium (NH_4) values reported by Al-Khashman (2005a, 2005b, 2009), (Al-Khashman et al., (2013); Al-Momani (2003); Al-Momani et al., (2000). For trace and heavy metals, the Aluminum (Al) concentrations, reported by Al-Khashman et al. (2013), Al-Momani (2003), and Al-Momani et al. (2000) exceeded the standard limit, as did the lead (Pb) values, reported by Al-Khashman et al. (2013) and Al-Momani (2003). For irrigation purposes, all reported values of the water quality parameters were within the limits of the standard, except for the Cadmium (Cd) value reported by Al-Momani (2003).

4.2 Roof runoff water

For drinking purposes, 86% of the reported water quality parameters in the reviewed articles were within the Jordanian standard limits (Table 2). Exceptions were the turbidity value, reported by Shatnawi (2019) and nitrate concentrations reported by Awawdeh et al., (2012). In addition, the reported lead (Pb) concentrations, reported by Awawdeh et al. (2012), were higher than the maximum standard limit. Regarding irrigation use, 71% of the investigated water quality parameters were suitable for all irrigation purposes. 82% of these values were suitable for both a slight to moderate degree of restricted irrigation and severely restricted irrigation, and 92% were suitable for severely restricted irrigation (Table 2). Prominent exceptions include the Total Suspended Solids (TSS) value, reported by Shatnawi (2019), which was only suitable for a severe degree of restricted irrigation and the Sodium (Na) and Bicarbonate (HCO_3) values by Al-Amoush et al., (2018) which were suitable for both slightly to moderately restricted irrigation and severely restricted irrigation. The Nitrate (NO_3) value, reported by Awawdeh et al. (2012), was only suitable for severely restricted irrigation, whereas the value of Zinc (Zn), reported by Awawdeh et al. (2012), exceeded the allowable limit for all irrigation purposes.

Table 1. Summary for the compliance of the quality of rainwater (direct rain) with the Jordanian standards

Jordanian Standards		% of compliance with water quality parameters	Rainwater (Direct rain)
Drinking water standard (JS 286:2015)		Physical and chemical parameters	83%
		Microbial parameters	Not investigated
		Metals and other parameters	88%
		Overall WQ parameters	86%
		Exceeded WQ parameters	pH, Turbidity, NH ₄ , Al, Cd, Pb
Irrigation water quality guideline (JS 1766:2014)	Non-restricted	Physical and chemical parameters	100%
		Microbial parameters	Not investigated
		Metals and other parameters	98%
		Overall WQ parameters	99%
		Exceeded WQ parameters	Cd
	Slight to moderate degree in restriction	Physical and chemical parameters	100%
		Microbial parameters	Not investigated
		Metals and other parameters	98%
		Overall WQ parameters	99%
		Exceeded WQ parameters	Cd
	Severe degree in restriction	Physical and chemical parameters	100%
		Microbial parameters	Not investigated
		Metals and other parameters	98%
		Overall WQ parameters	99%
		Exceeded WQ parameters	Cd

Table 2. Summary of the compliance of the quality of roof-runoff with the Jordanian standards

Jordanian Standards		% of compliance with water quality parameters	Roof Runoff water
Drinking water standard (JS 286:2015)		Physical and chemical parameters	83%
		Microbial parameters	Not investigated
		Metals and other parameters	90%
		Overall WQ parameters	86%
		Exceeded WQ parameters	Turbidity, NO ₃ , Pb
Irrigation water quality guideline (JS 1766:2014)	Non-restricted	Physical and chemical parameters	74%
		Microbial parameters	Not investigated
		Metals and other parameters	80%
		Overall WQ parameters	71%
		Exceeded WQ parameters	TSS, NO ₃ , Na, HCO ₃ , Zn
	Slight to moderate degree in restriction	Physical and chemical parameters	81%
		Microbial parameters	Not investigated
		Metals and other parameters	80%
		Overall WQ parameters	82%
		Exceeded WQ parameters	TSS, NO ₃ , Zn
	Severe degree in restriction	Physical and chemical parameters	100%
		Microbial parameters	Not investigated
		Metals and other parameters	80%
		Overall WQ parameters	92%
		Exceeded WQ parameters	Zn

4.3 Ground runoff water

The assessment of this category was limited to irrigation purposes only, as this type of water was not considered an appropriate source for drinking without prior treatment. Still, only 36% of the values were suitable for all irrigation purposes, 59% were suitable for a slight to moderate degree of restricted irrigation and a severe degree of restricted irrigation, and 66% were suitable for a severe degree of restricted irrigation (Table 3). The electrical conductivity

(EC) values for street runoff water at Amman's city center were only suitable for restricted irrigation (Jiries et al., 2001), whereas the Total Suspended Solids (TSS), Chemical oxygen demand (COD) and Biochemical oxygen demand (BOD₅) values at another urban site in Amman were suitable for slightly, to moderately, but mostly only for severely restricted irrigation (Al-Mashaqbeh et al., 2014). For the metal concentrations, the values, reported by Al-Mashaqbeh et al.

(2014) and Awawdeh et al. (2012) were within the irrigation guidelines, whereas the values for all metals in street runoff water in the study conducted by Jiries et al. (2001) exceeded the limits for all irrigation purposes. According to microbial

indicators, ground runoff at an urban site of Amman was only suitable for severely restricted irrigation, whereas a rural site of Jerash was more suitable for irrigation (Al-Mashaqbeh et al., 2014).

Table 3. Summary of the compliance of the quality of ground runoff water with the Jordanian standards

Jordanian Standards		% of compliance with water quality parameters	Ground runoff water
Irrigation water quality guideline (JS 1766:2014)	Non-restricted	Physical and chemical parameters	43%
		Microbial parameters	0%
		Metals and other parameters	33%
		Overall WQ parameters	36%
		Exceeded WQ parameters	EC, TSS, COD, BOD ₅ , NO ₃ , HCO ₃ , Na, Cl, Pb, Cu, Mn, Cr, Fe, Ni, Cd, <i>E. coli</i>
	Slight to moderate degree in restriction	Physical and chemical parameters	81%
		Microbial parameters	50%
		Metals and other parameters	33%
		Overall WQ parameters	59%
		Exceeded WQ parameters	TSS, COD, NO ₃ , Pb, Cu, Mn, Cr, Fe, Ni, Cd, <i>E. coli</i>
	Severe degree in restriction	Physical and chemical parameters	95%
		Microbial parameters	50%
		Metals and other parameters	33%
		Overall WQ parameters	66%
		Exceeded WQ parameters	Pb, Cu, Mn, Cr, Fe, Ni, Cd

4.4 Stored water in cisterns

In general, 78% of the reported water quality parameters were within the allowable limits of the drinking water standard (Table 4). Exceptions include the pH value, reported by Assayed et al. (2013) and the lead (Pb) value, reported by Radaideh et al., (2009). In terms of microbial indicators, most of the reported values for total coliforms, fecal coliforms,

and Escherichia coli (*E. coli*) exceeded the maximum limits of the standard. For compliance with the irrigation guideline, all the reported physical and chemical, microbial, and heavy metal parameters were within the allowable ranges in the guidelines for different irrigation aspects (non-restricted, slight to moderate degree of restriction, and severe degree of restriction).

Table 4. Summary of the compliance of the quality of stored water in cisterns with the Jordanian Standards

Jordanian Standards		% of compliance with water quality parameters	Stored water in cisterns
Drinking water standard (JS 286:2015)		Physical and chemical parameters	98%
		Microbial parameters	6%
		Metals and other parameters	92%
		Overall WQ parameters	78%
		Exceeded WQ parameters	pH, total coliforms, Fecal coliforms, <i>E. coli</i> , Pb
Irrigation water quality guideline (JS 1766:2014)	Non-restricted	Physical and chemical parameters	100%
		Microbial parameters	100%
		Metals and other parameters	100%
		Overall WQ parameters	100%
		Exceeded WQ parameters	None
	Slight to moderate degree in restriction	Physical and chemical parameters	100%
		Microbial parameters	100%
		Metals and other parameters	100%
		Overall WQ parameters	100%
		Exceeded WQ parameters	None
	Severe degree in restriction	Physical and chemical parameters	100%
		Microbial parameters	100%
		Metals and other parameters	100%
		Overall WQ parameters	100%
		Exceeded WQ parameters	None

5. Study limitations

Direct comparisons of water quality parameters between different water source categories were limited, mainly because test methods and units were different. Many studies investigating rainwater (direct rain) permitted a detailed analysis, comparing diverse geographical regions in Jordan. Less information was available on stored water or ground runoff quality. Overall, the investigated water quality parameters lacked consistency between categories, with heavy metal concentrations being a primary focus in rainwater (direct rain), while mainly microbial indicators were addressed in studies of stored water quality. Finally, it became clear that there is a lack of studies investigating treatment measures to improve water quality. Therefore, further research in this crucial area is inevitable.

6. Conclusion

This study aimed to investigate the water quality of rainwater harvesting systems through a review of studies conducted in Jordan. An analysis of the literature revealed that the quality of rainwater harvesting systems was influenced by natural and anthropogenic factors in addition to the characteristics of the system (catchment areas, storage facilities, etc.). Microbial contamination appeared to be the main factor limiting the use of harvested rainwater, especially for drinking purposes, while physical, chemical, and metal constituents mostly met Jordanian quality standards. Only a single study investigated the impact of applying prior treatment measures to improve water quality. Among the different sources of rainwater for harvesting, rainwater (direct rain) consistently had the highest water quality, and ground runoff had the lowest. Further research is needed to explore methods to improve the quality of harvested rainwater, including investigations of the impact of first-flush treatment, required diversion volumes, tank designs, and testing treatment options. Additionally, more attention is required to assess and improve the quality of ground runoff since it is becoming an increasingly viable resource in sponge cities and urban green infrastructure concepts for managing urban water and providing additional water for urban agriculture. Furthermore, more research is required on threats from emerging contaminants, as there is a growing concern related to these contaminants.

Acknowledgment:

This study was conducted within SAGE, a Global Climate Centre, funded by the German Academic Exchange Service (DAAD).

Conflicts of interest:

The authors declare no conflict of interest

References

- Abbasi, T., and Abbasi, S. A. (2011). Sources of pollution in rooftop rainwater harvesting systems and their control. *Critical Reviews in Environmental Science and Technology*, 41(23): 2097-2167. <https://doi.org/10.1080/10643389.2010.497438>.
- Abdulla, F. A., Al-Shareef, A. W., Abdulla, F. A., and Al, A. W. (2009). Roof rainwater harvesting systems for household water supply in Jordan. *Desalination*, 243 (1-3) : 195-207. <https://doi.org/10.1016/j.desal.2009>.
- Abu-Zreig, M., Ababneh, F., and Abdulla, F. (2019). Assessment of rooftop rainwater harvesting in northern Jordan. *Physics and Chemistry of the Earth*, 114. <https://doi.org/10.1016/j.pce.2019.08.002>.
- Al-Ajlouni, E., Hamid, S. A., Saad, L., Subbarini, M., and Wahdan, A. (2016). The Effect of Water Shortage on Water Quality of Different Resources in Jerash Governorate/Jordan, Based on New Water Quality Index. *Journal of Engineering Research and Application*, 6(6): 36-48.
- Al-Amoush, H., Al-Ayyash, S., and Shdeifat, A. (2018). Harvested Rainwater Quality of Different Roofing Material Types in Water Harvesting System at Al al-Bayt University/Jordan. *Jordan Journal of Civil Engineering*, 12(2): 2018-2228.
- Al-Jaralla, R., and Al-Fares, R. (2009). Quality of stormwater runoff in the State of Kuwait, Al-Asema governorate. *International Journal of Environmental Studies*, 66(2): 227-239. <https://doi.org/10.1080/00207230902859838>.
- Al-Khashman, O. A. (2005a). Ionic composition of wet precipitation in the Petra Region, Jordan. *Atmospheric Research*, 78(1-2): 1-12. <https://doi.org/10.1016/j.atmosres.2005.02.003>.
- Al-Khashman, O. A. (2005b). Study of chemical composition in wet atmospheric precipitation in Eshidiya area, Jordan. *Atmospheric Environment*, 39(33): 6175-6183. <https://doi.org/10.1016/j.atmosenv.2005.06.056>.
- Al-Khashman, O. A. (2009). Chemical characteristics of rainwater collected at a western site of Jordan. *Atmospheric Research*, 91(1): 53-61. <https://doi.org/10.1016/j.atmosres.2008.05.007>.
- Al-Khashman, O. A., Jaradat, A. Q., and Salameh, E. (2013). Five-year monitoring study of chemical characteristics of Wet atmospheric precipitation in the southern region of Jordan. *Environmental Monitoring and Assessment*, 185(7): 5715-5727. <https://doi.org/10.1007/s10661-012-2978-1>.
- Almanaseer, N. (2019). Rainwater Harvesting for Adaptation to Water Scarcity in Refugees Camps in Jordan. *Journal of Engineering and Applied Sciences*, 15(5): 1180-1189. <https://doi.org/10.36478/jeasci.2020.1180.1189>.
- Al-Mashaqbeh, O., Jiries, A., and El-Hajali, Z. (2014). Stormwater runoff quality generated from an urban and a rural area in the Amman-Zarqa basin. *WIT Transactions on Ecology and the Environment*, 182: 379-390. <https://doi.org/10.2495/WP140331>.
- Al-Momani, I. F. (2003). Trace elements in atmospheric precipitation at Northern Jordan measured by ICP-MS: Acidity and possible sources. *Atmospheric Environment*, 37(32) : 4507-4515. [https://doi.org/10.1016/S1352-2310\(03\)00562-4](https://doi.org/10.1016/S1352-2310(03)00562-4).
- Al-Momani, I. F., Momani, K. A., and Jaradat, Q. M. (2000). Chemical Composition of Wet Precipitation in Irbid, Jordan. *Journal of Atmospheric Chemistry*, 35: 47-57.
- Al-Momani, I. F., Momani, K. A., Jaradat, Q. M., Massadeh, A. M., Yousef, Y. A., and Alomary, A. A. (2008). Atmospheric deposition of major and trace elements in Amman, Jordan. *Environmental Monitoring and Assessment*, 136(1-3): 209-218. <https://doi.org/10.1007/s10661-007-9676-4>.
- Al-Momani, I. F., Ya'qoub, A. R. A., and Al-Bataineh, B. M. (2002). Atmospheric deposition of major ions and trace metals near an industrial area, Jordan. *Journal of Environmental Monitoring*, 4(6): 985-989. <https://doi.org/10.1039/b208697b>.
- Al-Shibli, F., Maher, W., and Thompson, R. (2017). The Need for a Quantitative Analysis of Risk and Reliability for Formulation of Water Budget in Jordan. *Jordan Journal of Earth and Environmental Sciences*, 8(2): 77-89.
- Assayed, A., Hatokay, Z., Al-Zoubi, R., Azzam, S., Qbailat, M., Al-Ulawayan, A., Saleem, M. A., Bushnaq, S., and Maroni, R. (2013). On-site rainwater harvesting to achieve household water security among rural and peri-urban communities in Jordan. *Resources, Conservation and Recycling*, 73:72-77. <https://doi.org/10.1016/j.resconrec.2013.01.010>.

- Awawdeh M, Al-Shraideh S, Al-Qudah K, and Jaradat R. (2012). Rainwater harvesting assessment for a small size urban area in Jordan. *International Journal of Water Resources and Environmental Engineering*, 4(12): 415–422. <https://doi.org/10.5897/IJWREE10.025>.
- Chakraborty, B., and Gupta, A. (2018). Study and interpretation of chemical composition of rainwater in selected urban and rural locations in India using multivariate analysis. *AIP Conference Proceedings*, 1952. <https://doi.org/10.1063/1.5031996>.
- Deng, Y. (2021). Pollution in rainwater harvesting: A challenge for sustainability and resilience of urban agriculture. *Journal of Hazardous Materials Letters*. 100037, 2. <https://doi.org/10.1016/j.hazl.2021.100037>.
- Department of Statistics (DOS). (2015). Department of Statistics Website. Population and Housing Census. <https://dosweb.dos.gov.jo/>. (July. 29, 2023)
- Despins, C., Farahbakhsh, K., and Leidl, C. (2009). Assessment of rainwater quality from rainwater harvesting systems in Ontario, Canada. *Journal of Water Supply: Research and Technology - AQUA*, 58(2): 117-134. <https://doi.org/10.2166/aqua.2009.013>.
- Domènech, L., and Saurí, D. (2011). A comparative appraisal of the use of rainwater harvesting in single and multi-family buildings of the Metropolitan Area of Barcelona (Spain): Social experience, drinking water savings and economic costs. *Journal of Cleaner Production*, 19(6–7): 598-608. <https://doi.org/10.1016/j.jclepro.2010.11.010>.
- Emmanuel, U., Samuel, K., and Ugonna, U. (2021). Assessment of the Suitability of Urban Residential Roof Catchments for Rainwater Capturing in Umuahia, Southeastern Nigeria. *Jordan Journal of Earth and Environmental Sciences*, 12(1): 22-35.
- Food and Agriculture Organization of the United Nations (FAO). (2016). Assessment of the water harvesting sector in Jordan. Final report. Retrieved from: <https://www.fao.org/3/i5390e/i5390e.pdf>.
- Förster, J. (1996). Patterns of roof runoff contamination and their potential implications on practice and regulation of treatment and local infiltration. *Water Science and Technology*, 33(6): 39-48. <https://doi.org/10.2166/wst.1996.0079>.
- Imo, T., Amosa, P., Latu, F., Vaurasi, V., and Ieremia, R. (2021). Chemical Composition of Rainwater at Selected Sites on Upolu Island, Samoa. *Atmospheric and Climate Sciences*, 11(03): 458–468. <https://doi.org/10.4236/acs.2021.113027>.
- Jiries, A. G., Hussein, H. H., and Halaseh, Z. (2001). The quality of water and sediments of street runoff in Amman, Jordan. *Hydrological Processes*, 15(5): 815–824. <https://doi.org/10.1002/hyp.186>.
- Jiries, A. G., Hussein, H. H., and Lintemann, J. (2003). Polycyclic aromatic hydrocarbon in rain and street runoff in Amman, Jordan. *Journal of Environmental Sciences*, 15(6): 848-853.
- Jordan standards and metrology organization (JSMO). (2014). Jordanian Irrigation water quality guideline, First edition (JS 1766:2014)..
- Jordan Standards and Metrology Organization (JSMO). (2015). Jordanian drinking water standard, Sixth edition (JS 286:2015).
- Keresztesi, Á., Nita, I. A., Boga, R., Birsan, M. V., Bodor, Z., and Szép, R. (2020). Spatial and long-term analysis of rainwater chemistry over the conterminous United States. *Environmental Research*, 188. <https://doi.org/10.1016/j.envres.2020.109872>.
- Kim, G., Chung, S., and Lee, C. (2007). Water quality of runoff from agricultural-forestry watersheds in the Geum River Basin, Korea. *Environmental Monitoring and Assessment*, 134(1–3): 441-452. <https://doi.org/10.1007/s10661-007-9635-0>.
- Lee, D. H., Kim, J. H., Mendoza, J. A., Lee, C. H., and Kang, J. H. (2016). Characterization and source identification of pollutants in runoff from a mixed land use watershed using ordination analyses. *Environmental Science and Pollution Research*, 23(10): 9774-9790. <https://doi.org/10.1007/s11356-016-6155-x>.
- Lee, J. Y., Yang, J. S., Han, M., and Choi, J. (2010). Comparison of the microbiological and chemical characterization of harvested rainwater and reservoir water as alternative water resources. *Science of the Total Environment*, 408(4): 896-905. <https://doi.org/10.1016/j.scitotenv.2009.11.001>.
- Martin, A. R., Coombes, P. J., and Dunstan, R. H. (2010). Investigating the influences of season and coastal proximity on the elemental composition of harvested rainwater. *Water Science and Technology*, 61(1): 25-36. <https://doi.org/10.2166/wst.2010.775>.
- Meera, V., Ahammed, M. (2006). Water quality of rooftop rainwater harvesting systems: A review. *Journal of Water Supply: Research and Technology - AQUA*, 55(4): 257-268. <https://doi.org/10.2166/aqua.2006.0010>.
- Meera, V., Ahammed, M. (2018). Factors Affecting the Quality of Roof-Harvested Rainwater. *Urban Ecology, Water Quality and Climate Change. Water Science and Technology Library*, 84: 195-202. https://doi.org/10.1007/978-3-319-74494-0_15.
- Ministry of Water and Irrigation. (2016). Jordan National Water Strategy 2016-2025. Retrieved from: <https://faolex.fao.org/docs/pdf/jor156264E.pdf>.
- Ministry of Water and Irrigation. (2023). Jordan National Water Strategy 2023-2040. Retrieved from: https://www.mwi.gov.jo/EBV4.0/Root_Storage/AR/EB_List_Page/national_water_strategy_2023-2040.pdf.
- Radaideh, J., Al-Zboon, K., Al-Harashsheh, A., and Al-Adamat, R. (2009). Quality Assessment of Harvested Rainwater for Domestic Uses. *Jordan Journal of Earth and Environmental Sciences*, 2(1): 26-31.
- Rivera-Rivera, D. M., Escobedo-Urías, D. C., Jonathan, M. P., Sujitha, S. B., and Chidambaram, S. (2020). Evidence of natural and anthropogenic impacts on rainwater trace metal geochemistry in central Mexico: A statistical approach. *Water* 2020, 12(1): 192. <https://doi.org/10.3390/w12010192>.
- Sharadqah, S. (2021). The Dead Sea and Geo-Environmental Trace Influence on the Rainwater Quality in Jordan. *International Journal of Agriculture and Environmental Science*, 8(1): 61–65. <https://doi.org/10.14445/23942568/ijaes-v8i1p110>.
- Shatnawi, R. S. (2019). Rooftop runoff water quality in university buildings, case study at Jordan Applied Science Private University. *Journal of Engineering Science and Technology*, 14(2): 987-997.
- Simmons, G., Hope, V., Lewis, G., Whitmore, J., and Gao, W. (2001). Contamination of potable roof-collected rainwater in Auckland, New Zealand. *Water Research*, 35(6): 1518-1524. [https://doi.org/10.1016/S0043-1354\(00\)00420-6](https://doi.org/10.1016/S0043-1354(00)00420-6).
- Sung, M., Kan, C. C., Wan, M. W., Yang, C. R., Wang, J. C., Yu, K. C., and Lee, S. Z. (2010). Rainwater harvesting in schools in Taiwan: System characteristics and water quality. *Water Science and Technology*, 61(7): 1767-1778. <https://doi.org/10.2166/wst.2010.107>.
- Tarawneh, Q., and Şen, Z. (2012). Spatial climate variation pattern and regional prediction of rainfall in Jordan. *Water and Environment Journal*, 26(2): 252-260. <https://doi.org/10.1111/j.1747-6593.2011.00284.x>.
- Zeng, J., and Han, G. (2021). Rainwater chemistry observation in a karst city: Variations, influence factors, sources, and potential environmental effects. *PeerJ*, 9. <https://doi.org/10.7717/peerj.11167>.

Evaluating the Impact of Rubber Particles on the Swelling Potential and Pressure of Tizi Soil in an Area Located in North Western Algeria

Benamar Balegh^{1*}, Hamid Sellaf², Adda Hadj Mostefa³, Nourdinne, Mahmoudi⁴

¹Department of Civil Engineering, Faculty of Sciences and Technology, Civil Engineering and Environmental Laboratory Sidi Bel Abbes, 01000, University of Adrar, DZ-01000, Algeria.

^{2,4}Department of Civil Engineering and Hydraulic, Faculty of Technology, Civil Engineering and Environmental Laboratory Sidi Bel Abbes University of Saida, DZ-20000, Algeria

³Civil Engineering Department, University of Relizane, Industrial Engineering and Sustainable Development Laboratory, DZ 48000, Algeria

Received July 11th, 2023; Accepted Oct. 30th, 2023

Abstract

Major climatic changes and heavy truck traffic are causing several problems in road base layers, leading to cracking and destruction. This work is part of a general framework aimed at characterizing and evaluating local materials (Tizi) from the Mascara area to valorize them in road and sidewalk construction. In addition to rubber's remarkable technical properties, its reuse as an additive in Tizi soil mixes can be effective in geotechnical projects while reducing its negative environmental impacts. A low mixing ratio experimental program was implemented to study the effect of rubber particles on the swelling of the Tizi. Grain size, specific gravity, Atterberg limit analysis, swelling consistency, and loading and unloading tests were carried out on Tizi soils and their mixtures with varying rubber particle percentages (3, 6, 9, and 12%). The results showed that liquid limits, swelling time, and swelling probability progressively decreased with increasing rubber particle contents in the samples. This reduction is significant for Tizi soil with medium swelling potential, due to the high compressibility of rubber particles, indicating that compaction and decompression indices increase significantly with rubber particle contents. The results highlighted the beneficial effect of particles and rubber powder, as it was found that Tizi soil samples, reinforced with rubber particles, are more ductile than unreinforced samples. This effect is highly desirable in many backfill applications.

© 2024 Jordan Journal of Earth and Environmental Sciences. All rights reserved

Keywords: Tizi soil, Rubber particles, Consistency limits, Swelling potential, Compressibility

1. Introduction

The infrastructure of developing and developed countries consists of a group of basic elements, including roads, bridges, railways, and airports. Roads are an important part of all the elements, as the cost of construction and maintenance are extremely high. Hence, understanding and improving performance are essential to using resources in the best possible way. In some areas, classic materials (good quality of gravel) are rare or even not present, so engineers and experts have to build roads at a low cost by adapting local materials (Xiaobing et al., 2022; Amakye et al., 2022). Lots of materials have proven to be very interesting in road design, such as tuff, quarry waste, dam sediments, and desert sand (Pan et al., 2020; Odari et al., 2021; López-Lara et al., 2017). Improving local materials for road engineering is an objective solution (Mlhem, 2023); the goal is to better support their physical and mechanical reactions under various climatic conditions, implement them, and achieve a description that enhances their ease of classification and use by experts. In Algeria, the area covered with tuff soil is about 300,000 square kilometers. It is used in roads, sidewalks, and the foundation layers of infrastructure airports according to Loualbia et al. (2016). Tuffs are non-homogeneous, porous, friable, and light rocks, often powdery, either of calcareous origin, derived from springs or "petrifying" gullies. The

presence of rich vegetation in tuffs accelerates limestone deposition or volcanic deposits' aggregates found in coarse strata, often under a thin layer of earth soil. Tuffs appear in a wide variety of colors, depending on their constituent elements.

Numerous studies have shown that tuffs are formed by a certain amount of excessive pressure and wet drying and continue to lose their consistency over time. This was well confirmed by their mechanical behavior under static and dynamic loading (Goual et al., 2011; Al Dwairi et al., 2018). This cohesion completely disappears after saturation, affecting the mechanical behavior of the tuff (Goual, et al 2008). Most previous technologies have not achieved the desired objective, and this research is a new window in the field of tuff improvement (Sarireh et al., 2021).

Several studies show that rubber waste improves geotechnical properties when mixed with soils (Anvari et al., 2017; Akbarimehr et al., 2020). The study, conducted by Ekincia et al. (2022), stated that weaved geotextile networks have been effectively employed to increase the longevity of roads by limiting soil slide, expansion, and ground pressures and sustained by increasing the capacity of these structures. Akbarimehr and Hosseini (2022), mixed pure clay samples with different rubber contents (from 2% to 30% by weight)

* Corresponding author e-mail: ben.balegh@univ-adrar.edu.dz

and found that the elastic plastic and accumulated plastic could change over different cycles and for two sizes of granular rubber. They concluded that it is well-recommended to use a maximum of 10% rubber in mixtures to obtain a homogeneous, resistant blend.

Jaramillo et al. (2022) used rubber tire granules in clay soils with different contents (5, 10 and 15% of the dry weight of the soil). The addition of 5% rubber led to similar maximum dry density values, while the optimum moisture content was affected by the selected surface. In addition to its use in improving the mechanical behavior of clay soils, the incorporation of recycled tire rubber is more effective in low-stress situations.

According to some relevant studies on fiber-reinforced soils, the percentage of polypropylene is generally 0.05, 0.015, and 0.025 % of the weight of the mother soil (Akbulut et al., 2007). For the rubber particles, the studied proportions were 1, 2, 3, 4, and 5% of the total weight of the knitting samples (Akbulut et al., 2007). For chemical additives, lime or cement was mixed with the soil in all the mentioned studies as suggested by Akbulut et al. (2007). The mixtures prepared with the sediment were studied with 10, 20, 25, and

50% of the purified tire (Sellaf et al., 2014).

This research mainly focused on the contribution of rubber particles to the swelling behavior of Tizi soil in comparison to tuff soil. It proposes a method for improving locally produced materials, including Tizi soil, by adding rubber particles for use in road engineering. In this study, Atterberg limit tests, swelling consolidation, and load discharge tests were combined to investigate the causes of strength changes in Tizi soil mixed with rubber particles.

2. Materials and Methods

2.1 The Tizi soil

The Tizi soil sample was obtained from the quarry, located in Tizi, northwest of Algeria (Figure 1). Samples are collected from quarries in the form of stones or gravel. After that, they are transported to the laboratory and placed in a microbial unit for grinding, then, passed through a 2 mm sieve. This soil underwent several laboratory tests (Consistency limits, Specific weight, Grains sizes analysis, Compaction, and Volume of blue) to determine its identity using standard procedures approved by AFNOR and ISO standards (NFP94-051, NFP94-054, NFP94-056, NFP94-057, and NFP 94-068).



Figure 1. Localization of site.

The results are explained in Table (1). The specific gravity (dimensionless) of the Tizi soil is 1.95, and the distribution of the grain size of the Tizi soil is determined. Table (2) displays the chemical analysis of the Tizi soil according to NF EN 1774.

Mineralogical analysis by X-ray Diffraction (Figure 2) reveals that Tizi soil is mainly composed of calcite (CaCO₃), with the presence of traces of quartz (SiO₂) and dolomite (CaMg(CO₃)₂). This high CaCO₃ content is favorable for the hardening and cementation of these compacted materials.

According to the results of Table 1, which is the study of consistency limits, specific weight, grain sizes analysis, compaction, and volume of blue, the Tizi soil is classified as highly plastic clay (CH) according to the Unified Soil Classification System (USCS).

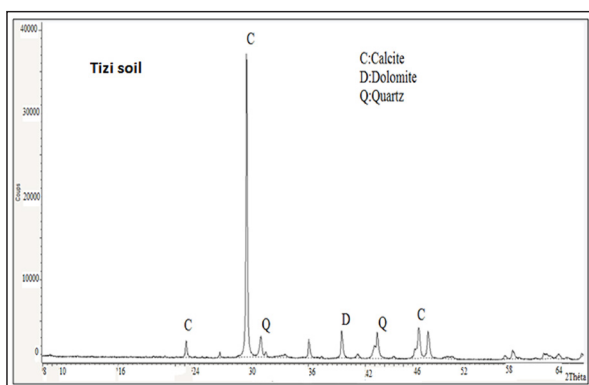


Figure 2. X-ray diffraction of the Tizi soil.

Table 1. Physical properties of Tizi soil

	Properties	Tizi soils
Consistency limits: NF:P94-051	Liquid limit, [%]	38.28
	Plastic limit, [%]	23
	Plasticity index, [%]	16
Specific gravity NF:P94-054	Specific gravity (dimensionless)	1.95
Grains sizes analysis NF:P94-057	Sand, [%]	18
	Silt, [%]	33.33
	Clay, [%]	48.67
Compaction NFP94-093	Maximum dry density: γ _{opm}	1.92
Volume of blue NFP94-068	Volume of blue VB (cm ³)	7.52

Table 2. Chemical compositions of Tizi soil

Property	Tizi soil
SiO ₂ , [%]	9.56
Al ₂ O ₃ , [%]	2.65
Fe ₂ O ₃ , [%]	0.58
CaO, [%]	70.25
MgO, [%]	2.61
Na ₂ O, [%]	4.90
Cl, [%]	0.25
SO ₃ , [%]	1.2
Loss on ignition, [%]	7.73

2.2 Rubber Particles

Rubber particles are obtained through two main processes: (1) the surrounding environment, which is a mechanical method, where scrap tires are ground and (2) the coolant, a process that uses liquid nitrogen to freeze rubber tires and, then, uses a mill to destroy the frozen rubber and convert it into a soft powder. Rubber particles consist of a compound mixture of citric acid (1.2 %), extension oil (1.9 %), carbon lions (31.0 %), zinc oxide (1.9%), and other materials (elastomers, polyisoprene and styrene-butadiene), that is, all the important ingredients for rubber (Balegh and Sellaf, 2022).

Rubber granules, used from five used car tires, are produced by mechanical cutting at the ocean temperature. After that, we separate the granules with a 2 mm dimension from the remainder of the powder, as the powder ratio was more than 41% of the total weight, and the powder tends to clump together (Figure 3). The scrap rubber frame is characterized by a qualitative specific weight of 0.83 g/cm³ and the absorption of little water.

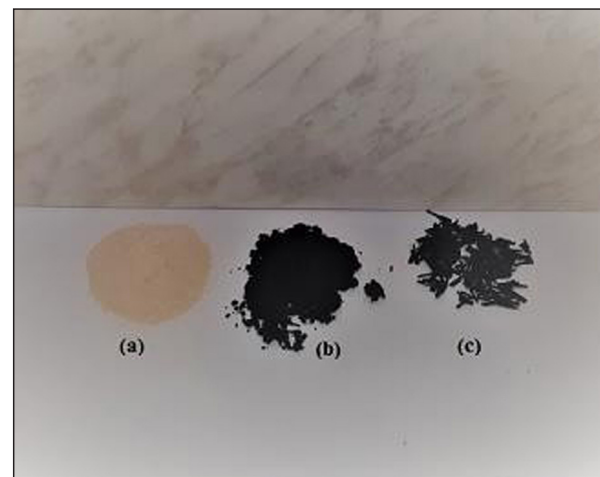


Figure 3. Tizi soil (a), and rubber particles (rubber powder (b), and rubber granules. (c).

2.3 Mix design preparation of Tizi soil-rubber mixtures

Because rubber is affected by temperature, the water content of samples was determined by drying at 35°C, and samples were considered completely dry when the difference did not exceed 2/1000 of the kidney weight in 24 hours.

In this study, the Tizi soil was mixed with rubber granules, and the granule content was chosen as 3, 6, 9, and 12 % of the total weight of the composite samples as illustrated in (Figure 4). The particles frequently clump together, so much care and time have been taken to obtain a homogeneous distribution of particles in mixtures. The materials used as T, P, and G were called Tizi soil T, rubber powder P, and rubber granules G. In the preparation of composite soil, samples are prepared in an optimal protector or in water content that corresponds to liquid reduction.

This study demonstrated that the specific gravity of the rubber is less than half of the soil, the mixing rates used are considered up to 12% of the rubber tires and 15% of the water content. The samples were constantly pressed in the

standard Proctor in three layers. To ensure a uniform dry density, samples are allowed to be absorbed in an additional cost of one Kilopascal, and this additional cost of the seat is caused by the great difference in the qualitative gravity of the components. After pressing the tuff and its mixtures, uninterrupted cylindrical samples were confirmed in the mold using a hydraulic crane. Samples are wrapped with plastic to prevent water from leaking into gout.

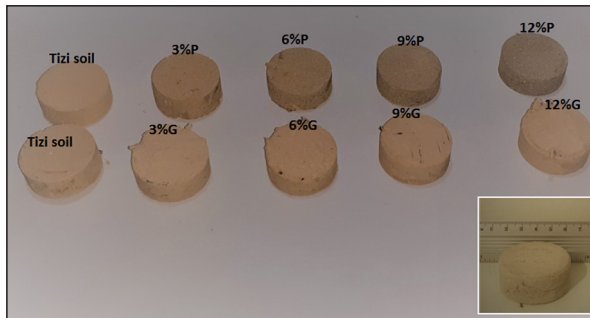


Figure 4. Tizi soil samples with different rubber content (granules or powder).

3. Results and Discussion

3.1 Consistency limits

To determine the consistency values of Tizi soil and mixtures, Atterberg limit tests were conducted in accordance with NF P94-051.

3.1.1 The liquid limit

Figure (5) illustrates the effect of rubber particles (granules and powder) on the boundaries of the consistency of the Tizi soil and its mixtures. The liquid limits are expected to decrease gradually when the content of the rubber particles increases. However, the liquid limit for the Tizi soil, reinforced with rubber granules, exceeds the liquid limit for the Tizi soil, reinforced with rubber powder. This is demonstrated by Akbarimehr and Aflaki (2018).

3.1.1 The plastic limit

As presented in Figure (5), for Tizi soil reinforced by rubber granules, the sample's plastic limit decreases by 3% of the granules, then gradually decreases under 15 % and 28 % of the plastic limit of Tizi, and this also applies for the granules' samples by 6 and 9 %. For Tizi soil, reinforced by rubber powder, the plastic limit of the sample decreases by 3% and 6% of the rubber powder, gradually increases, and, then, reaches the level of plastic of the Tizi soil (9 and 12% of the rubber powder). The results of the Atterberg limits indicate that the Tizi soil reinforced by rubber powder has a higher indicator than the Tizi soil reinforced by rubber grains (Sellaf et al., 2014). Changes in consistency limits of mixtures may be due to the mixture type, the cation exchange capacity, and the relative amount of clay mineral in the mixtures (Al-Mukhtar et al., 2010).

According to Kang et al. (2007) and Akbarimehr and Aflaki. (2018), it is interesting that the plastic limits that were studied for cohesive clay soils initially retain their form, then, undergo a certain degree of modification before returning to their original form. These results are comparable to those of a typical coherent soil with fine grains and medium plasticity.

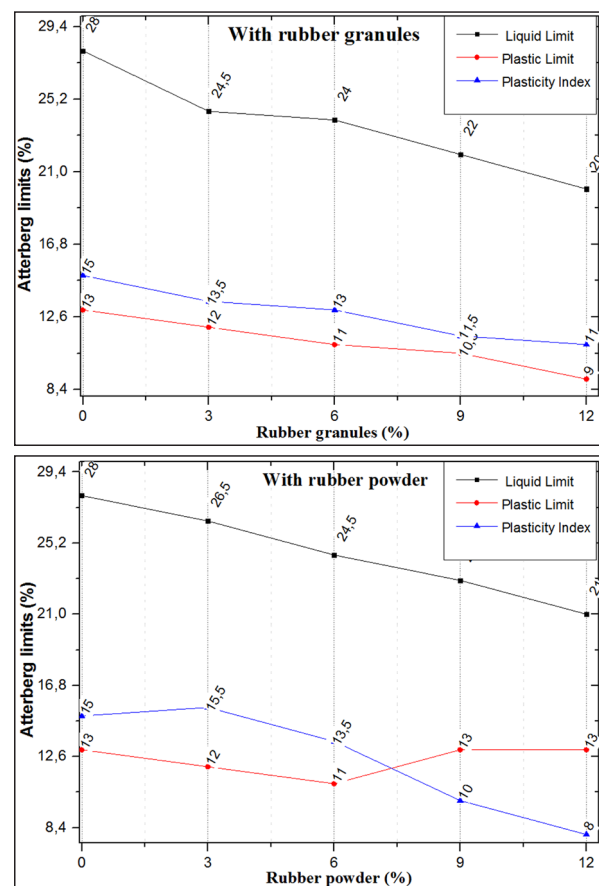


Figure 5. Effect of rubber particles on the consistency limits of Tizi soils.

3.2 Swell-consolidation Tests

Swell-consolidation experiments were carried out on all compacted specimens for the series of tests in accordance with AFNOR XP 94-91 (1995). These tests are conducted on an odometer (diameter 50 mm and thickness 20 mm). Considering how difficult the samples were to prepare, the initial vacuum ratio (e) varies with the contents of the rubber particles and their types. Samples are constantly pressed at a distance in four layers, each with a thickness of 4 mm to ensure a uniform dry density.

For homogeneous dry density, the specimens are statically compressed in the odometer into five layers, each 4 mm thick. Heave was permitted under a sitting surcharge based simply on the odometer for the sample (about 5 kPa) by continually allowing water into the soil specimen. After achieving the final heave (ΔH), the sample is compressed using increasing vertical loads until the original void ratio (e) is reached. For soils and their mixtures, swelling potential (S) and swelling pressure (PS) are measured. The swell potential is calculated as the ratio of the sample's original thickness (H) to its rise in thickness after submersion (ΔH). The pressure (PS) that corresponds to the initial void ratio (e), which is calculated from the e -log p curve, is identified as the swelling pressure (Akbarimehr et al., 2020).

3.2.1 Swell potential

Figure (6) shows the variation of swell potential (S) versus time for the Tizi soil sample compared to samples

mixed with 3, 6, 9, and 12% rubber granule contents and samples mixed with 3, 6, 9, and 12% rubber powder contents. Test results indicate that Tizi soil, reinforced with rubber granules, gives a potential of 3.88% in 21 days, whereas Tizi soil supported with rubber powder gives a 4.52% earned in 24 days.

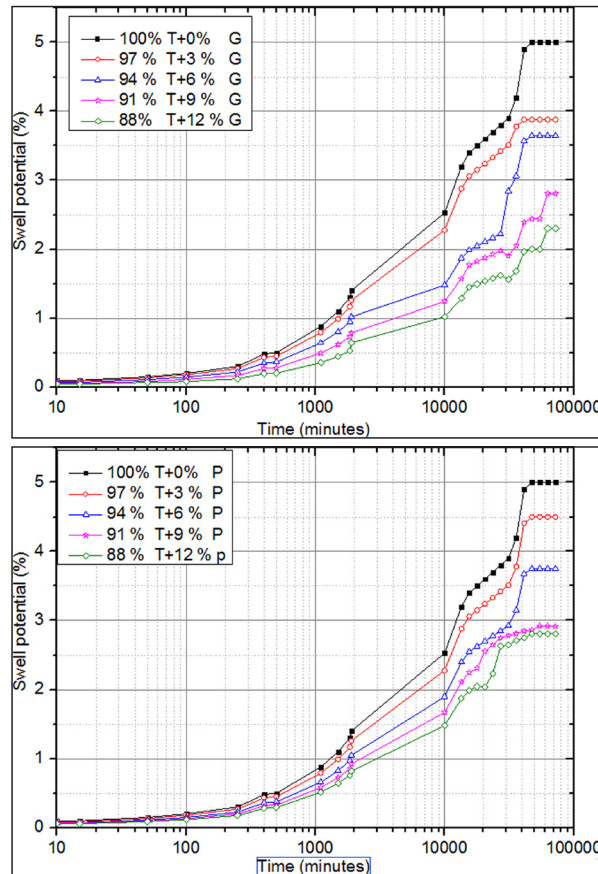


Figure 6. Effect of the rubber particles (granulated or powder) content on the swell potential of Tizi soil.

The final swelling of the compound samples is decreased, and, in practice, it reaches the same period for the compound samples with 3% of the rubber particles (granules or powder) and in less time for the compound samples with 6, 9, and 12% of the rubber particles.

Figure (6) indicates that rubber particles (granulated or powder) are very effective in reducing the swelling potential of Tizi. For the two rubber particles (Seda et al., 2007), the reduction of swell potential increases gradually with particle content. For Tizi soil reinforced with rubber granules, the reduction of swell potential is about 28.50% for a mixture with 3% of the granule content. It then ranges from 38.6% to 66.8% for respectively 9 and 12% of fiber content. Since all samples were prepared at 15% water content and rubber absorbs at most 4% of its weight, the water/Tizi soil rates at the beginning of the test were about 0.15, 0.18, 0.21, 0.24, and 0.28 for the mixture that contains 0, 3, 6, 9, and 12 % of the rubber particles (granules or powder), respectively, and these can be the reasons for reducing time. For Tizi soil reinforced with 3% rubber powder, the reduction of swell potential is about 11.5%, whereas with 6% of rubber powder, the reduction of the swell potential of the composite increases about 28.6%. A further reduction in the well potential of

Tizi soil in corporate with rubber powder is obtained by an increase in duration. The swell potential of 88% Tizi soil and 12% rubber decreases to 85% in 13 days (28 days for Tizi soil alone). This reduction in the reach time is undoubtedly due to the initial water: Tizi soil ratios, which were about 0.15 and 0.28 for samples with 0 and 12% of rubber particles. Their suction in the swell potential of the swell potential of Tizi soil increases gradually from 9 to 85% when powder content increases from 3 to 12%.

3.2.2 Swell pressure

Figure (7) illustrates the values of the swelling pressures of studied specimens. Swelling pressure (PS) decreases with particle content (Mistry et al., 2021). For Tizi soil reinforced with rubber granules, the swelling pressure was 6.40 kPa for Tizi soil samples, whereas the values of swelling pressure for composite samples at 3, 6, 9, and 12% are 6 kPa, 5.71 kPa, 5.42 kPa, and 5.12 kPa, respectively. The swelling pressure of Tizi soil and its mixtures decrease with rubber powder content. The swelling pressure was 4.35 kPa for Tizi soil samples, whereas the values of swelling pressure for powder-composite samples at 3, 6, 9, and 12% are 4.31 kPa, 4.28 kPa, 4.21 kPa, and 4.15 kPa, respectively.

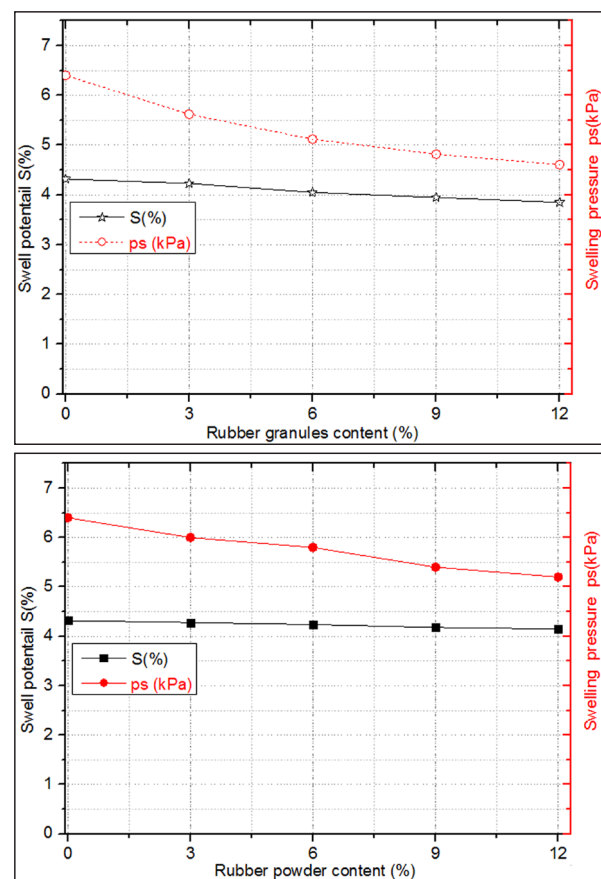


Figure 7. Effect of the rubber particles (granulated or powder) content on swell potential and swelling pressure of Tizi soil.

The swelling pressure values of Tizi soil reinforced with rubber granules were less than half those of Tizi soil reinforced with rubber powder (Ho et al., 2010). The reduction of swelling pressure for a composite sample with 12% rubber particles was about 8.5% and 13% for Tizi soil reinforced with granules and powder, respectively.

3.3 Loading–unloading tests

Due to the compressibility of the rubber particles to a greater degree and their qualitative weight being significantly lower than the specific weight of the Tizi soil (Nassim et al., 2019), a supplementary test program was performed under odometer conditions to obtain additional information on the mechanical behavior of Tizi soil and mixtures.

According to the method (AFNOR XP 94-090-1, 1997), the compression index (C_c) and the recompression Index (C_r) is determined for Tizi soil and composite samples.

3.3.1 Compression index

Figure (8) shows the compressibility indices of the Tizi soil and the mixtures reinforced with rubber granules of both types. It is known that the pressure index (C_c) is the slope of the linear part of the void pressure curve on a semi-logarithmic plot (Ming-Zhi et al., 2017; Ayeldeen and Kitazume, 2017). The C_c values are relatively small because the reshaped C_c has always been smaller than the non-isolated C_c .

The values vary from 0.22 to 0.28 for the Tizi soil that has been reinforced with rubber granules and its mixture and from 0.231 to 0.25 for Tizi soil reinforced with rubber powder and its mixtures. For the Tizi soil, C_c gradually increases with rubber particle content. This is what was found in the references (Soltani-Jigheh, 2016; Dang and Khabbaz, 2019).

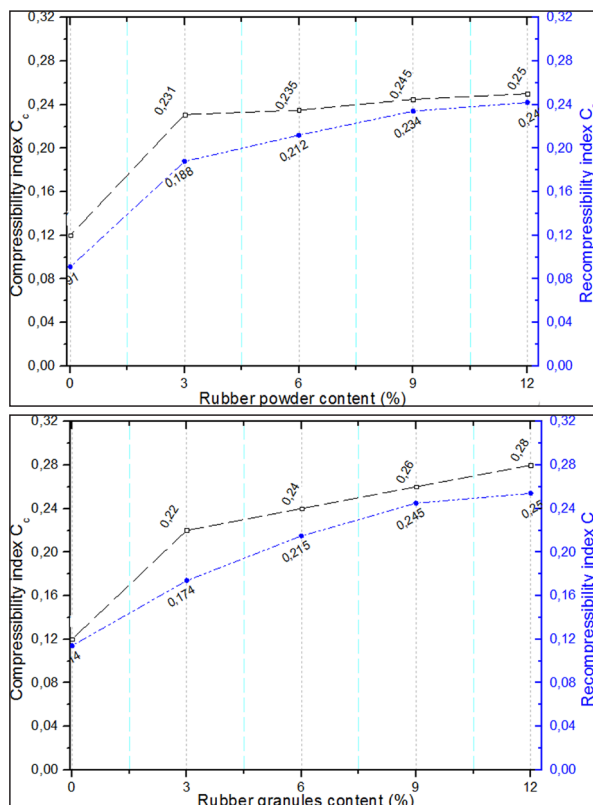


Figure 8. Effect of the rubber particles (granulated or powder) content on compression and recompression index of Tizi soils.

3.3.2 Recompression index

The Swell recompression has been calculated in this work as the decompression index C_r . The values of the swell recompression are generally about five times smaller than the compressibility (Prabakar and Sridhar, 2002; Liu et al., 2019). For all examined samples, C_r is approximately three

to four times smaller than C_c , and it rises with rubber particle content.

As it is shown in Figure (8), the values of C_r range from 0.0912 to 0.245 for the Tizi soil reinforced with rubber powder and its mixtures and from 0.0912 to 0.255 for the Tizi soil reinforced with rubber granules and its mixtures. The results of the present study also match the findings of the research conducted by Wu et al., (2022).

4. Conclusion

This investigation leads to the following findings:

- Mixing expansive Tizi soil samples with rubber particles (granules or powder) reduces heave and swelling pressure.
- Adding rubber particles (granules or powder) to swelling Tizi soil increases resistance to swelling due to contact fibers with the soil.
- The reduction in swelling potential at 3% rubber content is approximately 3.88% and 4.52% for low plasticity Tizi soil compared to high plasticity Tizi. For rubber particle contents of 6, 9, and 12%, the reduction is approximately the same for both rubber particles (granules and powder).
- As the rubber absorbs around 4% of the water as a percentage of its weight, the composite samples reach the final height in less time than the Tizi soil samples alone.
- Compression and decompression indices increase progressively with the rubber particle content of both particles (granules and powder). They exceed twice as much as 12% of the rubber particle content.
- Rubber particles, whether in granular or powder form, significantly reduce the probability of swelling and blistering of the tuff soil.
- The use of rubber waste, either powder or granules, as a stabilizing material result in a low-cost stabilization method and considerably reduces the problem of disposing of used tires.
- The current study focuses on the use of rubber waste as an additive to improve soil properties. The recycling of used tires would reduce the volume of solid waste redirected into a material that is useful for preserving the environment.

Data availability statement

The data that support the findings of this study are not available but can be provided upon reasonable request.

Conflicts of interest

The authors declare no conflict of interest.

Acknowledgments:

This work was supported by CNEPRU project code A01L02UN010120200004 and the Civil Engineering and Environmental Laboratory of the University of Sidi BelAbbes, Algeria.

References

- Akbarimehr, D., Hosseini, S.M. (2022). Elasto-plastic characteristics of the clay soil mixed with rubber waste using cyclic triaxial test results. *Arabian Journal of Geosciences* 15, 1280.

- Akbarimehr, D., Eslami, A., Aflaki, E. (2020). Geotechnical behavior of clay soil mixed with rubber waste. *Journal of Cleaner Production* 271: 122632.
- Akbarimehr, D., Aflaki, E. (2018). An experimental study on the effect of tire powder on the geotechnical properties of clay soils. *Civil Engineering Journal* 4(3): 594- 601, DOI: 10.28991/cej-0309118.
- Anvari, S.M., Shooshpasha, I., Kutanaei, S.S. (2017). Effect of granulated rubber on shear of fine-grained sand. *Journal of Rock Mechanics and Geotechnical Engineering* 9(5): 936-944, <https://doi.org/10.1016/j.jrmge.2017.03.008>.
- Ayeldeen, M., Kitazume, M. (2017). Using fiber and liquid polymer to improve the behavior of cement-stabilized of clay. *Geotextiles and Geo-membranes* 45(6): 592–602.
- Amakye, S.Y.O., Abbey,S.J., Booth,C.A., Oti,J. (2022). Road pavement thickness and construction depth optimization using treated and untreated artificially-synthesized expansive road subgrade materials with varying plasticity index. *Materials* 15: 2773.
- Akbulut, S., Arasan, S., Kalkan, E. (2007). Modification of clayey soils using scrap tire rubber and synthetic fibers. *Applied Clay Science* 38(2): 23–32.
- Al-Mukhtar, M., Lasledj, A., Alcover, J.F. (2010). Behavior and mineralogy changes in lime-treated expansive soil at 20°C. *Applied Clay Science* 50(2): 191-198.
- Al Dwairi, R.A., Al Saqarat, B., Shaqour, F., Sarireh, M. (2018). Characterization of Jordanian Volcanic Tuff and its Potential Use as Lightweight Aggregate. *Jordan Journal of Earth and Environmental Sciences* 9(2): 127 – 133.
- Ayala, S., Castaño, V. (2017). Expansion reduction of clayey soils through surcharge application and lime treatment. *Case Studies in Construction Materials* 7: 102-109.
- Balegh, B., Sellaf, H. (2022). Treatment of leachate of landfills using filters of ceramic waste and scrap rubber waste. *Water, Air, & Soil Pollution* 233 (12).
- Dang, L.C., Khabbaz, H. (2019). Experimental Investigation on the Compaction and Compressible Properties of Expansive Soil Reinforced with Bagasse Fiber and Lime. In: McCartney, J., Hoyos, L.(eds) *Recent Advancements on Expansive Soils. GeoMEast 2018. Sustainable Civil Infrastructures*. Springer, Cham. <https://doi.org/10.1007/978-3-030-01914-36>
- Ekincia, A., Vaz Ferreira, P. M., Rezaei, M. (2022). The mechanical behavior of compacted Lambeth-group clays without fiber reinforcement. *Geotextiles and Geomembranes* 50: 1-19.
- Goual, I., Goual, M.S., Gueddouda, M.K., & Ferhat, A. (2008). Effect of treatment with lime and cement on the mechanical behavior of calcareous tuffs: For use in pavement layers in the region of Laghouat – Algeria. *International Conference on Construction and Building Technology-A-* (10), 101–112.
- Goual, I., Goual, M.S., Taibi, S., & Abou-Bekr, N. (2011). The behavior of unsaturated tuff- limestones and mixture on drying–wetting and triaxial paths. *Geo-mechanics and Engineering*, 3, 267–284.
- Ho, M.H., Chan, C.M., Bakar, I. (2010). One Dimensional Compressibility Characteristics of Clay Stabilised with Cement-Rubber Chips. *International Journal of Sustainable Construction Engineering & Technology* 1(2): 91-104.
- Jaramillo, N.A.D., Dos Santos Ferreira, J.W., Malko, J.A.C. et al. (2022). Mechanical behavior of clayey soil reinforced with recycled tire rubber using chips and fibers. *Geotechnical and Geological Engineering* 40, 3365–3378. <https://doi.org/10.1007/s10706-022-02101-0>.
- Kang, G., Tsuchida, T., Tang, T.X., Kalim, T.P. (2017). Consistency measurements of cement-treated marine clay using fall cones and Casagrande liquid limit test. *Soils and Foundations* 57: 802-814.
- López-Lara, T., Hernández-Zaragoza, J., Horta-Rangel, J., Rojas-González, E., López- Liu, Y., Chang, C.W., Namdar, A., She, Y., Lin, C.H., Yuan, X., Yang, Q. (2019). Stabilization of expansive soil using cementing material from ricehusk ash and calcium carbide residue. *Construction and building materials* 221: 1-11, <https://doi.org/10.1016/j.conbuildmat.2019.05.157>.
- Loualbia, H., Sebaibi, Y., Duc, M. Goual, I. (2016). Effect of different drying methods on the mechanical behavior and the microstructure of an Algerian compacted limestone crust. *Journal of Adhesion Science and Technology* 3: 1045-1060.
- Mistry, M.K., Shukla, S.J., Solanki, C.H. (2021). Environmental Science and Pollution. Reuse of waste tyre products as a soil reinforcing material: a critical review. *Environmental Science and Pollution Research* 28: 24940–24971, <https://doi.org/10.1007/s11356-021-13522-4>.
- Ming-Zhi, Z., Qiang, L., Ming, W. (2017). Evaluation for intrinsic compressibility of reconstituted clay using liquid limit, initial water content and plasticity index. *European Journal of Environmental and Civil Engineering* 1: 1-19.
- Milhem, M. (2023). Chemical Effect on Soil Strength by adding Lime and Natural Pozzolana. *Jordan Journal of Earth & Environmental Sciences* 14 (1): 70-74.
- Nassim, A., Mumtaz, W., Fazal-e-Jalal, De Backer, H. (2019). Stabilization of expansive soil using tire rubber powder and cement kiln dust. *Soil Mechanics and Foundation Engineering* 56: 54–58.
- NF P 94-051, Sols: Reconnaissance et Essais – Détermination des limites d’Atterberg – Limite de liquidité à la coupelle – limite de plasticité au rouleau. Association Française de Normalisation.
- NF P 94-054, Sols: Reconnaissances et essais, Détermination de la masse volumique des particules solides des sols, Méthode du pycnomètre à eau. Association Française de Normalisation.
- NF P 94-056, Sols: Reconnaissances et essais, Analyse granulométrique, Méthode de tamisage à sec après lavage. Association Française de Normalisation.
- NF P 94-057, Sols: Reconnaissances et essais, Analyse granulométrique des sols, Méthode par sédimentation. Association Française de Normalisation.
- NF P 94-068, Sols : Reconnaissance et essais, Mesure de la capacité d’adsorption de bleu de méthylène d’un sol ou d’un matériau rocheux, Détermination de la valeur de bleu de méthylène d’un sol ou d’un matériau rocheux par l’essai à la tache. Association Française de Normalisation.
- NF EN 1744, Essais visant à déterminer les propriétés chimiques des granulats. Association Française de Normalisation.
- NF P94-093: Soils: recognition and tests – Determination of the compaction references of a material
- Normal Proctor test – Modified Proctor test. October 2014.
- Odari, N., Crispino, M., Toraldo, E. (2021). Laboratory investigation on using recycled materials in bituminous mixtures for dense-graded wearing course. *Case Studies in Construction Materials* 15.
- Pan, Q., Zheng, J. (2020). Mechanical calculation method and analysis of asphalt pavement considering different modulus in tension and compression. *China Civil Engineering Journal* 53 (1): 111-117.
- Prabakar, J., Sridhar, R.S. (2002). Effect of random inclusion of sisal fiber on strength behavior of soil. *Construction and Building Materials* 16: 123–131.
- Sarireh, M., Ghrair, A.M., Alsaqoor, S., Alahmer, A. (2021). Evaluation of the Use of Volcanic Tuff in concrete block production. *Jordan Journal of Earth & Environmental Sciences*, 12 (4): 275-284.
- Seda, J.H., Lee, J.C., Carraro, J.A.H. (2007). Beneficial Use of Waste Tire Rubber for Swelling

Potential Mitigation in Expansive Soils. Publication: Soil Improvement, [https://doi.org/10.1061/40916\(235\)5](https://doi.org/10.1061/40916(235)5).

Sellaf, H., Trouzine, H., Hamhami, M., Asron, (2014). Geotechnical properties of rubber tires and sediments mixtures. *Engineering, Technology & Applied Science Research* 4(2): 618–624.

Soltani-Jigheh, H. (2016). Compressibility and shearing behavior of clayey soil reinforced by plastic waste. *International Journal of Civil Engineering* 14: 479–489.

Wu, M., Liu, F., Li, Z., Bu, G. (2022). Micromechanics of granulated rubber–soil mixtures as a cost-effective substitute for geotechnical fillings. *Mechanics of Advanced Materials and Structures* 30(13): 2701-2717, DOI: 10.1080/15376494.2022.2062628.

Xiaobing, G., Zumei, Z., Mengyan, Z. (2022). A multi-sphere DE-FE method for traveling analysis of an off-road pneumatic tire on irregular gravel terrain. *Engineering Analysis with Boundary Elements* 139: 293-312. AFNOR. (1995). XP P 94-091, Sols: Reconnaissances et essais, Essai de gonflement à l'odomètre. Détermination des déformations par chargement de plusieurs éprouvettes. Association Française de Normalisation.

AFNOR. (1997). XP P 94-090-1, Sols: reconnaissance et essais. Essai œdométrique, Partie 1 : Essai de compressibilité sur matériaux fins quasi saturés avec chargement par

paliers: 23p.

The Development of Fine Precast Concrete Mix Using Local Materials

Mohmd Sarireh¹, Ayoup M. Ghrair², Sliiman M., M Zaidyeen³, and Mohmd Al-Jaraba⁴

¹Department of Civil Engineering, Faculty of Engineering, Tafila Technical University

²Department of Water Resources and Environmental Management-Al-Balqa Applied University, Al-Salt, Jordan

³Department of Civil Engineering, Faculty of Engineering, Al-Hussein Ben Talal University

⁴Tafila Technical University, Faculty of Engineering, Department of Civil Engineering

Received September 23th, 2023; Accepted November 15th, 2023

Abstract

The imperative to enhance the quality of precast concrete is evident, with a particular focus on augmenting its physical and mechanical attributes by incorporating concrete admixtures. This research centers on the utilization of phosphate minerals and finely ground glass within concrete mixes, with substitution ratios ranging from 15% to 60% of fine sand within the mix. The investigation encompasses multiple facets, including examining material blending, assessing fresh concrete properties (slump), and evaluating both physical and mechanical characteristics of hardened concrete at 7-day and 28-day intervals, juxtaposed against the properties of a control concrete mix. The findings reveal several significant outcomes. Firstly, the incorporation of phosphate minerals leads to a remarkable increase in the slump of concrete, reaching 75mm, in stark contrast to the 20mm slump observed in the control mix. Conversely, introducing fine glass elevates the slump to 60mm while maintaining a constant water-to-cement ratio of 0.48 across all concrete mixtures. Furthermore, the density of the hardened concrete demonstrates notable variations. The control mix boasts a density of 2375kg/m³, whereas the phosphate minerals and fine ground glass result in reduced densities of 2258kg/m³ and 2100kg/m³, respectively, at the 7-day and 28-day intervals. In terms of compressive strength, the 7-day results indicate a decrease to 8MPa with the use of phosphate and fine ground glass minerals, compared to the 13MPa strength observed in the control mix. At the same time, the compressive strength increases to 21MPa for phosphate “Shedyah,” compared to 20MPa for the control mix. Phosphate “Abiad” and fine ground glass yield compressive strengths of 15MPa and 16MPa, respectively, at the 28-day mark. Regarding tensile strength, the 7-day figures reveal 1.25MPa for the control mix, and the introduction of phosphate materials results in both increases and decreases, with values remaining similar to the control mix. Conversely, the 28-day tensile strength diminishes to 2.75MPa and 2.5MPa for “Shedyah” and “Abiad,” respectively, in contrast to the 3.5MPa exhibited by the control mix. The use of fine ground glass materials results in a tensile strength of 1.8MPa. Lastly, the flexural strength of the control mix stands at 2.5MPa, a value that can be maintained with “Shedyah” phosphate but reduces to 2MPa when “Abiad” phosphate is introduced. Fine ground glass fines maintain a flexural strength of 1.5MPa at 7-day, compared to the 3.25MPa of the control mix, with subsequent fluctuations resulting in strengths of 2.75MPa for “Shedyah” phosphate, 2.5MPa for “Abiad” phosphate, and 2.25MPa for ground glass fines.

© 2024 Jordan Journal of Earth and Environmental Sciences. All rights reserved

Keywords: Phosphate, Fine Ground Glass, Concrete Mix, Mix Design

1. Introduction

The construction industry is continuously evolving with a growing emphasis on sustainability and environmental responsibility. Fine precast concrete—a versatile and widely used construction material—has gained attention due to its potential for enhancing sustainability in the construction sector. Incorporating local materials, such as glass waste, into concrete mix design, is one approach that can reduce the environmental impact of concrete production. The addition of raw and natural materials is common in concrete mix production (Ghrair et al, 2022), while maintaining or even improving its performance characteristics (Smith & Brown, 2022). Furthermore, concrete is globally used as a building material for its economy, formability, durability, availability of components, and its suitability for use in a variety of environments, given its exceptional compressive strength

competitively, compared to other popular building materials (Kizilkanat et al.2015, Sadrmomtazi et al.2018). Though concrete is weak in tensile strength, it could be improved using fibers or using natural mineral materials. This literature review explores the development and utilization of fine precast concrete mixtures using local materials such as phosphates raw material and fine waste glass bottles as supplementary material. The improvement in properties of the concrete mix is essential in construction work and concrete technology to improve the quality in compliance with concrete specifications of contract, approval, and satisfaction of construction work (Sarireh et al, 2021; Ghrair et al, 2018). Also, Kennouche et al., 2022 applied the use of plastic waste and its effect on concrete properties.

Several case studies and real-world applications have demonstrated the feasibility and effectiveness of

* Corresponding author e-mail: m.sarireh@ttu.edu.jo

incorporating glass waste and local materials into fine precast concrete. The use of industrial products is common in concrete-based fiber content (Iqbal et al., 2015).

According to Johnson & Green (2020), glass waste, typically sourced from post-consumer glass products or industrial waste, has been identified as a promising supplementary material for concrete. It can replace a portion of traditional aggregates, such as sand and gravel and, thus, reduce the demand for natural resources. The incorporation of glass waste also offers the advantage of diverting waste from landfills, contributing to waste management and recycling efforts. In addition, Gonzalez & Patel (2019) reported that various studies have proposed optimization techniques to maximize the benefits of using glass waste in fine precast concrete. This process includes optimizing the particle size distribution of glass waste, adjusting the cement content and considering other supplementary materials, such as pozzolans and chemical admixtures. Also, the use of Jordanian volcanic tuff in aggregate for the production of light-weight concrete (Dwairi et al., 2018). Phosphate-based materials, such as phosphor content or glass fine materials are employed in low temperature building conditions (Aliha et al., 2017). Also, Anderson and Patel (2021) introduced the use of phosphate raw materials in concrete for sustainable aspects and objectives.

Adding fibers to a concrete mix enhances its mechanical qualities, such as strength when subjected to bending, tensile, and fatigue forces. Concrete's toughness, ductility, and non-linear behaviour are, thereby, improved by the fibers (Iqbal et al. 2015); Hannawi et al. (2016); Santarelli et al. (2014). In general, the fibers improve the crushing capacity of the members of the structure and stop micro cracks in concrete. As indicated that the use of local natural materials such as crushed and rounded aggregate in concrete production in Karak and Tafila area are shown in two studies on concrete mix. The first one is Sarireh, 2015-a. It uses local materials of crushed limestone aggregate and rounded valley aggregate for testing concrete properties, and the second one is Sarireh (2015-b) that uses the optimum percentage of volcanic tuff in concrete mix production. Also, the use of basalt aggregate materials in concrete mix production and improvements in concrete production and strength (Sarireh, 2017). In addition to the use of local materials of aggregate in concrete mix production in a national project in the twelfth governorates in Jordan (Sarireh and Al-Baijaj, 2019-a). Also, the use of blast furnace slag in concrete mix production is considered an important improvement in concrete compressive strength, tensile strength, and flexure of material of concrete (Al-Baijaj and Sarireh, 2019-a).

Fibers are randomly dispersed discrete components that are used to stop cracks from propagating or forming in concrete owing to external or internal stresses (Aliha et al. 2017 & Aliha, et al. 2018). Fibers play a key role in the post-cracking zone, and their inclusion could improve concrete's toughness and energy absorption capacity. Because a single fiber could only be successful in a single aspect dependent on fiber size and type, the total performance of concrete is improved by the addition of different fibers (Rooholamini

et al. 2018).

It is difficult and expensive to improve cement through the addition of additives and needs advanced technical solutions (Sarireh, 2020). The current case study is concerned with adding admixtures directly to the concrete mix. In this study, three fine materials (phosphate Shedyah, phosphate Abiad, and fine glass) of similar size of sand in the concrete mix are tested and used as samples for density, compressive strength, tensile strength, and flexural strength of concrete, compared with the control concrete mix. The study aims to test the impact of adding phosphate Shedyah, Abiad, and fine ground glass materials to the physical and mechanical properties of precast fine concrete.

2. Research Methodology

This study includes the design and testing of fresh and hardened properties of precast fine concrete mix through using phosphate Abiad, Shedyah, and glass fines in replacement with the fine sand in concrete mix at percentages of 15, 30, 45, and 60%. It is an effective and innovative procedure to use different materials to improve the properties of fresh and hardened concrete. A former study was done to use Tripoli materials as cement replacement to produce concrete mix and test its fresh and hardened properties (Sarireh and Al-Baijaj, 2019-b), and also, the use of Tripoli in the concrete mix in replacement with a sand component in the concrete mix (Al-Baijaj and Sarireh, 2019-b).

For the fine concrete mix design, the mix contains only Addaseyah as the maximum size of aggregate (12-6mm), Semsemeyah (6-2 mm), and fine sand (2-0.6 mm). The new mixed materials of phosphate of Abiad, phosphate of Shedyah, and fine ground glass were replaced with the sand portion in the concrete mix.

Physical and chemical analysis of proposed materials was conducted, and specific volumes of proposed materials were prepared for the concrete mix at the designed ratios of materials. Also, w/c ratio is considered constant at 0.4 for all concrete mixes following the instructions of testing methodology (Ghrais et al., 2018).

112 samples of concrete cubes were prepared to test density (unit weight) and compressive strength of concrete on 7-day and 28-day periods, in addition to 96 samples of cylinders for tensile strength test conducted at 7-day and 28-day periods. Also, 96 beam samples were prepared for flexural strength test at 7-day and 28-day periods. Samples were prepared for control mix and other mixes of phosphate and fine ground glass materials 15, 30, 45, and 60% ratios. Also, the slump of each fresh concrete mix was tested (3) times and the average of slump values was calculated for all concrete mixes. Samples were kept in distilled water tank for curing at 18°C temperature until testing times at 7-day and 28-day periods.

2.1 Cement

Cement is a material with adhesive and cohesive properties that allow it to bond with the components of the concrete mixture. Ordinary Portland Cement (OPC) Type I was used in the concrete mixes according to EN 197-1-2011 standards with 3.15 specific gravity. Table 1 shows the

chemical and physical properties of the OPC used.

Table 1. The Physical and Chemical Properties of OPC.

Chemical and physical properties	Percentages (%)
Silicon Oxide (SiO ₂)	20.41
Aluminum Oxide (Al ₂ O ₃)	4.51
Ferric Oxide (Fe ₂ O ₃)	3.43
Calcium Oxide (CaO)	64.74
Magnesium Oxide (MgO)	1.99
Sulfur Trioxide (SO ₃)	2.9
Potassium Oxide (K ₂ O)	0.52
Sodium Oxide (Na ₂ O)	0.32
Tricalcium Aluminate (C ₃ A)	7.5
Chloride (Cl)	0.03
Loss On Ignition (L.O.I)	1.15
Specific Service Area	3550 cm ² /g
Initial Setting Time	155 min.

2.2 Aggregate and Sand

Since aggregates represent the majority of the volume of concrete, it is important to determine their physical properties, including size, shape, texture, porosity, absorption, moisture content, and bulking of fine components. These characteristics influence concrete strength and durability, as well as the water to cement ratio (w/c), which influences concrete quality.

According to the ASTM C33/C33M-16 standard, the aggregate was chosen based on the original rocks, specific gravity, and particle size. All aggregates were provided by the Jordanian Manaseer Group. The aggregate types used in the experiment were as follows:

Limestone is the source of medium aggregate, and it was used in this study with a maximum size of 9.5 mm (3/8 in.) and also passing sieve No. 4 (4.75 mm). The medium aggregate is known as Adaseyah and has a Sp.Gr. (dry) of 2.57, Sp.Gr. (SSD) of 2.55, Sp.Gr. (Apparent) of (2.65), bulk density of 1500 kg/m³, absorption of 2.5%, and abrasion of 29%. Table 2 shows specific gravity of used materials in concrete mix.

Table 2. Specific Gravity of Mixing Materials.

Material	Sp. Gr. (Dry)	Sp. Gr. (SSD)	Sp. Gr. (App)	Bulk Density	Absorption	Abrasion
Medium Aggregate	2.566	2.546	2.649	1500	0.025	0.29
Sand	2.616	2.629	2.65	1577	0.005	-----
Glass	2.67	2.58	2.69	1680	0.004	----

Fig. (1) presents the mixing materials that were used in fine concrete mixing design in current project. Ordinary and original materials include Addaseyah medium aggregate, Semsemeyah fine aggregate, and fine sand. And the new mixing materials include phosphate material from Abiad mining site that is close to Al-Hasa area in Tafila and

Shedyah from Shedyah mining site in Ma'an, in addition to the fine ground glass by collecting waste glass bottles, cleaned and ground to sand gradation size. Also, phosphate materials were employed in fine precast concrete production as conducted by Smith and Greenfield, P. (2022).



Figure 1. Materials of Fine Concrete Mix Design.

For the quantities of mixed materials in concrete mix, Table 3 shows the quantity of concrete design for preparing mix 1m³ of concrete, in addition to the volume of cement and w/c ratio of the mix.

Table 3. Quantities of Mixing Materials of Fine Concrete Design.

Material	Gradation (mm)	Quantity Kg/m ³
Addaseyah	4-9.5	1,000
Semsemeyah	2-4	501
Sand	0.06-2	501
Cement	---	391
Water	---	190

*w/c ratio is 0.48

The admixtures of Phosphate (Shedeyah and Abiad) and glass fine were mixed separately at ratios 15, 30, 45, and 60% in replacement with sand materials in the mix are presented in Table 4.

Table 4. Ratios and Quantities of Admixtures in Fine Concrete Mix Design.

Material	Quantity Kg/m ³	Admixture Ratio			
		15%	30%	45%	60%
Sand or Fines	501	75.15	150.3	225.45	300.6

2.3 Chemical Composition of Fine Ground Glass

A quantity of 15kg of glass was collected and ground to get the size gradation relevant to that of fine sand to be mixed at 15, 30, 45, and 60% ratios in the concrete mix. Table 5 shows the chemical composition of glass fines that was used in the concrete mix.

Table 5. Chemical Composition of Glass

Oxides	SiO ₂	Al ₂ O ₃	Fe ₂ O ₃	MgO	Na ₂ O	K ₂ O
%	70.4	1.9	1.2	10.3	14	0.4

2.4 Chemical Composition of Jordanian Phosphate

The chemical analysis of constituents in phosphate materials and their percentages are important as the materials will be used in substitution of fine sand. The required quantities are prepared from Jordanian phosphate from Shedyah and Abiad mining sites in the south of Jordan. Table 6 presents the chemical composition of Jordanian Phosphate in Abiad and Shedyah in Jordan.

Table 6. Chemical Composition of Jordanian Phosphate

Phosphate Source	Na ₂ O	Al ₂ O ₃	SiO ₂	P ₂ O ₅	K ₂ O	CaO	Ti O ₂	MnO	Fe ₂ O ₃
Abiad	0.0	1.23	0.56	29.17	0.09	54	0.02	0.02	0.3
Shedyah	0.0	1.17	0.48	29.54	0.1	52.7	0.04	0.03	0.29

2.5 Mixing and Sampling

The required wooden fair-face molds were prepared to cast the concrete mix properly. The molds were prepared in the specific dimensions for each test. Molds for concrete compressive test and density were prepared in

(150x150x150mm) cubes, where cylindrical metal molds were considered for splitting the tensile strength of concrete, and wooden fair-face molds were prepared for the flexural strength of concrete. Fig. (2) shows the molds of sampling in the current Project.



(a) Molds of Concrete Compressive Strength

(b) Molds of Flexural Strength

(c) Molds of Tensile Strength

Figure 2. Molds of Concrete Samples

The mixing is done by hand in the work site for controlling the mix and other mixes with admixtures of Abiad and Shedyah phosphates and fine glass materials. Samples were taken as 6 samples for each parameter of physical and mechanical properties of concrete at 7-day and 28-day periods. Fig. (3) shows the mixing stage and quantity of concrete that was prepared each time.

2.5.1 Testing of Fresh Concrete Mix

One of the important test for fresh concrete is the slump test (ASTM C143) that is able to evaluate workability and

the presence of humidity and its required levels, considering construction type and application. After mixing concrete ingredients, concrete ingredients including aggregate, sand, cement, and water are mixed for control mix design and other mixes for added materials, and concrete is poured in the frustum cone on (3), layers and each layer is compacted (25) strokes to evaluate the workability and consistency (humidity) of concrete, slump is measured to the nearest mm for concrete. Fig. (4) presents the mechanism of conducting slump test to concrete.



Figure 3. Mixing Operation for the Study of Concrete Properties



(a) Layering and Free Compaction (b) Flipping of Slump Mold (c) Measuring of Slump Value

Figure 4. Slump Test for Fresh Concrete Mix

2.5.2 Sampling of Concrete Specimens

Cube samples (150x150x150mm) of 12 were taken to represent the test of compressive strength of control concrete mix and other mixes using Abiad phosphate and Shedyah phosphate and fine glass materials. 6 samples will be tested on 7-day, and other 6 ones will be tested on 28-day period. Samples of concrete are prepared according to

ASTM C31/C31M-22, the standard practice for making and curing concrete test specimens in the Field. Fig. (5) shows the preparation of samples of concrete mix. Also, 12 samples were taken for splitting tensile strength in order to be tested on 7-day and 28-day periods. In addition, 12 samples were taken to test the flexural strength of concrete.

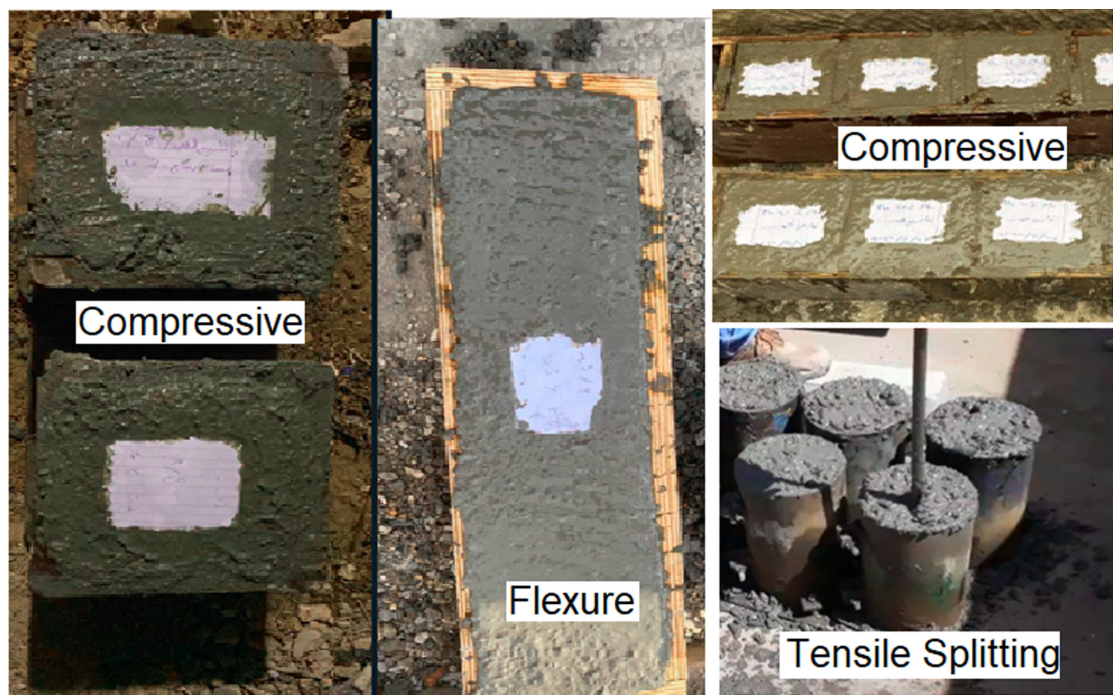


Figure 5. Samples of Concrete Mix for Compressive, Flexural, and Tensile Strengths

2.5.3 Curing and Testing of Concrete Samples

Samples of concrete, when prepared, were kept 24 hours in molds to insure drying process. Then, they were dismantled and kept in distilled water for curing up to 7-day and 28-day periods in order to be tested for density, compressive, tensile, and flexural strengths for control mix and all other mixes were made by Abiad phosphate, Shedyah phosphate, and glass fine materials. Fig. (6) presents the curing of concrete samples for 7-day and 28-day periods until testing samples.



Figure 6. Curing of Concrete Samples

After curing of samples for 7-day and 28-day periods, six samples are weighed and tested for compressive strength. After 28-day, other six samples were also weighed and tested for compressive strength. The weight is used to calculate density of concrete at 7-day and 28-day periods. Fig. (7) shows the compressive strength test of concrete. Also, the shape of failure or fracture of cube specimen is shown to be ideal for all samples.



Figure 7. Compressive Strength Test and Shape of Failure for Cube Specimens.

Also, similar numbers of samples are tested for tensile and flexural strengths of concrete on 7-day and 28-day periods when cured for the same periods respectively. Fig. (8) shows the test of tensile and flexural concrete strength.

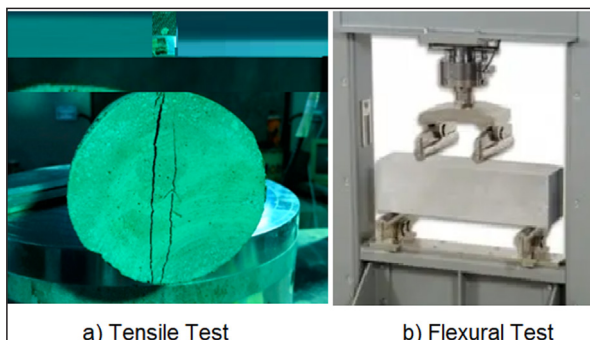


Figure 8. Tensile and Flexural Tests of Concrete.

3. Results and Discussion

3.1 Slump Test of Fresh Concrete

Slump value is an important property for concrete that the workability of concrete is measured using slump value at fresh state, in addition to other tests such as flow table and VB-Time. Figure (9) presents the slump values for control concrete mix, and other concrete mix of Phosphate Abiad, Phosphate Shedyah, and Glass fine at the mixing ratios 15, 30, 45, and 60% in concrete mix. Fig. (9) presents the value of slump for the concrete mix on different ratios of phosphate materials from Abiad and Shedyah mining and glass fines during mixing.

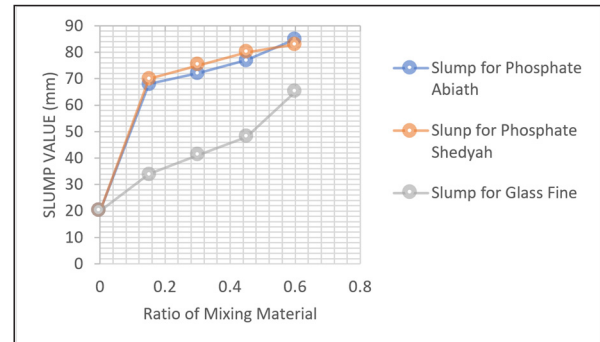


Figure 9. Slump Test of Fresh Concrete.

3.2 Density and Unit Weight of Hardened Concrete

Density and unit weight of concrete are both the most important properties of concrete to test and determine the type of concrete such as to be light weight, normal, or heavy weight concrete. Figure (10) presents the density of concrete at 7-day age of concrete when different materials are mixed in replacement with fine sand in concrete mix. Materials included Phosphate Abiath, Phosphate Shedyah, and Glass Fine materials mixed at once. Fig. (10) presents the density of concrete using the phosphate and glass fines in concrete.

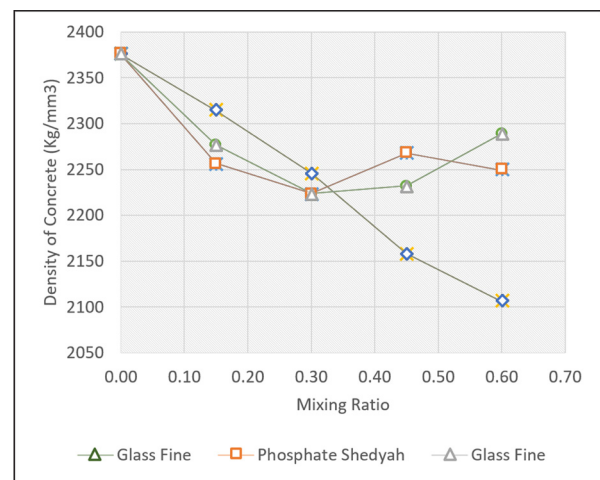


Figure 10. Density of Hardened Concrete at 7-day Period.

Also, it is necessary to evaluate density of concrete at 28-day period. The density of concrete at 28-day period is presented in Fig. (11).

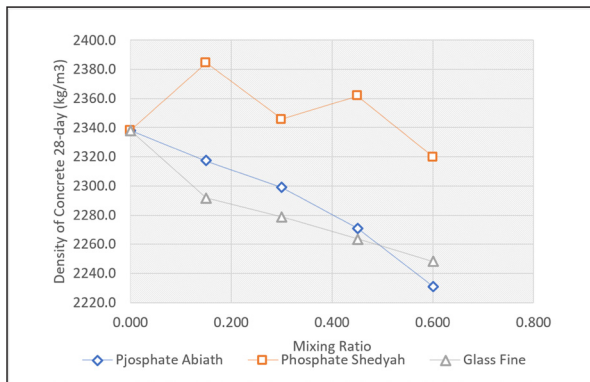


Figure 11. Density of Hardened Concrete at 28-day Period.

Also, Fig. (12) presents the unit weight of concrete using phosphate materials and glass fines material that were used in concrete mix.

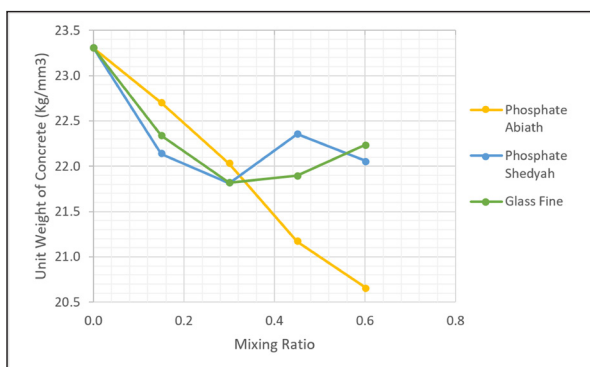


Figure 12. Unit Weight of Concrete at 7-day Period.

Fig. (13) presents the unit weight of concrete that was evaluated on 28-day period of concrete in the current project. The unit weight is an important property of concrete that is used in calculating the dead load of structures during design and evaluating of loads and structures.

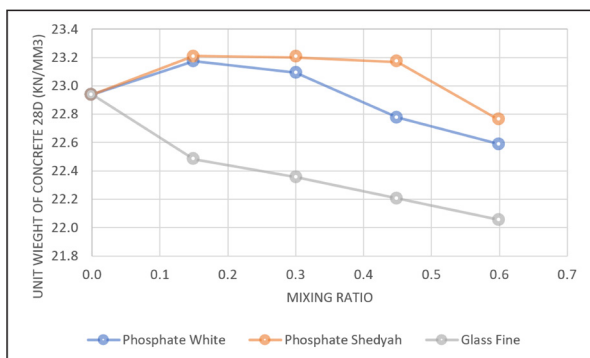


Figure 13. Unit Weight of Concrete at 28-day Period.

3.3 Compressive Strength

Compressive strength also is an important for concrete at the hardened state and is tested using cubic or cylinder molds. The cubic molds (15x15x15 cm) were used for testing and evaluating of compressive strength of concrete. Fig. (14) presents the compressive strength of concrete mix using phosphate materials and glass materials at 7-day age.

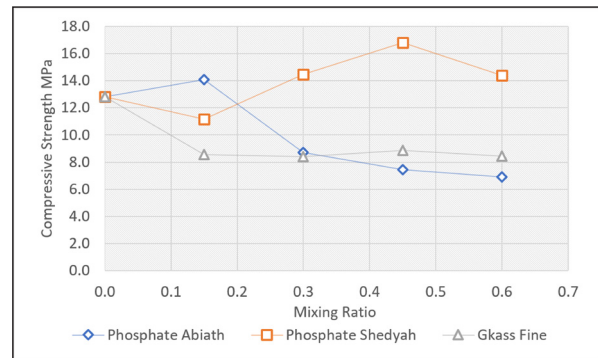


Figure 14. Compressive Strength of Concrete at 7-day Period.

Also, to follow the development of strength the compressive strength in concrete is evaluated at 28-day period. Fig. (15) presents the compressive strength of concrete at 28-day age of concrete.

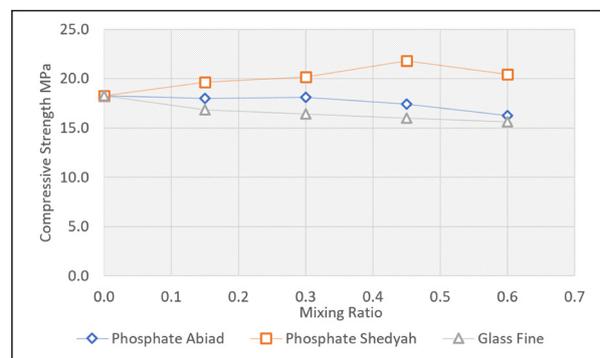


Figure 15. Compressive Strength of Concrete at 28-day Period.

3.4 Tensile Strength by Splitting

Tensile strength is an important property of concrete as the concrete can afford a minimal tensile strength when subjected to tension stresses in beams and slabs and columns. Fig. (16) presents the tensile of concrete, using phosphate and glass fine materials at 7-day period.

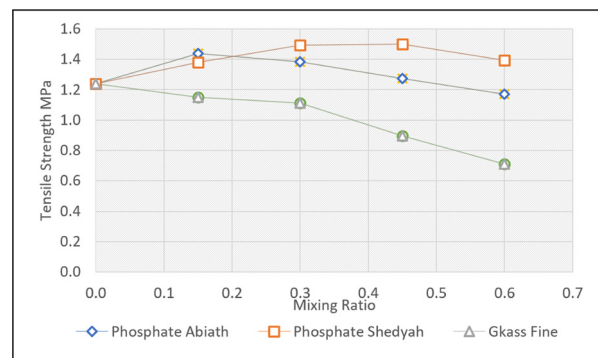


Figure 16. Tensile Strength of Concrete at 7-day Period.

The tensile strength of concrete is another indication on the quality of concrete and the improvement of concrete strength in general, Additional tests need to be made to adopt a decision that the concrete of good or specific quality. Fig. (17) presents the splitting tensile strength at 28-day age of concrete.

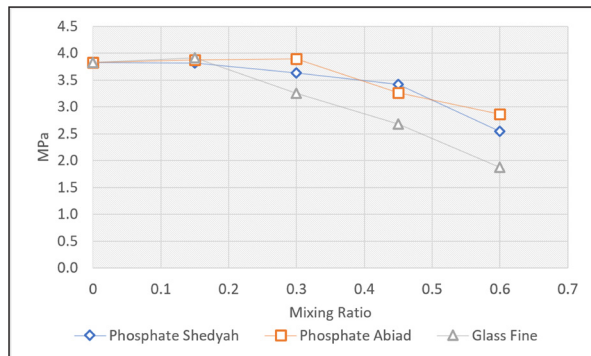


Figure 17. Tensile Strength of Concrete at 28-day Period.

3.5 Flexural Strength

Flexural strength, also, is an important property for the concrete specially for beams and slabs to resist flexural stresses and for columns to resist buckling. Fig. (18) and Fig. (19) present the flexural stresses in concrete using phosphate and glass fine materials 7-day and 28-day periods.

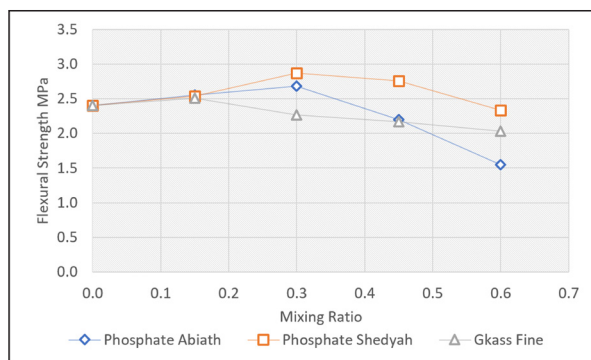


Figure 18. Flexural Strength of Concrete at 7-day Period.

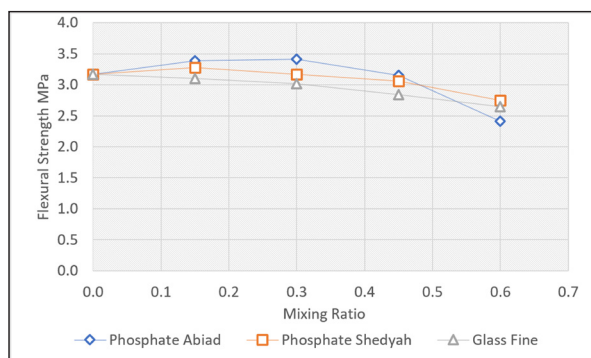


Figure 19. Flexural Strength of Concrete at 28-day Period.

4. Conclusion

According to the findings of the study, the following conclusions can be highlighted:

- Using phosphate materials from Abiad and Shedyah sources can increase slump value up to 70-80mm, compared to 20mm for control mix, without increasing of w/c ratio (0.4) to maintain the increase in compressive strength of concrete mix.
- Also, slump value is increased from 35mm to 65mm using glass fines in concrete mix.
- Density of control mix at 7-day is 2375 kg/m³, and density is decreased to 2275-2250 kg/m³ when Shedyah and Abiad materials of phosphate, while it could be decreased into 2100 kg/m³ when glass

fines materials are used at 7-day period. While the density at 28-day could be maintained using Shedyah, it still decreases using Abiad and glass fine materials. Similar conclusions could be elicited on unit weight of concrete.

- The compressive strength of the control mix is 13 MPa, while it was decreased to 8 MPa using phosphate of Shedyah and glass fines.
- Compressive strength at 28 days can be maintained, using phosphate of Shedyah up to 21 MPa compared to the compressive strength of control mix that maintained 20 MPa while it was decreased to 15MPa and 16MPa using glass fine and phosphate of Abiad respectively.
- The tensile stress of the control mix is 1.25MPa at 7-day, while it is increased and decreased again to maintain this strength using phosphate from Abiad and Shedyah, and it is decreased all the time using glass fine materials.
- Tensile strength of control mix is 3.75MPa at 28-day period, while it is maintained by Shedyah and Abiad to decrease to 2.75 and 2.5MPa respectively. And it is decreased using glass fine materials to 1.8MPa.
- The flexural stress of the control mix is 2.5MPa and could be maintained using Shedyah phosphate at 2.5MPa. It could also be decreased to 2MPa using Abiad Phosphate. By using glass fines, the flexural stresses is maintained on 1.5MPa at 7-day.
- The flexural strength is 3.25MPa of the control mix and starts to increase but to decrease to 2.75 for Shedyah, 2.5 for Abiad, and to 2.25 to glass fines.

5. Recommendations

- It is recommended to use materials that can help in reducing water/cement ratio and increase strength or do not affect strength adversely.
- It is recommended to use phosphate materials and glass fines up to 20% to increase and improve the slump of the concrete mix.
- It is recommended to use phosphate from Shedyah and/or Abiad sources up to 20% by replacing fine sand in concrete mix to keep strength parameters accepted.
- It is recommended to expand and apply the research widely to prove the results and generalize them clearly.

Acknowledgement

The researchers would like to direct their acknowledgements and thanks to the staff in the laboratories of concrete in Tafila Technical University, in Mu'tah University, The Southern Engineering laboratory in Karak, and the staff of Laboratory of Karak General Work Directorate. Also great thanks are granted to the students in Civil Engineering Department in Tafila Technical University: Ahmad Al Huwian, Omar Al Rubaihat, and Mohammad Saqrayeh for their efforts in fulfilling the current research.

References

- Al-Baijat Hamadallah and Sarireh, Mohmd (2019-a). The Use of Fine Blast Furnace Slag in Improvement of Properties of Concrete. *Open Journal of Civil Engineering*, 9 (2), 95-105, January 2019.
- Al-Baijat Hamadallah and Sarireh, Mohmd (2019-b). Concrete Properties Using Tripoli. *Electronic Journal of Geotechnical Engineering*, Vol. (24), 2019, Bund.2.
- Aliha, M. R., Razmi, A. and Mansourian (2017). The influence of natural and synthetic fibers on low temperature mixed mode I + II fracture behavior of warm mix asphalt (WMA) materials. *Engineering Fracture Mechanics*, Vol (182), pp: 322-336.
- Aliha, M. R., Razmi, A., Mousavi, A. (2018). Fracture study of concrete composites with synthetic fibers additive under modes I and III using ENDB specimen. *Construction and Building Materials*, Vol (190), pp: 612-622.
- Anderson, S. G., & Patel, R. (2021). Sustainable Construction Materials: Exploring the Use of Phosphate Raw Materials in Fine Precast Concrete Mix Design. *Journal of Sustainable Building and Construction*, 8 (2), 75-92.
- ASTM Standard Test Method C143: Slump of Hydraulic Cement Concrete.
- ASTM C31/C31M-22, Standard Practice for Making and Curing Concrete Test Specimens in the Field.
- Dwairi, R., Al Saqarat, B., Shaqour, F., Sarireh, M. Characterization of Jordanian Volcanic Tuff and its Potential Use as Lightweight Aggregate. 2018. *JJEES* 9(2): 127-133.
- Ghrrair, Ayouf M, Othman A Al-Mashaqbeh, Mohmd K Sarireh, Nedal Al-Kouz, Mahmoud Farfoura, Sharon B Megdal (2018). Influence of grey water on physical and mechanical properties of mortar and concrete mixes. *Ain Shams Engineering Journal* 9(4), 1519-1525.
- Ghrrair, A. M., Said, A. J., Al-Kroom, H., AL Daoud, N., Hanayneh, B., Mahanna, A., Gharaibeh, A. (2022) Utilization of Jordanian Bentonite Clay in Mortar and Concrete Mixtures. *JJEES* 14(1): 19-29. Gonzalez, M. C., & Patel, S. B. (2019). Optimization of Glass Waste-Infused Fine Precast Concrete Mixes for Sustainability and Durability. *Construction and Building Materials*, 185, 215-228.
- Hannawi, K. Bian, H. Prince-Agbodjan, W. and Raghavan, B. (2016). Effect of different types of fibers on the microstructure and the mechanical behavior of Ultra-High Performance Fiber-Reinforced Concretes. *Composites Part B: Engineering*, Vol. (86), pp: 214-220.
- Iqbal, S. Ali, A. Holschemacher, K. and Bier A. T. (2015). Mechanical properties of steel fiber reinforced high strength lightweight self-compacting concrete (SHLSCC). *Construction and Building Materials*, Vol. (98), pp: 325-333.
- Johnson, R. M., & Green, L. A. (2020). Sustainable Concrete Mix Design: Utilizing Glass Waste as Supplementary Material. *International Journal of Environmental Engineering and Sustainable Development*, 5(2), 87-102.
- Kennouche, S., Brahim, H., Abdelli, H. E. Aguiar, I. L. B., Jesus, C. (2022). Plastic Waste for the Enhancement of Concrete Properties - A review. *JJEES* 13(4): 263-270.
- Kizilkanat, A. B., Kabay, N., Akyüncü, Chowdhury, V. S. and Akça, A. H. (2015). Mechanical properties and fracture behavior of basalt and glass fiber reinforced concrete: An experimental study. *Construction and Building Materials*, Vol. (100), pp: 218-224.
- [Sadr-momtazi, A. Tahmouresi, and Saradar, A. (2018). Effects of silica fume on mechanical strength and microstructure of basalt fiber reinforced cementitious composites (BFRCC). *Construction and Building Materials*, Vol. (162), pp: 321-333.
- Santarelli, M.L., Iorio, M., González-Gaitano, G., González-Benito, J. (2018). Surface modification and characterization of basalt fibers as potential reinforcement of concretes. *Applied Surface Science*, Vol (427), pp: 12a48-1256.
- Sarireh, Mohmd (2015-a). The Use of Local Materials Crushed and Rounded Aggregate in Tafila and Karak Areas in Concrete Production. Dubai, 2015, Conference Poverty Alleviation Through Projects, American University, Dubai, United Arab Emirates, 25- 28/5/2015.
- Sarireh, Mohmd (2015-b). Optimum percentage of volcanic tuff in concrete productio. *Yanbu Journal of Engineering and Sciences*, Volume 11 (1), pp:43-50.
- Sarireh, Mohmd (2017). High Strength Concrete Using Basalt Aggregate in Concrete Mix Improvemnet. The International Academic Cluster Conference, Bangkok, Thailand, 5- 6 October 2017.
- Sarireh, Mohmd and Al-Baijat Hamadallah (2019-a). Local Aggregate in Production of Concrete Mix in Jordan. *Open Journal of Civil Engineering*, 9 (2), 81-94, January 2019.
- Sarireh, Mohmd and Al-Baijat Hamadallah (2019-b). Cement-Tripoli Admixture Replacement in Concrete Mix. *Electronic Journal of Geotechnical Engineering*, Vol. (24), 2019, Bund.2.
- Sarireh, Mohmd (2020). Examining the Suitability of Tripoli as Admixture in Cement Paste. *International Journal of Construction Management*. Accepted 2 November 2020, 2022, 22 (16), pp: 3169-3174.
- Sarireh, Mohmd, Sameh Al-Sqoor, Ayouf M. Ghrrair, and Ali Al-Ahmer (2021). Evaluation of the Use of Volcanic Tuff in Concrete Block Production. *Jordan Journal of Earth and Environmental Sciences (JJEES)*, 16 March 2021.
- Sarireh, Mohmd, Sameh Al-Sqoor, Ayouf M. Ghrrair, and Ali Al-Ahmer (2021). Evaluation of the Use of Volcanic Tuff in Concrete Block Production. *Jordan Journal of Earth and Environmental Sciences (JJEES)*, 16 March 2021.
- Smith, J. A., & Brown, K. L. (2022). Sustainable Construction Practices: A Focus on Fine Precast Concrete. *Journal of Sustainable Building Materials and Technology*, 9 (3), 145-160.
- Smith, A. J., & Greenfield, P. (2022). Sustainable Development of Fine Precast Concrete using Phosphate Raw Materials: Case Studies and Real-world Applications. *Journal of Sustainable Construction and Engineering*, 10 (1), 45-62.



الجامعة الهاشمية



صندوق دعم البحث العلمي



المملكة الأردنية الهاشمية

المجلة الأردنية
لعلوم الأرض والبيئة

JJEES

مجلة علمية عالمية محكمة

المجلد (١٥) العدد (٣)

<http://jjees.hu.edu.jo/>

ISSN 1995-6681

المجلة الأردنية لعلوم الأرض والبيئة

مجلة علمية عالمية محكمة

المجلة الأردنية لعلوم الأرض والبيئة: مجلة علمية عالمية محكمة ومفهرسة ومصنفة، تصدر عن عمادة البحث العلمي في الجامعة الهاشمية وبدعم من صندوق البحث العلمي - وزارة التعليم العالي والبحث العلمي، الأردن.

هيئة التحرير:

مساعد رئيس التحرير
- الدكتور محمد علي صلاحات
الجامعة الهاشمية، الزرقاء، الأردن.

رئيس التحرير:
- الأستاذ الدكتور عيد عبدالرحمن الطرزي
الجامعة الهاشمية، الزرقاء، الأردن.

أعضاء هيئة التحرير:

- الأستاذ الدكتور كامل خليف الزبون
جامعة البلقاء التطبيقية
- الأستاذ الدكتور محمود اسعد ابواللبن
الجامعة الهاشمية
- الأستاذ الدكتور هاني رزق الله العموش
جامعة آل البيت

- الأستاذ الدكتور إبراهيم مطيع العرود
جامعة مؤتة
- الأستاذ الدكتور خلدون عبدالكريم القضاة
جامعة اليرموك
- الأستاذ الدكتور عبدالله محمد بخيت ابوحمود
الجامعة الأردنية

فريق الدعم:

تنفيذ وإخراج
- عبادة محمد الصمادي

المحرر اللغوي
- الدكتور عبدالله فواز البدارنه

ترسل البحوث إلكترونياً إلى البريد الإلكتروني التالي:

رئيس تحرير المجلة الأردنية لعلوم الأرض والبيئة

jjees@hu.edu.jo

لمزيد من المعلومات والأعداد السابقة يرجى زيارة موقع المجلة على شبكة الانترنت على الرابط التالي:

www.jjees.hu.edu.jo



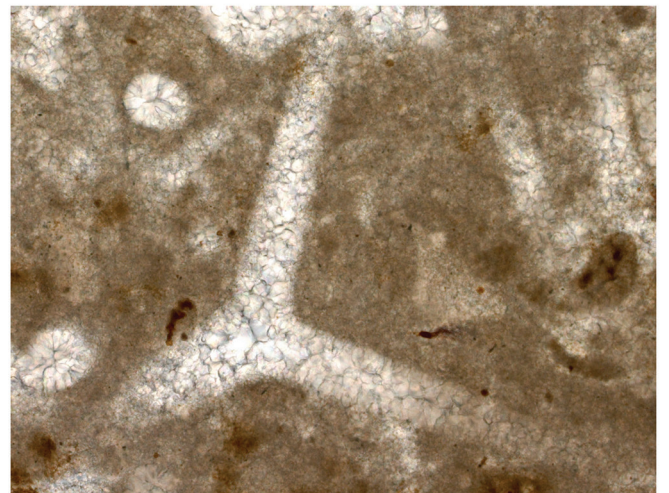
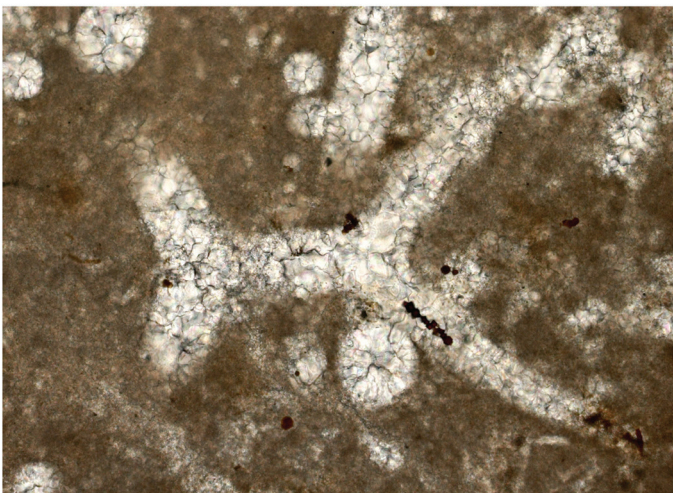
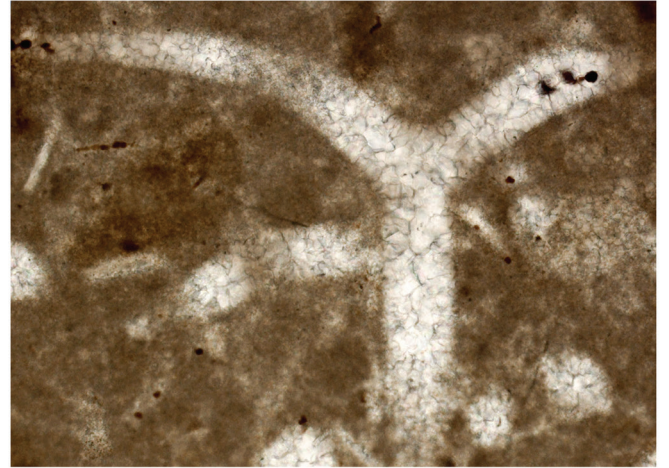
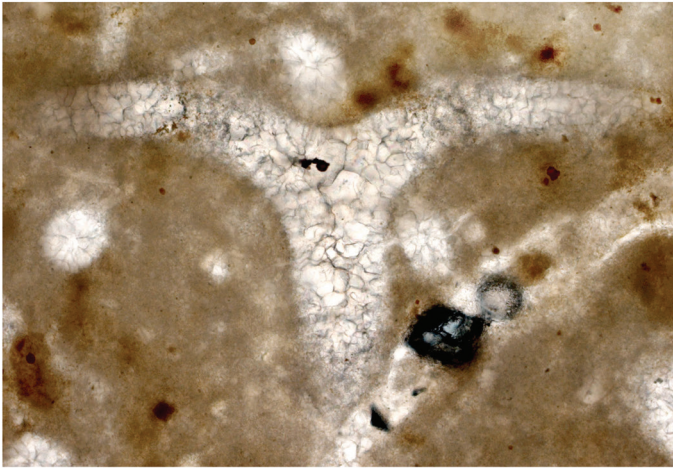
المملكة الأردنية الهاشمية صندوق دعم البحث العلمي الجامعة الهاشمية

JREES

المجلة الأردنية
لعلوم الأرض والبيئة



المجلد (15) العدد (3)



مجلة علمية عالمية مدعومة تصدر بدعم من صندوق دعم البحث العلمي